Physiology, syntrophy and viral interplay in the marine sponge holobiont

Dissertation

in fulfilment of the requirements for the degree
of Doctor in Natural Sciences
of the Faculty of Mathematics and Natural Sciences
at Kiel University

submitted by

Martin T. Jahn

Kiel, 2019

First examiner: Prof. Dr Ute Hentschel Humeida

Second examiner: Prof. Dr. Dr. Thomas Bosch

Date of the oral examination:
17. December 2019

Abstract

Holobionts result from intimate associations of eukaryotic hosts and microbes and are now widely accepted as ubiquitous and important elements of nature. Marine sponge holobionts combine simple morphology and complex microbiology whilst diverging early in the animal kingdom. As filter feeders, sponges feed on planktonic bacteria, but also harbour stable species-specific microbial consortia. This interaction with bacteria renders sponges to exciting systems to study basal determinants of animal-microbe symbioses. While inventories of symbiont taxa and gene functions continue to grow, we still know little about the symbiont physiology, cellular interactions and metabolic currencies within sponges. This limits our mechanistic understanding of holobiont stability and function. Therefore, this PhD thesis set out to study the questions of what individual symbionts actually do and how they interact.

The first part of this thesis focuses on the cell physiology of cosmopolitan sponge symbionts. For the first time, I characterised the ultrastructure of dominant sponge symbiont clades within sponge tissue by establishing fluorescence *in situ* hybridization-correlative light and electron microscopy (FISH-CLEM). In combination with genome-centred metatranscriptomics, this approach revealed structural adaptations of symbionts to process complex holobiont-derived nutrients (i.e., bacterial microcompartments and bipolar storage polymers). Next, we unravelled complementary symbiont physiologies and cell co-localisation indicating vivid symbiont-symbiont metabolic interactions within the holobiont. This suggests strategies of nutritional resource partitioning and syntrophy to dominate over spatial segregation to avoid competitive exclusion- a mechanistic framework to sustain high microbial diversity. By combining stable isotope pulse-chase experiments with metabolic imaging, we demonstrated that symbionts can account for up to 60 % of the heterotrophic carbon and nitrogen assimilation in sponges. Thus, sponge symbiont action determines sponge-driven biochemical cycles in marine ecosystems.

Finally, I explored the role of phages in the sponge holobiont focussing on tripartie phage-microbe-host interplay. Sponges appeared as rich reservoirs of novel viral diversity with 491 previously unidentified genus-level viral clades. Further, sponges harboured highly individual, yet species-specific viral communities. Importantly, I discovered that phages, termed "Ankyphages", abundantly encode ankyrin proteins. Such "Ankyphages" I found to be widespread in host-associated environments, including humans. Using macrophage infection assays I showed that phage ankyrins aid bacteria in eukaryote immune evasion by downregulating eukaryotic antibacterial immunity. Thus, I identified a potentially widespread mechanism of tripartite phage-prokaryote-host interplay where phages foster animal-microbe symbioses.

Altogether, I draw three main conclusions: The sponge holobiont is a metabolically intertwined ecosystem, with symbiont action impacting the environment, and tripartite phage-prokaryote-eukaryote interplay fostering symbiosis.

Zusammenfassung

Holobionten entstehen aus engen Verbindungen von eukaryontischen Wirten und Mikroben und sind heute als allgegenwärtige und wichtige Elemente in der Natur anerkannt. Marine Schwamm-Holobionten vereinigen eine einfache Morphologie und komplexe Mikrobiologie während sie früh im Tierreich divergierten. Als Filtrierer ernähren sich Schwämme von planktonischen Bakterien, beherbergen aber auch stabile artspezifische mikrobielle Konsortien. Diese Interaktion mit Bakterien macht Schwämme zu spannenden Systemen, um tiefzweigende Determinanten von Tier-Mikroben-Symbiosen zu untersuchen. Während die Inventare von Symbionten-Taxa und Genfunktionen stetig wachsen, wissen wir immer noch wenig über die Physiologie der Symbionten, zelluläre Interaktionen und ihren Stoffwechsel im Schwammkontext. Dies begrenzt unser tieferes Verständnis der Stabilität und Funktion von Holobionten. Deshalb untersucht diese Dissertation die Fragen, was die Funktion von Symbionten im Schwamm ist und wie sie miteinander interagieren.

Der erste Teil dieser Arbeit beschäftigt sich mit der Zellphysiologie von weit verbreiteten Schwammsymbionten. Durch Etablierung der Fluoreszenz *in situ* Hybridisierung - korrelative Licht- und Elektronenmikroskopie (FISH-CLEM) habe ich erstmals die Ultrastruktur dieser dominanten Schwamm-Symbionten im Schwammgewebe beschrieben. In Kombination mit genom-fokussierter Metatranskriptomik zeigte dieser Ansatz strukturelle Anpassungen zur Verarbeitung komplexer, aus dem Holobiont stammender Nährstoffe, d.h. bakterielle Mikrokompartimente und bipolare Speicherpolymere. Als Nächstes haben wir komplementäre Stoffwechselwege und Co-Lokalisationen der Symbionten aufgedeckt. Dies deutet darauf hin, dass Strategien der Ressourcenaufteilung und Syntrophie gegenüber räumlicher Trennung dominieren, um Wettbewerbsausschluss zu vermeiden- ein Ansatz, welcher der Erhaltung der hohen mikrobiellen Vielfalt dient. Durch die Kombination von stabilen Isotopen *pulse-chase* Experimenten mit metabolischer Bildgebung (NanoSIMS) konnten wir zeigen, dass Symbionten bis zu 60 % der heterotrophen Kohlenstoff- und Stickstoffassimilation in Schwämmen ausmachen können. Somit bestimmt die Aktivität von Schwammsymbionten die schwammgetriebenen biochemischen Zyklen in marinen Ökosystemen.

Zuletzt untersuchte ich die Rolle der Phagen im Schwamm-Holobionten und entdeckte eine Dreiecksbeziehung zwischen Phagen und Mikroben und dem Wirt. Schwämme erwiesen sich als reiche Quellen neuer viraler Vielfalt mit 491 bisher unbekannten Gruppen auf Gattungsebene und beherbergten sehr individuelle, aber artspezifische Virusgemeinschaften. Dabei entdeckte ich, dass Phagen, sogenannte "Ankyphagen", häufig Ankyrin-Proteine kodieren. Diese "Ankyphagen" fand ich in tierrischen Wirten, einschließlich des Menschen, weit verbreitet. Mit Hilfe von Makrophagen-Infektionstests konnte ich zeigen, dass Phagen- Ankyrine Bakterien helfen, dem Immunsystem von Eukaryoten zu entkommen, indem sie die antibakterielle Immunantwort von Eukaryoten herunterregulieren.

Zusammenfassend kann ich die folgenden wesentlichen Schlussfolgerungen ziehen: Der Schwamm-Holobiont ist ein metabolisch hochgradig vernetztes Ökosystem, dessen symbiontische Wirkung sich auf die Umwelt auswirkt und dessen trilaterales Interaktion zwischen Phagen-Prokayonten und Eukaryonten die Symbiose fördert.

Acknowledgments

So many people to thank across disciplines and places:

First of all, **Prof. Ute Hentschel**, for being an extraordinarily great supervisor, whilst allowing me the freedom to develop as an independent researcher. **Prof. Bas Dutilh** for hosting me in Utrecht, teaching me viromics Dutch cycling and chili and for becoming a mentor and friend. **Prof. Thomas Bosch** for kindly agreeing to examine this work and importantly for leading the CRC1182 in the way it is. Many thanks to **the CRC1182 community**- to **all of you**- for creating a most inspirational and friendly environment critical for the success of this thesis. **Dr. Tim Lachnit** for helping me with virus purification. **Dr. Stephanie Stengel** - the cell master - for your expertise and enduring support. The **Imaging Core Facility in Würzburg**, first and foremost **Prof. Christian Stigloher** and **Sebastian Markert** for sharing your excitement, equipment, time, and technical knowhow. Thanks to the whole Würzburg team making me feel as part of the group. Many thanks to current and former members of the **Marine Symbioses-Lab** I had the chance to work with. **Lucas** for being an invaluable colleague and friend. **Lucia** and **Laura** for making Barcelona happen and fun lunch discussions. **Hannes**, **Beate** and **Erik** for being amazing office mates who make me smile. **Kristina** for always being there to talk and laugh. Jazz, for being an almost reliable computation workhorse. **Florian Henkies** for being a great HIWI. **The Central Microscopy Facility** in Kiel- for providing me equipment to set up an own little EM processing lab. **Prof. Anders Meibom** for hosting us in Lausanne and introducing us into the art of NanoSIMS and trouble shooting. **Dr. Jean Vacelet** for sharing your perspective on the history of sponge microscopy and for providing early primary literature. **Prof. Forest Rohwer** for your interest and exciting discussions.

And there it is- obviously- my family. Thanks for your values and encouragement to follow my way.

This thesis was supported by a fellowship of the German Excellence Initiative to the Graduate School of Life Sciences, University of Würzburg, and a Young Investigator Award from the CRC1182.

Table of Contents

MAIN PUBLICATIONS & CONTRIBUTIONS

The thesis is based on the following publications and manuscripts:

1. **Jahn M.T.**, Markert S.M., Ryu T, Ravasi T, Stigloher C, Hentschel U, Moitinho-Silva L (2016). Shedding light on cell compartmentation in the candidate phylum *Poribacteria* by high resolution visualisation and transcriptional profiling. *Sci. Rep.* **6**, 35860; doi: 10.1038/srep35860

Participated in	**Author Initials,** Responsibility decreasing from left to right				
Study Design Methods Development	**MTJ** **MTJ**	LMS SMM/CS	UH		
Data Collection	LMS	**MTJ**	TRY	TRA	
Data Analysis and Interpretation	**MTJ**	LMS	UH	SMM	CS
Manuscript Writing Writing of Introduction Writing of Materials & Methods Writing of Discussion Writing of First Draft	 **MTJ** **MTJ** **MTJ** **MTJ** **MTJ**	 UH LMS LMS LMS	 LMS SMM UH		

2. Bayer K, **Jahn M.T.**, Slaby B.M., Moitinho-Silva L and Hentschel U (2018). Marine sponges as *Chloroflexi* hot spots: genomic insights and high-resolution visualization of an abundant and diverse symbiotic clade. *mSystems* 3:e00150-18; doi: 10.1128/mSystems.00150-18

Participated in	**Author Initials,** Responsibility decreasing from left to right				
Study Design Methods Development	KB **MTJ**	UH KB			
Data Collection	KB	**MTJ**	BS		
Data Analysis and Interpretation	KB	UH	**MTJ**	BS	
Manuscript Writing Writing of Introduction Writing of Materials & Methods Writing of Discussion Writing of First Draft	 UH KB KB UH KB	 KB **MTJ**/BS **MTJ**/BS KB	 **MTJ**/BS		

3. Moitinho-Silva L, Díez-Vives C, Batani G, Esteves A.I.S., **Jahn M.T.**, Thomas T (2017). Integrated metabolism in sponge-microbe symbiosis revealed by genome-centred metatranscriptomics. *ISME J* **11**(7); doi: 10.1038/ismej.2017.25

Participated in	**Author Initials,** Responsibility decreasing from left to right				
Study Design	LMS	TT			
Methods Development	LMS	TT	GB	MTJ	
Data Collection	LMS	DV	IE		
Data Analysis and Interpretation	LMS	TT	**MTJ**/GB		
Manuscript Writing					
Writing of Introduction	LMS	TT	DV	**MTJ**	
Writing of Materials &	LMS	TT	DV	**MTJ**	
Methods	LMS	TT	GB	**MTJ**	
Writing of Discussion	LMS	TT	DV	**MTJ**	
Writing of First Draft	LMS				

4. Rix L, Ribes M, Coma R, **Jahn, M.T.**, van Oevelen, D, de Goeij J, Escrig S, Meibom A, Hentschel U: Symbiont contributions to dissolved organic matter uptake by marine sponges. Manuscript in preparation.

Participated in	**Author Initials,** Responsibility decreasing from left to right				
Study Design	LR	UH	**MTJ**		
Methods Development	**LR/MTJ**				
Data Collection	LR	**MTJ**	SE		
Data Analysis and Interpretation	LR	**MTJ**	UH	SE	
Manuscript Writing					
Writing of Introduction	LR	LR	UH		
Writing of Materials &	LR	**MTJ**			
Methods	LR	**MTJ**			
Writing of Discussion	LR	UH	**MTJ**		
Writing of First Draft	LR				

5. **Jahn M.T.**, Arkhipova, K, Markert S.M., Stigloher C, Lachnit T, Pita L, Kupczok A, Ribes M, Stengel S.T., Rosenstiel P, Dutilh B.E., Hentschel U (2019). A phage protein aids bacterial symbionts in eukaryote immune evasion. *Cell Host & Microbe*; **26**(4); doi: 10.1016/j.chom.2019.08.019

Participated in	**Author Initials, Responsibility decreasing from left to right**				
Study Design	**MTJ**				
Methods Development	**MTJ**	BD			
Data Collection	**MTJ**	STS	SMM/CS	MR/PR/TL	
Data Analysis and Interpretation	**MTJ**	BD	KA	UH	
Manuscript Writing					
Writing of Introduction	**MTJ**	UH			
Writing of Materials &	**MTJ**	UH	BD		
Methods	**MTJ**	UH	KA		
Writing of Discussion	**MTJ**	UH			
Writing of First Draft	**MTJ**				

ADDITIONAL RELATED PUBLICATIONS

1.

Stengel S.T, Lipinski S., **Jahn M.T.**, Aden K., Ito G., Fazio A., Wottawa F., Kuiper J.W., Coleman O.I., Tran F., Bordoni D., Bernardes J.P., Jentzsch M., Luzius A., Bierwirth S., Messner B., Henning A., Welz L., Kakavand N., Schreiber S., Kaser A., Blumberg R.S., Haller D., Rosenstiel P (2019) ATF6 executes ER stress-dependent inflammatory signals in intestinal epithelial cells: *Submitted to Gastroenterology*

2.

Rausch, P., Rühlemann, M., Hermes, B. M., Doms, S., Dagan, T., Dierking, K., Domin, H., Fraune, S., von Frieling, J., Hentschel, U., Heinsen, F.-A., Höppner, M., **Jahn, M. T**., Jaspers, C., Kissoyan, K. A. B., Langfeldt, D., Rehman, A., Reusch, T. B. H., Roeder, T., Schmitz, R. A., Schulenburg, H., Soluch, R., Sommer, F., Stukenbrock, E., Weiland-Bräuer, N., Rosenstiel, P., Franke, A., Bosch, T., Baines, J. F. (2019). Comparative analysis of amplicon and metagenomic sequencing methods reveals key features in the evolution of animal metaorganisms. *Microbiome* **7**(1): 133.

3.

Slaby B.M., Franke A, Rix L, Pita L, Bayer K, **Jahn M.T**., Hentschel U (2019) marine sponge holobionts in health and disease. In: Li Z, editor. Symbiotic microbiomes of coral reefs sponges and corals. Dordrecht: *Springer Netherlands*. p.81-104.

4.

Hildebrand F, Moitinho-Silva L, Blasche S, **Jahn M.T.**, Gossmann T.I., Heuerta-Cepas J, Hercog R, Luetge M, Bahram M, Pryszlak A, Alves R.J., Waszak S.M., Zhu A, Ye L, Costea P.I., Aalvink S, Belzer C, Forslund S.K., Sunagawa S, Hentschel U, Merten C, Patil K.R., Benes V, Bork P (2019). Antibiotics-induced monodominance of a novel gut bacterial order. *Gut* **68**:1781-1790.

5.

Millins C, Dickinson E. R., Isakovic P, Gilbert L, Wojciechowska A, Paterson V, Tao F, **Jahn M.T.**, Kilbride E, Birtles R, Johnson R, Biek R (2018). Landscape structure affects the prevalence and distribution of a tick-borne zoonotic pathogen. *Parasit Vectors* **11**(1): 621

6.

Horn H, Slaby B, **Jahn M.T.**, Bayer K, Moitinho-Silva L, Förster F, Abdelmohsen U.R., Hentschel U (2016) An enrichment of CRISPR and other defense-related features in marine sponge-associated microbial metagenomes. *Front. Microbiol.* **7**:1751

"Each living creature must be looked as a microcosm – a little universe,
formed of a host of self-propagating organisms,
inconceivably minute and as numerous as the stars in heaven"

Charles Darwin (1868)
On the hypothesis of pangenesis
Animals and Plants under Domestication Vol.II p.404

CHAPTER 1
GENERAL INTRODUCTION

When the first animals evolved in the ocean's, microbes where around and they possibly interacted with animal hosts ever since (McFall-Ngai et al., 2013). While it is now widely accepted that animal-microbe symbioses are common themes in biology, the next challenge is to understand its functional underpinnings. Therefore, this thesis investigates the microbial activity and interplay in evolutionary basal sponges by taking the symbionts' perspective. I first establish and apply integrative methods to understand the physiology of cosmopolitan sponge symbionts in the context of their sponge host. Second, I focus on the metabolic interplay within the holobiont, and thirdly, explore the diversity and function of viruses as modulators of the holobiont. This chapter aims to give a brief overview of symbiosis literature, sets the conceptual framework and introduces relevant aspects of sponge holobiont biology.

1.1 Symbiosis

Symbioses- 'the living together of unlike organisms' (de Bary, 1879)- are extremely widespread in nature and set the stage for a tremendous variety of important interactions across the tree of life (Moya et al., 2008, Fisher et al., 2017b). Whole ecosystems are built on symbioses such as between corals and dinoflagellates, empowering sunlit coral-reefs (LaJeunesse et al., 2018, Venn et al., 2008), or between plants and mycorrhiza via the exchange of nutrients in about 60 % of trees on earth (Steidinger et al., 2019)). A key feature resulting from symbiotic interaction is that it allows for emergent properties, i.e. to perform new functions each symbiont alone would not be able to accomplish (Margulis and Fester, 1991). This enables hosts to conquer habitats they would otherwise be excluded from (Márquez et al., 2007, Simonsen et al., 2017), to access previously inaccessible nutrients and energy forms (i.e. nutritional symbiosis, (Dubilier et al., 2008, Salem et al., 2017)), or to equip with new weaponry to defend against opponents (i.e. defensive symbiosis, (Zan et al., 2019, Clay, 2014)). Such facilitative interactions between species are widespread and represent a mechanism to maintain symbioses (Zélé et al., 2018). Indeed, this is covered by the original symbiosis definition of de Bary (1879) that is inclusive of a variety of long-term interactions ranging from mutually beneficial (+/+), over commensal (+/0) to parasitic (+/-) but does not exclude mutually neutral (0/0).

For clarity, I will follow this broad symbiosis definition *sensu lato* throughout this thesis and specifically discuss the cases where assumptions on the type of interaction can be made. Diverse factors are explanatory for the type of such symbiotic associations which are compiled in Figure 1.

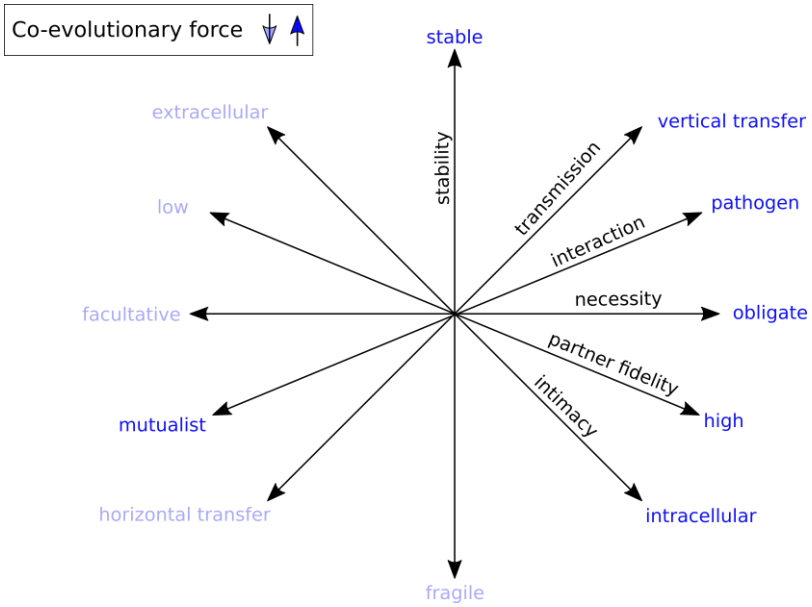

Figure 1: Important variables defining microbial symbioses (black) and their range (blue). The expected co-evolutionary force for each situation partly compiled based on data from van Vliet and Doebeli (2019).

Symbioses between microbes and animals are so ubiquitous, that there seems to be no permanently germ-free animal in nature (Margulis, 1998, McFall-Ngai et al., 2013, Thompson et al., 2017). These symbionts do not merely reflect environmental bacteria but are largely distinct and host-specific (Ley et al., 2008, Amato et al., 2019, Pollock et al., 2018, Hacquard et al., 2015). Notably, these widespread associations between microbial symbionts and their hosts only became possible to study following advances in bacterial genetics and sequencing technology (Sanger et al., 1965, Cohen et al., 1973). More recently, this has revealed an increasing number of cases where the microbiome similarity between species mirrors the host phylogeny (Brucker and Bordenstein, 2013, Pollock et al., 2018, van Opstal and Bordenstein, 2019, Groussin et al., 2017, Carrillo-Araujo et al., 2015, Ross et al., 2018). This eco-evolutionary pattern, termed phylosymbiosis (Brucker and Bordenstein, 2013), might indicate co-evolutionary trajectories between animals and their symbiont microbes.

Indeed, there is evidence that microbes have far-reaching effects on all central elements of the hosts biology. This includes its metabolism (Brune, 2014, Shabat et al., 2016), morphology (Kremer et al., 2018, Simonet et al., 2018), reproduction (Vala et al., 2004, Reyes et al., 2019), immune system (Arpaia et al., 2013, Lhocine et al., 2008), behaviour (Johnson and Foster, 2018, Schretter et al., 2018), development (Shikuma et al., 2014, van Opstal and Bordenstein, 2019), and ultimately host evolution (Shapira, 2016, Rudman et al., 2019).

How microbes specifically affect their host can best be illustrated in simple symbioses with one or a few main symbiont partners. It was shown that symbionts can provide essential nutrients such as amino acids in aphids (Douglas and Prosser, 1992, Douglas, 1998, Gündüz and Douglas, 2009), modulate body contraction behaviour in *Hydra* (Murillo-Rincon et al., 2017), allow bobtail squids active camouflage by counter illumination (McFall-Ngai, 2008), and even cause reproductive isolation in *Wolbachia*-insect symbioses (Shropshire and Bordenstein, 2019).

The animal hosts can also impact the ecology and evolution of their symbionts (Foster et al., 2017, McCutcheon and Moran, 2011, Fisher et al., 2017a). This includes the supply of symbiont tailored oligosaccharides in human breast milk (Zivkovic et al., 2011), the application of selective antimicrobial cocktails such as antimicrobial peptides in *Hydra* (Augustin et al., 2017, Franzenburg et al., 2013), or the selective vertical uptake of specific symbiont strains such as in the squid vibrio system (Nyholm and McFall-Ngai, 2004). Obviously, such partnerships do impact the hosts' and microbes' fitness and highlight that the biology of animal-microbe systems can't be fully understood when each associate is studied in isolation (reviewed in Gilbert et al. (2015)).

1.2 The holobiont concept

The holobiont concept offers an inclusive view on animals (and plants) as functional biological entities consisting of the host organism plus its microbial symbionts (Margulis and Fester, 1991). The microbial symbiont communities can be composed of a myriad of viruses, bacteria, archaea, fungi, protists, and microbial eukaryotes such as algae. The hologenome term was introduced to highlight the extended genetic repertoire of all combined genomes of the holobiont (Zilber-Rosenberg and Rosenberg, 2008, Rosenberg et al., 2007). While these concepts are widely accepted as structural definitions (such as a genome or chromosome), there is a fierce debate over the extent to which the holobiont and the hologenome are evolutionary units of selection (Queller and Strassmann, 2016, Moran and Sloan, 2015, Douglas and Werren, 2016, Doolittle and Booth, 2017, Theis et al., 2016, Hester et al., 2015, Bordenstein and Theis, 2015). However, examples are accumulating from different systems that point to co-evolution between specific microbes and their hosts (Russell et al., 2013, Clark et al., 2000, Nishiguchi et al., 1998, Wilson and Duncan, 2015, Moeller et al., 2016).

Animal holobionts are often complex systems with many symbiont species involved (O'Brien et al., 2019), resulting in non-trivial challenges to study them. Specifically, symbiosis characteristics (Figure **1**) may differ from symbiont to symbiont, depend on spatially confined niches (Mark Welch et al., 2016), can vary over (life)-time (Nyholm and McFall-Ngai, 2004, Kundu et al., 2017), and can also hinge on other symbionts (Zelezniak et al., 2015, Freilich et al., 2011) and the environment (Rothschild et al., 2018). One solution to cut through this complexity is to approach holobionts as ecological communities (Douglas and Werren, 2016, Miller et al., 2018) and to appreciate the complex and variable species interactions at play.

1.3 Sponge-microbe symbiosis– the players

Sponges are basal invertebrates that combine simplistic morphology with complex microbiology, making them an excellent model for investigating host-microbe interactions. The following sections present relevant aspects of sponge holobiont biology and introduce the relevant players with a focus on the host, prokaryotes and phages.

1.3.1 Sponges as animal hosts

Sponge ecology

Sponges perform key functions in benthic ecosystems from Pole to Pole and from shallow waters to the deep sea (Manconi and Pronzato, 2008, Van Soest et al., 2012). Sponges shape their ecosystem via bioerosion (reviewed in Schönberg et al. (2017)) and coral-reef consolidation (Wulff, 1984, Biggs, 2013), are competitors for reef-space (Brandt et al., 2019, Mateo et al., 2006) while providing at the same time habitat to others (Frith, 1976, Ávila and Briceño-Vera, 2018). Most remarkable, however, is their role in mediating biochemical fluxes in their respective ecosystems. Sponges filter up to about 24,000 litres of seawater per kg sponge per day (Reiswig, 1971). For illustration, it is estimated that giant barrel sponges process quantities equivalent to 7.7 meter of overlying water column per day (McMurray et al., 2014).

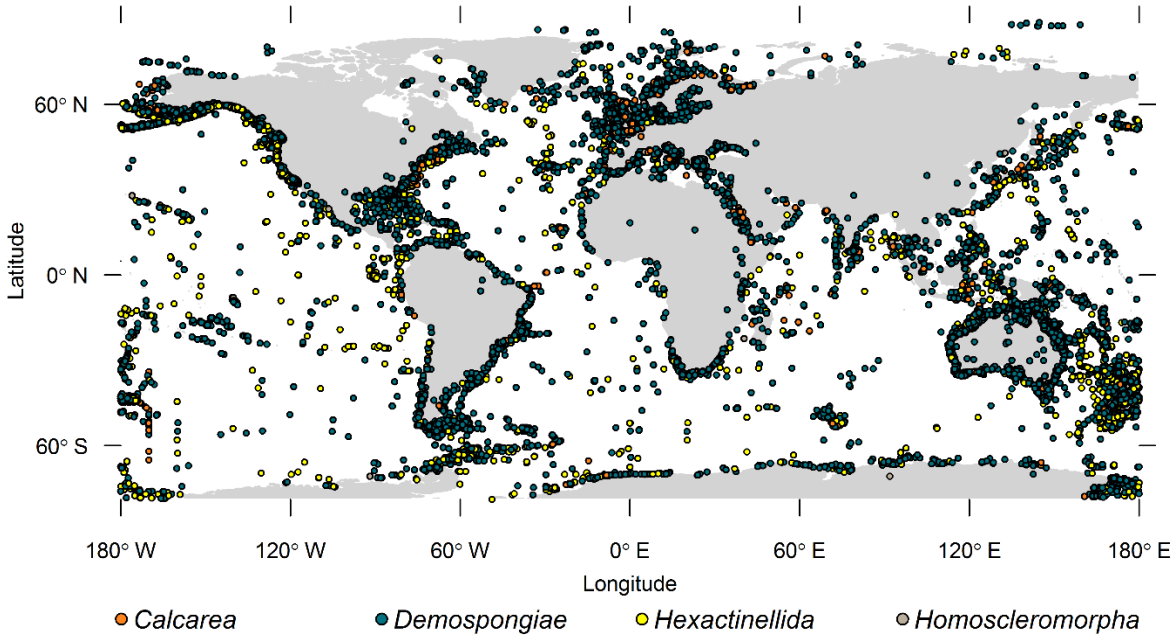

Figure 2 **Global distribution of *Porifera*.** The map illustrates sponge sightings (n=252,670 entries) as deposited in Ocean Biogeographic Information System (OBIS). Raw data was retrieved from OBIS as of July 2019 and plotted in R (for code see Appendix B1).

It is this enormous filtration capacity of sponges that drives a significant flow of energy and nutrients (C, N, P, and Si) from seawater to their benthic ecosystems (Maldonado et al., 2012, Jiménez and Ribes, 2007, Lopez-Acosta et al., 2019, Valentine and Butler, 2019). Thereby, sponges represent a critical trophodynamic link in the benthic-pelagic coupling that depends on the composition of sponge diet.

Traditionally, sponges are regarded as particulate organic matter (POM) specialists (Pile et al., 1996, Reiswig, 1971) with a diet spectrum that ranges in size from virions (Hadas et al., 2006) up to bacteria and phytoplankton (Ribes et al., 1999, Wehrl et al., 2007). Thus, sponges feed on the most abundant nano- and picoplankton components with retention efficiencies of up to 99 % (Pile et al., 1997, Hadas et al., 2009, Morganti et al., 2017). However, it was found that POM consumption alone was not sufficient to explain the observed respiratory rates of sponges (Reiswig, 1971, Reiswig, 1981). At ecosystem level, as well, there were nutritional budget gaps that could not be explained. Typically, DOM is of little direct use to higher organisms in the marine food web but is readily accessible to planktonic heterotrophic bacteria (i.e. microbial loop, (Azam et al., 1983)). This renders reports of sponges filtering DOM from seawater, as part, or most of their diet (Yahel et al., 2003, McMurray et al., 2018, Hoer et al., 2018, Wooster et al., 2019, Garrabou and Zabala, 2001, de Goeij et al., 2008) to exciting findings as DOM budgets critically impact the function and health of benthic ecosystems such as coral-reefs (Haas et al., 2016). Indeed, seawater DOM filtration by sponges is thought to reach equivalent magnitudes to the gross primary productivity of whole coral reef ecosystems (de Goeij et al., 2013, Hatcher, 1990, de Goeij and van Duyl, 2007) and thus close the aforementioned budget gaps. However, only a fraction of the consumed DOM is respired, or converted into body growth (Garrabou and Zabala, 2001), but is rather channelled into a massive cell turnover. Choanocytes can display with about 5-6 hours the shortest cell cycles in the animal kingdom (De Goeij et al., 2009), and when ejected into the environment, produce large amounts of detritus (POM). This POM is thought to be readily absorbed by higher trophic levels of the fauna, such as fish, which represents an extensive nutrient flux to higher trophic levels called the “sponge loop” (de Goeij et al., 2013). Overall, this highlights the importance of sponges in benthic nutrient cycles and ultimately for the health of benthic ecosystems. In spite of this importance, little is known about the nutrient fluxes within in the sponge holobiont, the mechanisms of conversion, and the elements involved.

Evolution, Taxonomy & Morphotypes

Evolutionarily, sponges (phylum *Porifera*) arose more than 600 million years ago (Yin et al., 2015, Maloof et al., 2010) in Precambrian oceans ranking them among most ancient extant animals, i.e. Metazoa (King and Rokas, 2017). A central element of their lasting success may have been their simple but plastic morphology (Wulff, 2006), which has remained largely unchanged for millennia (Yin et al., 2015). Unlike other metazoans, sponges lack true tissues, a nervous system, and internal organs (King and Rokas, 2017, Simpson, 1984). Further, while sponges lack an adaptive immune system, they

possess a well-developed innate immunity (Ryu et al., 2016, Srivastava et al., 2010, Riesgo et al., 2014). It is the deep evolutionary anchoring in the animal kingdom that propels sponges to important models for basic research on the evolution of multicellularity (Sogabe et al., 2019, Nichols et al., 2012), immunity in host-microbe interactions (Riesgo et al., 2014, Pita et al., 2018a, Steindler et al., 2007), as well as cell signalling (Ludeman et al., 2014, Leys and Degnan, 2001).

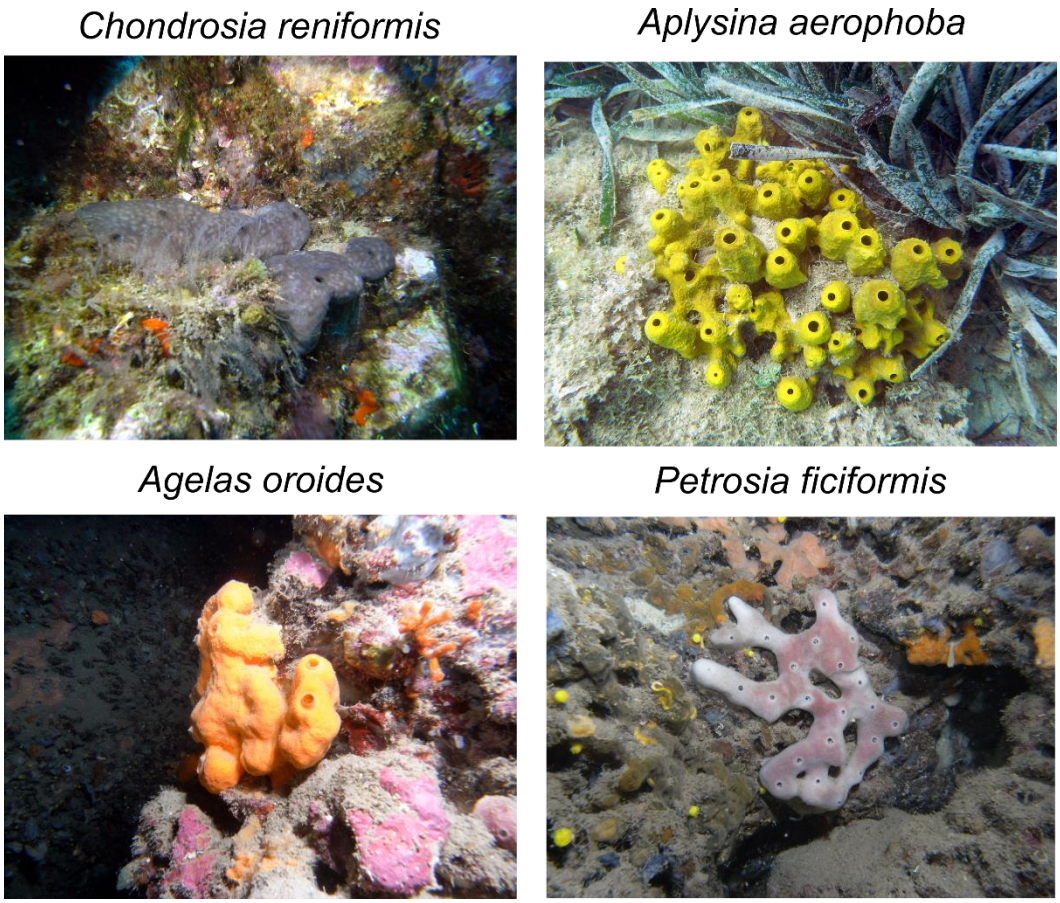

Figure 3: The Mediterranean sponges species studied in this PhD thesis.
1) *Chondrosia reniformis*, 2) *Aplysina aerophoba*, 3) *Agelas oroides*, 4) *Petrosia ficiformis*. Credit: Manel Bolivar; Images were corrected to remove blue cast.

To date, about 9,500 extant sponge species have been described (Van Soest et al., 2019, Van Soest et al., 2012, Hooper and Van Soest, 2002) and about 16,000 more species are predicted to exist (Hooper et al., 2013). The poriferan phylum is currently subdivided into four classes: demosponges (*Demospongiae*), glass sponges (*Hexactinellida*), calcareous sponges (*Calcarea*), and *Homoscleromorpha* (Van Soest et al., 2019, Thacker et al., 2013). Sponges display a magnificent variety in size, shape and colour (Figure 3), which is remarkable considering that sponges assemble from less than 20 different cell types (Simpson, 1984, Funayama, 2013). In addition to these manifold phenotypes between species, individuals can also display a notable degree of phenotypic heterogeneity (Hooper and Van Soest, 2002, Ávila and Ortega-Bastida, 2015). The size of adult sponges can range from thinly encrusting layers only millimetres thick (Simpson, 1984) up to massive organisms as big as a minivan (Wagner and Kelley, 2017). The shapes can be encrusting, massive, lobate, tubular,

branching, flabellate, cup shaped, or excavating (Hooper and Van Soest, 2002, Bell and Barnes, 2001). The rich colouring of sponges is frequently paralleled with a cocktail of secondary metabolites such as Uranidine yellow in *Aplysina aerophoba* (Cimino et al., 1984) or Prodigiosin red in *Xestospongia testudinaria* (Ibrahim et al., 2014). It is the diversity of sympatric sponges that can occur in the same habitat (Figure 3) that makes sponges a useful model for studying species-specific effects while minimizing environmental effects.

Morphology & function

Morphologically, the sponge body plan (except carnivores) is highly adapted for their lifestyle as sessile filter-feeders (Figure 4). This allows a sponge to filter seawater of up to a thousand times its own body weight per hour (Weisz et al., 2008, Nielsen et al., 2017) for nutrition and respiration (O_2 in; CO_2 out). Pumping further aids the sponges to excrete metabolic waste products such as ammonia and nitrate (Bayer et al., 2008), to perceive environmental cues, or to dispense reproductive cells (Vasconcellos et al., 2019). I will focus here on the stereotypic leuconoid type of demosponges as the poriferan class that comprises most modern species (Hooper and Van Soest, 2002, Thacker et al., 2013) and all studied specimens of this thesis.

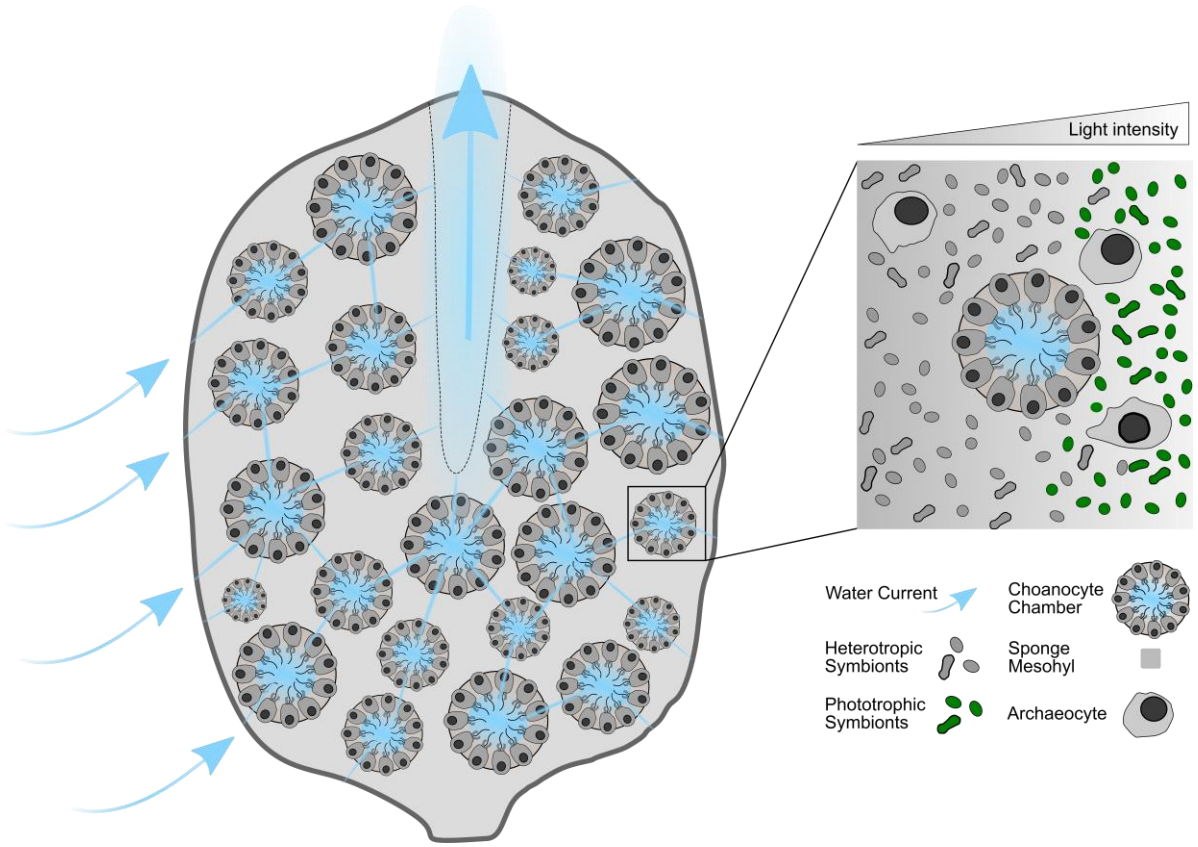

Figure 4: Schematic representation of the Demospongiae body plan in overview (left) and detail (right). The left part of the figure was modified from Godefroy et al. (2019).

Physiologically, water and dispensed food enter the branched aquiferous channel system of sponges through ostia, small pores of 10-100 µm, and the filtrate is expelled through larger openings termed oscula. The water stream is unidirectionally driven by beating flagellar choanocyte cells (choanoderm) lining densely packed choanocyte chambers (Figure 4). The large cross-sectional area in these chambers, as compared to the channel system, locally slows down the water flow allowing choanocytes to efficiently absorb nutrients and gases, therein (Westheide et al., 2013). Besides, absorption of gases and larger particles can be mediated via pinacocytes lining the outer sponge surface and water channels (Westheide et al., 2013). This setup allows the sponge to efficiently absorb a wide range of dissolved and particulate nutrients from the water column (see Sponge ecology). Following intravacuolar digestion the retained nutrients can then be passed over to archaeocytes, that further digest, and, as highly mobile amoeboid cells, distribute nutrients throughout the sponge body (Willenz, 1980). However, the exact uptake kinetics and transfer routes (i.e. lumen to mesohyl), and how it might explain observed selectivity of sponge feeding (McMurray et al., 2016, Maldonado et al., 2010, Wehrl et al., 2007), require further investigation (Godefroy et al., 2019).

The mesohyl, which is sandwiched between pinacoderm (exo- and endopinacoderm) and choanoderm, is the environmentally least exposed structure of the sponge body and frequently dominates the sponges' biomass. Mesohyl corresponds to the mesoglea of the coelenterates or the connective tissue in bilaterian animals. In sponges, it constitutes a gelatinous extracellular matrix, made by a collagen-like protein scaffold, where different cell types can freely move and differentiate into other cell types (e.g. archaeocytes; Sogabe et al. (2019)) generating high structural plasticity. Firmness of the sponge body is generated by spongin fibers secreted by spongocytes alone, or together with silica spicules manufactured by sclerocytes. Archaeocytes are abundant and patrol the mesohyl, much like macrophages, thus they critically function in the sponges' innate immunity on top of their role in catabolism (above). Importantly, it is the mesohyl that functions as a cellular melting pot where sponge cells intermingle and associate with their microbial symbionts (see 1.3.2), with drastic effects on both sides (see 1.4).

1.3.2 Sponge microbes

Abundance & diversity of sponge microbiomes

The microbiology of sponges spans all domains of life including bacteria, eukaryotes (e.g. unicellular algae, protists and fungi), and archaea (Taylor et al., 2007). In fact, prokaryotes can contribute up to about 40 % of sponge tissue volumes (Vacelet, 1975b, Wilkinson, 1978)) and thereby exceed the number of host cells' by up to 100-times (Figure 4) (Gloeckner et al., 2014a). It was early microscopic evidence that has repeatedly confirmed these sponge-microbe associations to be common in healthy sponges (Dosse, 1939, Lévi and Porte, 1962, Vacelet, 1975b, Vacelet and Donadey, 1977b, Wilkinson, 1978). But while some sponges host a myriad of microbes, others are reported to be nearly free of them

(Reiswig, 1981, Vacelet and Donadey, 1977a, Gloeckner et al., 2014a, Moitinho-Silva et al., 2017b). This dichotomy allows to classify sponge species as belonging to high microbial abundance (HMA; about 10^8–10^{10} prokaryotes g^{-1}) sponges or low microbial abundance (LMA; about 10^5–10^6 prokaryotes g^{-1}) sponges (Gloeckner et al., 2014a, Hentschel et al., 2006) and renders it a natural model to compare the influence of microbial abundance on sponge function.

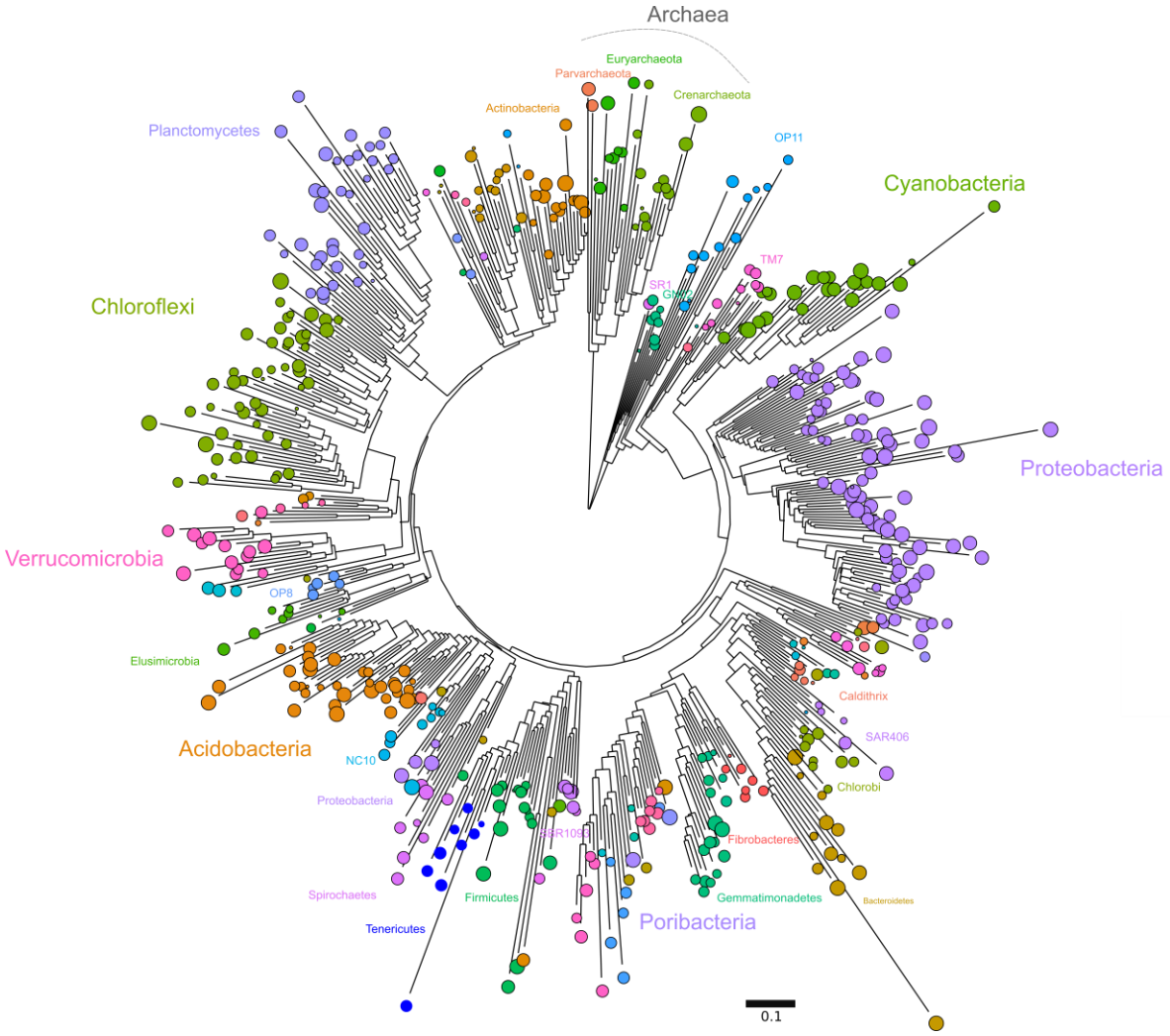

Figure 5: "Sponge Microbiome Project"-prokaryote diversity. The tree represents the 16S rRNA gene sequence-based phylogeny from *n* = 3569 sponge-associated microbial communities as described in Moitinho-Silva et al. (2017a). Data was analysed with phyloseq1.28 (McMurdie and Holmes, 2013) and branches were merged at order level, scale: substitutions per site (see Appendix B2;).

To date, at least 41 microbial phyla have been described in sponges (Thomas et al., 2016) with *Chloroflexi*, *Poribacteria*, *Cyanobacteria* and *Proteobacteria* representing abundant, diverse and widespread taxa (Karimi et al., 2018, Schmitt et al., 2012, Podell et al., 2018, Steinert et al., 2018b, Burgsdorf et al., 2015, Fieseler et al., 2004, Schmitt et al., 2011). This high rank taxonomic diversity (Figure 5) is extraordinary and distinguishes sponge microbiota from that of many other animals and plants that tend to be dominated by a few phyla (Thompson et al., 2017, Hacquard et al., 2015). A global

census of sponge microbial symbionts across five oceans extended previous findings showing that, collectively, sponges are a distinct reservoir of considerable marine microbial diversity in the oceans (~40,000 operational taxonomic units (OTUs); Thomas et al. (2016)). However, microbial complexity can differ considerably between sponge species ranging within two orders of magnitudes (50 - 3,820 OTUs host^{-1}, Thomas et al. (2016)). In this context, it has been shown that the HMA-LMA dichotomy is mirrored by diverging microbial symbiont profiles. Specifically, LMA sponges contain less diverse microbiomes, which are dominated by proteobacterial and cyanobacterial symbionts, whereas HMA sponge symbionts are more diverse and dominated by different clades such as *Poribacteria* and *Chloroflexi* (Moitinho-Silva et al., 2017b, Cleary et al., 2018, Erwin et al., 2015c, Schmitt et al., 2011). Therefore, lineages of *Poribacteria* and *Chloroflexi* are considered as indicator phyla of sponges.

Species-specificity, transmission & stability

Importantly, microbial sponge symbiont communities do not simply reflect the planktonic consortia filtered from seawater. Instead, the microbial communities of sponges are host species-specific, distinct to seawater and composed by a high fraction of specialist symbionts falling into monophyletic, sponge-specific sequence clusters (Schmitt et al., 2012, Simister et al., 2012, Thomas et al., 2016, Hentschel et al., 2002, Taylor et al., 2007, Reveillaud et al., 2014, Trindade-Silva et al., 2012). Transmission of symbiont communities between sponge generations is mediated by a mix of vertical and horizontal transmission (Björk et al., 2019, Schmitt et al., 2008). This is in line with reports of symbionts in reproductive cells (i.e. larvae, sperm, (Enticknap et al., 2006, Usher et al., 2005)), as well as rare observations in seawater, where they can only be detected with deep sequencing approaches (Webster et al., 2010, Moitinho-Silva et al., 2014a) and are likely metabolically inactive (Moitinho-Silva et al., 2014a, Taylor et al., 2013). Further, other biomes and reef animals might serve as reservoirs for horizontal transfer as showcased in a recent case study of Cleary et al. (2019), although the activity of sponge symbionts in these associations remains to be investigated. In contrast, within sponge species, symbiont communities were reported to be largely consistent at different sampling locations (Pita et al., 2013, Steinert et al., 2016), over time (Erwin et al., 2015b, Erwin et al., 2012) and facing some degree of environmental perturbation (Gerçe et al., 2009, Gantt et al., 2017, Glasl et al., 2018). To date, none of the core sponge symbionts is available in pure culture so that all insights were derived from culture independent approaches including imaging (Gloeckner et al., 2014b, Hardoim et al., 2014), meta-genomics (Slaby et al., 2017, Fan et al., 2012), meta-transcriptomics (Diez-Vives et al., 2017, Moitinho-Silva et al., 2014b, Radax et al., 2012) or meta-proteomics (Liu et al., 2012, De Mares et al., 2018). Thus, despite the ubiquity of abundant, stable and specific sponge-microbe symbioses, there is still limited knowledge about the activity and physiology of specific microbes in the host context and how their interplay translates to holobiont function.

1.3.3 Viruses

Viral loads impacting marine animals are substantial considering average titres of 10 million virions in each millilitre of seawater (Wommack and Colwell, 2000). This seems particularly true for filter feeding animals such as sponges that are highly exposed to this external virus pool by their filtration activity. This translates to 55.9 billion virions that are retained in a sponge per day when assuming an average virus concentration in seawater, the maximal filtration capacity of sponges (per kg and day), and an experimentally determined retention rate of about 23.3 % (Hadas et al., 2006), as calculated by:

$$\text{Viral uptake per day} = \text{Cv} * \text{Rr} * \text{Fv} = 10^7 \frac{\text{virions}}{\text{ml}} * 0.233 * 24{,}000 \frac{\text{l}}{\text{kg} * \text{d}}$$

$$= 55{,}920{,}000{,}000 \text{ virions / day}$$

where Cv is the average seawater virus concentration from Wommack and Colwell (2000);
Rr retained viral fraction 0.233 % from Hadas et al. (2006);
Fv filtered volume per day from Reiswig (1971).

While the presence of the first virus-like particles in sponge tissue was described already 1978 (Vacelet and Gallissian, 1978), it took almost 40 years, before sponge virology was starting to be explored. In fact, at the beginning of this PhD thesis, publications on sponge viruses using molecular approaches were not yet available. In this context, a recent electron microscopy based study extends the detected morphological diversity to 50 viral morphotypes (Pascelli et al., 2018). The observed virus like morphologies included non-enveloped, non-tailed icosahedral virus-like particles, tailed bacteriophages and geminate, filamentous, as well as brick-shaped viruses indicative of *Poxviridae* (Pascelli et al., 2018). In order to capture the molecular diversity of sponge associated viruses, a first attempt of sponge virome sequencing was established (Laffy et al., 2016) and applied to compare sponge viromes (i.e. *Amphimedon queenslandica, Xestospongia testudinaria, Ianthella basta and Rhopaloeides odorabile*) of Great Barrier Reef sponges (Laffy et al., 2018). Based on the comparisons of the four sponge species, it was suggested that patterns indicate species-specific viral signatures although specimen were sampled at different locations and timepoints, what also might explain the observed differences.

Taxonomically, the recovered sponge associated viruses showed low identity to known viruses and were dominated by clades of bacteriophages (Laffy et al., 2018) such as by tailed bacteriophages of the order *Caudovirales* (dsDNA) and *Microviridae* (ssDNA). Besides, there was evidence for eukaryote infecting viruses including members of *Megavirales* and *Parvoviridae* (Laffy et al., 2018). However, whether these viruses infect members of the sponge holobiont remains to be investigated. Further, while sponges are exposed to massive amounts of viruses, the composition and function of residual phages remains largely unexplored.

The high exposure to phages, a major bacteriolytic element (Figure 6), raises questions about how sponge microbiome homeostasis can be maintained. Morphologically, the lack of tissue boundaries along with high bacterial cell densities would favour viral outbreaks within sponge tissues. In this context, defence mechanisms to alien nucleotides from phages and plasmids are clearly enriched features of microbial sponge symbionts as indicated by single-cell genomics and metagenomics (Horn et al., 2016, Podell et al., 2018, Slaby et al., 2017, Fan et al., 2012, Burgsdorf et al., 2015, Thomas et al., 2010). These defence mechanisms are based on self-non-self-discrimination (e.g., restriction-modification system) or prokaryotic adaptive immunity (i.e. CRISPR-Cas system), representing major strategies against viral infection and for genetic resilience. While these are indications for the selective advantage of phage resistance for the bacterial symbiont lifestyle, there is still limited knowledge about the function of residual phages and their impact in shaping the sponge holobiont. Recent developments in sponge virology (Laffy et al., 2018, Pascelli et al., 2018, Laffy et al., 2019) will be discussed in light of my results in CHAPTER 8.

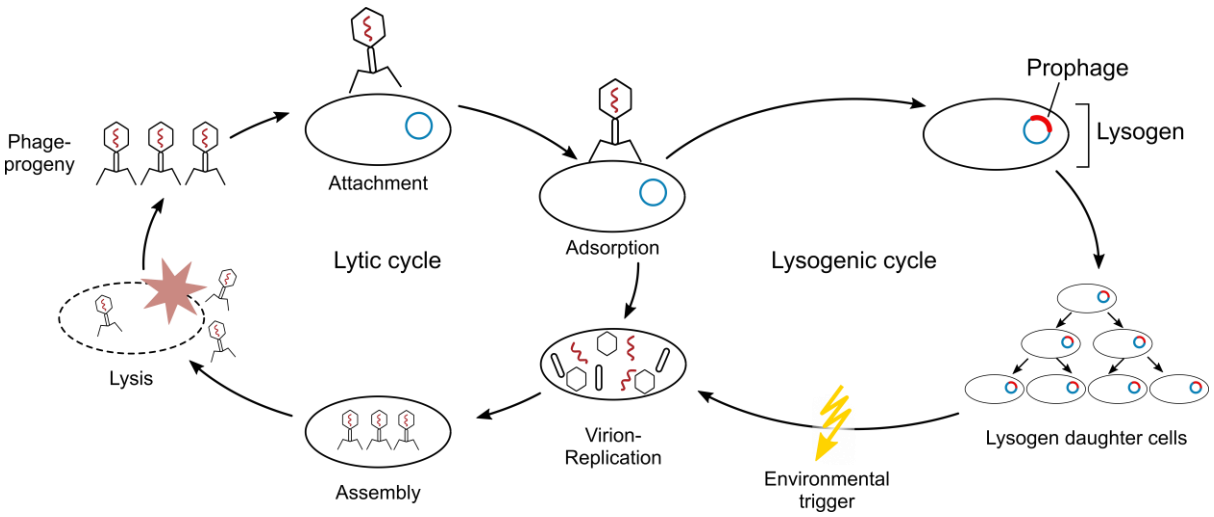

Figure 6: Lytic and lysogenic replication of bacteriophages. (**A)** For lytic replication phages rapidly take over the host cell for replication and assembly of progeny phage particles. Host cells are destroyed by lysis releasing new phage particles to the environment. Viral lysis promotes rapid nutrient turnover in their ecosystems (Weitz et al., 2015, Guidi et al., 2016), keeps the nutrients at lower trophic levels (viral shunt; Wilhelm and Suttle (1999)), and promotes bacterial diversity (kill-the-winner dynamics; (Thingstad, 2000, Winter et al., 2010). (**B**) For lysogenic replication temperate phages insert their genome into the host's chromosome (i.e. prophage) replicating with the host without destruction. Notably, at this stage, prophages can equip their hosts with beneficial genes (Hurwitz et al., 2013, Gao et al., 2016) and drive adaptive evolution (Davies et al., 2016, Fernández et al., 2018). Environmental triggers induce prophages to enter the lytic cycle. Modified from Breitbart et al. (2018).

1.4 Sponge-microbe symbiosis – the game

The sponge holobiont is characterized by an intimate association between sponge host cells and their symbionts (Figure 7). Heterotrophic and autotrophic symbionts can fill the mesohyl region in high densities with a degree of intimacy with their host cells ranging from mostly extracellular (Bruck et al., 2008, Taylor et al., 2007), to intracellular (Burgsdorf et al., 2019, Vacelet and Donadey, 1977a), and even intranuclear associations (Friedrich et al., 1999, Vacelet, 1970). This intimacy between sponge cells and their symbionts is very different from many other animals that maintain host cells and internal tissues sterile by keeping their symbionts in confined locations via epithelial barriers or specialised organs such as the gut. Instead, sponge cells (e.g. archaeocytes) intermingle with diverse symbionts in the extracellular mesohyl matrix, making it a vast space for potential symbiont-symbiont and symbiont-host interaction (Figure 7). Although this interplay might be decisive for holobiont stability and function, very little is known about the symbionts cell physiology, cellular interactions and metabolic currencies. The next paragraphs will introduce relevant aspects of what is known about sponge holobiont interplay.

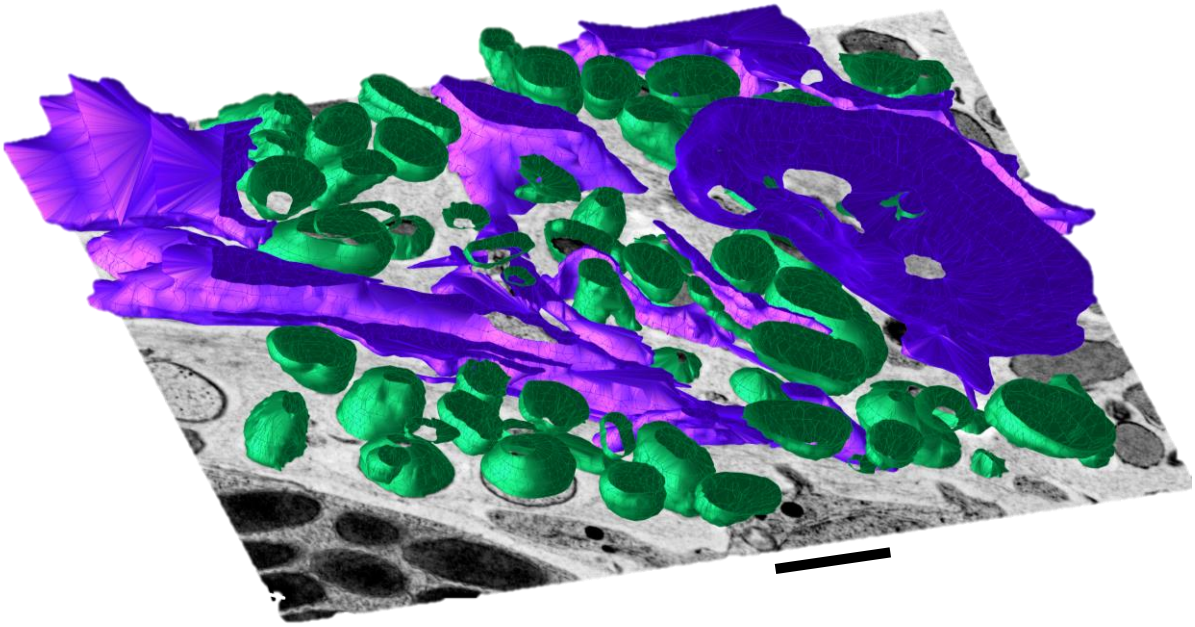

Figure 7: 3D reconstruction illustrating the intimate contact of symbionts and sponge cells in *A. aerophoba* mesohyl. Microbes, green; sponge cells, blue. Scale bar 2 µm. Jahn M.T.; unpublished

The symbiont perspective: sponges as landscapes

To a microbial symbiont, a typical sponge chimney would extend to a habitat 17 km wide and 170 km high, if scaled to human dimensions (assuming: 2 µm microbe length; a sponge vent of 2 x 20 cm; human size 1.70 m). In this context, microscopy was instrumental to study the niches of specific

symbionts in sponge tissues, and to identify morphotypes (Schmitt et al., 2011, Fieseler et al., 2004, Hardoim et al., 2014, Vacelet, 1975a). *Cyanobacteria* and other phototrophic symbionts position close to the sponge surface, close to available light, while heterotrophic microbes, such as *Poribacteria*, dominate inside of the sponge body (Achlatis et al., 2018, Bayer et al., 2014, Wilkinson, 1978). Besides, steep oxygen gradients were observed within sponge bodies decreasing towards the inside as well as with distance to the aquiferous system (Hoffmann et al., 2008, Schläppy et al., 2010). Notably, by reducing pumping rates, sponges can also expose their symbionts to anaerobic conditions located at alternating locations (Lavy et al., 2016, Hoffmann et al., 2005). These spatial-temporal oxygen gradients explain the paradox that sponges - as aerobic animals without specialized organs - can host anaerobic bacteria and metabolic processes exemplified by anaerobic ammonium oxidation (anammox) performed by members of *Planctomycetales* (Hoffmann et al., 2009, Mohamed et al., 2009). Therefore, such biochemical gradients within the sponge including pH (Webb et al., 2019), or bioactive secondary metabolites (Simmons et al., 2008, Yarnold et al., 2012), collectively assemble distinct niches in sponge tissues. In this context, dense assemblages of symbionts were repeatedly reported in the surroundings of choanocyte chambers (Webster et al., 2001, Rubin-Blum et al., 2019, Liu et al., 2012) representing the major food inlets into the mesohyl (Figure 4). However, there is limited knowledge about the fine scale distribution of symbiont accessible nutrients and how this distribution impacts spatial microbiome structure. In summary, sponges represent vast heterogeneous landscapes to their symbionts offering a variety of distinct micro-environments. While this indicates that space matters to understand symbiont physiology, interaction, and function, systematic knowledge is scarce in this regard.

The host perspective: The microbiome as bioreactor

The symbiont communities of sponges typically encode many times more unique proteins than their host and thus significantly extend the metabolic potential of the sponge holobiont (Ryu et al., 2016). Indeed, autotrophic and heterotrophic symbionts equip the sponge holobiont with key biochemical pathways to cycle carbon (C), nitrogen (N), sulphur (S) and phosphorus (P) sources prevalent in the host and its environment (Fan et al., 2012, Slaby et al., 2017, Radax et al., 2012, Karimi et al., 2018, Moitinho-Silva et al., 2014b, Lackner et al., 2017, Gauthier et al., 2016, Astudillo-Garcia et al., 2018, Fiore et al., 2015). Here, I shall focus on how sponge symbionts engage in C and N transformation and refer to extensive reviews for further factors such as vitamin cross-feeding and the production of defensive compounds (Maldonado et al., 2012, Webster and Thomas, 2016, Hentschel et al., 2012).

Sponge symbionts were reported to facilitate all major steps of nitrogen cycling. These steps include N_2 fixation, nitrification, denitrification, anammox and remineralisation (Maldonado et al., 2012). Specifically, microbial nitrification represents a direct mutualistic trophic link between sponges and their symbionts. In this scenario, excess quantities of ammonia from organic matter degradation are excreted by the sponge and are readily metabolised to nitrite and nitrate by its symbionts (Bayer et al.,

2008, Hoffmann et al., 2009). This aids the microbes to retain energy whereas the sponge benefits from being detoxified from ammonia that can accumulate to toxic levels in times of non-pumping (Boardman et al., 2004, Moeller et al., 2019). Importantly, this symbiont mediated transformation shifts the nitrogen release from ammonia to nitrate, making sponges major sources of this compound in their environment (Lopez-Acosta et al., 2019, Southwell et al., 2008, Morganti et al., 2017). This process requires syntrophic cooperation between different microbial groups within the holobiont (i.e. ammonia-oxidizing prokaryotes and nitrite oxidizing bacteria) rendering this an excellent example of metabolic interplay within the sponge holobiont.

Sponge symbionts also equip their host with broad metabolic capabilities to utilize various C substrates for growth and respiration. Specifically, a diverse genetic repertoire for heterotrophic metabolism seems to be a core feature of sponge symbionts as indicated by studies across host species and symbiont lineages (Tian et al., 2014, Siegl et al., 2011, Astudillo-Garcia et al., 2018, Slaby et al., 2017, Kamke et al., 2013). *Poribacteria* are recognised specialists for the degradation and transformation of complex carbohydrates as indicated by abundant carbohydrate active enzymes (Kamke et al., 2013, Karimi et al., 2018). Interestingly, glycoside hydrolases that enable the degradation of glycosaminoglycan (GAG) chains of proteoglycans were particularly abundant on poribacterial genomes. Notably, these GAGs are major elements of the sponge extracellular matrix (Zierer and Mourao, 2000, Vilanova et al., 2009). This was in line with further observations that *Poribacteria* encode sulfatases to cleave GAG sulphur residues along with pathways to degrade resulting sugars as uronic acid (Kamke et al., 2013). Comparative genomics revealed that the ability to feed on sponge sulfated polysaccharides is also shared by further symbiont including *Caldilineales* or *Spirochaetes* (Slaby et al., 2017). Further, a nutritional guild of symbionts was identified, comprising SAR202 and others, with the repertoire to metabolise carnitine, an abundant compound within the mesohyl (Slaby et al., 2017). Therefore, it is conceivable that the extracellular matrix has a dual function to these symbionts by representing food and scaffold at the same time. However, although the heterotrophic potential of sponge symbionts potentially involves the filtered organic matter from the sponge host, the role of the symbionts in degrading these and the underlying nutritional interdependencies remain an enigma.

Cellular dialogue within the sponge holobiont

The underlying mechanisms that allow the sponge to discriminate between food, symbiont, and pathogen are key to understand how the symbiosis is maintained stable (Pita et al., 2018b). However, while the sponge's discriminative ability was indicated in targeted feeding studies (i.e. symbiont vs. food, Wehrl et al. (2007)), the mechanisms behind remain largely unclear. In this context, it is interesting to note that sponges display a surprisingly complex innate immune system (Riesgo et al., 2014, Ryu et al., 2016, Srivastava et al., 2010). This includes an expansion of immunological and receptor domains, as well as bactericidal effectors such as antimicrobial proteins and peptides. Further, HMA and LMA sponges seem to actively respond to microbial-associated molecular patterns (MAMPs) with divergent strategies (Pita et al., 2018a, Wiens et al., 2005).

Several symbiont mechanisms to escape host digestion are conceivable which can be broadly classified into cases where microbes either avoid or antagonise host immune reaction (reviewed in Finlay and McFadden (2006)). Thick capsular sheaths and extended cell walls were described for sponge associated bacterial morphotypes and were discussed as factors to potentially prevent phagocytosis (Wilkinson et al., 1984, Wehrl et al., 2007). Other symbionts, such as *Cyanobacteria*, seem to modulate epitopes within their lipopolysaccharides and miss the widespread O-antigen as compared to non-symbiont relatives (Burgsdorf et al., 2015). Besides, with the increasing amount of (meta-) genomic sequencing data, a common theme is emerging that many sponge symbionts are enriched in so-called eukaryotic-like protein domains (ELPs, hereafter) compared to ambient seawater bacteria (Thomas et al., 2010, Fan et al., 2012, Burgsdorf et al., 2019, Burgsdorf et al., 2015, Gao et al., 2014, Rubin-Blum et al., 2019, Kamke et al., 2014, Liu et al., 2011, Alex and Antunes, 2019). These ELPs are operationally defined as classes of proteins that are found in prokaryotes, but likely originated from eukaryotes and comprise amongst others tetratricopeptide repeats and ankyrins-repeats (Reynolds and Thomas, 2016). Being abundant in symbiont genomes, ELPs were also found to be actively expressed as transcripts (Diez-Vives et al., 2017) and proteins (Liu et al., 2012, Rubin-Blum et al., 2019). Specifically, ankyrin containing proteins in sponge symbionts need to be highlighted as these widespread protein-protein interaction motives (Jernigan and Bordenstein, 2014) were reported to modulate eukaryote-microbe interplay and to mediate intracellular survival (Price et al., 2010, Pan et al., 2008). Nguyen et al. (2014) were able to show that chromosomally encoded sponge symbiont ankyrins indeed modulated eukaryote-microbe interplay in an amoebal surrogate model. This renders ankyrins as potential symbiosis factors that might antagonise sponge host immunity although the mode of action and impact on the host remain unclear.

1.5 Research gaps

To truly approach the ecology within the sponge holobiont, one must understand both the activity and interplay of its members. In addition to the open questions I touched on in the introduction, I identify the following points as key gaps in our understanding of sponge holobiont biology:

Symbiont cell biology and metabolic interplay in the host context

How do symbiont physiology, morphology and cell function assemble in the holobiont space? While there is increasing knowledge about the taxonomic and functional composition of microbial sponge symbionts there is a lack of methods to link community level signatures to the cell biology of its members. In fact, most microbial symbionts are exclusively known from nucleotide sequencing data and there is little knowledge on how this data relates to the symbiont's cell ultrastructure and physiology. However, it is the level of cells at which microbial symbionts function and interact and is therefore likely to bear valuable information on the foundations of sponge-microbe symbiosis. Commonly used methods in microbial ecology to study spatial holobiont association are light- or electron microscopy, where each method allows to retain different information from symbiont tissues. While light microscopy applications, such as fluorescence microscopy, allow to stain biomolecules to specifically identify microbes and proteins therein, the unstained ultrastructure remains elusive. Electron microscopy provides this ultrastructure but has yet limited ability to localise multiple, specific biomolecules. Therefore, there is a gap between these imaging modalities that hinders to study the link between symbiont ultrastructure, identity and function in the context of their sponge host. Consequently, the morphology of even the most prevalent sponge symbionts such as *Poribacteria* and *Chloroflexi* remains unknown which hinders inference of their function.

How are symbiont-host and symbiont-symbiont metabolisms intertwined? Although sponge symbionts are well acknowledged to form complex communities within the sponge holobiont, little is known about their interplay. Specifically, details on metabolic interactions among symbionts and with their host remain elusive (Webster and Thomas, 2016). However, syntrophic interdependencies are key to understand the joint physiology of the holobiont with potentially cascading effects on ecosystem function. In this context, a recurring observation was that feeding physiology of sponges seems to critically differ depending on the microbial load (i.e. along the HMA/LMA dichotomy). Specifically, HMA sponges generally display a more complex aquiferous system, extended mesohyl, and reduced pumping rates compared to LMA sponges (Weisz et al., 2008, Vacelet and Donadey, 1977b). While these HMA features were suggested to foster microbiome mediated DOM nutrient cycling (Reiswig, 1974, Weisz et al., 2008, Maldonado et al., 2010, Leys et al., 2018), it is, besides initial evidence from bulk stable isotope probing (de Goeij et al., 2008, Rix et al., 2016, Rix et al., 2017a, Shih et al., 2019), not yet clear how sponge symbionts engage in heterotrophic holobiont nutrition and thereby in ecosystem scaled processes.

Viral diversity and function in sponge holobionts

What role do viruses play in the sponge holobiont? While recent sequencing-driven studies throughout animal taxa highlight phages as an ubiquitous part of host-associated microbiota, surprisingly little is known about the taxonomic association and mode of interaction between phages, their bacterial hosts and the animals that harbour the microbial communities (Keen and Dantas, 2018). Importantly, few studies systematically embraced viral complexity across biological scales ranging from protein- and cellular-level interactions up to viral associations among tissues, individuals and species. Further, knowledge is limited about the tripartite interplay between phages, microbes, and their sponge host. While direct phage-eukaryote interaction would be phagocytosis or transcytosis of virions by eukaryote cells, an indirect interaction would function via manipulation of the microbiome by the phage or eukaryote. However, such evidence in host associated environments such as sponges is still scarce, and the underlying mechanisms are often unknown.

1.6 Aims & outline of the PhD thesis

This thesis aims to study the activity and interplay of sponge symbionts. The overall goal is to contribute to a better understanding of the molecular processes that determine the stability, composition and function of the sponge holobiont. To achieve this my specific aims and associated questions were as follows:

1. Investigate the cell physiology of cosmopolitan sponge symbionts & metabolic interactions within the sponge holobiont

- **CHAPTER 3** aims to follow up on genomic evidence of *Poribacteria* by asking: *Which poribacterial functions are actively transcribed in the host context?* Further, I aim to step beyond genomics by approaching structure-function relationships with the question: *Does the long-standing hypothesis of poribacterial compartmentation hold true? Can information about Poribacteria' physiology and function in the host context be derived from their morphology?*
- With Chapters 4-6 I further developed the importance of spatial-functional relationships from a microbial community perspective: **CHAPTER 4** applies a combined genomics and imaging approach in the context of functional redundancy and symbiont niche specialisation in taxonomically related symbiont clades. **CHAPTER 5** elucidates the aspect of spatial association in the context of metabolic interactions among sponge symbionts. **CHAPTER 6** then sets sponge symbiont activity into ecological context by quantifying the contribution of sponge microbial symbionts in sponge DOM cycling.

2. Explore the diversity and function of viruses in sponge microbiomes

- In **CHAPTER 7** I employ an integrative viromics approach to answer the following questions: *Are there sponge species-specific viral signatures? Are there tissue specific viral signatures in sponges?* And, *do symbiont phages encode auxiliary genes tailored to the symbiosis context?* I hypothesize that sponges have species-specific viral signatures different from surrounding seawater. Functionally, I focussed on the phage repertoire to modulate cell interaction and functioning in the sponge environment. Finally, **CHAPTER 7-APPENDIX A** aims to gain more insight into the lifestyle of the newly discovered phages in sponges. In particular, the following questions are examined: *Who are the bacterial hosts of the discovered phages*?, *What are their replication strategies?*, and *How are symbiont phages spatially distributed in sponges?*

Following a description of the newly established methods (Chapter 2) the core research of this thesis (Chapter 3-7) is presented leading to a general discussion of the key findings (Chapter 8). Each chapter is a peer-reviewed publication or a manuscript. Additional publications from this PhD research that were not included in the main text are listed above (vii) and abstracts are available at the end of the thesis.

CHAPTER 2

METHODOLOGY

2.1 A toolset for sponge microbial ecology

To advance our understanding of the mechanisms acting in host-microbe symbioses, we need to improve our technological repertoire to study the physiology of uncultivated bacteria in their host context. In order to meet this challenge, I have established new procedures in various projects of my doctoral thesis, which are outlined below (2.1.1-2.1.4).

2.1.1 Fluorescence *in situ* hybridization - correlative light and electron microscopy (FISH-CLEM)

FISH-CLEM allowed, for the first time, to characterise the morphology of the core sponge symbiont clades *Poribacteria* (CHAPTER 3) and *Chloroflexi* (CHAPTER 4). To enable the localization of proteins of interest within bacterial cells, I then complemented FISH-CLEM with immunohistochemistry (IHC) super-resolution imaging (FISH-IHC-CLEM). This extension of array tomography (Micheva and Smith, 2007, Markert et al., 2016) enables bacterial genomics to be linked with the spatial organisation of symbiont cells *in situ* and to detect proteins within at subcellular resolution. Therefore, FISH-IHC-CLEM represents a potentially widely applicable interface to follow up on yet untested hypotheses from sequencing-based microbiome studies.

2.1.2 Genome-centred metatranscriptomics

Genome-centred metatranscriptomics was instrumental to learn about what individual symbiont groups do in sponges by estimating their transcriptional activity *in situ* (CHAPTER 3, CHAPTER 5). Compared to studying metatranscriptomic reads alone this provides a more comprehensive picture on the transcriptional activity of clades while simulation-based parameter optimisation was used to increase the specificity of this estimation (CHAPTER 3).

2.1.3 Sponge-associated particle purification and virome sequencing

The virion purification and sequencing protocol, complementing an alternative version of Laffy et al. (2016), has been proven to be robust and effective in different Mediterranean HMA sponge species (CHAPTER 7). New insights into the diversity and function of sponge associated viruses we achieved by an integrative approach where I combined tissue resolved virome sequencing with novel imaging, and synthesis-based cell assays (Figure 8).

2.1.4 Enhanced PhageFISH (ePhageFISH)

ePhageFISH (Figure 8; Appendix A3) is an extension of FISH-CLEM (CHAPTER 7) in order to stain phages within host tissues at about single particle sensitivity. Therefore, I modified and extended the ViewHIV approach of Chin et al. (2015) that detects HIV in laboratory cell cultures. This allowed to confirm tissue signatures identified from virome sequencing (CHAPTER 7, Appendix A3) as well as to validate the symbiont phage lifestyle (i.e. lysogenic or lytic) *in-situ* by localising selected phages in sponge tissues. This approach potentially allows to stain the whole spectrum of viruses in host tissues including single-and double stranded DNA and RNA viruses and therefore should be widely applicable in the field of environmental virology.

Detailed methods are included in the research chapters (Chapter 3-7) as indexed in Figure 8 as a coherent toolset. Further, to make my established key methods available to a wider audience, and to foster reproducibility, I submitted detailed step-by-step protocols for FISH-CLEM hybridisation and ePhageFISH to the science repository *protocols.io* presented in section 2.2 and 2.3, respectively.

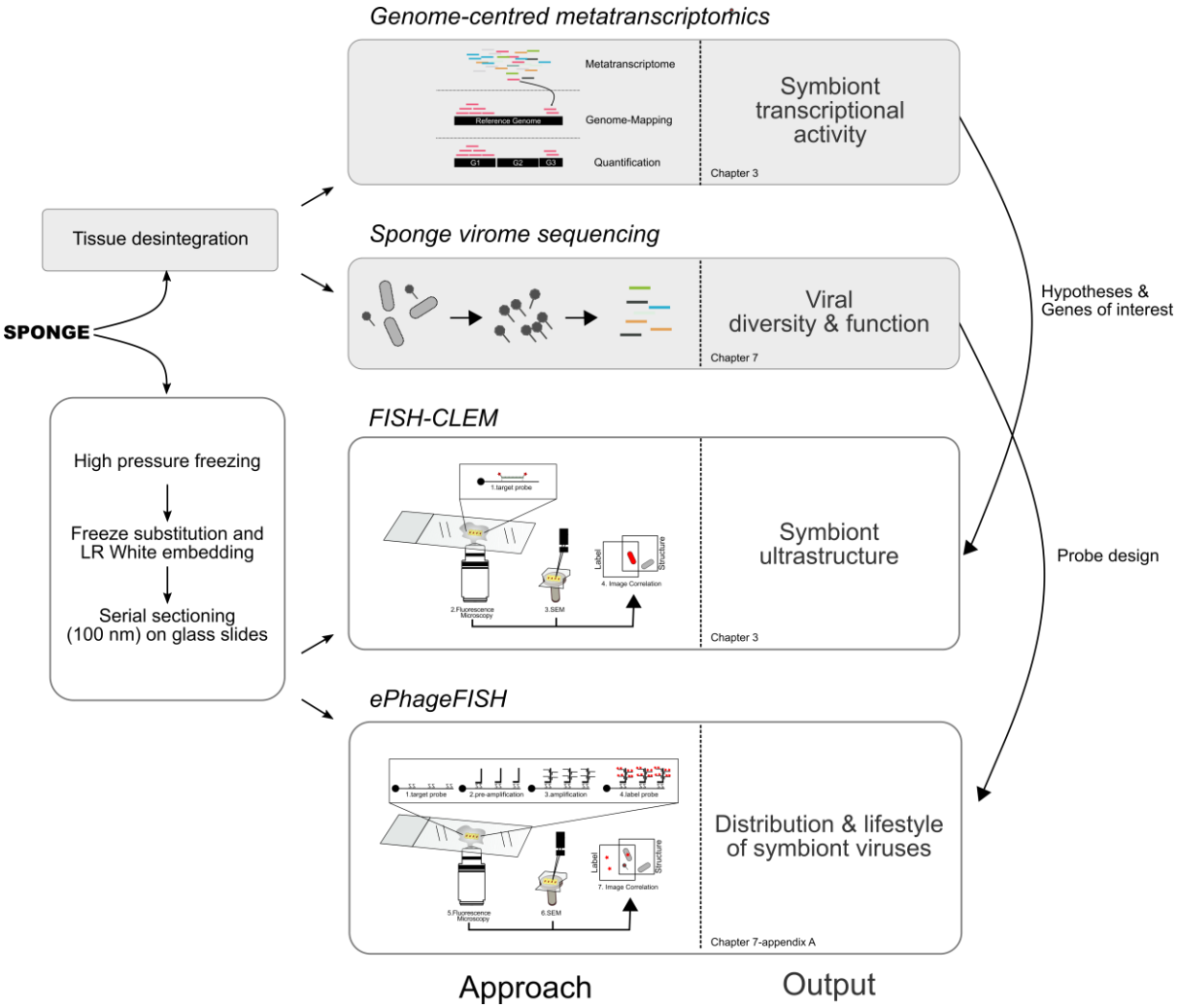

Figure 8: Established approaches to sponge microbial ecology. The scheme illustrates the basic steps (left) leading the established approaches. Note the references to detailed protocols in the respective chapters.

2.2 FISH-CLEM Protocol

Published online under DOI: *dx.doi.org/10.17504/protocols.io.hptb5nn*

OPEN ACCESS protocols.io

FISH-CLEM hybridisation

Martin Thomas Jahn[1]

[1]CRC1182 Metaorganism

Works for me dx.doi.org/10.17504/protocols.io.hptb5nn

Martin Thomas Jahn
CRC1182 Metaorganism

ABSTRACT

The majority of environmental microorganisms remains uncultivated and are commonly referred to as microbial dark matter. Here we present our protocol for fluorescence *in situ* hybridization-correlative light and electron microscopy (FISH-CLEM) that enabled the identification of poribacterial cells in sponge tissue at electron microscopy resolution.

This method allows to combine -omics approaches with spatial studies and should thus be applicable in the wider context of microbial ecology.

EXTERNAL LINK

https://www.nature.com/articles/srep35860

THIS PROTOCOL ACCOMPANIES THE FOLLOWING PUBLICATION

Jahn MT, Markert SM, Ryu T, Ravasi T, Stigloher C, Hentschel U, Moitinho-Silva L. 2016. Shedding light on cell compartmentation in the candidate phylum Poribacteria by high resolution visualisation and transcriptional profiling. Sci Rep 6:35860.

MATERIALS

NAME	CATALOG #	VENDOR
10% Sodium dodecyl sulfate (SDS)	L4509	Sigma Aldrich
PAP PEN Liquid Blocker Japan	Z377821	Sigma Aldrich
DAPI	62248	Thermo Fisher Scientific

MATERIALS TEXT

WaterWater

%Formamide	Formamide	Water	NaCL [5M]	1M Tris 7.4	10%SDS
0.00%	0	1598	360	40	2
5.00%	100	1498	360	40	2
10.00%	200	1398	360	40	2
15.00%	300	1298	360	40	2
20.00%	400	1198	360	40	2
25.00%	500	1098	360	40	2
30.00%	600	998	360	40	2
35.00%	700	898	360	40	2
40.00%	800	798	360	40	2
45.00%	900	698	360	40	2
50.00%	1000	598	360	40	2
55.00%	1100	498	360	40	2
60.00%	1200	398	360	40	2
65.00%	1300	298	360	40	2
70.00%	1400	198	360	40	2
75.00%	1500	98	360	40	2

Hybridisation Buffers (µl volume to add depending on applied Formamide concentration)

%Formamide	5M NaCL	1M Tris/HCL	0.5M EDTA	Water	10%SDS
0.00%	9000	1000	0	39,950	50
5.00%	6300	1000	0	42,650	50
10.00%	4500	1000	0	44,450	50
15.00%	3180	1000	0	45,770	50
20.00%	2150	1000	500	46,800	50
25.00%	1490	1000	500	47,460	50
30.00%	1020	1000	500	47,930	50
35.00%	700	1000	500	48,250	50
40.00%	460	1000	500	48,490	50
45.00%	300	1000	500	48,650	50
50.00%	180	1000	500	48,770	50
55.00%	100	1000	500	48,850	50
60.00%	40	1000	500	48,910	50
65.00%	0	1000	500	48,950	50
70.00%	0	1000	500	48,950	50
75.00%	0	1000	500	48,950	50

Wash Buffers (µl volume to add depending on applied Formamide concentration)

SAFETY WARNINGS

Formamide & SDS

BEFORE STARTING

obtain: double labelled probe (5' & 3') for target organism of interest.
Tested Dyes are: Cy3 and various Alexa dyes. Atto dyes are too hydrophobic on LR white and do not work for FISH-CLEM.

Preparations

1 **Prepare Hybridisation chamber (airtight box):**
1. Add 5 Kimwipes at bottom and place a slide support on top (e.g. 96 Well plate)
2. Add dd H_20 (to soak Kimwipe tissues)
3. Close chamber airtight and equilibrate at 46 °C for at least 01:00:00

It is critical that the slide support is flat. Otherwise the PAP pen will not hold the buffers in subsequent steps.

2 **Prepare buffers:**
Prepare Prehybridisation buffer:
(NN mM NaCl, 20 mM Tris/HCL pH 7.4, %FA , 0.01% sodium dodecyl sulphate)

Prepare Hybridisation buffer:
(NN mM NaCl, 20 mM Tris/HCL pH 7.4, %FA , 0.01% sodium dodecyl sulphate+ 10% dextran sulfate)

Then prewarm buffers in hybridisation-oven for at least 00:30:00 depending in volume.

%FA= Formamide % (v/v) in Buffer (depending on probe melting temperature)
NN = NaCl (depending on probe melting temperature; see materials)

can be stored at -80°C and thawed in oven prior use

volume per slide depends on PAP pen cycle but is per slide typically ~ 150 µl for pre-hybridisaiton buffer and ~300 µl for hybridisation buffer

3 **Prepare slides:**

- Prepare serial LR-white sections as described in Jahn et al (2016) here: https://media.nature.com/original/nature-assets/srep/2016/161028/srep35860/extref/srep35860-s2.pdf
- Clean slide with airbrush
- Mark position of slices on backside of slide. Mark also position of In/Outflow for pipetting
- Encircle slices with PAP-pen and let dry at least 00:15:00 (until smell is gone)

Pre-hybridisation

4 Place slides in hybridisation chamber within hybridisation oven and apply Pre-hybridisation (see Step 2) incubate at 46 °C for 01:00:00

5 30 min prior end of pre-hybridisation dilute probes
8 ng/µl in hybridisation buffer to the needed volume + 25%

Pre-warm in oven at 46 °C

Hybridisation

6 Exchange pre-hybridisation buffer with hybridisation buffer incl. probe
hybridise for 03:00:00 at 46 °C

Critical step: Apply perfusion method using twp parallel pipets. Orientate according to inflow/outflow markings (see Step 3). Any contact with the sections must be avoided.

7 45 min prior end of the hybridisation time prepare:
- 1 ng/µl solution of DAPI in pre-hybridisation buffer and put in oven
- wash buffers and place at 48 °C

DAPI staining

8 Exchange hybridisation buffer with DAPI solution using perfusion method and incubate at 46 °C for 00:20:00

Washing

9 Rinse slide with 1ml wash buffer and put in 50 ml falcon with wash buffer. Place at 48 °C for 00:25:00 slightly shaking.

Mounting

10
- Prepare coverslips with Mowiol.
- Get slide out of tube with forceps and instantly rinse with ice cold RNAse free ddH_2O.
- Leave water on slices and put on kim wipe.
- Air-brush remaining water and instantly apply coverslip

Slides should be imaged within 1-2 days.

2.3 ePhage FISH Protocol

Published online under DOI: *dx.doi.org/10.17504/protocols.io.74thqwn*

OPEN ACCESS protocols.io

ePhageFISH protocol

Martin Thomas Jahn[1]

[1]CRC1182 Metaorganism

Works for me dx.doi.org/10.17504/protocols.io.74thqwn

Martin Thomas Jahn
CRC1182 Metaorganism

ABSTRACT

This protocol walks you through the steps required to identify environmental eukaryote viruses and bacteriophages associated with host-tissues or biofilms using enhanced phage FISH (**ePhageFISH**). As an application of single molecule FISH (smFISH) it was successfuly tested to stain single virions and lysiogens. The method was a great advance for us as it combines **high specificity, sensitivity** and **lateral resolution**. To be widely reproducible the reagents are mainly based on the commercially available Affymetrix RNA-view kit. Overall, I would be glad if this approach would help the field to a better understanding of viruses in nature.

GUIDELINES

This protocol aims to localise specific viruses on LR white sections.
Total execution time is ~ 10 hours

MATERIALS

NAME	CATALOG #	VENDOR
Ethanol (100%, Molecular Biology Grade)	BP2818500	Fisher Scientific
SSC, RNase-free, 20×	AM9763	Ambion
PAP PEN Liquid Blocker Japan	Z377821	Sigma Aldrich
Phosphate Buffered Saline	P7059-1L	Sigma Aldrich
ViewRNA Cell Plus Assay	88-19000-99	Thermo Fisher Scientific

SAFETY WARNINGS

Read safety instructions of the RNAview kit before you start

BEFORE STARTING

3 weeks before experiment

- Design and order a specific probe-set against your target virus
- Order ViewRNA Cell Plus Assay kit (see materials)

1 day before experiment

- wash 4 coplin jars with 3% H_2O_2 1h to overnight
- prepare 500 ml 1x PBS
- prepare 5 ml EtOH 70%, 85%, 100% and put at -20°C
- select slides and encircle by PAP-pen and let dry overnight in fridge (~100 µl field size)
- Prepare 2x SSC 1.5 ml (to prepare denat. solution later)

Setup Chamber

1 Turn on hybridisation oven set to 40 °C (best ~3 h before experiment start)

Assemble humid chamber (airtight box) :
add ~ 5 trimmed tissues (Kim Wipes)
add 100 ml water
add base to place microscope slides on (recommended are 12/24/96Well plates that fit 4 microscope slides)

place humid chamber with flat surface (check with bubble-level, like the ones for running gels)
Equilibrate for 02:00:00

I assemble the chamber the day before and use a timer that starts the oven automatically
Accurate temperature at 40°C+-0.5°C is critical for success

Turn on denaturation oven set to 72°C

Setup hybridisation

2
- Pre-warm detergent solution QC (stored at RT)
- Pre-warm probe-set diluent (4 °C) 105 µl per sample
- Pre-warm amplifier diluent (4 °C) 210 µl per sample (if done same day, see stop point)
- Pre-warm label probe diluent (4 °C) 105 µl per sample (if done same day, see stop point)

Before taking subsets of these solutions carefully check if stock is preticipated. If this is the case put stock bottles from kit at 40°C until completely dissolved. Then take subsamples.

Setup denaturation

3 Prepare 200 µl of denaturation solution per slide pre-heat in 72 °C oven
- 70% Formamide in 2X SSC pH 7.5 (980 µl FA+ 420 SSC)

Initial washes

4 use this also to evaluate the needed amount of solution per slide

1x PBS in coplin jar	5 min
2x PBS in coplin jar	2 min

Setup hybridisation buffer

5 Mix probe set 1:100 with probe set diluent e.g. 1 µl Probeset in 99 µl probe set dilutend and bring to 40 °C

Denaturation

6 Add 100 µl of prewarmed denaturation solution per slide and place in denaturation

00:10:00 **incubaction at 72°C**

Don't do that on Parafilm that gets really sticky at this temperature

7 Immediately dehydrate with a EtOH gradient. EtOH needs to be ice cold at -20 °C .

1. 70% 00:02:00
2. 85% 00:02:00
3. 100% 00:02:00
4. 100% 00:02:00

then let air dry.

Use low amounts of ethanol here as excess ethanol destroys the PAP-pen!

Hybridisation for 3h at 40°C

8 Add solution from step 5 to sections and place within humid chamber into hybridisation oven
40 °C for 03:00:00

Setup Wash probeset

9 During hybridisation prepare:

800 ml selfmade washbuffer
- 0.1x SSC 0.1% SDS
- 4 ml 20% SDS 4 ml 20x SSC
- 792 ml autoclaved MilliQ (using scale)
- adjust PH 7

60 ml Affymetrix wash buffer
- 180 µl component 1
- 300 µl component 2
- add to 60 ml with water

Setup Amplify (~1h before hybridisation ends)

10 Thaw on ice :
- PreAmp Mix Solition (A)
- Amplifier Mix soluiton (B)
- label probe mix (prevent from light!)

then pre-warm Amplifier Diluent QF at 40°C

Wash probeset

11 wash at Room temperature

50 ml	self-made wash buffer	5 min
50 ml	self-made wash buffer	5 min
50 ml	self-made wash buffer	5 min
20 ml	Affymetrix Wash Buffer	5 min

Potential Stop point

12 Leave slide in Affymetrix Wash Buffer Overnight in Fridge.

Although this is easier as the long protocol is split into 2 days I found signals to be not as good as when the whole protocol is done in one day.

Pre-Amplify

13 Per Slide mix:

96 µl Amplifier Dilient QF (prewarmed 40 °C)

4 µl **Pre**AmpMix

vortex briefly and incubate slides for 00:30:00 at 40 °C

Wash Pre-Amplify

14 wash at RT

50 ml	self-made wash buffer	5 min
50 ml	self-made wash buffer	5 min
50 ml	self-made wash buffer	5 min
20 ml	Affymetrix Wash Buffer	5 min

Amplify

15

Per Slide mix:

96 µl Amplifier Dilient QF (prewarmed 40 °C)

4 µl **AmpMix**

vortex briefly and incubate slides for 00:30:00 at 40 °C

Wash Amplify

16 wash at RT

50 ml	self-made wash buffer	5 min
50 ml	self-made wash buffer	5 min
50 ml	self-made wash buffer	5 min
20 ml	Affymetrix Wash Buffer	5 min

Label (keep dark from now on)

17 Per Slide mix:

96 µl Amplifier Dilient QF (prewarmed **40 °C**)

4 µl Label Probe Mix

vortex briefly and incubate slides for **00:30:00** at **40 °C**

Wash Label

18 wash at RT in **dark**

50 ml	self-made wash buffer	5 min
50 ml	self-made wash buffer	5 min
50 ml	self-made wash buffer	5 min
20 ml	PBS	5 min

Stain with DAPI in PBS then wash briefly in PBS

19

00:20:00 RT in Dark

Mount

20 Mount in Mowiol.

- Spinning Mowiol before helps removing potential particles
- Bigger cover slips make imaging easier as lateral stability is improved avoiding wrinkling of sections
- Keeping slides in fridge for several hours improves stability of coverslip
- Image within two days

Image

21 Image with a fluorescence microscope within two days.

Bleaching can be avoided by searching region of interest using long excitation wavelength and at low light intensity.

CHAPTER 3

SHEDDING LIGHT ON CELL COMPARTMENTATION IN THE CANDIDATE PHYLUM PORIBACTERIA BY HIGH RESOLUTION VISUALISATION AND TRANSCRIPTIONAL PROFILING

Jahn M.T., Markert S.M., Ryu T, Ravasi T, Stigloher C, Hentschel U, Moitinho-Silva

Scientific Reports, 2016

doi: 10.1038/srep35860

www.nature.com/scientificreports

SCIENTIFIC REPORTS

OPEN

Received: 19 May 2016
Accepted: 05 October 2016
Published: 31 October 2016

Shedding light on cell compartmentation in the candidate phylum Poribacteria by high resolution visualisation and transcriptional profiling

Martin T. Jahn[1,2], Sebastian M. Markert[3], Taewoo Ryu[4], Timothy Ravasi[4], Christian Stigloher[3], Ute Hentschel[2,5] & Lucas Moitinho-Silva[6]

Assigning functions to uncultivated environmental microorganisms continues to be a challenging endeavour. Here, we present a new microscopy protocol for fluorescence *in situ* hybridisation-correlative light and electron microscopy (FISH-CLEM) that enabled, to our knowledge for the first time, the identification of single cells within their complex microenvironment at electron microscopy resolution. Members of the candidate phylum Poribacteria, common and uncultivated symbionts of marine sponges, were used towards this goal. Cellular 3D reconstructions revealed bipolar, spherical granules of low electron density, which likely represent carbon reserves. Poribacterial activity profiles were retrieved from prokaryotic enriched sponge metatranscriptomes using simulation-based optimised mapping. We observed high transcriptional activity for proteins related to bacterial microcompartments (BMC) and we resolved their subcellular localisation by combining FISH-CLEM with immunohistochemistry (IHC) on ultra-thin sponge tissue sections. In terms of functional relevance, we propose that the BMC-A region may be involved in 1,2-propanediol degradation. The FISH-IHC-CLEM approach was proven an effective toolkit to combine -omics approaches with functional studies and it should be widely applicable in environmental microbiology.

The majority of microorganisms in nature remains uncultivated and is commonly referred to as "microbial dark matter"[1]. This uncultivated microbial majority holds new insights into biology and biotechnology as well as evolution[2–4]. Cultivation-independent high throughput sequencing surveys have provided comprehensive insights towards diversity and function of the microbial dark matter. However, these insights fail to provide spatial information with respect to bacterial function in its microenvironment. While electron microscopy is an established method to study structure and ultrastructure, fluorescence microscopy allows the identification of specific molecules such as taxonomic marker genes[5] or proteins[6]. Correlative light and electron microscopy (CLEM) combines the advantages of both modalities allowing to put molecular identity into structural context[7]. CLEM is therefore predestined to shed light on uncultivated prokaryotes thriving in complex microbiomes. Marine sponges for example contain massive amounts of microorganisms within their mesohyl matrix, which may contribute up to 35% of the animal's biomass[8–10]. Members of at least 47 bacterial phyla and archaeal lineages were so far identified by high-throughput sequencing technologies within sponge hosts[11–13]. The candidate phylum Poribacteria is among the predominant microorganisms in these microbial consortia[14,15]. Much of our knowledge about their genomic potential was obtained by single-cell genome analyses[16–18]. This approach revealed details

[1]Julius-von-Sachs Institute for Biological Sciences, University of Würzburg, Würzburg, 97082, Germany. [2]Marine Microbiology, GEOMAR Helmholtz Centre for Ocean Research, Kiel, 24105, Germany. [3]Division of Electron Microscopy, Biocenter, University of Würzburg, 97074, Würzburg, Germany. [4]Division of Biological and Environmental Sciences & Engineering, King Abdullah University of Science and Technology, Thuwal, 23955-6900, Kingdom of Saudi Arabia. [5]Christian-Albrechts-University of Kiel, Germany. [6]School of Biotechnology and Biomolecular Sciences & Centre for Marine Bio-Innovation, University of New South Wales, Sydney, 2052, Australia. Correspondence and requests for materials should be addressed to U.H. (email: uhentschel@geomar.de)

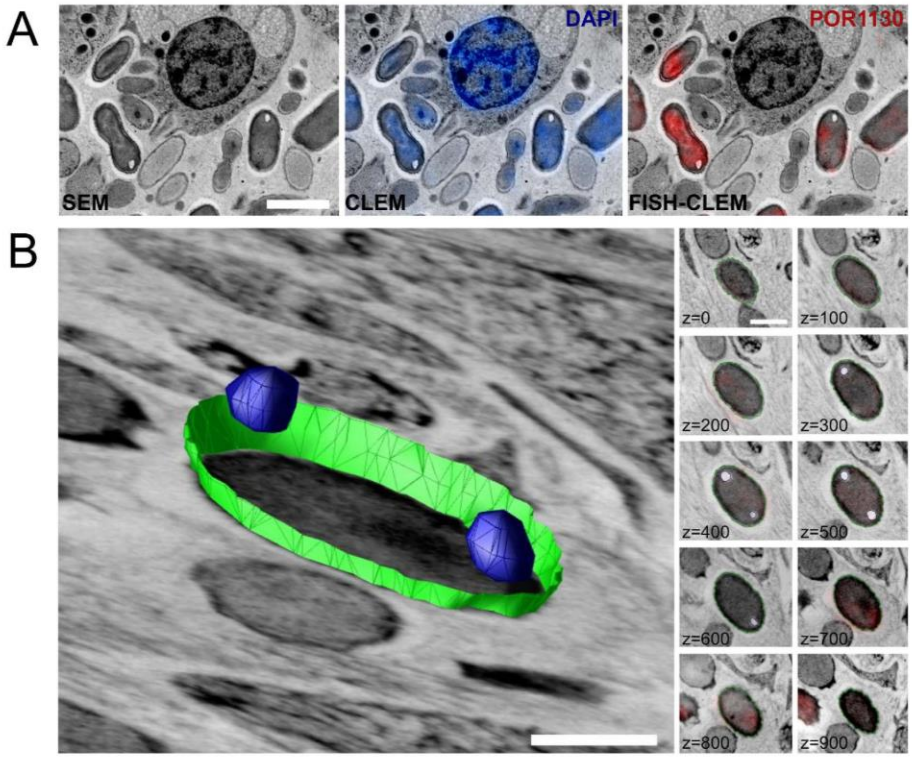

Figure 1. Identification of Poribacteria cells in the sponge microbiome using FISH-CLEM. (**A**) Scanning electron microscopy images (SEM) were correlated with fluorescence signal of the nucleotide stain DAPI (blue; CLEM) and the Poribacteria specific 16S rRNA probe POR1130 (red; Alexa546; FISH-CLEM) allowing the identification of microbes within the host in close proximity to a sponge cell at ultrastructure resolution. Separate channels are shown in Figure S1. (**B**) Three-dimensional reconstruction of a representative Poribacteria cell. Polar spherical structures (blue), which represent about 2% of cell volume, are typically observed at different z-intervals. Cell envelope is shown in green. Right panel displays FISH-CLEM micrographs used as basis for the reconstruction, where consistent POR1130 signals were observed across 10 consecutive slices totaling 1 μm of depth in z-dimension (z-values in nm). Scale bars, 2 μm (**A**) and 500 nm (**B**).

of their potential primary and secondary metabolism, including the description of a complex carbon degradation enzymatic repertoire[17], as well as putative symbioses factors[16,18]. Since their first description, Poribacteria were suggested to display cellular compartmentalisation. Few experimental findings support this idea, including the observation of ring-shaped Poribacteria-specific FISH (fluorescence *in situ* hybridisation) signals[19] and the presence of protein shell genes[16]. Structurally, protein shells can form bacterial compartments (BMC) and gas vesicles[20–22]. The ability for compartmentation is widespread in bacteria (reviewed in Kerfeld and Erbilgin[23]). Bacterial compartments provide confined biochemical environments within the cell where enzymatic reaction conditions are optimised, nutrients and volatiles are stored, and toxic compounds are isolated[24–27].

In the present study, we aimed to resolve the ultrastructure as well as the transcriptional activity profile of poribacterial symbionts of marine sponges. To achieve this we standardised transcriptome retrieval from metatranscriptomes and present a novel protocol that extends the principles of array tomography[28] by combining fluorescence *in situ* hybridisation (FISH) and immunohistochemistry (IHC) with scanning electron microscopy (SEM).

Results

High resolution visualisation and 3D reconstruction of Poribacteria. The FISH-CLEM method enabled the taxon-specific identification of bacterial cells at ultrastructural resolution. Poribacteria probe (POR1130, Alexa546) signals co-localised with DAPI signals and microbial cells from electron micrographs of *Aplysina aerophoba* mesohyl (Fig. 1A; Supplementary Figure S1). On the average of four areas, 21.8% (±2.9 s.d.; 792 of 2,697) of the prokaryotic cells, detected by DAPI, emitted also poribacterial probe signal. Besides, 5.4 (±1.8) poribacterial cells per sponge cell (792/154) were observed at a density of $32.8*10^3$ ($\pm 5.0 \times 10^3$) cells/mm^2. Poribacterial cells showed a consistent morphotype that appeared ovoid-shaped, with 1.5–2.2 μm in length and 0.9–1.2 μm in width. At the poles of poribacterial cells, intracellular structures of low electron density were consistently observed. Multiple structures per cell pole were observed only rarely (<1% of cells). The cellular

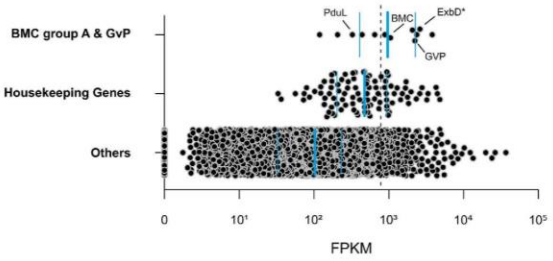

Figure 2. Active functions of poribacterial SAG 3G related to compartmentation in the sponge *X. testudinaria*. Expression estimations (FPKM) are shown for genes of selected functional categories. Blue horizontal lines indicate the first and third quartiles and the median (thick line) of each category. Dashed line indicates average expression level of housekeeping genes. Genes highlighted ExbD*, gas vesicle protein (GvP), BMC-shell marker, and propanediol utilization protein (PduL). The FPKM values represent the average of three biological replicates.

morphology of Poribacteria was further investigated by array tomography of FISH-CLEM micrographs. The three dimensional reconstruction of seven representative poribacterial cells confirmed the presence of two bipolar intracellular structures per each cell (Fig. 1B). DAPI signals were evenly distributed within poribacterial cells without local maxima. Generally, the bipolar structures were spherical, with an average volume of $5.28*10^{-3}\,\mu m^3$ each and 168.0 nm (±25.6 nm) in diameter. Together, they made up about 1.1% (±0.7%; n = 4) of the poribacterial cell volume and did not appear to be membrane bound.

Cell compartmentation-related genes are highly expressed. Metatranscriptomic datasets from 3 biological replicates of *Xestospongia testudinaria* were obtained and processed resulting, on average, in 43,076,693 (±7,840,577) quality filtered paired-end reads (Supplementary Table 1). These datasets were each mapped against the poribacterial single amplified genome (SAG) 3G, which was isolated from *A. aerophoba*. The retrieved Poribacteria 3G transcriptomes represented between 3.12% (1,582,793 reads; *XT2*) and 4.05% (1,417,774 reads; *XT3*) of the sequenced *X. testudinaria* metatranscriptomes. Gene expression, as estimated by FPKM values, was significantly positively correlated among biological replicates (average Pearson's correlation coefficient $P = 0.82 \pm 0.11$; p value < 0.001). The most abundant genes in poribacterial SAG 3G transcriptomes in *X. testudinaria* were analysed in relation to their functional classification and a set of housekeeping genes (Supplementary Data S1). We defined genes as highly expressed when expression levels were above those of housekeeping genes (average 780.1FPKM, the fold difference to this level is referred to as times $FPKM_{HK,}$ hereafter). This included a set of 258 coding sequences (CDS) being slightly overrepresented by functionally annotated genes compared to the rest of the SAG 3G genome (76.7% vs. 68.8%).

Specifically, genes related to cell compartmentation involving the BMC-shell marker protein (1.3 $FPKM_{HK}$) and gas vesicle protein (GvP) (2.9 $FPKM_{HK}$) were found to be highly transcribed (Fig. 2). The first gene is localised in the conserved BMC-A genomic region of poribacterial SAGs[16]. Three genes coding for membrane components of biopolymer transporters found on this region were highly transcribed (Fig. 3A; Supplementary Figure S1): the ExbD* (3.3 $FPKM_{HK}$), the ExbD (2.6 $FPKM_{HK}$), and a protein with MotA/TolQ/ExbB proton channel family and carboxypeptidase regulatory-like domain (BTP, 4.9 $FPKM_{HK}$). Notably, in all three sponge individuals, zero coverage was observed flanking these genes, thus indicating polycistrons, i.e. genes that are expressed in a single transcript (Fig. 3A, red bars). Additionally, the genes encoding the BMC-shell marker and the propanediol utilization protein, PduL, also appeared to be part of one polycistron.

Subcellular localisation of cell compartmentation-related proteins. The BMC-A genomic region was further investigated by localising the proteins BMC-shell marker and ExbD* using the newly developed FISH-IHC-CLEM method. Additionally, FISH-IHC-CLEM was applied to localise the gas vesicle protein (GvP)[29], which showed high transcription levels. Protein-specific signals were observed in the majority of the cells labelled with Poribacteria FISH probes. Specifically, BMC-specific signals were detected in 92.5% (37/40), ExbD* in 91.4% (32/35), and GvP in 100% (10/10) of Poribacteria-positive cells. The GvP protein signals were observed throughout the cytosol (Supplementary Figure S2), while the ring-shaped BMC-shell marker protein and the ExbD* protein signals were associated with cell membranes (Fig. 3B).

Additional highly expressed functional genes in Poribacteria. Only three studies have so far reported metatranscriptome data from sponges[30–32]. We thus expand our analysis to provide a compilation of additional highly expressed functional genes detected here in the Poribacteria 3G transcriptomes (Supplementary Figure S3). A strong transcriptional activity was observed for genes related to: (a) central metabolism, mainly tricarboxylic acid (TCA) cycle [PATH:ko00020] (n = 2); (b) energy metabolism, including several NADH-quinone oxidoreductase subunits involved in oxidative phosphorylation [PATH:ko00190], and (c) genetic information processing, specifically genes of transcription and translation machinery (n = 43). In particular, nucleotide binding proteins such as the RNA binding domain with a RNA recognition motif (RRM; PF00076; 47.1 $FPKM_{HK}$) and the DNA-binding protein HU (heat unstable)-beta (K03530; 25.3 $FPKM_{HK}$) were remarkably highly transcribed.

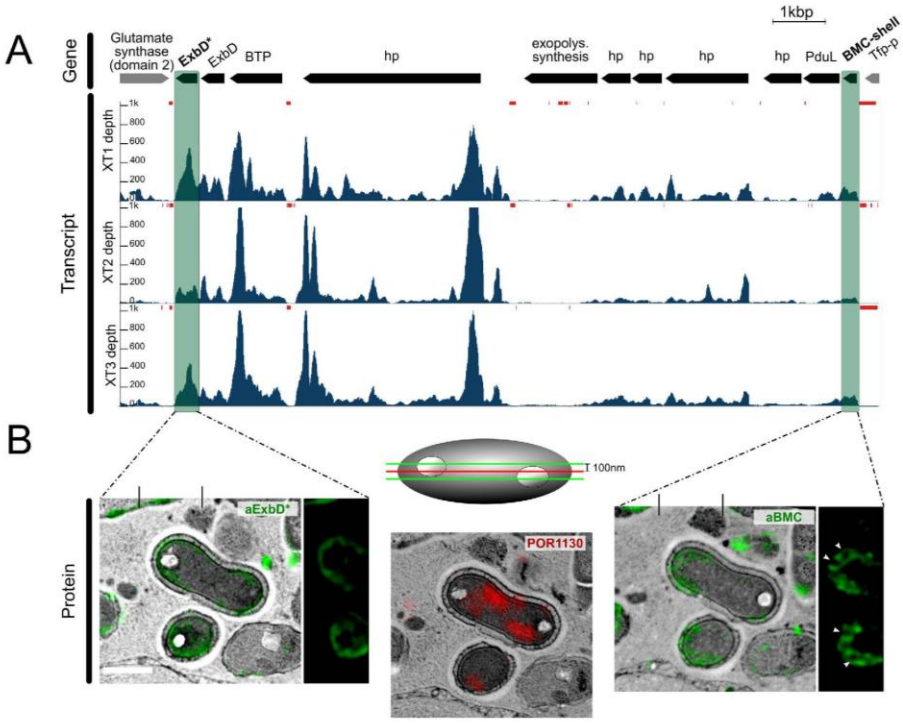

Figure 3. Integrative omics and microscopy study of the BMC-A genomic region. (**A**) The genomic region and transcriptional profile of poribacterial SAG 3G. Gene abbreviations are: BTP = biopolymer transport protein, hp = hypothetical protein, Tfp-p = Tfp-pilus protein. Arrows indicate gene intervals and orientation. BMC group A genes are shown in black, others in grey. The transcript coverage (reads per genomic base) for three *X. testudinaria* metatranscriptiomes (*XT*1, *XT*2, and *XT*3) was illustrated using the Integrated Genome Viewer (IGB) tool. Loci with no read coverage are highlighted by red bars. (**B**) Proteins encoded in the BMC-A, BMC-shell marker (right; green; FITC) and ExbD proteins (left; green; FITC), were localised within poribacterial cells by FISH-IHC-CLEM. Ring shaped BMC-shell signals are indicated by arrowheads. Poribacteria cells were identified at ultrastructural resolution in *Aplysina aerophoba* tissue by FISH-CLEM using the Poribacteria-specific 16S rRNA probe POR1130 (middle image, red; Alexa546 double 5′3′ labelled). Micrographs represent the same cells on 3 consecutive sections of 100 nm distance as illustrated in the scheme. Separate channels are shown in Figure S1. Scale bars, 500 nm.

Besides, metabolism of co-factors and vitamins was abundantly represented in SAG 3G transcriptomes, in particular genes coding for pathways of folate biosynthesis ([PATH:ko00790]; folE, 1.3 $FPKM_{HK}$, queE, 1.1 $FPKM_{HK}$), biotin metabolism (fabF, 2.1 $FPKM_{HK}$) and nicotinate/nicotinamide metabolism ([PATH:ko00760]; nadA, 1.4 $FPKM_{HK}$).

Further, specific sets of genes associated with nutrient acquisition were highly transcribed, such as genes encoding enzymes that control cellular nitrogen levels, i.e., the nitrogen regulatory protein PII (17.1 $FPKM_{HK}$) and two glutamine synthases (4.6 $FPKM_{HK}$, 2.0 $FPKM_{HK}$). Besides, two ammonium permeases were expressed, although at a lower level (>75^{th} FPKM percentile, 0.5 $FPKM_{HK}$, 0.5 $FPKM_{HK}$). With respect to sulfur metabolism, genes of the enzymatic pathway transforming thiosulfate to acetate and L-cysteine were abundant in the transcriptome, i.e. thiosulfate sulfurtransferase (TST, 1.5 $FPKM_{HK}$), NADPH-dependent sulfite reductase (cysI, 2.0 $FPKM_{HK}$), and cysteine synthase A (cysK, 1.2 $FPKM_{HK}$). On the other hand, carbohydrate degradation genes, such as glycoside hydrolases[17], were not particularly highly expressed (≤0.6 $FPKM_{HK}$; Supplementary Data S1).

Thirdly, genes of several other functional categories were also abundant in the Poribacteria SAG 3G transcriptome, including cell redox homeostasis related genes: superoxide dismutase (SOD2; 7.0 $FPKM_{HK}$), thioredoxin (4.9 $FPKM_{HK}$), and rubrerythrin (2.6 $FPKM_{HK}$). Further, genes coding for membrane transport-associated proteins were highly expressed, particularly components of several ABC-transporters, biopolymer transporters, and the Sec dependent pathway translocation system. Notably, 11 transposase genes were present among the most expressed and 3 among the top 100. Few genes encoding Eukaryote-like repeat proteins (ELP), Bacterial Ig-like domains (n = 3) and Tetratricopeptide repeats (n = 2) were also highly transcribed, including TonB (1.7 $FPKM_{HK}$) and the hypothetical protein CDS #2265144549 (1.4 $FPKM_{HK}$). Additionally, the secondary metabolism related gene phosphotransferase ispE (2.6 $FPKM_{HK}$), which encodes a protein that is part of the almost

complete alternative nonmevalonate pathway for terpenoid biosynthesis, was highly transcribed. Finally, genes encoding phyH—domain containing proteins were abundant in the transcriptome, in particular with putative involvement in the biosynthesis of mitomycin antibiotics/polyketide fumonisin (1.3 $FPKM_{HK}$; 1.1 $FPKM_{HK}$). The functional elucidation of highly transcribed but poorly understood genes is an important undertaking to increase our understanding of Poribacteria physiology.

Discussion

The present study provided novel, transcriptome-derived insights into poribacterial cell compartmentation as well as other highly expressed functions related to core metabolism and nutrient utilisation. A newly established microscopy protocol allowed the taxon-specific identification and 3D visualisation of Poribacteria within the extracellular sponge matrix as well as the subcellular localisation of highly transcribed poribacterial proteins involved in cell compartmentation. We combined here, to our knowledge for the first time, FISH and IHC with SEM on ultrathin sections of sponge tissue. The preparation of the samples with HPF allowed us to achieve superior cellular structure preservation over chemical fixation[33,34] (Supplementary Figure S4). To date, there are only two FISH-CLEM protocols published both employing chemical sample fixation[35,36]. The presented FISH-IHC-CLEM toolset presents a significant step forward as it integrates taxonomic, functional, and structural information.

We consistently observed the ovoid-shaped morphotype with two granules in correlation with poribacterial-specific FISH signals, which may represent carbon-rich polymers such as poly-β-hydroxybutyrate (PHB)[37] or glycogen[38]. This hypothesis is supported by the observed electron permeability of the structures since neither uranyl acetate nor lead citrate stain polysaccharides or polyesters. Moreover, their bipolar localisation is in agreement with descriptions for PHB-granules in other bacteria[39]. The ring-shaped fluorescent signals for Poribacteria specific FISH-probes that were originally observed by Fieseler, *et al.*[40] using conventional microscopy might be attributed to the granules described here that might have caused probe exclusion.

Bacterial microcompartments (BMCs) and their structural and functional diversity have received much recent attention[23,41]. Unlike the granules described above, they are protein-based and they contain enzymes and metabolic pathways. Here, we focused on the BMC-A genomic region that is structurally conserved among three poribacterial genomes (3G, 4CII and 4E) representing two distant clades[16]. These genomic regions are composed of CDSs encoding components of TonB-dependent periplasmatic energy transduction (ExbD, BPT), which are involved in biopolymer transport[42], the outer membrane-predicted RhoGEF (COG5422), which is involved in the regulation of signal transduction pathways[43], the propanediol utilisation protein PduL[44], the BMC-shell marker protein (PF00936; 70% identity to PduA; SMTL id 4p2s.1), and several hypothetical proteins (Fig. 3). We showed that genes of the BMC-A region were highly transcribed with evidence of at least two polycistrons: one composed by BMC-shell marker and propanediol utilisation genes and the other composed by genes of the TonB-dependent energy transduction system. The functional relations within the BMC-A cluster genes were further supported by FISH-IHC-CLEM, where both the BMC-shell marker protein and ExbD* were co-localised at the cellular membrane (Fig. 3). In terms of functional relevance, we propose that the BMC-A region may be involved in 1,2-propanediol (1,2-PD) degradation (Fig. 4). The import of the cofactor vitamin B_{12}[45], may be driven by components of the TonB-system[42], which are also encoded in the BMC-A gene region. Besides PduL, poribacterial SAGs encode further homologues of propanediol utilisation enzymes, which may convert propionaldehyde to propionate (exergonic reaction; PduP, PduW) or propanol (endergonic reaction, PduQ)[17,46].

In conclusion, we obtained a better understanding of the candidate phylum Poribacteria biology by integrating information from different biological levels, i.e. DNA, RNA, protein, and cellular ultrastructure. Specifically, we identified poribacterial cells in the sponge tissue and studied their morphology, revealing the presence of characteristic bipolar granules possibly representing polymer depots. With respect to the function of the BMC-A region, the most conceivable hypothesis is that Poribacteria may perform propanediol utilisation reactions at the cytoplasmic membrane in areas confined by BMC-like proteins, including transformations of the toxic and volatile intermediate propionaldehyde. With regard to the methodological advances, the assembled microscopical FISH-IHC-CLEM toolset enables the simultaneous identification of specific microbes at high resolution in their environmental context, the study of their cellular structures, and the localisation of target proteins. Altogether, these methods contribute to and will facilitate an improved understanding of the uncultured environmental microorganisms.

Methods

Sample collection. *Aplysina aerophoba* individuals were collected by SCUBA diving in the Gulf of Piran (GPS: 45°31′N, 13°34′E), Piran, southwestern Slovenia, on May 15th, 2014 at 2 to 5 meters depth. Existing metatranscriptomes of the sponge *Xestospongia testudinaria* (Moitinho-Silva PhD thesis) were used for poribacterial transcriptome retrieval because all major poribacterial lineages were present in this dataset.

Prokaryotic mRNA enrichment, sequencing and read processing. Prokaryotic mRNA was enriched from sponge total RNA and linearly amplified as previously described[32]. Sequencing was performed with Illumina HiSeq 2000 standard protocols, resulting in paired-end reads (101 bp) with an estimated mean insert size of 149 bp. The raw Illumina reads were processed according to Moitinho-Silva, *et al.*[32]. Briefly, (a) reads containing low quality bases were truncated to the first base below Phred score < 20; (b) sequencing adapters, including partial adapters, were trimmed; (c) remaining read pairs containing reads shorter than 16 bps were removed. Raw Illumina reads have been submitted to the National Center for Biotechnology Information under Biosample IDs SAMN02903553 (*XT*1), SAMN02903554 (*XT*2), and SAMN02903555 (*XT*3).

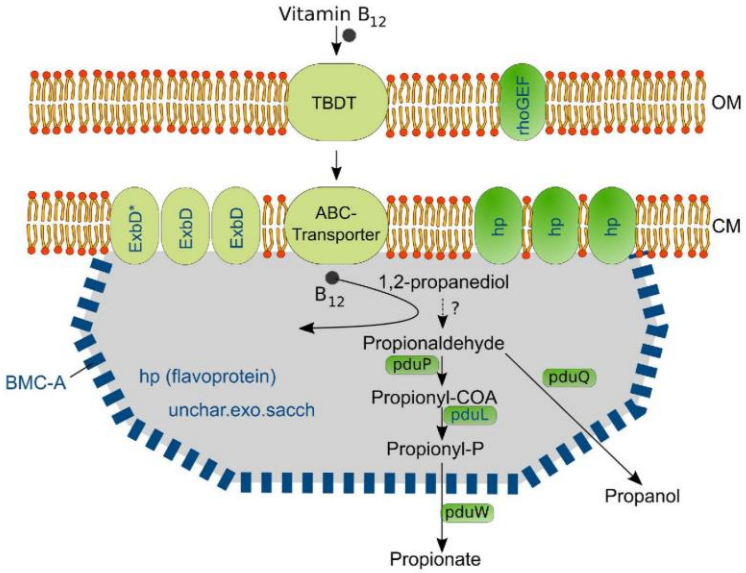

Figure 4. Hypothetic model for the BMC-A gene region function. Vitamin B-12 transport by Ton-B dependent systems occurs closely to reactions of the 1,2-propanediol degradation pathway, which is confined by BMC-shell like proteins. BMC-A encoded proteins are shown in blue color. Proteins are localised based on prediction (all but the BMC-shell marker), microscopic evidence (of BMC, and ExbD*) and literature (TonB-dependent transport system, Pdu proteins). OM, outer membrane; CM, cytoplasmic membrane; TBDT, TonB-dependent transporter; hp, hypothetical protein; unchar.exo.sacch, uncharacterized protein exopolysaccharide synthesis. Propenediol degradation pathway and localization of Pdu proteins relative to BMC-shell is assumed based on characterized BMCs[41].

Poribacteria transcriptome retrieval and gene expression estimation from metatranscriptomes. All six available single amplified genomes (SAGs) of Poribacteria (3G, 4C, 4CII, 4G, 4E and A3)[17,18] were included in this study as reference for initial transcriptome abundance estimation. Genome-related files containing annotated sequence information were obtained from the Department of Energy (DOE) Joint Genome Institute (http://genome.jgi-psf.org). The success of the transcriptome retrieval procedure, i.e. mapping of metatranscriptomic reads to single-cell genomes, was optimised and validated based on a simulation experiment (see Suplementary Information, Section 1). Read mapping was performed with Bowtie2 v2.1.0 (Langmead & Salzberg, 2012), with the parameters: "--very-sensitive -I 20 -X 450". In this step, unassembled, quality-processed, metatranscriptomic reads from 3 biological replicates were mapped to each poribacterial SAG. Read-mapping results in SAM format (Sequence Alignment/Map) were manipulated using SAMtools v0.1.18[47].

To estimate transcript abundance, the reads aligned to coding sequences (CDS) were quantified using the htseq-count function of the HTSeq package[48] in "no strand-specific" (-s no) and "union mode" (-m union). Non-uniquely mapped reads were discarded. The HTSeq "-samout" option was used to create SAM files, in which read pairs were uniquely assigned to a given CDS. Gene expression was estimated by normalising read counts to FPKM (Fragments Per Kilobase of exon, per Million fragments mapped), the paired-end equivalent of RPKM (Reads Per Kilobase of exon, per Million reads mapped), a measure used earlier[49]. In order to compare gene expression derived from the mapping of the three metatranscriptomic datasets, i.e. biological replicates, Pearson's product-moment correlation, and standard deviation were calculated based on FPKM values in R v3.1.1[50].

Among the poribacterial genotypes, 3G represented by far the most comprehensive transcriptomes retrieving 78.3% (2,345,508 of 2,995,024) of all sequences that were assigned to Poribacteria genomes (Supplementary Table S2). Besides, a proportion of 98.8% of SAG 3G genes was represented by the metatranscriptomic data set by at least one read-pair. Altogether, these results indicate a sufficient dynamic range for Poribacteria 3G transcriptional expression estimations[51]. Therefore, functional analyses of this study were based on Poribacteria SAG 3G. The gene functional annotations were based on the KEGG Ontology (KO)[52], COG (clusters of orthologous groups, http://www.ncbi.nlm.nih.gov/COG/), and Pfam[53] databases integrated with annotations deposited by Kamke, *et al.*[17] at the Joint Genome Institute. Genomic regions were visualised using the Integrative Genomics Viewer[54] and edited using Inkscape (https://www.inkscape.org).

Microscopy

HPF and freeze substitution. For high pressure freezing (HPF), *A. aerophoba* chimneys were dissected within 1 minute and placed into the 200 μm deep well of the freezing chamber (Specimen Carriers Type A (200 μm)

and B (0 μm), Bal-Tec AG, Liechtenstein) filled with 1-hexadecene. Mesohyl samples were loaded into the HPF machine (EM HPM100, Leica Microsystems GmbH, Wetzlar, Germany) and cryo-immobilised at >20,000 K/s freezing speed and >2,100 bar pressure. Three specimens were processed for two sponge individuals. The freeze substitution protocol, as adapted from Weimer[55], the embedding procedure, and the sectioning protocol are provided in the Supplementary Information, Sections 2 and 3.

Fluorescence *in situ* hybridisation (FISH) for FISH-CLEM. Poribacterial cells were identified within the *A. aerophoba* tissue by *in situ* hybridisation on ultrathin LR-white embedded-array-sections. Poribacteria 16S rRNA was hybridized using the double labelled probe POR1130 (5′-[Alexa546]GGC TCG TCA CCA GCG GTC[Alexa546]-3′; Fieseler, *et al.*[40]) at a concentration of 7 ng/μl. Hybridisation took place within Sylgard chambers (in-house production) inside an equilibrated humid chamber at 46 °C for 3 h in hybridisation buffer (900 mM NaCl, 20 mM Tris/HCL pH 7.4, 30% formamide, 0.01% sodium dodecyl sulphate). For counter-staining of bacterial nucleic acids and sponge cell nuclei, the hybridisation solution was exchanged with pre-warmed DAPI in hybridisation buffer (1 ng/μl), followed by 20 min incubation at 46 °C. After this, the arrays were incubated in pre-warmed wash buffer (20 mM Tris/HCL; 112 mM NaCl, 5 mM EDTA; 0.005% sodium dodecyl sulphate) at 48 °C for 25 min. Finally, the slides were carefully rinsed with a laminar flow of ice cold ddH_2O and were directly mounted in Mowiol medium (Mowiol® 40–88, Kuraray Europe GmbH, Tokyo, Japan). In addition to Poribacteria-specific probes, FISH was performed with a Chloroflexi probe (sponge cluster I, GNS934, Alexa488, 10 ng/μl). No co-localisation was observed indicating specificity of the Poribacteria probe. The POR1130 sense probe (5′-[Alexa546]GAC CGC TGG TGA CGA GCC[Alexa546]-3′) was used as a control for false positive staining and did not show detectable signals.

Antibody design and immunohistochemistry (IHC). Affinity purified polyclonal antibodies (Genscript, NJ, USA) were raised in rabbit based on peptides of highly transcribed poribacterial SAG 3G genes. Peptides were selected aiming for maximum antigenicity (OptimumAntigen™ Design Tool; Genscript) and minimum host similarity. Additionally, peptides with less than 60% identity to other poribacterial proteins were chosen. For each target protein, two (BMC-shell marker protein, ID 2265142951) or three (ExbD protein, ID 2265142941; gas vesicle protein, ID 2265144305) peptides were picked for antibody production. The immunological staining procedure was adapted from Micheva and Smith[28] with modifications (Suplementary Information, Section 4). Arrays only incubated with secondary antibody were used as a negative control, showing few background fluorescence signals. The sensitivity of the primary antibodies was confirmed by immuno-dot-blotting. Monoclonal b-tubulin (mouse) antibody was used as positive control during protocol standardisation.

Scanning electron microscopy preparations. After the light microscopic images were taken, the cover slip was carefully removed with a razor blade and the whole slide was washed in ddH_2O to remove the mounting medium. After drying, the sections were contrasted in 2.5% uranyl acetate in ethanol for 15 min and in 50% Reynolds' lead citrate[56] in boiled ddH_2O for 10 min. The slides were size-reduced with a diamond pen and attached to a scanning electron microscopy (SEM) pin stub specimen mount. Electrically conductive adhesive was added to one side of the glass piece to allow electron flow from the surface to the specimen mount. Finally, the sample was coated with a carbon layer to prevent charging of the sample.

Image acquisition. The fluorescence signals of IHC and FISH were captured using the ELYRA S.1 super-resolution structured illumination microscope (Zeiss, Göttingen, Germany) and the Axio Observer.Z1 microscope (Zeiss, Göttingen, Germany), respectively. In order to follow regions of interest on consecutive sections by fluorescence- and electron microscopy, reference maps were established based on relative positions to section edges and structures with large and consistent z dimension. Initial processing of the obtained fluorescence images was carried out with the ImageJ distribution Fiji[57,58]. Briefly, background signal levels were determined as average maximum intensities of three cell-free mesohyl regions, the brightness and contrast were adjusted accordingly and custom lookup tables were applied. On the same sections, that were used for fluorescence microscopy, SEM was carried out using a field emission scanning electron microscope JSM-7500F (JEOL, Japan) with LABE detector (for back scattered electron imaging at extremely low acceleration voltages) directly on the microscope slides.

Correlation and set alignment. Using the rough reference map described above, regions of fluorescence microscopy were identified at SEM resolution based on sponge heterochromatin patterns. The obtained z-stacks of fluorescence microscopy and SEM images were automatically aligned in TrackEM2[59] using the align layers function in least square mode with 8 steps per octave, a maximum image size of 3,000 pixels and rigid mode for feature extraction whilst allowing a maximum alignment error of 100 pixels. The applied desired transformation was rigid and affine for light and electron micrographs, respectively. For FISH-CLEM, the aligned stacks were collectively correlated based on the middle serial section of an array. In order to enable the correlation precision required for high resolution IHC fluorescence images, IHC-CLEM correlation was established using the Fiji implemented Landmark Correspondences plugin (moving least squares; mesh resolution 200; affine), referencing characteristic features of both fluorescence and electron microscopy, such as sponge nuclei heterochromatin. The correlation of FISH and IHC with electron microscopy is termed "FISH-IHC-correlative light and electron microscopy" (FISH-IHC-CLEM). For the combination of IHC and FISH, in the current setup, images were taken on consecutive sections of 100 nm distance with alternating protocols (3 slices IHC; 1 slice FISH; 3 slices IHC pattern). The segmentation, 3D tomographic reconstruction and subsequent analysis of consecutive FISH-CLEM sections was carried out using the IMOD software package v.4.7[60].

References

1. Rinke, C. *et al.* Insights into the phylogeny and coding potential of microbial dark matter. *Nature* **499,** 431–437 (2013).
2. Wilson, Micheal C. & Piel, J. Metagenomic Approaches for Exploiting Uncultivated Bacteria as a Resource for Novel Biosynthetic Enzymology. *Chem Biol* **20,** 636–647 (2013).
3. Spang, A. *et al.* Complex archaea that bridge the gap between prokaryotes and eukaryotes. *Nature* **521,** 173–179 (2015).
4. Brown, C. T. *et al.* Unusual biology across a group comprising more than 15% of domain Bacteria. *Nature* **523,** 208–211 (2015).
5. Amann, R. I., Ludwig, W. & Schleifer, K. H. Phylogenetic identification and *in situ* detection of individual microbial cells without cultivation. *Microbiological reviews* **59,** 143–169 (1995).
6. Newton, I. L., Savytskyy, O. & Sheehan, K. B. Wolbachia utilize host actin for efficient maternal transmission in Drosophila melanogaster. *PLoS Pathog* **11,** e1004798 (2015).
7. de Boer, P., Hoogenboom, J. P. & Giepmans, B. N. G. Correlated light and electron microscopy: ultrastructure lights up! *Nat Meth* **12,** 503–513 (2015).
8. Hentschel, U., Piel, J., Degnan, S. M. & Taylor, M. W. Genomic insights into the marine sponge microbiome. *Nat Rev Microbiol* **10,** 641–654 (2012).
9. Taylor, M. W., Radax, R., Steger, D. & Wagner, M. Sponge-associated microorganisms: evolution, ecology, and biotechnological potential. *Microbiology and molecular biology reviews: MMBR* **71,** 295–347 (2007).
10. Webster, N. S. & Taylor, M. W. Marine sponges and their microbial symbionts: love and other relationships. *Environ Microbiol* **14,** 335–346 (2012).
11. Webster, N. S. *et al.* Deep sequencing reveals exceptional diversity and modes of transmission for bacterial sponge symbionts. *Environ Microbiol* **12,** 2070–2082 (2010).
12. Schmitt, S. *et al.* Assessing the complex sponge microbiota: core, variable and species-specific bacterial communities in marine sponges. *ISME J* **6,** 564–576 (2012).
13. Reveillaud, J. *et al.* Host-specificity among abundant and rare taxa in the sponge microbiome. *ISME J* **8,** 1198–1209 (2014).
14. Lafi, F. F. *et al.* Widespread Distribution of *Poribacteria* in *Demospongiae*. *Appl Environ Microbiol* **75,** 5695–5699 (2009).
15. Schmitt, S., Hentschel, U. & Taylor, M. In *Ancient Animals, New Challenges* Vol. 219 *Developments in* Hydrobiology (eds Maldonado, Manuel, Turon, Xavier, Becerro, Mikel & Uriz, Maria Jesús) Ch. 28, 341–351 (Springer Netherlands, 2012).
16. Kamke, J. *et al.* The Candidate Phylum Poribacteria by Single-Cell Genomics: New Insights into Phylogeny, Cell-Compartmentation, Eukaryote-Like Repeat Proteins, and Other Genomic Features. *Plos One* **9** (2014).
17. Kamke, J. *et al.* Single-cell genomics reveals complex carbohydrate degradation patterns in poribacterial symbionts of marine sponges. *ISME J* **7,** 2287–2300 (2013).
18. Siegl, A. *et al.* Single-cell genomics reveals the lifestyle of Poribacteria, a candidate phylum symbiotically associated with marine sponges. *ISME J* **5,** 61–70 (2011).
19. Fieseler, L., Horn, M., Wagner, M. & Hentschel, U. Discovery of the novel candidate phylum "Poribacteria" in marine sponges. *Applied and Environmental Microbiology* **70,** 3724–3732 (2004).
20. Murat, D., Byrne, M. & Komeili, A. Cell biology of prokaryotic organelles. *Cold Spring Harbor perspectives in biology* **2,** a000422 (2010).
21. Pfeifer, F.Distribution, formation and regulation of gas vesicles. *Nat Rev Micro* **10,** 705–715 (2012).
22. Chowdhury, C., Sinha, S., Chun, S., Yeates, T. O. & Bobik, T. A. Diverse Bacterial Microcompartment Organelles. *Microbiology and Molecular Biology Reviews* **78,** 438–468 (2014).
23. Kerfeld, C. A. & Erbilgin, O. Bacterial microcompartments and the modular construction of microbial metabolism. *Trends in microbiology* **23,** 22–34 (2015).
24. Cornejo, E., Abreu, N. & Komeili, A. Compartmentalization and organelle formation in bacteria. *Current opinion in cell biology* **26,** 132–138 (2014).
25. van Niftrik, L. *et al.* Linking Ultrastructure and Function in Four Genera of Anaerobic Ammonium-Oxidizing Bacteria: Cell Plan, Glycogen Storage, and Localization of Cytochrome c Proteins. *J Bacteriol* **190,** 708–717 (2008).
26. Tocheva, E. I. *et al.* Polyphosphate Storage during Sporulation in the Gram-Negative Bacterium Acetonema longum. *J Bacteriol* **195,** 3940–3946 (2013).
27. Alvarez, H. M., Pucci, O. H. & Steinbüchel, A. Lipid storage compounds in marine bacteria. *Appl Microbiol Biotechnol* **47,** 132–139 (1997).
28. Micheva, K. D. & Smith, S. J. Array tomography: a new tool for imaging the molecular architecture and ultrastructure of neural circuits. *Neuron* **55,** 25–36 (2007).
29. Pfeifer, F. Distribution, formation and regulation of gas vesicles. *Nat Rev Microbiol* **10,** 705–715 (2012).
30. Fiore, C. L., Labrie, M., Jarett, J. K. & Lesser, M. P. Transcriptional activity of the giant barrel sponge, Xestospongia muta Holobiont: Molecular Evidence for Metabolic Interchange. *Front Microbiol* **6** (2015).
31. Radax, R. *et al.* Metatranscriptomics of the marine sponge Geodia barretti: tackling phylogeny and function of its microbial community. *Environ Microbiol* **14,** 1308–1324 (2012).
32. Moitinho-Silva, L. *et al.* Revealing microbial functional activities in the Red Sea sponge Stylissa carteri by metatranscriptomics. *Environ Microbiol* **16,** 3683–3698 (2014).
33. Leunissen, J. L. & Yi, H. Self-pressurized rapid freezing (SPRF): a novel cryofixation method for specimen preparation in electron microscopy. *J Microsc* **235,** 25–35 (2009).
34. Fischer, K., Beatty, W. L., Weil, G. J. & Fischer, P. U. High pressure freezing/freeze substitution fixation improves the ultrastructural assessment of Wolbachia endosymbiont-filarial nematode host interaction. *PLoS One* **9,** e86383 (2014).
35. Laming, S. R. & Duperron, S. In *Hydrocarbon and Lipid Microbiology Protocols: Ultrastructure and Imaging* (eds Terry McGenity, J., Kenneth Timmis, N. & Nogales, Balbina) 163–174 (Springer Berlin Heidelberg, 2016).
36. Halary, S., Duperron, S. & Boudier, T. Direct image-based correlative microscopy technique for coupling identification and structural investigation of bacterial symbionts associated with metazoans. *Appl Environ Microbiol* **77,** 4172–4179 (2011).
37. Jendrossek, D. & Pfeiffer, D. New insights in the formation of polyhydroxyalkanoate granules (carbonosomes) and novel functions of poly(3-hydroxybutyrate). *Environ Microbiol* **16,** 2357–2373 (2014).
38. Khadem, A. F. *et al.* Genomic and Physiological Analysis of Carbon Storage in the Verrucomicrobial Methanotroph "Ca. Methylacidiphilum Fumariolicum" SolV. *Front Microbiol* **3,** 345 (2012).
39. Becking, J. *The prokaryotes, 2nd edition* 2254–2267 (Springer Verlag, 1992).
40. Fieseler, L., Horn, M., Wagner, M. & Hentschel, U. Discovery of the novel candidate phylum "Poribacteria" in marine sponges. *Appl Environ Microbiol* **70,** 3724–3732 (2004).
41. Chowdhury, C., Sinha, S., Chun, S., Yeates, T. O. & Bobik, T. A. Diverse bacterial microcompartment organelles. *Microbiology and molecular biology reviews: MMBR* **78,** 438–468 (2014).
42. Noinaj, N., Guillier, M., Barnard, T. J. & Buchanan, S. K. TonB-dependent transporters: regulation, structure, and function. *Annu Rev Microbiol* **64,** 43–60 (2010).
43. Kozasa, T., Hajicek, N., Chow, C. R. & Suzuki, N. Signalling mechanisms of RhoGTPase regulation by the heterotrimeric G proteins G12 and G13. *J Biochem* **150,** 357–369 (2011).
44. Daniel, R., Bobik, T. A. & Gottschalk, G. *Biochemistry of coenzyme B12-dependent glycerol and diol dehydratases and organization of the encoding genes*. Vol. 22 (1998).

45. Liu, Y. *et al.* PduL is an evolutionarily distinct phosphotransacylase involved in B12-dependent 1,2-propanediol degradation by *Salmonella enterica* serovar typhimurium LT2. *J Bacteriol* **189,** 1589–1596 (2007).
46. Bobik, T. A., Havemann, G. D., Busch, R. J., Williams, D. S. & Aldrich, H. C. The propanediol utilization (pdu) operon of *Salmonella enterica* serovar Typhimurium LT2 includes genes necessary for formation of polyhedral organelles involved in coenzyme B(12)-dependent 1, 2-propanediol degradation. *J Bacteriol* **181,** 5967–5975 (1999).
47. Li, H. *et al.* The Sequence Alignment/Map format and SAMtools. *Bioinformatics* **25,** 2078–2079 (2009).
48. Anders, S., Pyl, P. T. & Huber, W. HTSeq—a Python framework to work with high-throughput sequencing data. *Bioinformatics* **31,** 166–169 (2015).
49. Mortazavi, A., Williams, B. A., McCue, K., Schaeffer, L. & Wold, B. Mapping and quantifying mammalian transcriptomes by RNA-Seq. *Nat Methods* **5,** 621–628 (2008).
50. R: A Language and Environment for Statistical Computing (Vienna, Austria, 2012).
51. Haas, B. J., Chin, M., Nusbaum, C., Birren, B. W. & Livny, J. How deep is deep enough for RNA-Seq profiling of bacterial transcriptomes? *BMC Genomics* **13,** 734 (2012).
52. Kanehisa, M. & Goto, S. KEGG: kyoto encyclopedia of genes and genomes. *Nucleic acids research* **28,** 27–30 (2000).
53. Finn, R. D. *et al.* Pfam: the protein families database. *Nucleic acids research* **42,** D222–D230 (2014).
54. Robinson, J. T. *et al.* Integrative genomics viewer. *Nat Biotechnol* **29,** 24–26 (2011).
55. Weimer, R. M. Preservation of C. elegans tissue via high-pressure freezing and freeze-substitution for ultrastructural analysis and immunocytochemistry. *Methods Mol Biol* **351,** 203–221 (2006).
56. Reynolds, E. S. The use of lead citrate at high pH as an electron-opaque stain in electron microscopy. *The Journal of cell biology* **17,** 208–212 (1963).
57. Schindelin, J. *et al.* Fiji: an open-source platform for biological-image analysis. *Nat Methods* **9,** 676–682 (2012).
58. Schneider, C. A., Rasband, W. S. & Eliceiri, K. W. NIH Image to ImageJ: 25 years of image analysis. *Nat Methods* 9, 671–675 (2012).
59. Cardona, A. *et al.* Identifying neuronal lineages of Drosophila by sequence analysis of axon tracts. *J Neurosci* **30,** 7538–7553 (2010).
60. Kremer, J. R., Mastronarde, D. N. & McIntosh, J. R. Computer visualization of three-dimensional image data using IMOD. *Journal of structural biology* **116,** 71–76 (1996).

Acknowledgements

We thank the KAUST Coastal and Marine Resources Core Lab for support with sample collection and the KAUST Biosciences Core Laboratory for support with sequencing. We further acknowledge the expert advice of Uriel Koziol for valuable suggestions on the IHC protocol (University of Würzburg). Harald Engelhardt provided helpful insights into the interpretation of the intracellular granules. SMM was supported by the German National Academic Foundation. This work was supported by the Deutsche Forschungsgemeinschaft (CRC 1182, project B1). MTJ and LMS were each supported by grants of the German Excellence Initiative to the Graduate School of Life Sciences, University of Würzburg.

Author Contributions

L.M.-S., M.T.J. and U.H. conceived the experiments; microscopy and sample preparation were performed by M.T.J. and S.M.M. under supervision of C.S. T.R. and T.R. contributed sequencing data and TR pre-processed reads; M.T.J. and L.M.-S. analysed sequencing data and M.T.J. imaging data; M.T.J., L.M.-S. and U.H. wrote the main manuscript text; All authors read and approved the final manuscript.

Additional Information

Supplementary information accompanies this paper at http://www.nature.com/srep

Competing financial interests: The authors declare no competing financial interests.

How to cite this article: Jahn, M. T. *et al.* Shedding light on cell compartmentation in the candidate phylum Poribacteria by high resolution visualisation and transcriptional profiling. *Sci. Rep.* **6**, 35860; doi: 10.1038/srep35860 (2016).

Publisher's note: Springer Nature remains neutral with regard to jurisdictional claims in published maps and institutional affiliations.

CHAPTER 4

MARINE SPONGES AS CHLOROFLEXI HOT SPOTS: GENOMIC INSIGHTS AND HIGH-RESOLUTION VISUALIZATION OF AN ABUNDANT AND DIVERSE SYMBIOTIC CLADE

Bayer, K., **Jahn, M.T.**, Slaby, B.M., Moitinho-Silva, L., Hentschel, U.

mSystems, 2018

doi: 10.1128/mSystems.00150-18

AMERICAN SOCIETY FOR MICROBIOLOGY | mSystems®

RESEARCH ARTICLE
Host-Microbe Biology

Marine Sponges as *Chloroflexi* Hot Spots: Genomic Insights and High-Resolution Visualization of an Abundant and Diverse Symbiotic Clade

Kristina Bayer,[a] Martin T. Jahn,[a,b] Beate M. Slaby,[a] Lucas Moitinho-Silva,[c] Ute Hentschel[a,d]

[a]GEOMAR-Helmholtz Centre for Ocean Research, RD3-Marine Ecology, RU-Marine Microbiology, Kiel, Germany
[b]University of Wuerzburg, Imaging Core Facility at the Theodor Boveri Institute of Bioscience, Wuerzburg, Germany
[c]Centre for Marine Bio-Innovation, University of New South Wales, Sydney, New South Wales, Australia
[d]Christian-Albrechts University of Kiel, Kiel, Germany

ABSTRACT Members of the widespread bacterial phylum *Chloroflexi* can dominate high-microbial-abundance (HMA) sponge microbiomes. In the Sponge Microbiome Project, *Chloroflexi* sequences amounted to 20 to 30% of the total microbiome of certain HMA sponge genera with the classes/clades SAR202, *Caldilineae*, and *Anaerolineae* being the most prominent. We performed metagenomic and single-cell genomic analyses to elucidate the functional gene repertoire of *Chloroflexi* symbionts of *Aplysina aerophoba*. Eighteen draft genomes were reconstructed and placed into phylogenetic context of which six were investigated in detail. Common genomic features of *Chloroflexi* sponge symbionts were related to central energy and carbon converting pathways, amino acid and fatty acid metabolism, and respiration. Clade-specific metabolic features included a massively expanded genomic repertoire for carbohydrate degradation in *Anaerolineae* and *Caldilineae* genomes, but only amino acid utilization by SAR202. While *Anaerolineae* and *Caldilineae* import cofactors and vitamins, SAR202 genomes harbor genes encoding components involved in cofactor biosynthesis. A number of features relevant to symbiosis were further identified, including CRISPR-Cas systems, eukaryote-like repeat proteins, and secondary metabolite gene clusters. *Chloroflexi* symbionts were visualized in the sponge extracellular matrix at ultrastructural resolution by the fluorescence *in situ* hybridization-correlative light and electron microscopy (FISH-CLEM) method. Carbohydrate degradation potential was reported previously for "*Candidatus* Poribacteria" and SAUL, typical symbionts of HMA sponges, and we propose here that HMA sponge symbionts collectively engage in degradation of dissolved organic matter, both labile and recalcitrant. Thus, sponge microbes may not only provide nutrients to the sponge host, but they may also contribute to dissolved organic matter (DOM) recycling and primary productivity in reef ecosystems via a pathway termed the sponge loop.

IMPORTANCE *Chloroflexi* represent a widespread, yet enigmatic bacterial phylum with few cultivated members. We used metagenomic and single-cell genomic approaches to characterize the functional gene repertoire of *Chloroflexi* symbionts in marine sponges. The results of this study suggest clade-specific metabolic specialization and that *Chloroflexi* symbionts have the genomic potential for dissolved organic matter (DOM) degradation from seawater. Considering the abundance and dominance of sponges in many benthic environments, we predict that the role of sponge symbionts in biogeochemical cycles is larger than previously thought.

KEYWORDS *Chloroflexi*, DOM degradation, FISH-CLEM, metabolism, metagenomic binning, single-cell genomics, sponge symbiosis

Received 26 July 2018 **Accepted** 29 November 2018 **Published** 26 December 2018

Citation Bayer K, Jahn MT, Slaby BM, Moitinho-Silva L, Hentschel U. 2018. Marine sponges as *Chloroflexi* hot spots: genomic insights and high-resolution visualization of an abundant and diverse symbiotic clade. mSystems 3:e00150-18. https://doi.org/10.1128/mSystems.00150-18.

Editor Karen G. Lloyd, University of Tennessee at Knoxville

Address correspondence to Kristina Bayer, kbayer@geomar.de.

Marine sponges as Chloroflexi hot spots: Genomic insights and high-resolution visualization of an abundant and diverse symbiotic clade. @GEOMAR_en @sponge_papers @SpongeLoop @Symbiosispapers #SpongeThursday

Sponges (*Porifera*) represent one of the oldest, still extant animal phyla. Fossil evidence shows their existence in the Precambrian long before the radiation of all other animal phyla (1, 2). Nowadays, sponges are globally distributed in all aquatic habitats from warm tropical reefs to the cold deep sea and are even present in freshwater lakes and streams (3). Sponges are increasingly recognized as important components of marine environments due to their immense filter-feeding capacities and consequent impacts upon coastal food webs and biogeochemical (e.g., carbon, nitrogen) cycles (4, 5). Many marine sponges contain dense and diverse microbial consortia within their extracellular mesohyl matrix. To date, 41 bacterial phyla (among them many candidate phyla) have been recorded from sponges, with recent amplicon sequencing studies suggesting up to 14,000 operational taxonomic units (OTUs) per sponge individual (6, 7). Sponges also constitute one of the most abundant natural sources of secondary metabolites, which are of commercial interest for the development of pharmaceuticals and new drugs (8) and are often produced by the microbial symbionts (9, 10).

Sponges can be classified into the so-called high-microbial-abundance (HMA) sponges harboring dense and diverse microbial consortia within their mesohyl tissues and the low-microbial-abundance (LMA) sponges containing microbial numbers on the order of those found in seawater (11–13). While HMA sponges are enriched in *Chloroflexi*, *Acidobacteria*, and "*Candidatus* Poribacteria," the LMA sponges are dominated by *Gamma-* and *Betaproteobacteria* as well as *Cyanobacteria*, while *Chloroflexi* are typically absent. Differences have also been observed with respect to functional gene content (14), pumping rates (15), and exchange of carbon and nitrogen compounds (16). There is mounting evidence that HMA sponges are specialized to feed on dissolved organic matter (DOM), while the LMA sponges preferably feed on particulate organic matter (POM) (7, 17, 18). It is thus tempting to speculate that the symbiotic microbiota of HMA sponges is involved in DOM degradation, and indeed, the microbiomes analyzed so far encode a diverse repertoire for carbon metabolism pathways and transporters for low-molecular-weight compounds (10, 19–21). However, the precise fluxes and mechanisms how DOM and POM are taken up and processed within the sponge holobiont remain unknown. Recently, it was proposed that members of the phylum *Chloroflexi* are involved in recalcitrant DOM recycling in the water column (22, 23).

In the present study, we focused our metagenomic analyses on *Chloroflexi* as abundant and characteristic, yet understudied members of HMA sponge microbiota. The phylum *Chloroflexi* comprises taxonomically and physiologically highly diverse lineages that populate a wide range of habitats (24–27) including the deep sea (22), uranium-contaminated aquifers (28), and the human oral cavity and gut (29, 30). *Chloroflexi* metabolism is very diverse, ranging from anoxygenic photosynthesizers, obligate aerobic/anaerobic heterotrophs, thermophiles, halophiles, clades capable of reductive halogenation, and even predators with gliding motility. Because only a few *Chloroflexi* lineages have been cultivated (87) and because draft genomes are limited in number (22, 23, 32), the specific functions of *Chloroflexi* within the marine ecosystem but especially in the symbiont context remain largely unknown.

Chloroflexi are members of HMA sponge microbiota, with representatives of classes/clades SAR202, *Anaerolineae*, and *Caldilineae* being the most abundant (31). Visualization of *Chloroflexi* by fluorescence *in situ* hybridization (FISH) revealed bright and abundant signals (32, 33). Because *Chloroflexi* likely play an important role in the HMA sponge holobiont, we had the following aims: (i) to assess their relative abundances and distributions in diverse HMA sponge species by using the largest data set currently available (Earth Microbiome Project [EMP] sponge microbiome [31]), (ii) to provide their phylogenetic affiliation, (iii) to characterize the functional gene repertoire with a particular focus on carbon degradation and symbiotic lifestyle, and (iv) to visualize *Chloroflexi* in mesohyl tissues at ultrastructural resolution by FISH-correlative light and electron microscopy (CLEM) methodology. We applied a broad range of state-of-the-art methods, from global sponge surveys to single-cell genomics and microscopy, to acquire comprehensive insights into the lifestyle of *Chloroflexi* symbionts.

RESULTS AND DISCUSSION

***Chloroflexi* abundance in HMA sponges.** Recently, members of the phylum *Chloroflexi* were shown to be present in much higher abundance and diversity in HMA sponges than in LMA sponges, which is why they were termed indicator species for HMA sponges (12). Here, we provide further details for the presence and abundance of *Chloroflexi* in HMA sponges (12) (Fig. 1; see also Tables S2A and S2B in the supplemental material). The recently compiled Sponge Microbiome Project (6, 31) was used as a reference database. In these 63 investigated sponge species, *Chloroflexi* abundances ranged from 4.39% ± 3.02% (*Chondrilla caribensis*) to 31.89% ± 5.27% (*Aplysina* spp.) (Fig. 1, right panel, and Table S2A). With respect to the *Chloroflexi* classes, the SAR202 clade was the most abundant, contributing on average to 47.74% ± 22.00% of the phylum total abundance (Fig. 1, top panel, and Table S2B). Members of the classes *Caldilineae* (22.35% ± 17.93%) and *Anaerolineae* (11.64% ± 12.30%) were also abundant in some sponges but not others. Unclassified OTUs at the class level represented 14.50% ± 10.77% of *Chloroflexi* sequences, indicating that there is phylogenetic novelty still to be discovered. Despite some variability (Fig. 1, heatmap), the classes/clades SAR202, *Caldilineae*, and *Anaerolineae* as well as diverse hitherto unclassified OTUs dominated the *Chloroflexi* population in the HMA sponges. The remaining classes/clades amounted to 3.78% of total phylum abundance. At the OTU level, there was a significant effect of geographical location [$F(15, 725) = 15.9$, $P = 0.001$] and of sponge taxonomy [$F(9, 725) = 18.6$, $P = 0.001$] on beta diversity (Table S2C). For example, a Mediterranean cluster and several Caribbean clusters become visible as shown by Bray-Curtis cluster analysis. In addition, a host taxonomic signature was revealed for example for the sponge genera *Aplysina* and *Agelas*. However, there were also exceptions (i.e., *Neopetrosia* species from the Caribbean did not cluster together, and *Stelletta maori* from New Zealand fell into the Mediterranean cluster). Altogether, this analysis showed the high abundance and consistency of the three above-mentioned main clades of *Chloroflexi* in HMA sponges and revealed a geographic and host taxonomic signature for the *Chloroflexi* community.

Phylogeny of *Chloroflexi* metagenome bins and single amplified genomes. In total, 260 single amplified genomes (SAGs) were screened for the presence of the phylogenetic marker. A total of 125 16S rRNA genes were identified in 112 SAGs, of which some were duplicates per well. Sequencing revealed that 39 genes (31.2%) were affiliated with the phylum *Chloroflexi* (33). We randomly chose 13 SAGs for genome sequencing. Phylogenetic analysis of 16S rRNA genes revealed that one SAG (3D), four SAGs (1B, 1G, 1H, and 4H), and eight SAGs (2D, 3B, 3H, 4A, 5H, 6B, 6C, and 6F) belonged to the classes/clades SAR202, *Anaerolineae*, and *Caldilineae*, respectively, forming a well-supported sequence cluster (bootstrap, 100) with other sponge-derived sequences (Fig. S2). The binning of metagenomic sequence data (21) resulted in additional five high-quality bins (Table 1). The only metagenome bin containing a 16S rRNA gene (S156) belonged to SAR202. The SAR202 sequences formed a well-supported cluster (bootstrap value, 98) with other sponge-derived 16S rRNA gene sequences (Fig. S1). To elucidate the clade affiliation of the remaining four metagenome bins lacking 16S rRNA genes of appropriate length, a concatenated genome tree based on nine ribosomal genes was calculated (Fig. 2). One bin (A154) was affiliated with the class *Anaerolineae*, two metagenome bins were associated with the *Caldilineae* (C141 and C174), and two bins were associated with the SAR202 clade (S152 and S156) within the phylum *Chloroflexi*. The phylogenetic affiliation of metagenome bin S156 was congruent with the 16S rRNA gene analysis. SAGs were included in the protein-based phylogenetic analysis when they encoded at least three of the nine ribosomal genes. Due to the lack of more-complete reference genomes from SAR202 microorganisms, the most complete one (ca. 25%, SAR202 cluster bacterium sp. strain SCGC AAA240-N13, IMG Gold Study ID Gs0017605 [22]) was included in this analysis, although only one ribosomal protein could be used for tree construction. Both analyses showed a stable phylogeny of all SAGs and metagenome bins to above-described classes or clades within the

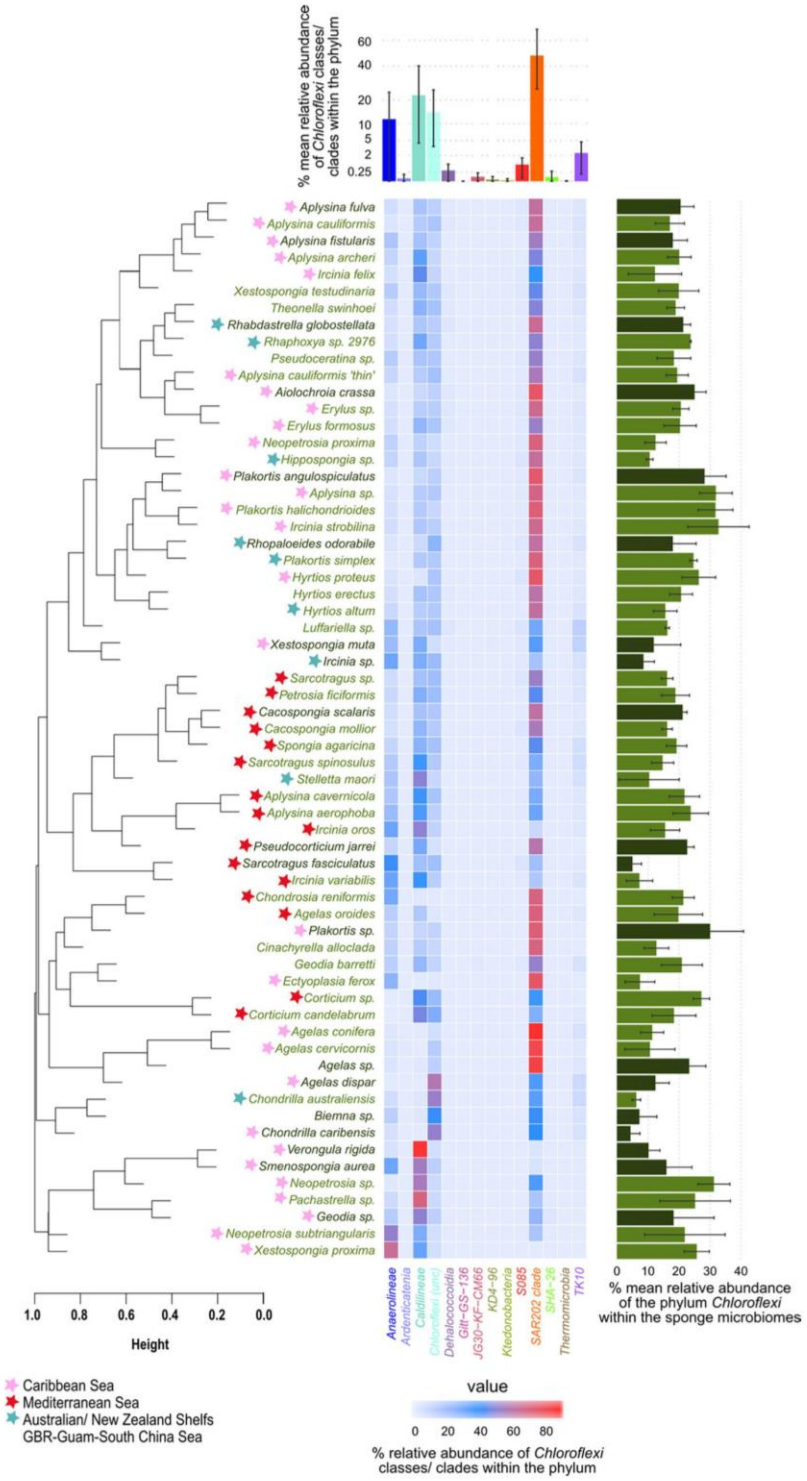

FIG 1 Heatmap showing the relative abundance of *Chloroflexi* classes/clades in 63 HMA sponges extracted from Earth Microbiome Project (EMP) data (31). The top panel shows the mean relative abundance of

(Continued on next page)

TABLE 1 Genomic features overview of single amplified genomes (SAGs) and metagenome bins of *A. aerophoba* associated *Chloroflexi* and closest relative reference genomes analyzed in this study

Class/clade and SAG/bin[a]	Taxon ID	Genome size (Mbp)	No. of scaffolds	N50 (kbp)	GC (%)	Contamination (CheckM)	% completeness estimation (IMG)	No. of genes				
								Total	CDS	RNA	tRNA	Without function
Anaerolineae												
SAG 1B	2617270794	2.78	325	46.4	58.9	8.64	55.8	2,714	2,679	35	24	639
SAG 1G	2617270795	1.69	307	22.6	58.1	0.91	32.0	1,694	1,676	18	14	438
SAG 1H	2617270796	1.73	352	16.6	59.1	0.00	31.9	1,774	1,752	22	17	458
SAG 4H	2617270812	0.16	51	4.0	58.4	0.00	0.0	175	168	7	4	43
A154*	2619619053	3.73	107	63.9	59.3	1.82	91.8	3,358	3,307	51	47	613
Caldilineae												
SAG 2D	2617270806	3.51	489	17.8	58.4	0.91	65.5	3,207	3,177	30	24	855
SAG 3B	2617270807	2.02	310	15.3	59.2	0.00	38.7	1,844	1,823	21	17	444
SAG 3H	2617270810	2.47	290	31.1	58.9	0.00	50.9	2,271	2,242	29	24	641
SAG 4A	2617270811	3.35	437	31.3	59.4	0.00	64.8	3,024	2,994	30	26	777
SAG 5H	2617270814	1.26	183	17.5	58.4	0.00	17.2	1,132	1,112	20	17	288
SAG 6B	2617270816	4.25	685	14.6	58.7	3.18	66.8	3,943	3,901	42	35	1,154
SAG 6C	2617270818	2.75	414	18.6	58.5	1.82	45.9	2,579	2,544	35	28	703
SAG 6F	2617270820	3.66	839	8.4	58.4	0.91	56.5	3,594	3,561	33	25	1,063
C141*	2619619051	4.59	507	13.3	63.0	0.91	90.9	4,288	4,236	52	46	1,246
C174*	2619619055	6.36	647	13.0	58.4	10.20	96.3	5,662	5,601	61	55	1,472
SAR202												
SAG 3D	2617270809	0.58	106	22.8	60.5	0.00	25.4	622	608	14	13	145
S152*	2619619052	5.03	890	6.9	56.9	16.31	91.1	5,448	5,378	70	60	1,938
S156*	2619619054	3.35	334	15.2	65.6	2.97	98.0	3,463	3,402	61	52	964

[a]IMG Gold Study IDs are Gs0114494 and Gs0099546 (marked with an asterisk). The letters of the bins reflect the phylogenetic identity of the bin (A for *Anaerolineae*, C for *Caldilineae*, and S for SAR202). The gray shaded bins/SAGs were used for further detailed metabolic analysis.

phylum *Chloroflexi*. All three classes/clades were visualized in the *A. aerophoba* sponge mesohyl matrix by fluorescence *in situ* cohybridization (FISH) on ultrathin tissue sections using class/clade-specific probes. The *Chloroflexi* cell signal was abundant as judged by the stained versus unstained bacterial signal, and SAR202 (green) seemed to dominate over either *Anaerolineae* (red) or *Caldilineae* (orange). The cells were metabolically active as judged by the brightness of the FISH probe (Fig. 3). These visual observations are consistent with the relative abundance of the phylum *Chloroflexi* within sponge microbiomes (24% ± 6% within *A. aerophoba* sponge microbiome; Fig. 1 and Table S2A) and the representation of *Chloroflexi* cells among SAGs (31%).

General description of genomes. The final genome assembly sizes for the sponge-associated *Chloroflexi* single cells (SAGs) ranged from 0.16 to 4.25 Mbp, representing up to 66.85% of genome completeness derived from IMG-based estimations (Table 1). The guanine-cytosine (GC) content ranged from 58.08 to 59.32%, 58.36 to 62.98%, and 56.93 to 65.59% for *Anaerolineae*, *Caldilineae*, and SAR202, respectively. The numbers of identified genes were highly variable, ranging from 3,358 genes for *Anaerolineae* genome bin A154 to 5,448 for the SAR202 bin S152 and 5,662 genes for the *Caldilineae* bin C174 (Table 1). The five metagenome bins (two for *Caldilineae* [C141 and C174], two for SAR202 [S152 and S156], and one for *Anaerolineae* [A154]) which had >90% coverage were chosen for detailed metabolic analysis and inner-phylum comparison. The letters of the bins were chosen to reflect their phylogenetic identity (A for *Anaerolineae*, C for *Caldilineae*, and S for SAR202). Additionally, the most complete *Anaerolineae* SAG 1B (55.76% genome completeness estimation) was included in the

FIG 1 Legend (Continued)

Chloroflexi classes/clades in all sponges (means ± standard deviations [error bars]). The right panel displays the mean relative abundance of the phylum *Chloroflexi* in predicted (light green names and medium green bars) and classified (dark green names and bars) HMA sponges (means ± standard deviations) determined by machine learning (12). Results of cluster analysis based on Bray-Curtis dissimilarities on mean relative abundances of OTUs within the phylum are presented on the left side. Sponges are marked with stars when all species samples came from one of the three major sample locations.

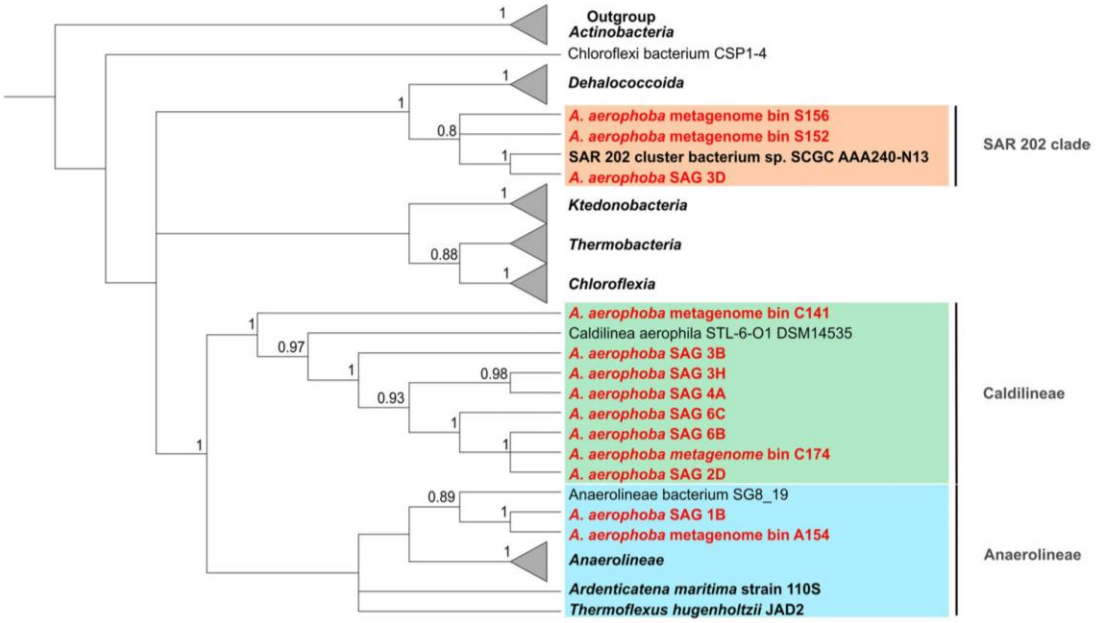

FIG 2 Concatenated protein tree. Maximum likelihood phylogenetic analysis of *Chloroflexi* metagenome bins and SAGs (in red) from 1,914 positions of 60 sequences using ribosomal proteins. The percentage of replicate trees in which the associated taxa clustered together in the bootstrap test (100 replicates) are shown. The initial tree for the heuristic search was obtained automatically by applying neighbor-joining and BioNJ algorithms to a matrix of pairwise distances estimated using a JTT model. Multiple sequences are included in the collapsed branches representing *Chloroflexi* classes/clades (bold). To root the tree, three representative genomes from the phylum *Actinobacteria* were used. Reference genomes with accession numbers can be found in Table S1 in the supplemental material.

analysis. Due to the lack of complete genomes of marine representatives of the *Anaerolineae*, *Caldilineae*, and SAR202 available at the time of analysis, sponge-derived *Chloroflexi* genomes could not be fully assessed. Taking the pitfalls inherent to metagenome sequencing into account (i.e., fragmented assemblies, unresolved ambiguities),

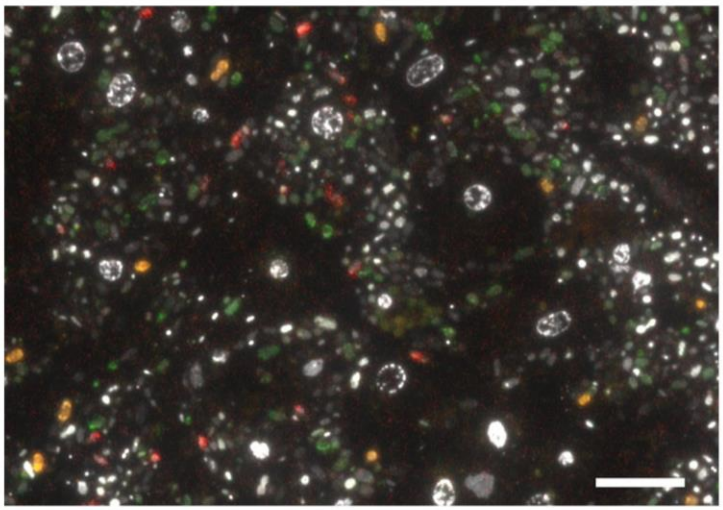

FIG 3 Distribution of *Chloroflexi* clades in *Aplysina aerophoba* mesohyl using fluorescence *in situ* hybridization (FISH). The image shows the overlay of all probes. SAR202 cells are displayed in green, *Caldilineae* cells in orange, and *Anaerolineae* cells in red. The nucleotide stain DAPI (white/gray) served as a reference for the localization of unstained cells. Bar, 10 μm.

we have opted for a presence/absence approach: a gene or enzyme was considered present when it was identified in both bins of the corresponding clade. For *Anaerolineae*, we consider an enzyme or gene present when identified in bin A154, and the SAG 1B was taken as additional support.

Central metabolism of sponge-associated *Chloroflexi*. Metabolic reconstruction suggests that *Chloroflexi* are aerobic and heterotrophic bacteria including glycolysis, tricarboxylic acid (TCA) cycle, pentose phosphate pathway (PPP) (see Text S1 and Fig. S3A to C for details), and the respiratory chain as energy-producing pathways in all three clades.

With respect to autotrophic carbon fixation, the reductive citrate acid cycle (Arnon-Buchanan cycle), which is largely present, and the Wood-Ljungdahl pathway, which was partially identified (Fig. S2D) might be functional in times when sponges are not pumping and the mesohyl turns anoxic (34). Genes encoding components involved in ammonia import and assimilation are carried on all investigated genomes, but SAR202 and *Caldilineae* have additional genes for glutamate synthesis from glutamine and directly from ammonia. The transport of nitrite (and possibly also nitrate) is encoded on all investigated genomes, while the reduction to ammonia is encoded only by SAR202 (Fig. S3E). The incorporation of sulfur (with, e.g., thiosulfate as donor) into S-containing amino acids might be possible in all clades, whereas the assimilatory reduction of sulfate is restricted to *Anaerolineae* and *Caldilineae* genomes (Fig. S3F).

These processes additionally provide precursors for further metabolic pathways such as biosynthesis of purines and pyrimidines, amino acids, and cofactors, or structural compounds. Machinery for transcription, translation, and purine and pyrimidine metabolism are largely present. Fatty acid (FA) biosynthesis and degradation pathways were detected in all six genomes. All genomes encode a high number of different ABC transporters compared to genomes of free-living bacteria (22, 35) to supplement for nutrition and cell growth-related compounds [including oligopeptides, phosphate, L- and branched-chain amino acids, minerals such as iron(III) and molybdate, metal ions such as zinc, manganese, and iron(II)]. Additionally, all six genomes largely encode enzymes needed for biosynthesis of most amino acids (Text S1). We could not identify any of the typical phosphotransferase systems, as was the case for *Ca.* Poribacteria described previously (19).

We found genomic potential for aromatic degradation in *Chloroflexi* genomes, but pathways remain incomplete (Text S1). Several genes encoding components involved in phenylpropionate and cinnamate degradation, terephthalate degradation, catechol degradation, and xylene degradation were identified in *Chloroflexi* genomes. Also, genes encoding enzymes involved in ring cleavage by Baeyer-Villinger oxidation and beta oxidation as well as ring-hydroxylating dioxygenases and isomerases were identified which could be involved in degradation of aromatic compounds possibly synthesized by the sponge host or other microbes. This finding is interesting in the context that many sponge species contain secondary metabolites that often contain aromatic ring structures that serve as a defense strategy against predators and biofouling (36). Sponge symbionts may be able to degrade such substances, enabling them to a life within sponge hosts. These findings fit with the potential degradation of organic compounds which was suggested for *Chloroflexi* bacteria of the class SAR202 by (meta)genomic studies (22, 23, 35). The highest (20 to 30% relative to the total microbiome) and most consistent presence of *Chloroflexi* within a sponge genus was found in the sponge genera *Plakortis*, *Agelas* (with the exception of *Agelas dispar*), and *Aplysina* and sister taxon *Aiolochroia*. Interestingly, all of them contain characteristic natural products with aromatic ring structures. It is therefore tempting to speculate that the presence and abundance of *Chloroflexi* and especially SAR202 are shaped, at least to some extent, by the natural products present in the corresponding host sponges.

With respect to cell wall structure, the *Anaerolineae* and *Caldilineae* genomes carry the gene repertoire for peptidoglycan biosynthesis. The noticeable lack of peptidoglycan biosynthesis genes in the SAR202 genomes (Text S1) is consistent with previous

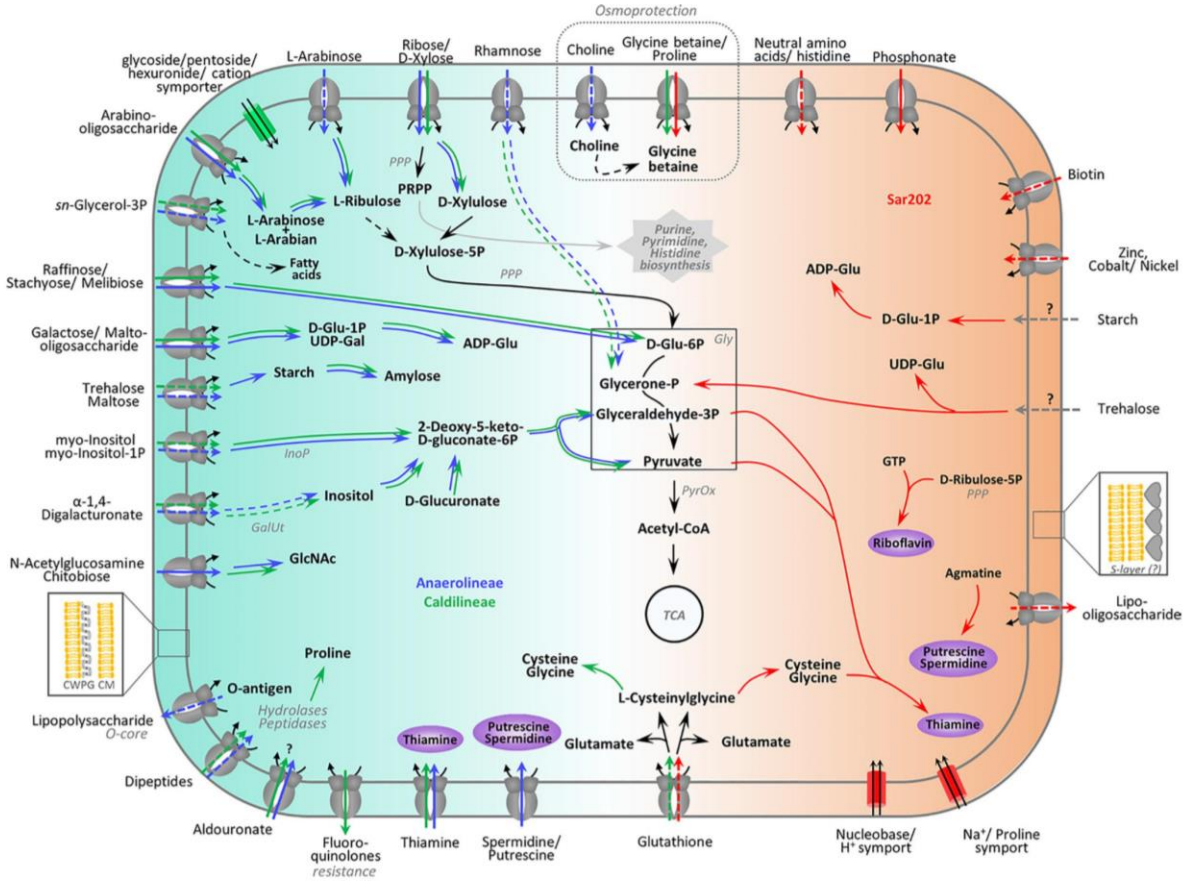

FIG 4 Summarized metabolic features which were found only in *Anaerolineae* and *Caldilineae* (left side, blue and green arrows, respectively) or in SAR202 genomes (right side, red arrows). The central metabolic pathways (glycolysis, TCA cycle, purine, pyrimidine histidine biosynthesis) located in the middle of the figure are general features found in all genomes. Lines are dashed when pathways or transporter could not be annotated completely (single enzymes of the pathway or single genes from the transporter were missing) or could not be annotated in both genomes of one clade. Gray dashed arrows indicate that those transporters were not identified.

analyses of three *Chloroflexi* genomes derived from uranium-contaminated aquifers (28) and hyperoxic zones from the Gulf of Mexico (37). Additionally, consistent with previous observations (38), none of the six genomes contained flagellar or chemotaxis genes.

Metabolic specialization: extensive carbohydrate uptake and degradation in *Anaerolineae* and *Caldilineae*. The following features are metabolic specialties of *Anaerolineae* and *Caldilineae* and appear to be missing in SAR202, unless otherwise mentioned (Fig. 4). We found a number of ABC transporters for the import of diverse monosaccharides (ribose/xylose, inositol, glycerol-3-phosphate [glycerol-3P], and rhamnose) and oligosaccharides (sorbitol, raffinose/stachyose/melibiose, maltose, *N*-acetylglucosamine, and arabinosaccharide) into *Anaerolineae* and *Caldilineae* cells. Xylose can be processed to xylulose which may enter the pentose phosphate cycle finally leading into glycolysis. Ribose can be converted to 5-phosphoribosyl 1-pyrophosphate (PRPP), which is a precursor for the biosynthesis of the amino acid histidine or it may fuel purine and pyrimidine synthesis (Text S1). Both groups may also be able to import glycerol-3P, which is a phosphoric ester of glycerol (a component of glycerophospholipids) which can be converted to fatty acids. Additionally, we found evidence for arabinose and rhamnose import and degradation; however, annotation was incomplete (Text S1).

Arabinooligosaccharides (such as α-L-arabinofuranosides, α-L-arabinans, arabinoxylans, and arabinogalactans) result from degradation of plant-like cell material entering

the sponge by filtration. These substances may be imported by the almost completely annotated AraNPQ and MsmX transporters and be utilized to L-arabian and L-arabinose by the enzyme α-*N*-arabinofuranosidase (EC 3.2.1.55, GH3). The enzyme L-arabinose isomerase (EC 5.3.1.4, AraA) is present in all four genomes of *Anaerolineae* and *Caldilineae* and converts L-arabinose to L-ribulose, which can further be converted by reactions of PPP to glucose-6P suitable for entering glycolysis. Additionally, other oligosaccharides such as stachyose, raffinose, melibiose, and galactose can be imported and used in central metabolism (Fig. 4 and Text S1).

The utilization of *myo*-inositol as a carbon source and possibly as a regulatory agent was hypothesized previously for sponge-associated *Ca.* Poribacteria (19). Similarly, sponge-associated *Anaerolineae* and *Caldilineae* genes encode almost all the components involved in the inositol degradation pathway (Text S1). *myo*-Inositol is likely degraded to glyceraldehyde-3-phosphate and acetyl-CoA, which are further used in the central metabolism. Inositol phosphates are found as part of eukaryotic and archaeal cell wall components (39). Phosphorylated inositol is a precursor for several lipid molecules, including sphingolipids, ceramides, and glycosylphosphatidylinositol anchors (40), as well as many stress-protective solutes of eukaryotes (39), and it might be part of the signal transduction in sponges (41). Therefore, the sponge itself or eukaryotic microorganisms can probably provide inositol as a carbon source or regulatory agent for the microbial symbionts.

Uronic acids are sugar acids that can be found in biopolymers of plants, animals, and bacteria (42, 43) and are known to occur in glycosaminoglycans (GAGs). GAGs in sponges are mainly composed of fucose, glucuronic acid (glucoronate), mannose, galactose, *N*-acetylglucosamine, and sulfate (44–46). Genes encoding enzymes involved in degradation of uronic acids were found in *Anaerolineae* and *Caldilineae* genomes. The possibility of galacturonate and glucuronate catabolism is supported by the conversion of 2-dehydro-3-deoxy-D-gluconate by the enzymes glucoronate isomerase (EC 5.3.1.12), tagaturonate reductase (EC 1.1.1.58), and altronate hydrolase (EC 4.2.1.7). Furthermore, the presence of genes encoding oligogalacturonide lyase (EC 4.2.2.6), 2-deoxy-D-gluconate 3-dehydrogenase (EC 1.1.1.125), and 2-dehydro-3-desoxy-D-glucokinase (EC 2.7.1.45) supports possible 4(4-α-D-gluc-4-enuronosyl)-D-galacturonate degradation activity. The products could then enter the Entner-Doudoroff (ED) pathway via 2-dehydro-3-desoxyphophogluconate aldolase (EC 4.1.2.14). Uronic acid degradation could principally be connected to the inositol degradation pathway via D-galacturonate even though additional genome evidence, such as genes encoding the enzyme inositol oxidase (EC 1.13.99.1), remain wanting (Fig. 4 and Text S1). A number of transporters for *N*-acetylglucosamine, digalacturonate, mannose, and galactose (Fig. 4 and Text S1) were identified in *Anaerolineae* and *Caldilineae* genomes. Digalacturonate can be utilized by the uronic acid degradation pathway (Text S1), and *N*-acetylglucosamine can be used directly in amino sugar and nucleotide sugar synthesis. The presence of uronic acid degradation pathways provides strong support that *Anaerolineae* and *Caldilineae*, similar to the previously described *Ca.* Poribacteria, degrade glycosaminoglycan chains of proteoglycans, which are important components of the sponge host matrix (19). In that line, *Anaerolineae* and *Caldilineae* genomes were enriched in arylsulfatases A (Fig. S4A), which are thought to be involved in metabolization of sulfated polysaccharides from the sponge extracellular matrix (19, 21) and in the heterotrophic ability of symbionts to use sponge components for nutritional purposes.

Expanded carbohydrate-active enzyme (CAZymes) repertoire in *Caldilineae* and *Anaerolineae*. In order to search for CAZymes, we screened the *Chloroflexi* genome data against dbCAN (47) and classified the enzymes according to the CAZy database (48). Most *Chloroflexi* hits were against glycosyl hydrolases (GH), glycosyltransferases (GT), and carbohydrate-binding modules (CBM). Consistent with the above-described metabolic specializations, these enzyme classes were present in larger amounts in *Caldilineae* and *Anaerolineae* than in SAR202 (Fig. S4B and Table S3). Altogether, 40 GH families were identified in all *Chloroflexi* genomes (Table S3). Glycosyl hydrolase family 109 was the most abundant family of GHs and was identified in all six

genomes. GH109 family proteins are predicted as α-*N*-acetylgalactosaminidases (EC 3.2.1.49) with putative substrates such as glycolipids, glycopeptides, and glycoproteins, all of which are common constituents of sponge mesohyl as well as dissolved organic matter from seawater. The GH74 family is the second most abundant and is also present in all six genomes. These appear to be xyloglucan-hydrolyzing enzymes, that act on β-1,4 linkages and might help degrade various oligo- and polysaccharides. The previously reported glycosylhydrolases GH33 and GH32 (19, 20) were the third most abundant, but they were restricted to *Caldilineae* bin C174. This enzyme family is annotated as sialidase (EC 3.2.1.18), capable of hydrolyzing glycosidic linkages of terminal sialic acid residues, which are present in sponge mesohyl (49). Altogether, 17 glycosyltransferases were identified on *Chloroflexi* genomes with families GT2, GT4, and GT83 being the most abundant. Among the 11 CBM families identified on *Chloroflexi* genomes, CBM50 was the most abundant, but it was restricted to *Caldilineae* and *Anaerolineae*. CMB50 modules, also known as LysM domains, attach to various GH enzymes which are involved in the cleavage of chitin or peptidoglycan. The numbers of carbohydrate-active enzymes on *Chloroflexi* symbiont genomes reflect their extensive potential to degrade complex carbohydrates as reported previously for *Ca.* Poribacteria and the sponge-associated unidentified lineage SAUL (19, 20).

Metabolic specialization: cofactor biosynthesis in SAR202 genomes. There is mounting evidence that vitamins and cofactors produced by diverse symbiont lineages could be beneficial to the sponge host (50–53). Parallel transcriptional activity profiling of the symbionts and the sponge showed that the symbionts had the capacity for vitamin B biosynthesis, whereas the host transcripts displayed the capacity for vitamin catabolism (54). It is thus tempting to speculate that the sponges' nutrition is augmented by symbiont-derived vitamins and cofactors. In the present study, at least two biosynthetic pathways for cofactor biosynthesis were identified on SAR202 genomes, which were absent in *Anaerolineae* and *Caldilineae* (Fig. 5). Thiamine is an essential cofactor which is involved in central metabolism. The biosynthesis of the biologically active form thiamine diphosphate (TPP) from L-cysteine, glycine, pyruvate, and glyceraldehyde-3P is encoded on the SAR202 genomes (Fig. 4 and 5A). Although the pathway is incomplete, the data strongly suggest that the synthesis of TPP is restricted to SAR202 bacteria. Instead, *Anaerolineae* and *Caldilineae* appear to import thiamine via an ABC transporter (TbpA, ThiPQ) and convert it to TPP by using thiamine pyrophosphokinase (EC 2.7.6.2). Additionally, thiamine synthesis might be a symbiosis-related feature, since free-living SAR202 members lack the synthesis ability (22, 37).

Second, riboflavin (vitamin B2) is required by enzymes and proteins to perform certain physiological functions. Specifically, the active forms, flavin mononucleotide (FMN) and flavin adenine dinucleotide (FAD), serve as cofactors for a variety of flavoprotein enzyme reactions. Most genomes carry genes encoding the enzymes FMN adenylyltransferase (EC 2.7.7.2) and FAD riboflavin kinase (EC 2.7.1.26) which activate riboflavin into FMN. However, only the SAR202 genomes contain genes encoding the riboflavin biosynthesis enzymes which rely on GTP and ribulose-5P (Fig. 4 and 5B). Both substrates can be provided by pathways of the central metabolism (purine metabolism and PPP). Only one free-living SAR202 bacterium (unclassified *Chloroflexi* bin 43) (37) has genes encoding components involved in riboflavin synthesis.

Potential for degradation of recalcitrant DOM in SAR202. The uptake of the amino acid L-Asp was shown before in subtropical Atlantic waters (35), and the possible participation of deep sea SAR202 bacteria in degradation of recalcitrant or refractory DOM was recently postulated by Landry et al. (22). Even though the exact composition of DOM in the world's oceans remains to be elucidated, refractory DOM is an important component of the global carbon budget in terms of sheer mass. Landry et al. (22) argue that SAR202 genomes have an expanded repertoire of oxidative enzymes that may help in the oxidation of recalcitrant compounds. Interestingly, some of the described enzymes were also found to be enriched in SAR202 symbionts of sponges (Table S4). Among them are genes encoding proteins from the CaiB/BaiF family as well as related

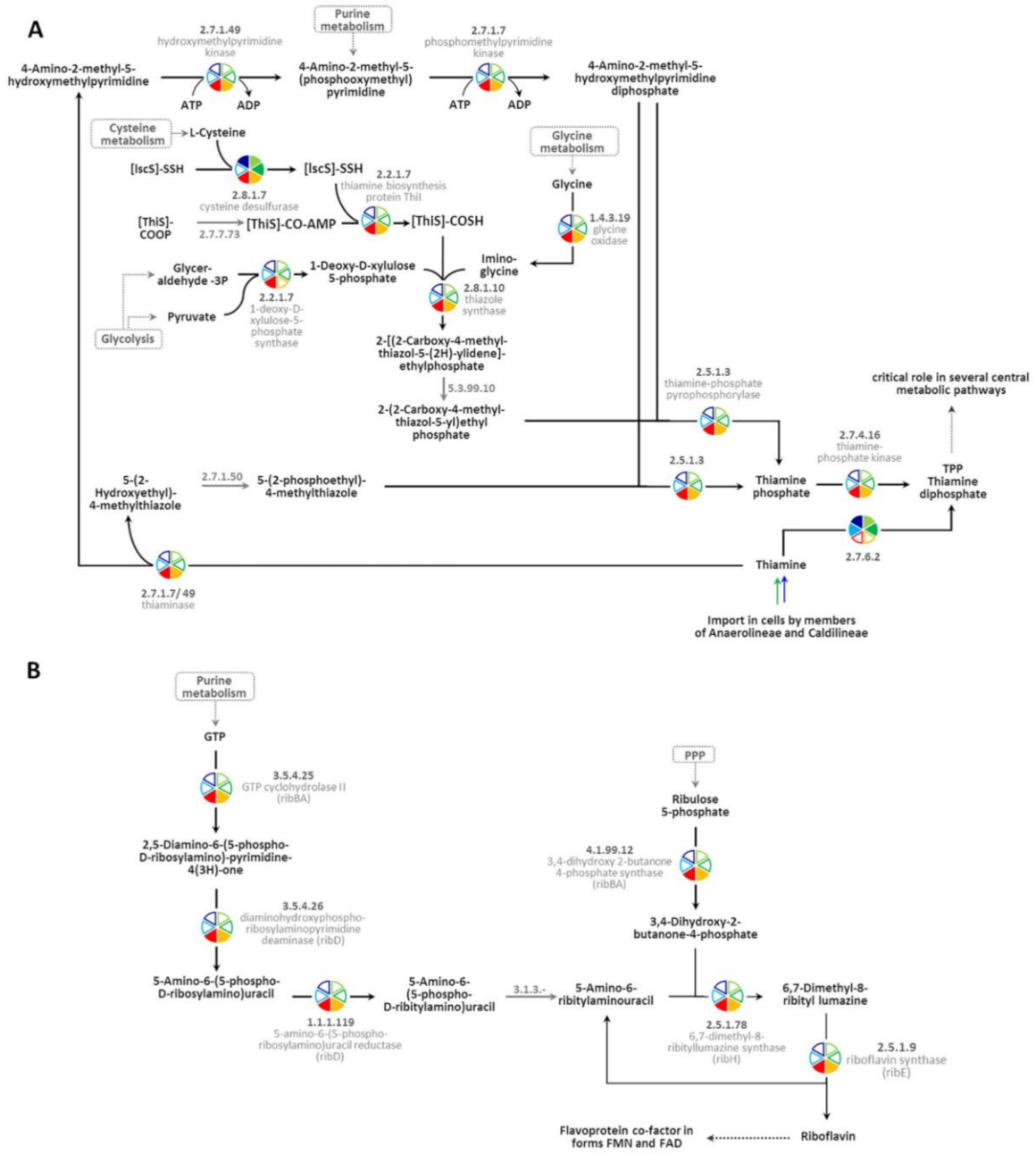

FIG 5 Pathway for synthesis of thiamine (A) and riboflavin (B) in both SAR202 genomes. (A) Members of classes *Anaerolineae* and *Caldilineae* carry genes encoding components involved in the import of thiamine (see also Fig. 4). (B) The conversion of riboflavin into the biologically active forms (flavin mononucleotide [FMN] and flavin adenine dinucleotide [FAD]) was encoded by genes in the genomes of all three classes (filled pies compared to empty pies). The colors represent the genomes. The numbers are KEGG identifiers. PPP, pentose phosphate pathway. Gray arrows and numbers indicate unidentified enzymes.

family III transferases. While the enrichment of CaiB was previously interpreted as carnitine being a carbon and nitrogen source for sponge symbionts (21), an alternative explanation may be that it serves to funnel substrates into degradation pathways without consumption of energy by shuffling CoA, thus generating free electrons (Text

S1). Even though the precise function of CaiB/BaiF family proteins cannot be elucidated at this time, the enrichment in SAR202 genomes is noteworthy. Further, a total of 53 flavin-dependent, class C oxidoreductases of the luciferase family (flavin mononucleotide monooxygenases [FMNOs], COG2141) which include alkanesulfonate monooxygenase SsuD and methylene tetrahydromethanopterin reductase, were present and enriched in SAR202 genomes compared to the genomes of *Anaerolineae* and *Caldilineae* bacteria (Table S4). These enzymes are proposed to participate in the oxidation of (long-chain) aldehydes to carboxylic acids and/or cleavage of carbon-sulfur bonds in a variety of sulfonated alkanes (55). The SAR202 genomes contained 22 genes encoding short-chain alcohol dehydrogenases (COG0300) which might be involved in canalization of ketone body derivate release. Some of these genes from bin S152 showed homologies to cyclopentanol and 3-α (or 20-β)-hydroxysteroid dehydrogenases which convert alicyclic-bound alcohol groups to ketones (22, 56). The combination of the enzymes described above could allow sponge-associated *Chloroflexi* to convert recalcitrant alicyclic ring structures to more labile carboxylic acid, as proposed recently for SAR202 bacteria from deep sea (22).

Additionally, a number of genes encoding oxidative enzymes were identified on the *Chloroflexi* genomes but were not enriched in SAR202 (Table S4). These enzymes include a 2-oxoglutarate:ferrodoxin oxidoreductase (EC 1.2.7.11) which oxidizes acetyl-CoA, carbon monoxide dehydrogenase (EC 1.2.99.2) which might allow the bacteria to oxidize CO as described for some members of the Ktedonobacteria (57), CO- or xanthine dehydrogenases (COG1529) which are possibly involved in oxidation of a broad range of complex substrates (22), choline dehydrogenase (EC 1.1.99.1) being possibly involved in the oxidation of alcohols to aldehydes, sarcosine oxidase (EC 1.5.3.1), the serine hydroxymethyltransferase (2.1.2.1) with predicted function in choline degradation, formaldehyde dehydrogenase (EC 1.2.1.46), and subunits of formate dehydrogenase (EC 1.2.1.2/43) which oxidize formaldehyde and formate and might be involved in demethylation of various compounds. The overall presence and frequent enrichment of enzymes with oxidative capacity in SAR202 would be consistent with gene functions in degradation of recalcitrant DOM. However, owing to the sponges' existence in shallow-water sun-lit benthic environments, it remains unclear whether the sponge symbionts encounter recalcitrant DOM derived from seawater sources. Interestingly, Colatriano et al. recently proposed the degradation of terrestrial DOM (tDOM) by members of the SAR202 clade (23). Shallow-water sponges and associated symbionts could be faced by tDOM via freshwater inflow in ocean waters they inhabit. Alternatively, and similar to other high-diversity microbiota, for example, of ant, ruminant, and human guts, the resident microbes were likely to specialize in certain substrates, thus promoting maximum nutrient exploitation and also securing their individual niche in the holobiont ecosystem.

Symbiosis-related features. Eukaryotic-like proteins (ELPs) seem to be a general genomic feature of sponge symbionts (20, 38, 50, 51, 58–60). Ankyrin (ANK), tetratricopeptide (TPR), and leucine-rich (LRR) repeat proteins are postulated to be involved in mediating host-microbe interactions (61, 62). Ankyrin and ankyrin repeat-containing proteins were detected in all six genomes of sponge symbionts (Fig. S4C and Table S5A) in higher numbers than in free-living bacteria (22, 37). It was recently proposed that the expression of sponge symbiont-derived ankyrin protein prevents phagocytosis by amoeba (63), and it is tempting to speculate that they protect the symbionts from digestion by the sponge archaeocytes *in vivo*. TPRs, possibly functioning as a module for protein-protein interaction involved in a variety of cellular functions, including those that participate in bacterial pathogenesis (64) were found in all six genomes. However, LRR genes were identified only in *Caldilineae* and SAR202 genomes (Fig. S4C and Table S5A). Many LRR proteins are involved in protein-ligand interactions; these interactions include plant immune response and the mammalian innate immune response (for a review, see reference 65), such as the detection of pathogen-associated molecular patterns by recogni-

TABLE 2 Genomic characteristics of the six genomes investigated in detail[a]

Class/clade and SAG/bin[b]	Taxon ID	CRISPR: CRISPRfinder total (no. of repeats per spacer)	CRISPR: IMG total	ANK	Secondary metabolite gene cluster: Type 1 PKS	Terpene	Other
Anaerolineae							
SAG 1B	2617270794	-	-	1	-	-	-
A154*	2619619053	-	-	2	-	-	-
Caldilineae							
C141*	2619619051	7 (27, 24, 13, 7, 3, 30, 4)	9	9	2	-	-
C174*	2619619055	5 (21, 24, 8, 32, 27)	8	1	-	1	-
SAR202							
S152*	2619619052	5 (7, 34, 26, 7, 4)	9	5	3	4	1
S156*	2619619054	1 (13)	3	2	1	2	1

[a]The absolute numbers of CRISPR arrays defined by CRISPRfinder and IMG, the number of ankyrins and ankyrin repeat-containing proteins (ANK), as well as the number of secondary metabolite (antiSMASH) gene clusters per genome are shown. The IMG Gold Study IDs are Gs0114494 and Gs0099546. Secondary metabolite clusters were found using antiSMASH 3.0; the values are total numbers of genes per genome.
[b]Asterisks on bins indicate extracted metagenome bins from IMG Gold Study ID Gs0099546. The letters of the bins reflect the phylogenetic identity of the bin (A for *Anaerolineae*, C for *Caldilineae*, and S for SAR202).

tion receptors (66). Our findings are in good agreement with general patterns previously found in the metagenomes of sponge symbionts (38, 51), in enriched (mini)metagenomes of cyanobacterial sponge symbionts (59) and single amplified genomes from members of SAUL (20) and *Ca.* Poribacteria (58).

Another example of sponge-symbiont enriched features are the clustered, regularly interspaced, short, palindromic repeats (CRISPRs) and their associated proteins (Cas) that have recently been reported from the genomes of sponge symbionts (20, 38, 50, 51, 59). Here, the investigated *Caldilineae* and SAR202 genomes contained CRISPR-Cas systems, while the two most complete *Anaerolineae* genomes did not (Table 2). The presence of CRISPRs can be explained by the extensive filter-feeding activity of sponge hosts that result in high exposure of sponge symbionts to phages and other sources of free DNA from ambient seawater.

The synthesis of secondary metabolites is an important defense mechanism of sessile organisms such as sponges to protect themselves against predators or biofouling (36). Many of these compounds are in fact produced by the sponge microbiome (10, 36). In particular, genes for polyketide synthases (PKS), nonribosomal peptide synthetases (NRPS), and halogenases are regularly enriched in sponge symbionts, often with new structures and putatively novel activities (51, 67–72). Here, we assessed the genomic repertoire of sponge-associated *Chloroflexi* for secondary metabolism using antiSMASH (73). In both SAR202 genomes and in *Caldilineae* C141, we found up to three polyketide synthase (PKS) gene clusters, all of which showed homologies to the previously reported type I PKS gene cluster from other sponge symbionts. Additional gene clusters for the production of terpenes and other yet to be identified substances were identified in the two SAR202 genomes and in *Caldilineae* C174 (Table 2 and Table S5B). Both *Anaerolineae* genomes did not contain any gene clusters for the biosynthesis of secondary metabolites. While the exact functions of these gene clusters putatively involved in defense remain unknown, it appears that at least SAR202 bacteria and *Caldilineae* have the genomic repertoire for chemical defense within the sponge holobiont.

Ultrastructural identification of sponge-specific *Chloroflexi*. The correlation of probe-specific fluorescence with scanning electron microscopy (SEM) images allowed taxon-specific identification of *Chloroflexi* cells at ultrastructural resolution. Overall, distributions of all three *Chloroflexi* clades in *Aplysina aerophoba* indicate that SAR202 cells were more abundant than the other two *Chloroflexi* classes (Fig. 6). This is consistent with the relative abundances of *Chloroflexi* classes in HMA sponges extracted from EMP data (Fig. 1). Cells belonging to the SAR202 clade (green signals in Fig. 6A and

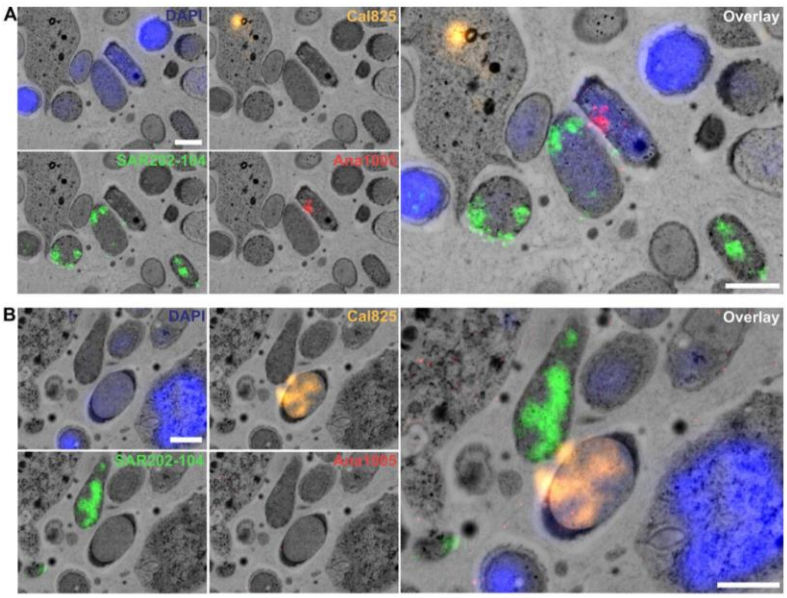

FIG 6 Visualization of sponge-associated *Chloroflexi* in *Aplysina aerophoba* mesohyl using FISH-CLEM. (A and B) SAR202 cells are displayed in green, *Anaerolineae* in red (A), and *Caldilineae* in orange (B). The nucleotide stain DAPI (blue) served as reference for the localization of unstained cells. In both panels, the picture on the right is the overlay of all probes and DAPI. Bars, 1 μm.

B) are generally rod shaped (0.8 μm by 1 to 2 μm) with a regular distribution of cell cytosol content. The *Anaerolineae*-specific probe targeted rod-shaped cells (0.8 by 2.0 μm) (red signal in Fig. 6A). The characteristic feature of *Caldilineae*-positive cells (ca. 1 by 2 μm) was the presence of electron-dense capsules or mucus-like structures located at the cell poles (orange signal in Fig. 6B). All cells that were stained positive with a corresponding FISH probe showed a consistent morphology, which was taken as a measure of probe specificity.

Conclusions. Owing to the lack of cultivation and difficult experimental access for the majority of *Chloroflexi* clades, advancing knowledge has been limited to few lineages (22, 28, 74). The present study provides a new experimental opportunity, as HMA sponges were identified as true *Chloroflexi* hot spots, both in terms of biomass and biodiversity. Metagenomic and single-cell genomic analyses revealed metabolic specialization in that *Anaerolineae* and *Caldilineae* have an expanded gene repertoire for carbohydrate degradation. SAR202 genomes lack transporter and degradation pathways for carbohydrates, and we therefore speculate that they may gain the energy needed by degradation of amino and fatty acids. Similarly, while *Anaerolineae*/*Caldilineae* take up cofactors, SAR202 has the genomic repertoire for their synthesis. A combination of FISH-CLEM allowed us, for the first time, to visualize *Chloroflexi* in the host context and to identify characteristic cellular morphotypes. The results of this study suggest that *Chloroflexi* symbionts have the genomic potential for DOM degradation from seawater, both labile and recalcitrant. These findings are in line with previous reports that have shown extensive carbohydrate degradation potential in other HMA sponge symbionts (10, 19, 20). Thus, we hypothesize that collectively, sponge microbes not only provide nutrients to the HMA sponge host but also contribute to DOM cycling and primary productivity in reef ecosystems via a pathway termed the "sponge loop." Considering the abundance and dominance of sponges in many benthic environments, we predict that the role of sponge symbionts in biogeochemical cycles is larger than previously thought.

MATERIALS AND METHODS

Relative abundance of *Chloroflexi* in high-microbial-abundance sponges. To investigate the abundance of the bacterial phylum *Chloroflexi* on a global scale, microbiome data from HMA sponges, classified and predicted (cluster 1), were obtained from Moitinho-Silva et al. (31). This data set is a rarefied operational taxonomic unit (OTU) abundance matrix (23,455) from the mothur processed data of the Sponge Microbiome Project (31). The abundance of *Chloroflexi* OTUs was grouped according to the class level based on SILVA taxonomy (75). Relative abundances were calculated and displayed using the R packages ggplot2 version 3.0.0 (76) and ggpubr version 0.1.8 (https://CRAN.R-project.org/package=ggpubr). and complete-linkage hierarchical clustering was performed. For this purpose, Bray-Curtis dissimilarities were calculated on relative abundance values of *Chloroflexi* classes/clades within the phylum using the R package vegan version 2.4-5 (https://cran.r-project.org/package=vegan). To test the effect of geography and sponge phylogenetic on the beta diversity of *Chloroflexi* communities, Bray-Curtis dissimilarities were calculated on *Chloroflexi* abundances. Here, the rarified OTU abundance matrix that contained only *Chloroflexi* OTUs from classified and predicted HMA species was used. Samples with less than 100 sequences were excluded from the analysis. Type II permutation MANOVA using distance matrices was performed with RVAideMemoire package version 0.9-69-3 (https://CRAN.R-project.org/package=RVAideMemoire), using 999 permutations and an alpha level of 5%. For this test, each sample was assigned to the geographic region according to their collection sites. Sponge taxonomic order following NCBI taxonomy was used as a proxy of sponge phylogeny. Graphs and tests were performed in R environment version 3.4.3 (https://www.R-project.org/).

Sponge sampling and cell separation and handling. *Aplysina aerophoba* was collected from Piran, Slovenia (45.5099 N; 13.5600 E) in May 2013 and transported to the laboratory in Würzburg, Germany, in ambient seawater. Sponge-associated prokaryotes (SAPs) were enriched from fresh sponge tissues within 1 week of collection, for mesohyl and pinacoderm separately, by differential centrifugation as described previously (32). DNA was extracted from frozen SAP aliquots either from pinacoderm or mesohyl tissue (three replicates each) using the FastDNA SPIN kit for Soil (MP Biomedicals, Illkich, France) by the method of Slaby et al. (21). Briefly, different cell lysis protocols were applied for each triplicate to obtain differential sequencing coverage: (i) bead beating, following the manufacturer's protocol, (ii) freeze-thaw cycling (three cycles of 20 min at −80°C and 20 min at 42°C), (iii) proteinase K digestion for 1 h at 37°C (TE buffer with 0.5% SDS and proteinase K at a final concentration of 100 ng/ml). The quantity and quality of the extracted DNA were assessed by Nanodrop, Qubit high-sensitivity assay, and agarose gel electrophoresis. The DNA from two extraction rounds was pooled for each extraction approach separately, and the six sets of metagenomic DNA were sequenced on an Illumina HiSeq2000 platform (150-bp paired-end reads), quality filtered, and assembled at the DOE Joint Genome Institute (Walnut Creek, CA, USA) within the JGI sequencing and data processing pipeline (77). Differential coverage binning was performed with CONCOCT v. 0.2.1 (78) at default settings utilizing the coverage values from the six metagenomic data sets differing in tissue type and/or cell lysis method. A fasta file for each bin was created with the in-house python script mkBinFasta.py (https://github.com/bslaby/scripts/). Assembly statistics were obtained from QUAST v. 3.1 (79).

Single cells from cell preparations which were freshly prepared from a sponge from Rovinj/Croatia were sorted and their DNA was amplified by the method of Kamke et al. (19) and stored in 96-well plates at −80°C. Single amplified genomes (SAGs) were PCR screened using the universal primers 27f and 1492r to detect *Chloroflexi* 16S rRNA genes (67). SAGs that tested positive for the presence of a single *Chloroflexi* 16S rRNA gene were sequenced at GATC GmbH (Konstanz, Germany) on an Illumina MiSeq personal sequencer (300 bp; paired end). Sequences were trimmed with Trimmomatic-0.32 (minlen 150, avgqual 25, slidingwindow 4:25) (80) and filtered against eukaryotic, archaeal, and *Delftia* reads (known betaproteobacterial contaminant of the single-cell amplification kit) using blastn (nt database). The SAGs were assembled with SPAdes 3.5.0 (--sc, --careful, keep contigs >1000 bp) (81) decontaminated using the IMG/MER (Integrated microbial genomes & environmental samples) web tools following the single-cell data decontamination protocol provided at the JGI webpage (https://img.jgi.doe.gov/w/doc/SingleCellDataDecontamination.pdf). Only contigs showing clearly different GC/kmer frequency profiles from those of the bulk and that were not identified as *Chloroflexi* derived were filtered out. The SAGs were named according to the columns and rows of the 96-well plate they were identified.

Phylogenetic tree construction. 16S rRNA genes from one metagenome bin (S165) and all 13 single amplified genomes (SAGs) were manually quality checked and aligned with closely related sponge- and non-sponge-derived environmental reference sequences obtained from the Silva database (SSU release 132) using the SINA aligner (82). The program MEGA 7.0.4 (83) was used to align the amino acid sequences of 60 genomes, in total 1,914 positions from nine ribosomal proteins (L2, L4, L14, L15, L22, L24, S3, S17, and S19). The determination of best tree construction model (JTT model), and final tree construction (neighbor-joining method) was conducted in MEGA. As references for the protein tree, sequences from publicly available genomes, basically from cultured *Chloroflexi* were included (see Table S1 in the supplemental material). Due to low genome completeness, some of the proteins used were missing in the relevant genomes. For the 16S rRNA gene-based tree, the neighbor-joining method (GTR+G+I model) was also applied using 1,787 positions from 182 sequences. The trees were visualized using iTOL (interactive tree of life; https://itol.embl.de/).

Fluorescence *in situ* hybridization and FISH-CLEM. FISH probes were designed based on the 16S rRNA gene alignment for sponge-specific clades within the classes *Anaerolineae* and *Caldilineae* using the probe design tool implemented in ARB (84). Candidate probes were tested *in silico* for their specific hybridization conditions using different target and nontarget reference sequences using mathFISH (http://mathfish.cee.wisc.edu/). The probes with the best performance were tested for hybridization

specificity on fixed (4% paraformaldehyde) *A. aerophoba* microbial cell preparations by the method of Fieseler et al. (32) using formamide (FA) concentration gradients. Finally, we used for the *Caldilineae* probe Cal825 (5′-[Cy3]-ACACCGCCCACACCTCGT-[Cy3]-3′; *E. coli* binding positions, 825 to 843) and for the *Anaerolineae* probe Ana1005 (5′-[Alexa Fluor 647]-TCCGCTTTCGCTTCCGTA-[Alexa Fluor 647]-3′; *E. coli* binding positions, 1005 to 1023). Additionally, probe SAR202-104 (5′-[Alexa Fluor 488]-GTTACTCAGCCG TCTGCC-[Alexa Fluor 488]-3′; *E. coli* binding positions, 104 to 122) was used to identify members of the SAR202 group in sponges (85). All probes were double labeled at 5′ and 3′ ends (Sigma-Aldrich, Steinheim, Germany). To test the efficiencies of the newly designed sponge-specific *Chloroflexi* probes and the previously published SAR202-104R probe for the sponge microbiome, FISH conditions were optimized using microbial cell preparations from *A. aerophoba*. The three probes did not colocalize using 10%, 20%, and 30% FA, demonstrating specific binding of the probes to the *Chloroflexi* classes/clades in standard FISH experiments (Fig. S1).

For ultrastructural visualization of sponge *Chloroflexi*, we applied a recently established FISH-CLEM (fluorescence *in situ* hybridization-correlative light and electron microscopy) protocol (86). Briefly, freshly sampled *A. aerophoba* sponges were transported to the University of Wuerzburg where small mesohyl discs (2-mm diameter, 200-μm thickness) were subjected to high-pressure freezing (HPF) and freeze substitution. Samples were embedded in LR white, and 100-nm ultrathin sections were cut using a Histo Jumbo Diamond knife (Diatome AG, Biel, Switzerland) on a Leica EM UC7 ultramicrotome (Leica Microsystems, Wetzlar, Germany). The sections were placed on poly-L-lysine-coated slides and subjected to fluorescence *in situ* hybridization with the *Chloroflexi* clade-specific probes at 10% FA concentration (900 mM NaCl, 20 mM Tris-HCl [pH 7.4], 0.01% sodium dodecyl sulfate, 20% dextran sulfate). All three class- or clade-specific probes were cohybridized, and fluorescence signals were detected using an Axio Observer.Z1 microscope equipped with AxioCam 506 and Zen 2 version 2.0.0.0 software (Carl Zeiss Microscopy GmbH, Göttingen, Germany). On the same sections that were used for fluorescence microscopy, scanning electron microscopy (SEM) was carried out using a field emission scanning electron microscope JSM-7500F (JEOL, Japan) with LABE detector (for back scattered electron imaging at extremely low acceleration voltages) directly on the microscope slides. FISH and SEM images of same regions were computer correlated based on sponge heterochromatin pattern by the method of Jahn et al. (86).

Functional genomic analysis. Genomic data from SAG sequences and the extracted metagenome bins were loaded and analyzed in IMG (https://img.jgi.doe.gov/) using the KEGG Orthology (KO) terms assigned to our data sets, and metabolic pathways (KEGG) were analyzed. To identify CRISPR-related genes, CRISPRfinder (http://crispr.i2bc.paris-saclay.fr/Server/) was used. For the search of specific metabolite gene clusters, antiSMASH was used (73). The genomic potential of investigated microbial symbionts to degrade and transform complex carbohydrates was assessed by screening the IMG-predicted open reading frames (ORFs) of the genome data against the dbCAN (47) and classified according to the carbohydrate-active enzymes (CAZymes) database (48).

Data availability. Data sets for SAGs and the metagenomic bins are available at the NCBI Sequence Read Archive under the BioProject accession numbers or identifiers (IDs) PRJNA506133 and PRJNA366444 to PRJNA366449, respectively. Complete assembled and annotated data are available from IMG (https://img.jgi.doe.gov/) under the Gold Study IDs Gs0114494 and Gs0099546 (for more details, see Table 1).

SUPPLEMENTAL MATERIAL

Supplemental material for this article may be found at https://doi.org/10.1128/mSystems.00150-18.

TEXT S1, PDF file, 2 MB.
FIG S1, TIF file, 0.1 MB.
FIG S2, TIF file, 0.8 MB.
FIG S3, TIF file, 0.6 MB.
FIG S4, TIF file, 0.1 MB.
TABLE S1, DOCX file, 0.02 MB.
TABLE S2, DOCX file, 0.02 MB.
TABLE S3, DOCX file, 0.04 MB.
TABLE S4, DOCX file, 0.02 MB.
TABLE S5, DOCX file, 0.01 MB.

ACKNOWLEDGMENTS

We acknowledge Laura Rix and Lucia Pita Galan for many insightful discussions on sponge ecology and Sebastian M. Markert and Christian Stigloher at University of Wuerzburg for help with FISH-CLEM.

This study was supported by DFG (CRC1182-TPB1) and European Union's Horizon 2020 research and innovation program grants (679849 SponGES). M.T.J. was supported by a grant of the German Excellence Initiative to the Graduate School of Life Sciences, University of Wuerzburg. The funders had no role in study design, data collection and interpretation, or the decision to submit the work for publication.

REFERENCES

1. Li CW, Chen JY, Hua TE. 1998. Precambrian sponges with cellular structures. Science 279:879–882.
2. Yin Z, Zhu M, Davidson EH, Bottjer DJ, Zhao F, Tafforeau P. 2015. Sponge grade body fossil with cellular resolution dating 60 Myr before the Cambrian. Proc Natl Acad Sci U S A 112:E1453–E1460. https://doi.org/10.1073/pnas.1414577112.
3. Van Soest RWM, Boury-Esnault N, Vacelet J, Dohrmann M, Erpenbeck D, De Voogd NJ, Santodomingo N, Vanhoorne B, Kelly M, Hooper JNA. 2012. Global diversity of sponges (Porifera). PLoS One 7:e35105. https://doi.org/10.1371/journal.pone.0035105.
4. Bell JJ. 2008. The functional roles of marine sponges. Estuar Coast Shelf Sci 79:341–353. https://doi.org/10.1016/j.ecss.2008.05.002.
5. Maldonado M, Ribes M, van Duyl FC. 2012. Nutrient fluxes through sponges: biology, budgets, and ecological implications. Adv Mar Biol 62:113–182. https://doi.org/10.1016/B978-0-12-394283-8.00003-5.
6. Thomas T, Moitinho-Silva L, Lurgi M, Björk JR, Easson C, Astudillo-García C, Olson JB, Erwin PM, López-Legentil S, Luter H, Chaves-Fonnegra A, Costa R, Schupp PJ, Steindler L, Erpenbeck D, Gilbert J, Knight R, Ackermann G, Victor Lopez J, Taylor MW, Thacker RW, Montoya JM, Hentschel U, Webster NS. 2016. Diversity, structure and convergent evolution of the global sponge microbiome. Nat Commun 7:11870. https://doi.org/10.1038/ncomms11870.
7. McMurray S, Stubler A, Erwin P, Finelli C, Pawlik J. 2018. A test of the sponge-loop hypothesis for emergent Caribbean reef sponges. Mar Ecol Prog Ser 588:1–14. https://doi.org/10.3354/meps12466.
8. Blunt JW, Copp BR, Keyzers RA, Munro MHG, Prinsep MR. 2017. Marine natural products. Nat Prod Rep 34:235–294. https://doi.org/10.1039/c6np00124f.
9. Wilson MC, Mori T, Rückert C, Uria AR, Helf MJ, Takada K, Gernert C, Steffens UAE, Heycke N, Schmitt S, Rinke C, Helfrich EJN, Brachmann AO, Gurgui C, Wakimoto T, Kracht M, Crüsemann M, Hentschel U, Abe I, Matsunaga S, Kalinowski J, Takeyama H, Piel J. 2014. An environmental bacterial taxon with a large and distinct metabolic repertoire. Nature 506:58–62. https://doi.org/10.1038/nature12959.
10. Lackner G, Peters EE, Helfrich EJN, Piel J. 2017. Insights into the lifestyle of uncultured bacterial natural product factories associated with marine sponges. Proc Natl Acad Sci U S A 114:E347–E356. https://doi.org/10.1073/pnas.1616234114.
11. Hentschel U, Usher KM, Taylor MW. 2006. Marine sponges as microbial fermenters. FEMS Microbiol Ecol 55:167–177. https://doi.org/10.1111/j.1574-6941.2005.00046.x.
12. Moitinho-Silva L, Steinert G, Nielsen S, Hardoim CCP, Wu YC, McCormack GP, López-Legentil S, Marchant R, Webster N, Thomas T, Hentschel U. 2017. Predicting the HMA-LMA status in marine sponges by machine learning. Front Microbiol 8:752. https://doi.org/10.3389/fmicb.2017.00752.
13. Pita L, Rix L, Slaby BM, Franke A, Hentschel U. 2018. The sponge holobiont in a changing ocean: from microbes to ecosystems. Microbiome 6:46. https://doi.org/10.1186/s40168-018-0428-1.
14. Bayer K, Moitinho-Silva L, Brümmer F, Cannistraci CV, Ravasi T, Hentschel U. 2014. GeoChip-based insights into the microbial functional gene repertoire of marine sponges (high microbial abundance, low microbial abundance) and seawater. FEMS Microbiol Ecol 90:832–843. https://doi.org/10.1111/1574-6941.12441.
15. Weisz JB, Lindquist N, Martens CS. 2008. Do associated microbial abundances impact marine demosponge pumping rates and tissue densities? Oecologia 155:367–376. https://doi.org/10.1007/s00442-007-0910-0.
16. Ribes M, Jiménez E, Yahel G, López-Sendino P, Diez B, Massana R, Sharp JH, Coma R. 2012. Functional convergence of microbes associated with temperate marine sponges. Environ Microbiol 14:1224–1239. https://doi.org/10.1111/j.1462-2920.2012.02701.x.
17. Hoer DR, Gibson PJ, Tommerdahl JP, Lindquist NL, Martens CS. 2018. Consumption of dissolved organic carbon by Caribbean reef sponges. Limnol Oceanogr 63:337–351. https://doi.org/10.1002/lno.10634.
18. Maldonado M. 2016. Sponge waste that fuels marine oligotrophic food webs: a re-assessment of its origin and nature. Mar Ecol 37:477–491. https://doi.org/10.1111/maec.12256.
19. Kamke J, Sczyrba A, Ivanova N, Schwientek P, Rinke C, Mavromatis K, Woyke T, Hentschel U. 2013. Single-cell genomics reveals complex carbohydrate degradation patterns in poribacterial symbionts of marine sponges. ISME J 7:2287–2300. https://doi.org/10.1038/ismej.2013.111.
20. Astudillo-García C, Slaby BM, Waite DW, Bayer K, Hentschel U, Taylor MW. 2017. Phylogeny and genomics of SAUL, an enigmatic bacterial lineage frequently associated with marine sponges. Environ Microbiol 20:561–576. https://doi.org/10.1111/1462-2920.13965.
21. Slaby BM, Hackl T, Horn H, Bayer K, Hentschel U. 2017. Metagenomic binning of a marine sponge microbiome reveals unity in defense but metabolic specialization. ISME J 11:2465–2478. https://doi.org/10.1038/ismej.2017.101.
22. Landry Z, Swan BK, Herndl GJ, Stepanauskas R, Giovannoni SJ. 2017. SAR202 genomes from the dark ocean predict pathways for the oxidation of recalcitrant dissolved organic matter. mBio 8:e00413-17. https://doi.org/10.1128/mBio.00413-17.
23. Colatriano D, Tran PQ, Guéguen C, Williams WJ, Lovejoy C, Walsh DA. 2018. Genomic evidence for the degradation of terrestrial organic matter by pelagic Arctic Ocean Chloroflexi bacteria. Commun Biol 1:90. https://doi.org/10.1038/s42003-018-0086-7.
24. Woese CR. 1988. Bacterial evolution. Can J Microbiol 34:547–551.
25. Hugenholtz P, Goebel BM, Pace NR. 1998. Impact of culture-independent studies on the emerging phylogenetic view of bacterial diversity. J Bacteriol 180:4765–4774.
26. Gupta RS, Chander P, George S. 2013. Phylogenetic framework and molecular signatures for the class Chloroflexi and its different clades; proposal for division of the class Chloroflexi class. nov. into the suborder Chloroflexineae subord. nov., consisting of the emended family Oscillochlorida. Antonie Van Leeuwenhoek 103:99–119. https://doi.org/10.1007/s10482-012-9790-3.
27. Garrity G, Boone DR, Castenholz RW (ed). 2001. Bergey's manual of systematic bacteriology. Springer, New York, NY.
28. Hug LA, Castelle CJ, Wrighton KC, Thomas BC, Sharon I, Frischkorn KR, Williams KH, Tringe SG, Banfield JF. 2013. Community genomic analyses constrain the distribution of metabolic traits across the Chloroflexi phylum and indicate roles in sediment carbon cycling. Microbiome 1:22. https://doi.org/10.1186/2049-2618-1-22.
29. Campbell AG, Schwientek P, Vishnivetskaya T, Woyke T, Levy S, Beall CJ, Griffen A, Leys E, Podar M. 2014. Diversity and genomic insights into the uncultured Chloroflexi from the human microbiota. Environ Microbiol 16:2635–2643. https://doi.org/10.1111/1462-2920.12461.
30. Edmonds-Wilson SL, Nurinova NI, Zapka CA, Fierer N, Wilson M. 2015. Review of human hand microbiome research. J Dermatol Sci 80:3–12. https://doi.org/10.1016/j.jdermsci.2015.07.006.
31. Moitinho-Silva L, Nielsen S, Amir A, Gonzalez A, Ackermann GL, Cerrano C, Astudillo-Garcia C, Easson C, Sipkema D, Liu F, Steinert G, Kotoulas G, McCormack GP, Feng G, Bell JJ, Vicente J, Björk JR, Montoya JM, Olson JB, Reveillaud J, Steindler L, Pineda MC, Marra MV, Ilan M, Taylor MW, Polymenakou P, Erwin PM, Schupp PJ, Simister RL, Knight R, Thacker RW, Costa R, Hill RT, Lopez-Legentil S, Dailianis T, Ravasi T, Hentschel U, Li Z, Webster NS, Thomas T. 2017. The sponge microbiome project. Gigascience 6:1–7. https://doi.org/10.1093/gigascience/gix077.
32. Fieseler L, Horn M, Wagner M, Hentschel U. 2004. Discovery of the novel candidate phylum "Poribacteria" in marine sponges. Appl Environ Microbiol 70:3724–3732. https://doi.org/10.1128/AEM.70.6.3724-3732.2004.
33. Bayer K, Kamke J, Hentschel U. 2014. Quantification of bacterial and archaeal symbionts in high and low microbial abundance sponges using real-time PCR. FEMS Microbiol Ecol 89:679–690. https://doi.org/10.1111/1574-6941.12369.
34. Hoffmann F, Røy H, Bayer K, Hentschel U, Pfannkuchen M, Brümmer F, De Beer D. 2008. Oxygen dynamics and transport in the Mediterranean sponge Aplysina aerophoba. Mar Biol 153:1257–1264. https://doi.org/10.1007/s00227-008-0905-3.
35. Varela MM, van Aken HM, Herndl GJ. 2008. Abundance and activity of Chloroflexi-type SAR202 bacterioplankton in the meso- and bathypelagic waters of the (sub)tropical Atlantic. Environ Microbiol 10:1903–1911. https://doi.org/10.1111/j.1462-2920.2008.01627.x.
36. Pawlik JR. 2011. The chemical ecology of sponges on Caribbean reefs: natural products shape natural systems. Bioscience 61:888–898. https://doi.org/10.1525/bio.2011.61.11.8.
37. Thrash JC, Seitz KW, Baker BJ, Temperton B, Gillies LE, Rabalais NN, Henrissat B, Mason OU. 2017. Metabolic roles of uncultivated bacterioplankton lineages in the northern Gulf of Mexico "dead zone." mBio 8:e01017-17. https://doi.org/10.1128/mBio.01017-17.
38. Horn H, Slaby BM, Jahn MT, Bayer K, Moitinho-Silva L, Förster F, Abdel-

mohsen UR, Hentschel U. 2016. An enrichment of CRISPR and other defense-related features in marine sponge-associated microbial metagenomes. Front Microbiol 7:1751. https://doi.org/10.3389/fmicb.2016.01751.
39. Michell RH. 2011. Inositol and its derivatives: their evolution and functions. Adv Enzyme Regul 51:84–90. https://doi.org/10.1016/j.advenzreg.2010.10.002.
40. Reynolds TB. 2009. Strategies for acquiring the phospholipid metabolite inositol in pathogenic bacteria, fungi and protozoa: making it and taking it. Microbiology 155:1386–1396. https://doi.org/10.1099/mic.0.025718-0.
41. Müller WE, Rottmann M, Diehl-Seifert B, Kurelec B, Uhlenbruck G, Schröder HC. 1987. Role of the aggregation factor in the regulation of phosphoinositide metabolism in sponges. Possible consequences on calcium efflux and on mitogenesis. J Biol Chem 262:9850–9858.
42. Sutherland IW. 1985. Biosynthesis and composition of Gram-negative bacterial extracellular and wall polysaccharides. Annu Rev Microbiol 39:243–270. https://doi.org/10.1146/annurev.mi.39.100185.001331.
43. Rehm BHA. 2010. Bacterial polymers: biosynthesis, modifications and applications. Nat Rev Microbiol 8:578–592. https://doi.org/10.1038/nrmicro2354.
44. Misevic GN, Burger MM. 1986. Reconstitution of high cell binding affinity of a marine sponge aggregation factor by cross-linking of small low affinity fragments into a large polyvalent polymer. J Biol Chem 261:2853–2859.
45. Misevic GN, Burger MM. 1993. Carbohydrate-carbohydrate interactions of a novel acidic glycan can mediate sponge cell adhesion. J Biol Chem 268:4922–4929.
46. Misevic GN, Finne J, Burger MM. 1987. Involvement of carbohydrates as multiple low affinity interaction sites in the self-association of the aggregation factor from the marine sponge Microciona prolifera. J Biol Chem 262:5870–5877.
47. Yin Y, Mao X, Yang J, Chen X, Mao F, Xu Y. 2012. dbCAN: a web resource for automated carbohydrate-active enzyme annotation. Nucleic Acids Res 40:W445–W451. https://doi.org/10.1093/nar/gks479.
48. Lombard V, Golaconda Ramulu H, Drula E, Coutinho PM, Henrissat B. 2014. The carbohydrate-active enzymes database (CAZy) in 2013. Nucleic Acids Res 42:D490–D495. https://doi.org/10.1093/nar/gkt1178.
49. Garrone R, Thiney Y, Pavans de Ceccatty M. 1971. Electron microscopy of a mucopolysaccharide cell coat in sponges. Experientia 27:1324–1326. https://doi.org/10.1007/BF02136717.
50. Thomas T, Rusch D, DeMaere MZ, Yung PY, Lewis M, Halpern A, Heidelberg KB, Egan S, Steinberg PD, Kjelleberg S. 2010. Functional genomic signatures of sponge bacteria reveal unique and shared features of symbiosis. ISME J 4:1557–1567. https://doi.org/10.1038/ismej.2010.74.
51. Fan L, Reynolds D, Liu M, Stark M, Kjelleberg S, Webster NS, Thomas T. 2012. Functional equivalence and evolutionary convergence in complex communities of microbial sponge symbionts. Proc Natl Acad Sci U S A 109:E1878–E1887. https://doi.org/10.1073/pnas.1203287109.
52. Hentschel U, Piel J, Degnan SM, Taylor MW. 2012. Genomic insights into the marine sponge microbiome. Nat Rev Microbiol 10:641–654. https://doi.org/10.1038/nrmicro2839.
53. Radax R, Hoffmann F, Rapp HT, Leininger S, Schleper C. 2012. Ammonia-oxidizing archaea as main drivers of nitrification in cold-water sponges. Environ Microbiol 14:909–923. https://doi.org/10.1111/j.1462-2920.2011.02661.x.
54. Fiore CL, Labrie M, Jarett JK, Lesser MP. 2015. Transcriptional activity of the giant barrel sponge, Xestospongia muta holobiont: molecular evidence for metabolic interchange. Front Microbiol 6:364. https://doi.org/10.3389/fmicb.2015.00364.
55. Eichhorn E, Van Der Ploeg JR, Leisinger T. 1999. Characterization of a two-component alkanesulfonate monooxygenase from Escherichia coli. J Biol Chem 274:26639–26646.
56. Griffin M, Trudgill PW. 1972. The metabolism of cyclopentanol by Pseudomonas N.C.I.B. 9872. Biochem J 129:595–603.
57. King CE, King GM. 2014. Description of Thermogemmatispora carboxidivorans sp. nov., a carbon-monoxide-oxidizing member of the class Ktedonobacteria isolated from a geothermally heated biofilm, and analysis of carbon monoxide oxidation by members of the class Ktedonobacteria. Int J Syst Evol Microbiol 64:1244–1251. https://doi.org/10.1099/ijs.0.059675-0.
58. Kamke J, Rinke C, Schwientek P, Mavromatis K, Ivanova N, Sczyrba A, Woyke T, Hentschel U. 2014. The candidate phylum Poribacteria by single-cell genomics: new insights into phylogeny, cell-compartmentation, eukaryote-like repeat proteins, and other genomic features. PLoS One 9:e87353. https://doi.org/10.1371/journal.pone.0087353.
59. Burgsdorf I, Slaby BM, Handley KM, Haber M, Blom J, Marshall CW, Gilbert JA, Hentschel U, Steindler L. 2015. Lifestyle evolution in cyanobacterial symbionts of sponges. mBio 6:e00391-15. https://doi.org/10.1128/mBio.00391-15.
60. Liu M, Fan L, Zhong L, Kjelleberg S, Thomas T. 2012. Metaproteogenomic analysis of a community of sponge symbionts. ISME J 6:1515–1525. https://doi.org/10.1038/ismej.2012.1.
61. Díez-Vives C, Moitinho-Silva L, Nielsen S, Reynolds D, Thomas T. 2017. Expression of eukaryotic-like protein in the microbiome of sponges. Mol Ecol 26:1432–1451. https://doi.org/10.1111/mec.14003.
62. Reynolds D, Thomas T. 2016. Evolution and function of eukaryotic-like proteins from sponge symbionts. Mol Ecol 25:5242–5253. https://doi.org/10.1111/mec.13812.
63. Nguyen MTHD, Liu M, Thomas T. 2014. Ankyrin-repeat proteins from sponge symbionts modulate amoebal phagocytosis. Mol Ecol 23:1635–1645. https://doi.org/10.1111/mec.12384.
64. Cerveny L, Straskova A, Dankova V, Hartlova A, Ceckova M, Staud F, Stulik J. 2013. Tetratricopeptide repeat motifs in the world of bacterial pathogens: role in virulence mechanisms. Infect Immun 81:629–635. https://doi.org/10.1128/IAI.01035-12.
65. Matsushima N, Enkhbayar P, Kamiya M, Osaki M, Kretsinger R. 2005. Leucine-rich repeats (LRRs): structure, function, evolution and interaction with ligands. Drug Des Rev - Online 2:305–322. https://doi.org/10.2174/1567269054087613.
66. Ng ACY, Eisenberg JM, Heath RJW, Huett A, Robinson CM, Nau GJ, Xavier RJ. 2011. Human leucine-rich repeat proteins: a genome-wide bioinformatic categorization and functional analysis in innate immunity. Proc Natl Acad Sci U S A 108:4631–4638. https://doi.org/10.1073/pnas.1000093107.
67. Bayer K, Scheuermayer M, Fieseler L, Hentschel U. 2013. Genomic mining for novel FADH2-dependent halogenases in marine sponge-associated microbial consortia. Mar Biotechnol 15:63–72. https://doi.org/10.1007/s10126-012-9455-2.
68. Hooper JA, Van Soest RM. 2002. Systema Porifera: a guide to the classification of sponges. Springer US, Boston, MA.
69. Taylor MW, Radax R, Steger D, Wagner M. 2007. Sponge-associated microorganisms: evolution, ecology, and biotechnological potential. Microbiol Mol Biol Rev 71:295–347. https://doi.org/10.1128/MMBR.00040-06.
70. Siegl A, Hentschel U. 2010. PKS and NRPS gene clusters from microbial symbiont cells of marine sponges by whole genome amplification. Environ Microbiol Rep 2:507–513. https://doi.org/10.1111/j.1758-2229.2009.00057.x.
71. Pimentel-Elardo SM, Grozdanov L, Proksch S, Hentschel U. 2012. Diversity of nonribosomal peptide synthetase genes in the microbial metagenomes of marine sponges. Mar Drugs 10:1192–1202. https://doi.org/10.3390/md10061192.
72. Rua CPJ, de Oliveira LS, Froes A, Tschoeke DA, Soares AC, Leomil L, Gregoracci GB, Coutinho R, Hajdu E, Thompson CC, Berlinck RGS, Thompson FL. 2018. Microbial and functional biodiversity patterns in sponges that accumulate bromopyrrole alkaloids suggest horizontal gene transfer of halogenase genes. Microb Ecol 76:825–838. https://doi.org/10.1007/s00248-018-1172-6.
73. Weber T, Blin K, Duddela S, Krug D, Kim HU, Bruccoleri R, Lee SY, Fischbach MA, Müller R, Wohlleben W, Breitling R, Takano E, Medema MH. 2015. antiSMASH 3.0—a comprehensive resource for the genome mining of biosynthetic gene clusters. Nucleic Acids Res 43:W237–W243. https://doi.org/10.1093/nar/gkv437.
74. Mehrshad M, Rodriguez-Valera F, Amoozegar MA, López-García P, Ghai R. 2018. The enigmatic SAR202 cluster up close: shedding light on a globally distributed dark ocean lineage involved in sulfur cycling. ISME J 12:655–668. https://doi.org/10.1038/s41396-017-0009-5.
75. Yilmaz P, Parfrey LW, Yarza P, Gerken J, Pruesse E, Quast C, Schweer T, Peplies J, Ludwig W, Glöckner FO. 2014. The SILVA and "All-species Living Tree Project (LTP)" taxonomic frameworks. Nucleic Acids Res 42:D643–D648. https://doi.org/10.1093/nar/gkt1209.
76. Wickham H. 2016. ggplot2: elegant graphics for data analysis. Springer-Verlag, New York, NY.
77. Markowitz VM, Chen I-MA, Palaniappan K, Chu K, Szeto E, Grechkin Y, Ratner A, Jacob B, Huang J, Williams P, Huntemann M, Anderson I, Mavromatis K, Ivanova NN, Kyrpides NC. 2012. IMG: the Integrated

Microbial Genomes database and comparative analysis system. Nucleic Acids Res 40:D115–D122. https://doi.org/10.1093/nar/gkr1044.
78. Alneberg J, Bjarnason BS, De Bruijn I, Schirmer M, Quick J, Ijaz UZ, Lahti L, Loman NJ, Andersson AF, Quince C. 2014. Binning metagenomic contigs by coverage and composition. Nat Methods 11:1144–1146. https://doi.org/10.1038/nmeth.3103.
79. Gurevich A, Saveliev V, Vyahhi N, Tesler G. 2013. QUAST: quality assessment tool for genome assemblies. Bioinformatics 29:1072–1075. https://doi.org/10.1093/bioinformatics/btt086.
80. Bolger AM, Lohse M, Usadel B. 2014. Trimmomatic: a flexible trimmer for Illumina sequence data. Bioinformatics 30:2114–2120. https://doi.org/10.1093/bioinformatics/btu170.
81. Bankevich A, Nurk S, Antipov D, Gurevich AA, Dvorkin M, Kulikov AS, Lesin VM, Nikolenko SI, Pham S, Prjibelski AD, Pyshkin AV, Sirotkin AV, Vyahhi N, Tesler G, Alekseyev MA, Pevzner PA. 2012. SPAdes: a new genome assembly algorithm and its applications to single-cell sequencing. J Comput Biol 19:455–477. https://doi.org/10.1089/cmb.2012.0021.
82. Pruesse E, Peplies J, Glöckner FO. 2012. SINA: accurate high-throughput multiple sequence alignment of ribosomal RNA genes. Bioinformatics 28:1823–1829. https://doi.org/10.1093/bioinformatics/bts252.
83. Kumar S, Stecher G, Tamura K. 2016. MEGA7: Molecular Evolutionary Genetics Analysis version 7.0 for bigger datasets. Mol Biol Evol 33:1870–1874. https://doi.org/10.1093/molbev/msw054.
84. Ludwig W, Strunk O, Westram R, Richter L, Meier H, Yadhukumar, Buchner A, Lai T, Steppi S, Jobb G, et al. 2004. ARB: a software environment for sequence data. Nucleic Acids Res 32:1363–1371. https://doi.org/10.1093/nar/gkh293.
85. Morris RM, Rappé MS, Urbach E, Connon SA, Giovannoni SJ. 2004. Prevalence of the Chloroflexi-related SAR202 bacterioplankton cluster throughout the mesopelagic zone and deep ocean. Appl Environ Microbiol 70:2836–2842. https://doi.org/10.1128/AEM.70.5.2836-2842.2004.
86. Jahn MT, Markert SM, Ryu T, Ravasi T, Stigloher C, Hentschel U, Moitinho-Silva L. 2016. Shedding light on cell compartmentation in the candidate phylum Poribacteria by high resolution visualisation and transcriptional profiling. Sci Rep 6:35860. https://doi.org/10.1038/srep35860.
87. Yamada T, Sekiguchi Y. 2009. Cultivation of uncultured *Chloroflexi* subphyla: significance and ecophysiology of formerly uncultured *Chloroflexi* "subphylum I" with natural and biotechnological relevance. Microbes Environ 24:205–216. https://doi.org/10.1264/jsme2.ME09151S.

CHAPTER 5

INTEGRATED METABOLISM IN SPONGE-MICROBE SYMBIOSIS REVEALED BY GENOME-CENTERED METATRANSCRIPTOMICS

Moitinho-Silva, L., Diez-Vives, C., Batani, G., Esteves, A.I., **Jahn, M.T.**, Thomas, T

The ISME Journal, 2017

doi: 10.1038/ismej.2017.25

The ISME Journal (2017), 1–16

www.nature.com/ismej

ORIGINAL ARTICLE

Integrated metabolism in sponge–microbe symbiosis revealed by genome-centered metatranscriptomics

Lucas Moitinho-Silva[1], Cristina Díez-Vives[1], Giampiero Batani[1], Ana IS Esteves[1], Martin T Jahn[2] and Torsten Thomas[1]
[1]*Centre for Marine Bio-Innovation and School of Biological, Earth and Environmental Sciences, The University of New South Wales, Sydney, New South Wales, Australia and* [2]*Marine Microbiology, GEOMAR Helmholtz Centre for Ocean Research, Kiel, Germany*

Despite an increased understanding of functions in sponge microbiomes, the interactions among the symbionts and between symbionts and host are not well characterized. Here we reconstructed the metabolic interactions within the sponge *Cymbastela concentrica* microbiome in the context of functional features of symbiotic diatoms and the host. Three genome bins (CcPhy, CcNi and CcThau) were recovered from metagenomic data of *C. concentrica*, belonging to the proteobacterial family *Phyllobacteriaceae*, the *Nitrospira* genus and the thaumarchaeal order *Nitrosopumilales*. Gene expression was estimated by mapping *C. concentrica* metatranscriptomic reads. Our analyses indicated that CcPhy is heterotrophic, while CcNi and CcThau are chemolithoautotrophs. CcPhy expressed many transporters for the acquisition of dissolved organic compounds, likely available through the sponge's filtration activity and symbiotic carbon fixation. Coupled nitrification by CcThau and CcNi was reconstructed, supported by the observed close proximity of the cells in fluorescence *in situ* hybridization. CcPhy facultative anaerobic respiration and assimilation by diatoms may consume the resulting nitrate. Transcriptional analysis of diatom and sponge functions indicated that these organisms are likely sources of organic compounds, for example, creatine/creatinine and dissolved organic carbon, for other members of the symbiosis. Our results suggest that organic nitrogen compounds, for example, creatine, creatinine, urea and cyanate, fuel the nitrogen cycle within the sponge. This study provides an unprecedented view of the metabolic interactions within sponge–microbe symbiosis, bridging the gap between cell- and community-level knowledge.
The ISME Journal advance online publication, 24 March 2017; doi:10.1038/ismej.2017.25

Introduction

A wide range of animals are found in symbiosis with microorganisms, from basal metazoans, such as marine sponges (phylum *Porifera*), to humans (phylum *Chordata*) (Taylor *et al.*, 2007; Cho and Blaser, 2012). Animal–microbe symbioses encompass a variety of acquisition modes (that is, vertical, horizontal and a combination of both; for example, Cary and Giovannoni (1993); Kikuchi *et al.* (2007); Schmitt *et al.* (2008)), and levels of diversity (ranging from monoclonal populations to highly complex assemblages; Martens *et al.* (2003); Schmitt *et al.* (2012)). Additionally, a gradient of interactions may occur, ranging from competition to mutualism (Dethlefsen *et al.*, 2007; Coyte *et al.*, 2015; Thomas *et al.*, 2016). To account for this spectrum of patterns, Douglas and Werren (2016) have recently argued that host–microbe symbioses are productively approached as ecological communities. Therefore, to further our understanding of the biology of animal–microbe symbioses, research should contemplate the members of the association, that is, the microbial populations and the host, and how they relate to each other.

Marine sponges are filter-feeders found in a wide range of benthic environments, across gradients of depth and latitude (Wulff, 2012). Sponges perform a broad range of functional roles in benthic habitats (Bell, 2008), including the retention of nutrients and energy within the coral reef through the consumption of dissolved organic matter (DOM) and high cell turnover rates (Yahel *et al.*, 2003; de Goeij *et al.*, 2013). In addition to DOM, sponges feed on detritus and microorganisms of diverse sizes (from 0.5 to 70 μm) (Marta *et al.*, 1999; Hadas *et al.*, 2009). Owing to their basal position in metazoans phylogeny and their association with microbial communities, sponges are emerging as models for the evolutionary study of animal–microbe symbiosis (for example, Fan *et al.*, 2012; Ryu *et al.*, 2016).

Microbial communities can account for up to 40% of the sponge tissue volume and often contain novel and uncharacterized diversity (Taylor *et al.*, 2007; Schmitt *et al.*, 2012). Microorganisms are generally

Correspondence: T Thomas, Centre of Marine Bio-Innovation and School of Biological, Earth and Environmental Sciences, The University of New South Wales, High Street, Sydney, New South Wales 2052, Australia.
E-mail: t.thomas@unsw.edu.au
Received 3 October 2016; revised 10 January 2017; accepted 19 January 2017

found in the animal's extracellular matrix (mesohyl), although they are not restricted to this location (Taylor *et al.*, 2007). Owing to the lack of culturable representatives of the microbiome, most of the understanding of the functional roles of microbial symbiont have been acquired by approaches either centered on the community, for example, using meta-omics, 16S rRNA gene analysis and compound-uptake experiments, or on specific genomes, pathways and genes (reviewed by Taylor *et al.*, 2007 and Webster and Thomas 2016). Together, these studies have revealed important metabolic attributes of sponge-associated microorganisms, such as different energy acquisition strategies (for example, heterotrophism and autotrophism), complex element cycling, functional equivalence, production of bioactive compounds and nutrient transfer to the host (Hoffmann *et al.*, 2009; Fan *et al.*, 2012; Freeman *et al.*, 2013; Kamke *et al.*, 2013; Wilson *et al.*, 2014). Nevertheless, the metabolic interactions among the microbiome members and between them and the host cells are rarely explored and thus remain largely unknown (Webster and Thomas, 2016).

The sponge *Cymbastela concentrica* contains consistently dominant and uncharacterized alphaproteobacterial symbionts, particularly within the family *Phyllobacteriaceae* (Taylor *et al.*, 2004; Fan *et al.*, 2012; Esteves *et al.*, 2016) as well as community members belonging to the *Gammaproteobacteria*, the *Nitrospira* and the archaeal phylum *Thaumarchaeota* among others (Fan *et al.*, 2012; Esteves *et al.*, 2016). In addition, *C. concentrica* hosts an abundant population of diatoms (Taylor, 2005). The overall community composition and function of the *C. concentrica* microbiome have been previously characterized on the community level using metagenomics, metaproteomics and metatranscriptomics (Díez-Vives *et al.*, 2016; Thomas *et al.*, 2010; Liu *et al.*, 2011; Fan *et al.*, 2012; Liu *et al.*, 2012). Here we build on these data sets to unveil nutritional interactions in *C. concentrica*. Towards this goal, we reconstructed three new prokaryotic genomes and estimated their activity by analyzing metatranscriptomic sequences, while metabolic features of the sponge and diatoms were inferred from an eukaryotic transcriptomic data set produced from *C. concentrica*.

Materials and methods

Genome assembly, binning and annotation

Metagenomic shotgun sequencing reads for three replicates (BBAY40, 41 and 42) of the microbiome of *C. concentrica* from a previous study (Fan *et al.*, 2012) were co-assembled using the Newbler assembler (Roche, Penzberg, Germany). Sequence reads for each replicate were then mapped back against assembled contigs >500 bp using the Bowtie aligner (Langmead *et al.*, 2009). Coverage file and contigs were then used to bin and refine genomes using the GroopM tool (Imelfort *et al.*, 2014). Genome bins were checked for completeness and contamination using CheckM (Parks *et al.*, 2015) and then annotated using the IMG system (Markowitz *et al.*, 2014). Genome assembly and annotation are avaiable at IMG (http://img.jgi.doe.gov) under the genome IDs 2608642157, 2608642160 and 2626541593. Phylogenetic analysis of 16S rRNA genes and deduced amino-acid sequences for those bins are described in Supplementary Information.

Transcriptomic analysis

We used the metatranscriptomic reads from the microbiome of three *C. concentrica* individuals (Díez-Vives *et al.*, 2016) to estimate the gene expression of binned genomes. Briefly, mRNA was previously enriched from three individuals (ind1, ind2, and ind3; biological replicates), which were processed with Dynabeads Oligo $(dT)_{25}$ (Thermo Fisher Scientific, Waltham, MA, USA) and the Ribo-Zero Bacteria Kit (Epicentre, Madison, WI, USA) in technical replicates (aR and bR). Enriched prokaryotic mRNA was sequenced with HiSeq2000 platform (Illumina, San Diego, CA, USA) with 100 bp paired-end reads. Transcript expression for the coding DNA sequences (CDS) of each genome bin was estimated with RSEM v. 1.2.21 (Li and Dewey, 2011) with default parameters, which implements the Bowtie aligner (Langmead *et al.*, 2009). Transcripts per million (TPM) measures were used as estimations of expression (Li *et al.*, 2010; Wagner *et al.*, 2012). Gene expression estimates in each sponge individual were obtained by averaging TPM values of the technical replicates. Only genes with mapped reads (replicate-average TPM>0) coming from at least two of the three sponge individuals were considered expressed. The global expression estimate for each gene was obtained by averaging TPM values (TPM_{av}) across the three sponge individuals.

The analysis of eukaryotic transcripts is described in Supplementary Information. Briefly, transcripts were taxonomically sorted using the Lowest Common Ancestor algorithm implemented in MEGAN v. 5.11.3 (Huson *et al.*, 2011). Peptides deduced from predicted coding sequences were annotated based on the Kyoto Encyclopedia of Genes and Genomes (KEGG) Orthology (KO). Expression estimates of KEGG functions were calculated by summing TPM values (TPM_{sum}) across coding sequences.

Localization analysis of symbionts

Three individuals of *C. concentrica* were collected by SCUBA diving from Botany Bay near Bare Island, Sydney, Australia (33.99222° S, 151.23111° E) during October 2015. Specimens were processed, fixed and dehydrated. Probes specific for the obtained genome bins (that is, CcPhy, CcNi and CcThau; see

Table 1 Assembly and annotation statistics of genome bins

	CcPhy (Ga0068441)	*CcNi (Ga0068443)*	*CcThau (Ga0078905)*
Assembly size (bp)	2 116 962	1 594 656	2 161 854
Individual coverage in three replicate metagenomes	19.5 × /58.4 × /37.5 ×	3.2 × /0.8 × /7.2 ×	0.9 × /15.2 × /2.3 ×
Estimated genome completeness (%)	69.17	66.56	97.12
Estimated contamination (%)	0.39	0	4.01
Number of contigs	918	126	637
Average GC content (%)	60.34	48.03	38.42
Number of CDS	2411	1679	2745
Number of rRNA genes	1	3	5
Number of tRNA genes	16	25	44

Abbreviations: CDS, coding DNA sequence; GC, guanine–cytosine; rRNA, ribosomal RNA; tRNA, transfer RNA.

below) were designed and cells were detected using fluorescence *in situ* hybridization. Sample processing, probe design and fluorescence *in situ* hybridization conditions are fully described in Supplementary Information.

Results and discussion

Genomes and transcriptomes of the dominant community members in C. concentrica

Three genomes were reconstructed (Table 1) from a previous metagenomic sequence data set of the microbial community of *C. concentrica* (Fan *et al.*, 2012). Phylogenetic analysis of the 16S rRNA gene sequence recovered from one of the genomes (Ga0068441) placed it with members of the family *Phyllobacteriaceae*, order *Rhizobiales*, class *Alphaproteobacteria* (Supplementary Information; Supplementary Figure S1). Thus the genome will be hereafter referred to as CcPhy (*C. concentrica Phyllobacteriaceae*). The 16S rRNA gene sequence is only 96% similar to its closest cultured bacterium (*Mesorhizobium amorphae* CCNWGS0123) and has >99% similarity to sequences that have been previously found in *C. concentrica* (for example, GenBank: AY942778.1). The cluster represented by these *C. concentrica*-derived sequences represents a distinct and novel clade within the *Phyllobacteriaceae* (Supplementary Figure S1). The 16S rRNA gene sequence of the second genome (Ga0068443) was phylogenetically close to other sequences derived from several sponge species (for example, *Agelas dilatata*, *Geodia barretti*, *Xestospongia testudinaria*). These sequences were related yet distinct from sequences of the lineage IV of the *Nitrospira* genus within the phylum *Nitrospirae* (Supplementary Information; Supplementary Figure S2). The genome will be hereafter named CcNi. The 16S rRNA gene sequence of the last genome obtained (Ga0078905) clustered within the candidate order *Nitrosopumilales* (known as group I.1a) (Konneke *et al.*, 2005; Stieglmeier *et al.*, 2014b) within the *Thaumarchaeota* phylum (Supplementary Information; Supplementary Figure S3). It will be referred as CcThau. The 16S rRNA sequence from CcThau was 99% similar to the sequence from *Candidatus* Nitrosopumilus sediminis AR2 (GenBank: CP003843.1). According to studies based on OTUs recovered from metagenomic data sets and 16S rRNA gene sequencing, these three organisms are among the most dominant members of the *C. concentrica* microbiome (Thomas *et al.*, 2010; Fan *et al.*, 2012; Esteves *et al.*, 2016). For example, based on 16S rRNA gene sequencing, the *Phyllobacteriaceae* OTU may account approximately 17% of all bacteria in the sponge, while the *Nitrospira* OTU has a relative abundance of ~6% (Thomas *et al.*, 2010). Metagenomic sequencing further indicated that the thaumarchaeal organism has similar relative abundances than the *Nitrospira* bacterium (Fan *et al.*, 2012).

CcThau has the largest genome assembly with a size of 2.16 mega basepairs (Mb), followed by CcPhy with 2.11 Mb and CcNi with 1.59 Mb (Table 1). Genome completeness estimations based on lineage-specific marker genes were higher in CcThau (97.12%) in comparison to CcPhy (69.17%) and CcNi (66.56%). The estimated contamination of genome bins was low, ranging from 0% to 4.01%. GC content varied from 38.42% for CcThau and 48.03% for CcNi to 60.34% for CcPhy. Metatranscriptomic sequencing reads mapped to these genomes at different extent, where most of the reads mapped to the CcThau CDS (88 303 ± 23 580; mean ± s.d.), followed by CcPhy (16 540 ± 6128) and CcNi (7054 ± 3542) (Supplementary Table S1). Expressed genes represented 86.7% of the total CDS in CcPhy (2092 of 2411), 80.5% in CcNi (1353 of 1679) and 64.6% in CcThau (1775 of 2745). High gene expression correlation among biological replicates, as estimated by TPM values, indicated low variability between sponge individuals (Supplementary Information; Supplementary Figures S4). Average TPM values (TPM_{av}) of expressed genes across sponge individuals varied from 1.09 to 27 022.43, with a median of 191.54 in CcPhy, 354.2 in CcNi and 49.18 in CcThau (Supplementary Figure S7).

A heterotrophic, facultative anaerobic metabolism of CcPhy

The genomic and transcriptomic data suggest that the population represented by CcPhy has a

heterotrophic metabolism, which is broadly consistent with other members of the family *Phyllobacteriaceae* (Willems, 2014). The CcPhy expressed an almost complete set of genes for glycolysis (Embden–Meyerhof–Parnas pathway) (TPM_{av} 24–343; lower value – higher value), as well as the anabolic enzyme fructose-1,6-bisphosphatase (TPM_{av} 281 ± 39; mean ± s.d.) and tricarboxylic acid (TCA) pathways (TPM_{av} 121–1396), which are linked by the pyruvate dehydrogenase complex (TPM_{av} 88–1316) (Figure 1; Supplementary Table S2). Additionally, CcPhy is able to process sugars via the pentose phosphate pathway. In support of a heterotrophic lifestyle, approximately 13.5% of the protein-coding genes ($n = 328$) were involved in membrane transport (according to Transporter Classification Database (TCDB); Supplementary Table S2). From these, 164 CDS were assigned to the adenosine triphosphate (ATP)-binding cassette (ABC) superfamily (TC: 3. A.1), which were among the most expressed genes in the CcPhy transcriptome (Figure 2). The most expressed genes classified by TCDB encoded for components of different transport systems involved in the uptake of general L-amino acids, glycine betaine/proline, multiple sugars, spermidine/putrescine, monosaccharides, mannitol/chloroaromatic compounds, amino acid/amide and manose/fructose/ribose. Genes encoding for Amt-type ammonium transporters (TPM_{av} 1729 ± 351) and the glutamine synthase-glutamine oxoglutarate aminotransferase pathway (TPM_{av} 168–1157) were expressed, allowing for import and assimilation of extracellular ammonium (Javelle *et al.*, 2005).

Genes for the malate synthase and isocitrate lyase (TPM_{av} 211–605) were also expressed. These two enzymes are key for the glyoxylate cycle and their expression is an indication of aerobic growth on fatty acids and acetate (White, 2007). Active uptake of fatty acids could be carried by the product of expressed genes encoding for the proposed fatty acid transporter family (TPM_{av} 80–790). Several genes, whose products are involved in the fatty acid β-oxidation pathway and the downstream propanoyl-CoA degradation pathway were also found expressed (TPM_{av} 88–790) (Supplementary Table S2). Despite existing characterization of the fatty acid contents in sponges and associated bacteria (Gillan *et al.*, 1988; Koopmans *et al.*, 2015), this is to our knowledge the first report of heterotrophic fatty acid-based metabolism of bacteria associated with sponges. Future research focusing on the importance of fatty acids as energy source for sponge microbiome members and the origin of these compounds has the potential to elucidate the ecological relevance of this metabolic feature.

Creatinine degradation via creatine is used by bacteria to assimilate carbon and/or nitrogen (Kim *et al.*, 1986; Shimizu *et al.*, 1986). CcPhy expressed genes related to the degradation of creatine to glycine, that is, creatinase (TPM_{av} 151 ± 25) and the sarcosine oxidase alpha, beta, gamma and delta subunits (TPM_{av} 122–296). A gene encoding for creatinine amidohydrolase was present in the genome but not expressed. Urea is a product of this pathway, which is generated by the hydrolysis of creatine by creatinase (Shimizu *et al.*, 1986). The genome bin CcPhy lacked genes encoding for enzymes involved in the breakdown of urea into ammonium and inorganic carbon (Solomon *et al.*, 2010). Because the genome is not complete and the fact that urease activity has been described in the species of the *Phyllobacteriaceae* family (for example, Peix *et al.*, 2005), the existence and expression of *Phyllobacteriaceae*-like urease genes was further investigated for the *C. concentrica* microbiome. We found transcripts encoding for sequences similar to urease subunits and accessory proteins in the metatranscriptome of *C. concentrica* (Díez-Vives *et al.*, 2016), but none were related to sequences from *Phyllobacteriaceae* (Supplementary Information; Supplementary Table S3), further corroborating the absence of urea breakdown in CcPhy.

Members of the *Phyllobacteriaceae* family are described as having respiratory metabolism with oxygen as the terminal electron acceptor, while anaerobic nitrate respiration and facultative chemolithotrophic metabolism also exist for some members of the family (Willems, 2014). CcPhy has the genetic repertoire to thrive in a variety of oxygenic conditions. The genome encodes for the subunits of two different heme–copper terminal oxidases, the mitochondrial-like aa3-type cytochrome *c* oxidase and the cbb3-type cytochrome *c* oxidase. Both these oligomeric cytochrome complexes transfer electrons of the respiratory chain to its final destination, oxygen, but have different O_2 affinities and can be differentially regulated according to available oxygen concentrations (Garcia-Horsman *et al.*, 1994; Morris and Schmidt, 2013). For instance, in *Bradyrhizobium japonicum* (family *Bradyrhizobiaceae*) the low affinity aa3-type is favored in fully aerobic conditions, while the high affinity cbb3-type is used in microaerobic conditions (Gabel and Maier, 1993; Preisig *et al.*, 1996; Swem *et al.*, 2001).

Genomic data also indicated that, in the absence of O_2, CcPhy can perform nitrate (NO_3^-) respiration, where the membrane-bound nitrate reductase NarGHI complex transfers the electrons to nitrate, reducing it to nitrite (NO_2^-; Bertero *et al.*, 2003). In this case, it is likely that nitrite is excreted via a nitrate/nitrite transporter NarK as the final product of the CcPhy anaerobic respiration. Nitrite excretion is likely because the genome lacked genes encoding for enzymes capable to further reduce nitrite to nitric oxide (NO), that is, a copper or a cytochrome cd1-containing nitrite reductase (NirK and NirS, respectively), or to ammonium (NH_4^+), that is, cytochrome *c* nitrite reductase (NrfA) (Kraft *et al.*, 2011; Zheng *et al.*, 2013). The components and related genes of the cytochrome *c* oxidases and respiratory nitrate reductase were all expressed and also at similar

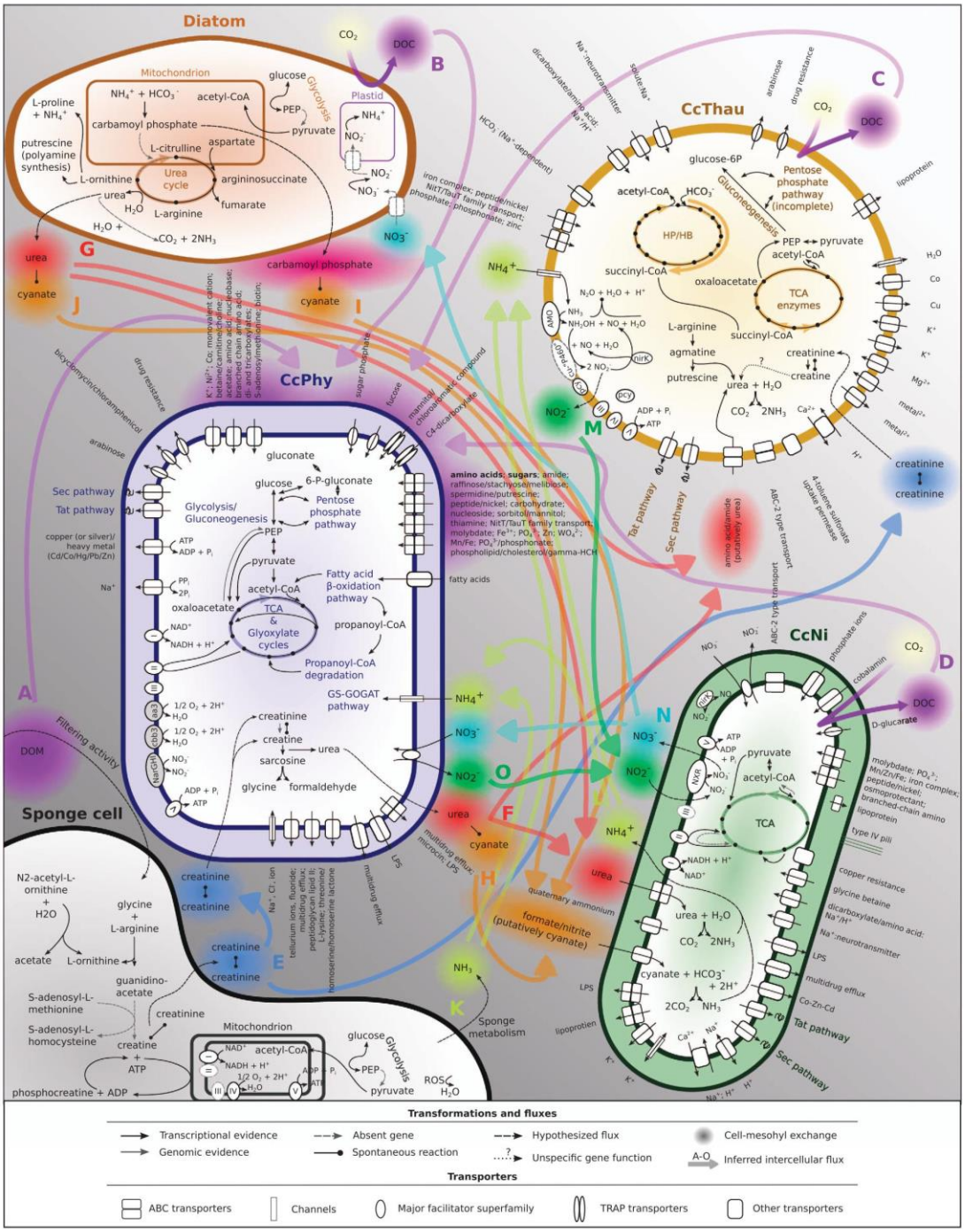

Figure 1 Predicted model of integrated metabolic processes within *Cymbastela concentrica*. Selected pathways and gene functions are shown. Transporters with at least partial genomic evidence and expression detected were included. Inferred nutrient fluxes (A–O) are discussed in the section 'Model of integrated metabolism of the microbial community members in *C. concentrica*'. Expressed genes are listed in Supplementary Tables S2.

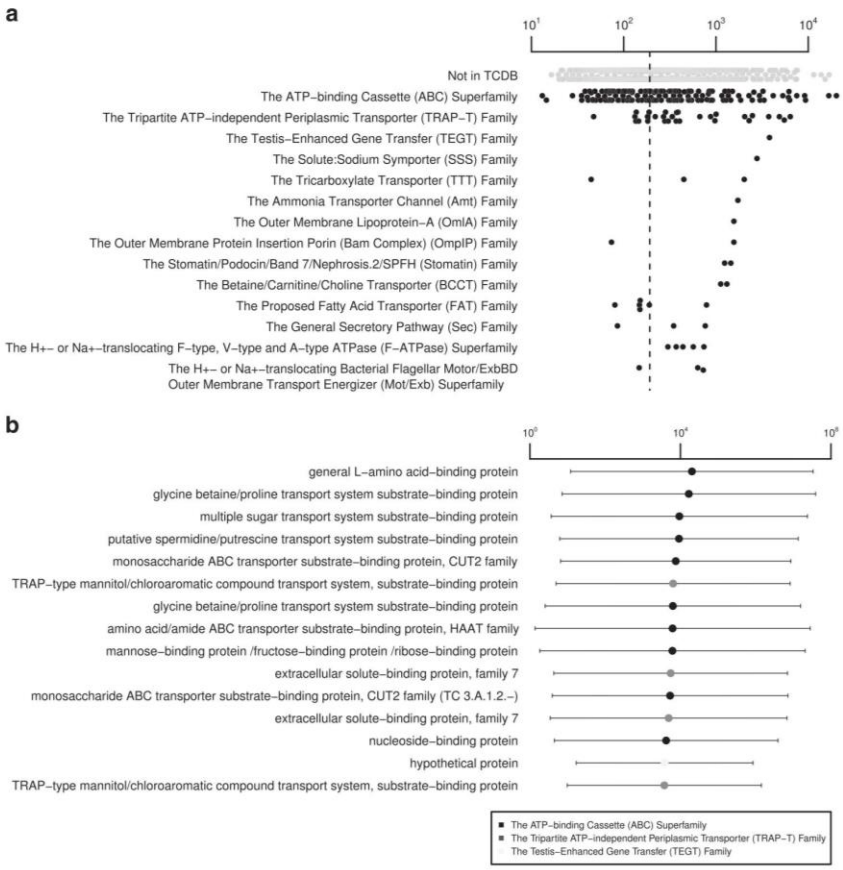

Figure 2 Most expressed CcPhy genes related to membrane transport. (**a**) CDS assigned to TCDB were grouped by families and super families. Groups were ordered according to maximum TPM_{av} values (*x* axis), and only the top 15 are shown. For reference, CDS not classified by TCDB are shown (not in TCDB). The median of all expressed genes is represented by the dashed line. (**b**) Most expressed transport-related genes. Gray scale refer to gene family or superfamily. Genes are ordered according to TPM_{av} values (*x* axis). Whiskers represent s.d. of biological replicates ($n = 3$).

levels for the aerobic, microaerobic and anaerobic respiratory pathways (Supplementary Figure S8). It is unlikely that any given individual cell within a population performs all three modes of respiration at the same time and therefore our observation indicates that subpopulations within the sponge tissue experience distinct oxygen environments.

Nitrite-dependent chemolithoautotrophy and use of organic nitrogen compounds by CcNi

Nitrospira are known to obtain energy by oxidizing nitrite to nitrate using the key enzyme nitrite oxidoreductase (NXR) (Spieck and Bock, 2005). The NXR of *Nitrospira* was proposed to be a membrane-bound periplasmic complex composed of at least two subunits, the subunits alpha (nxrA) and beta (nxrB) (Spieck *et al*., 1998; Lucker *et al*., 2010). Two adjacent genes encoding for nxrA (gene locus Ga0068443_101117) and nxrB (Ga0068443_101118) were found in CcNi (see Supplementary Information for phylogenetic analysis) representing the fourth and second most abundant transcripts in CcNi transcriptome (TPM_{av} 17 252 ± 9822 and TPM_{av} 26 308 ± 13 520, respectively; Figure 3). Electron transport and ATPase encoding genes were also expressed (Supplementary Table S2), supporting a nitrite-dependent chemolithotrophic electron flow (Lucker *et al*., 2010). Expressed genes related to other nitrogen transformations were also found and are discussed in Supplementary Information. Taken together, these results indicate an active chemolithotrophic conversion of nitrite to nitrate by the CcNi population (Figure 1).

Few *Nitrospira* species can decompose urea using the resulting ammonia for nitrification and biomass production, where urea would be imported from the extracellular milieu by the urea ABC transporter and hydrolyzed by urease (Koch *et al*., 2015; van Kessel *et al*., 2015). CcNi possess an putative operon with genes related to the transport and decomposition of urea, including those encoding for subunits of

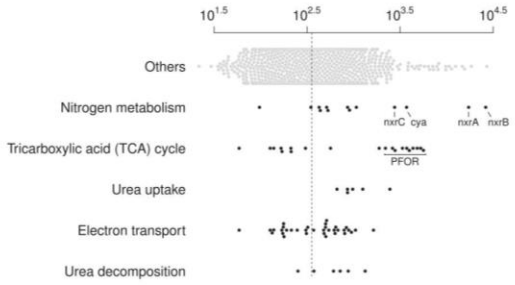

Figure 3 Expression of selected functional genes of CcNi. TPM_{av} values are shown for genes of selected functions. 'Others' stands for genes not grouped in the specific functions shown. The median of all expressed genes is represented by the dashed line. Highlighted genes encode for the nitrite oxidoreductase alpha (nxrA), beta (nxrB), putative C (nxrC) subunits (Supplementary Information), cyanate lyase (cya) and pyruvate ferredoxin oxidoreductase (PFOR).

urease, urea ABC transporter, as well as auxiliary proteins (Ga0068443_100614-16, Ga0068443_100619-27) (Supplementary Figure S9). Some of these genes were highly expressed, such as gene for the urtA urea transport system substrate-binding protein (TPM_{av} 2458 ± 357), the urease subunit alpha (TPM_{av} 1332 ± 420) and the urtD and urtE urea transport system ATP-binding proteins (TPM_{av} 978–1255; Figure 3). We did not find genomic evidence for the internal production of urea by CcNi, such as genes encoding for agmatinase or arginase. Because nitrite-oxidizing bacteria encode urea-producing enzymes (Palatinszky *et al*., 2015), the possibility of *Nitrospira*-like genes encoding for agmatinase or arginase to be expressed in *C. concentrica* was investigated. Transcripts encoding for sequences similar to agmatinase or arginase were found in the metatranscriptome of *C. concentrica* (Díez-Vives *et al*., 2016), but none of them were related to *Nitrospira* (Supplementary Information; Supplementary Table S4). This result further supports the absence of pathways for internal production of urea in CcNi.

The gene encoding for cyanate lyase (*cya*) was abundantly expressed in the transcriptome (TPM_{av} 3712 ± 1501) of CcNi (Figure 3). Cyanate lyase decomposes cyanate to CO_2 and ammonia in a reaction dependent of bicarbonate (Johnson and Anderson, 1987). Its activity was described in *N. moscoviensis* and its proposed biological roles include nitrogen assimilation, cyanate detoxification and energy acquisition (Anderson *et al*., 1990; Palatinszky *et al*., 2015). The *cya* gene was localized downstream from two genes encoding for proteins of the formate/nitrite transporter family (TPM_{av} 513–904) (Supplementary Figure S9). Members of the formate/nitrite transporter family (TC 2.A.44) have broad specificity for small monovalent anions (Lu *et al*., 2013). It is likely that CcNi putative formate/nitrite transporter is also permeable to cyanate, as similarly inferred for the ammonia-oxidizing archaea *Candidatus* Nitrososphaera gargensis due to the proximity of genes for transporter and enzymatic degradation (Spang *et al*., 2012).

Nitrospira species are proposed to fix carbon via the reductive TCA (rTCA) cycle (Starkenburg *et al*., 2006; Lucker *et al*., 2010, 2013; Koch *et al*., 2015). The rTCA cycle shares most of its enzymes with the oxidative TCA (oTCA) cycle, with the exception of three key enzymes, which are characteristic of the reductive cycle: ATP citrate lyase, 2-oxoglutarate: ferredoxin oxidoreductase (also named as α-ketogluterate synthase), and fumarate reductase (Berg, 2011). Alternatively, ATP-dependent cleavage of citrate can be carried by citryl-CoA synthetase and citryl-CoA lyase enzymes (Aoshima *et al*., 2004a, b). CcNi encoded enzymes that are shared between the two forms of TCA cycles. In addition, CcNi encoded a pyruvate ferredoxin oxidoreductase, which can act as pyruvate synthase (EC 1.2.7.1), carboxylating acetyl-CoA to pyruvate (Evans *et al*., 1966; Furdui and Ragsdale, 2000) (Figure 3). However, the characteristic rTCA key enzymes were not annotated in the genome (Figure 1). The annotation of genes encoding for A, B and C subunits of succinate dehydrogenase (complex II) or fumarate reductase (Ga0068443_100221-23) could indicate fumarate reductase activity and be considered an evidence for the rTCA cycle. These two enzymes are structurally similar and carry opposite reactions, that is, succinate oxidation and fumarate reduction (Hagerhall, 1997). Succinate dehydrogenase/fumarate reductase subunit genes are localized immediately adjacent to citrate synthase gene (Ga0068443_100220) in the CcNi genome. Although the mapping of metatranscriptomic reads to CDS does not allow us to verify whether they are co-expressed as an operon, their adjacent localization and similar expression levels (TPM_{av} 58–169) are suggestive of the participation of succinate dehydrogenase/fumarate reductase in the oTCA cycle as succinate dehydrogenase and not fumarate reductase. In the absence of evidence of other carbon fixation pathways (Supplementary Information), we hypothesize that CcNi fix carbon via rTCA cycle as conducted by other *Nitrospira* members, despite the lack of the key genes of this pathway in the genome bin.

Ammonia-dependent chemolithoautotrophy and use of organic nitrogen compounds by CcThau

Cultured members of the *Thaumarchaeota* are able to aerobically oxidase ammonia to nitrite (Stieglmeier *et al*., 2014a). Genes related to energy acquisition through ammonia oxidation were among the most abundantly transcribed in CcThau (TPM_{av} 3566–31 115, Figures 1 and 4). Ammonia oxidation is carried by ammonia monooxygenase, which in bacteria is composed of three subunits encoded by *amoA*, *amoB* and *amoC* genes (Arp *et al*., 2007). Additionally, a gene named '*amoX*' was proposed to be associated with the archaeal ammonia monooxygenase, due to

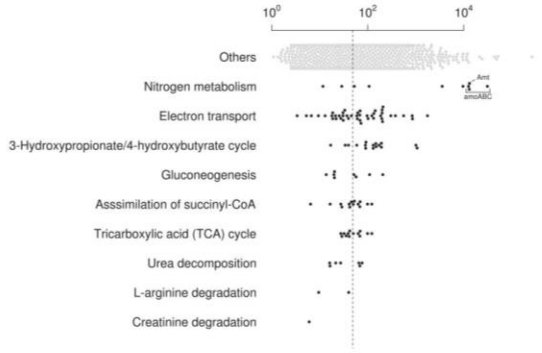

Figure 4 Expression of selected functional genes of CcThau. TPM_{av} values are shown for genes of selected functions. 'Others' stands for genes not grouped in the specific functions shown. The median of all expressed genes is represented by the dashed line. Highlighted genes encode for the ammonia monooxygenase subunits alpha (amoA), beta (amoB) and C (amoC) subunits as well as ammonium transporter (Amt).

the conserved co-localization with the subunit genes across ammonia-oxidizing archaea (Bartossek *et al.*, 2012). Single copies of genes putatively related to archaeal ammonia monooxygenase were present in pairs, amoA–amoX (Ga0078905_11462, Ga0078905_11463) and amoB–amoC (Ga0078905_103916-17), in the edge of two contigs, possibly forming a single gene array (*amoAXCB*) as observed in the genomes of *Nitrosoarchaeum limnia* SFB1 and *Nitrosopumilus maritimus* SCM1 (Walker *et al.*, 2010; Blainey *et al.*, 2011; Bartossek *et al.*, 2012). The gene encoding for an ammonium transporter (Ga0078905_100724, TPM_{av} 13 184 ± 1736) was estimated to be expressed at an approximate ratio of 1:1 to *amoA*. In addition, several genes putatively involved in ammonia-dependent chemolithotrophy in *Thaumarchaeota* were expressed at different levels by CcThau (Kozlowski *et al.*, 2016), including genes encoding for nitrite reductase (NO-forming) (TPM_{av} 107–9653), plastocyanins (TPM_{av} 37–1761), copper-binding proteins of the plastocyanin/azurin family (TPM_{av} 19–200), ubiquinol–cytochrome *c* reductase cytochrome *b* subunit (TPM_{av} 304 ± 26), multicopper oxidase (TPM_{av} 18 ± 4) and ATPase subunits (TPM_{av} 26–847). These findings are consistent with the observation of a large transcriptional effort invested in genes related to ammonia-dependent chemolithotrophy by archaeal populations in marine sponges (Radax *et al.*, 2012; Moitinho-Silva *et al.*, 2014).

Genomic analysis of several Thaumarchaea species revealed the presence of genes related to transport, production and degradation of urea (Palatinszky *et al.*, 2015). Urea can be used by *Thaumarchaeota* members as source of ammonia, as shown by biochemical assays of cultivated species (Lehtovirta-Morley *et al.*, 2016), and as carbon source, as inferred from ^{14}C-labeled urea incorporation of prokaryotic communities of Artic waters (Alonso-Saez *et al.*, 2012). The genes encoding for urease subunits, as well as auxiliary proteins, were present in two separate contigs of CcThau but lowly expressed (TPM_{av} 16–77). No encoded urea transporter was found. A set of genes encoding for amino acid/amide ABC transporter of the hydrophobic amino-acid uptake transporter (HAAT) family (TCDB:3.A.1.4), which includes urea transporters (Hosie *et al.*, 2002), were found in the genome. Thus it is conceivable that the encoded products may participate in urea transport. Urea can also be internally produced from the degradation of the amino-acid L-arginine (Shaibe *et al.*, 1985), and the genes encoding for arginine decarboxylase and agmatinase were expressed at low levels (TPM_{av} 10–40).

The expression of a gene encoding for creatinine amidohydrolase, albeit at low levels (TPM_{av} 6 ± 7), further indicates that CcThau degrades creatinine. Creatinine amidohydrolase genes are also present in other members of the candidate order *Nitrosopumilales*, for example, *Nitrosopumilus maritimus* SCM1 (Nmar_0222) (Walker *et al.*, 2010). The gene encoding for a creatinase, which would carry the downstream hydrolysis of creatine to sarcosine and urea (Shimizu *et al.*, 1986), was however not found in the CcThau genome bin. The most similar sequence to characterized creatinases from bacteria species was a gene encoding for a Xaa-Pro aminopeptidase (Ga0078905_10021), which is structurally related to creatinase (Supplementary Information; Supplementary Table S5; Bazan *et al.*, 1994). This similarity, however, does not provide enough evidence that CcThau converts creatinine to creatine in order to produce urea and, consequently, ammonia. Therefore, it is unclear in which biochemical context creatinine degradation is carried out by CcThau.

An almost complete set of genes for the 3-hydroxypropionate/4-hydroxybutyrate (HP/HB) pathway was expressed (Figure 1; Supplementary Table S2). The HP/HB pathway is an autotrophic CO_2 fixation cycle recently discovered in archaea and present in all *Thaumarchaeota* species characterized so far (Berg *et al.*, 2007; Bayer *et al.*, 2016). CcThau uses the same set of enzymes as *N. maritimus*, including 3-hydroxypropionyl-CoA synthetase (ADP-forming) (TPM_{av} 173 ± 53) and 4-hydroxybutyryl-CoA synthetase (ADP-forming) (TPM_{av} 90 ± 31) (Konneke *et al.*, 2014). In one cycle of the HP/HB pathway, two bicarbonate molecules are converted to one acetyl-coA. It is possible that the CcThau HP/HB pathway mainly connects to the central carbon metabolism via succinyl-CoA, which is produced from the generated acetyl-CoA and another pair of bicarbonate molecules by an additional half turn of the cycle (Estelmann *et al.*, 2011). With the exception of the gene for fumarase, for which no orthologous was identified, CcThau showed the expression of the enzymatic repertoire capable to further transform succinyl-coA into precursor metabolites, such as oxaloacetate,

phosphoenolpyruvate (PEP), pyruvate and 2-oxoglutarate (TPM_{av} 6–122). This set includes enzymes that are components of the oxidative TCA cycle. In addition, genes encoding for enzymes of the rTCA cycle were also found expressed, such as citrate lyase subunit beta/citryl-CoA lyase and 2-oxoglutarate ferredoxin oxidoreductase (TPM_{av} 32–39). In *Thaumarchaeota*, oTCA cycle was assumed to be used for anaplerotic reactions and the capacity of *Thaumarchaeota* to fix carbon via rTCA cycle was not demonstrated (Spang *et al.*, 2012; Zhalnina *et al.*, 2014; Stieglmeier *et al.*, 2014a). Mixotrophic growth has been reported in the *Thaumarchaeota* phylum (for example, Qin *et al.*, 2014). For CcThau, the possible uptake of urea and amino acids by the amino acid/amide ABC transporter of the HAAT family and the degradation of creatinine by creatinine amidohydrolase were the only evidence to suggest the use of external organic carbon sources (Supplementary Information).

Metabolic features of diatoms and the sponge

From the 184 053 eukaryotic transcripts recovered from *C. concentrica* (Díez-Vives *et al.*, 2016), the number of transcripts assigned to diatoms (*Bacillariophyta*) was similar to the combined number of transcripts classified as *Porifera* or as metazoans with best BLAST hit against sequences from sponges (Figure 5a). Higher expression, estimated from the sum of TPM values, was found for the host compared with the diatom symbiont (Figure 5b). Most transcripts could not be functionally classified for both organisms. Environmental information processing, genetic information processing and metabolism were the pathways with highest overall sums of TPM (Figure 5c). The comprehensive description of the diatom and sponge transcriptomes is beyond the scope of this study and therefore we focused here on key metabolic pathways.

The diatom symbionts invested a large transcriptional effort in functions for energy harvesting via photosynthesis and consumption via glycolysis (Figure 6a; Supplementary Table S6). In addition, functions related to arginine and proline metabolism were found to be abundantly expressed by the diatoms, in particular prolyl 4-hydroxylase (TPM_{sum} 46, Supplementary Table S6), the enzyme that carries out posttranslational modifications of proline (Gorres and Raines, 2010). The expression of carbamoyl-phosphate synthase, argininosuccinate synthase, argininosuccinate lyase and arginase (TPM_{sum} 3–10) are indicative of an active urea cycle in the diatom symbionts. Additional support for this metabolic cycle is provided by the expression of ornithine cyclodeaminase (TPM_{sum} 4) and ornithine decarboxylase (TPM_{sum} 5), which produce proline and putrescine from ornithine, respectively. The urea cycle in diatoms is proposed to redistribute and turnover inorganic carbon and nitrogen coming from catabolism and/or photorespiration (Allen *et al.*, 2011). With respect to sources of nitrogen, the diatoms expressed functions related to nitrate assimilation (nitrate reductase (NADPH), ferredoxin-nitrite

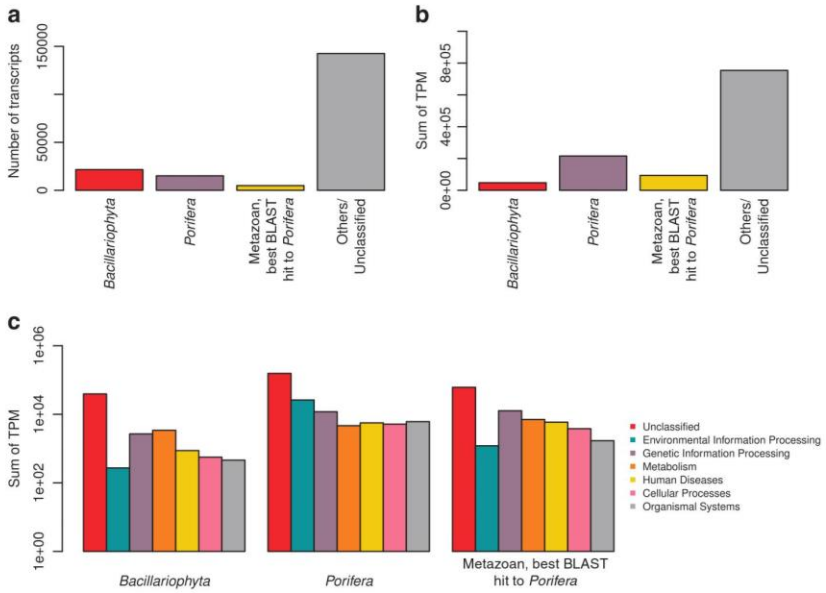

Figure 5 Expression of diatom and sponge transcripts in *Cymbastela concentrica*. (**a**) Transcripts taxonomically classified as diatoms (*Bacillariophyta*) or sponge (*Porifera* or Metazoan with best BLAST hit to sponge sequences) were sorted from other eukaryotic transcripts recovered from *C. concentrica*. (**b**) Overall expression of diatom and sponge is indicated by the sum of transcripts' TPM. (**c**) Deduced peptide sequences from transcripts' coding sequences were used for KEGG functional classification. Expression of KEGG functions was inferred from the sum of TPM values across coding sequences.

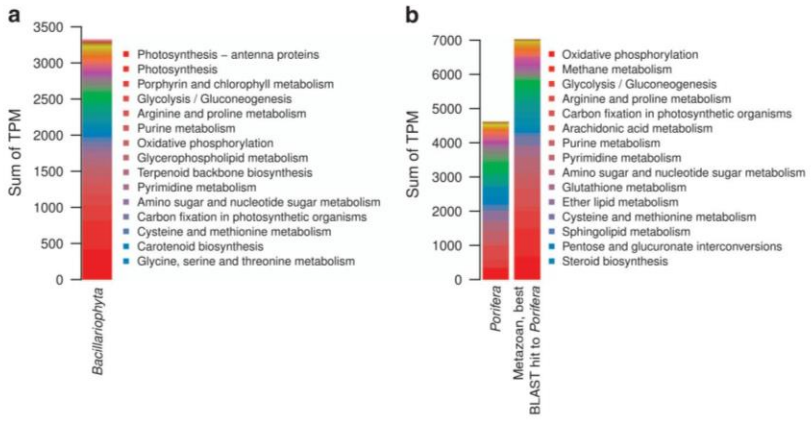

Figure 6 Expressed metabolic functions in diatoms and the sponge. Sums of TPM are shown for KEGG metabolic pathways found in (**a**) diatoms (*Bacillariophyta*) and (**b**) sponge (*Porifera* and Metazoan or Metazoan with best BLAST hit to sponge sequences). Legends list the top expressed pathways.

reductase, TPM_{sum} 2–5) and production of ammonia via nitrite generated from the oxygenation of alkyl nitronates (nitronate monooxygenase TPM_{sum} 1). The co-expression of these pathways at different intensities has also been recently observed in metatranscriptomes of *Skeletonema* spp. recovered from surface seawater (Alexander *et al.*, 2015) and indicates the simultaneous use of multiple sources of nitrogen by the diatom symbiont.

Sponge cells abundantly expressed functions of the oxidative phosphorylation (for example, cytochrome *c* oxidase subunit 6a, TPM_{sum} 418, Supplementary Table S7) and glycolysis (glyceraldehyde 3-phosphate dehydrogenase, TPM_{sum} 418) (Figure 6b). The expression of functions assigned to methane metabolism was largely due to antioxidant enzymes, catalase (TPM_{sum} 468) and peroxiredoxin 6, 1-Cys peroxiredoxin (TPM_{sum} 353), which may protect the sponge cells from reactive oxygen species (Tate *et al.*, 1995; Chen *et al.*, 2000). The most abundant functions related to arginine and proline metabolism were acetylornithine deacetylase (TPM_{sum} 237) and glycine amidinotransferase (TPM_{sum} 94). Both enzymes carry out reactions that produces L-ornithine, the former from N2-acetyl-L-ornithine and H_2O and the latter from L-arginine and glycine. The reaction of glycine amidinotransferase is the first of the two-step creatine biosynthesis (Wyss and Kaddurah-Daouk, 2000). Along with creatine, creatinine is expected to be found in sponge cells, as it is a product of spontaneous, non-enzymatic conversion of the former. In addition, the sponge expressed a creatine kinase function (TPM_{sum} 34), which reversibly converts creatine and ATP to phosphocreatine and ADP. This result is in support of previous detection of creatine kinase activity in the tissue of the sponge *Tethya aurantia* (Ellington, 2000; Sona *et al.*, 2004). In sponges, the creatine kinase/phosphocreatine system was proposed as an intracellular spatial buffer of energy, connecting the ATP produced in the mitochondria with distant cytosolic sites of ATP consumption (Sona *et al.*, 2004; Ellington and Suzuki, 2007).

Model of integrated metabolism of the microbial community members in C. concentrica

Based on the genomic and transcriptomic information of these three prokaryotic symbionts and the expression of eukaryotic transcripts assigned to diatoms and sponges, we developed a metabolic model for the sponge–microbe symbiosis in which nutrient fluxes between cells and the extracellular milieu, that is the sponge mesohyl, were inferred from our data set (see Figure 1).

As shown above, CcPhy is a heterotrophic bacterium with the capacity to uptake a range of organic and inorganic compounds. Such nutrients are likely found across the sponge tissue, which is consistent with a scattered distribution of CcPhy cells throughout the mesohyl (see Figure 7; Supplementary Figure S10). Considering the high relative abundance of *Phyllobacteriaceae* within the symbiont community (Fan *et al.*, 2012; Esteves *et al.*, 2016), CcPhy may thus be a major contributor to uptake and utilization of DOM by the microbiome. The DOM used by CcPhy may come from the sponge's filtering activity (Figure 1a; de Goeij *et al.*, 2008, 2013) or from diatoms (Figure 1b) that were found throughout the mesohyl (Figure 7), especially considering that axenic cultures of diatoms have been shown to release between 5% and 21% of their total fixed carbon as dissolved organic carbon (Wetz and Wheeler, 2007). In support of this, photosynthesis functions were abundantly expressed in the diatom transcriptome (Figure 6a). Another source of carbon for the members of the sponge–microbe symbiosis may be from the autotrophic metabolism of CcThau and CcNi (Figures 1c and d, see above).

Creatine and creatinine are products of the sponge metabolism, as indicated by the expression

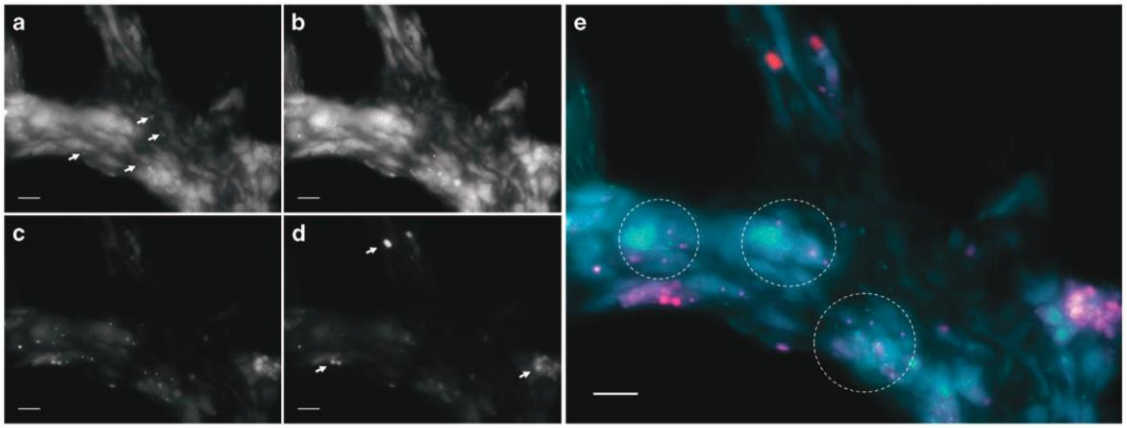

Figure 7 Visualization of microorganisms associated with *Cymbastela concentrica* by fluorescence *in situ* hybridization. (**a**) Rod-shaped cells (white arrows) were observed from hybridization with a Pacific Blue-labeled CcPhy-specific probe. Signals from (**b**) fluorescein-isothiocyanate-labeled CcNi-specific and (**c**) Cy3-labeled CcThau-specific probes are shown. (**d**) Red autofluorescence signals from diatoms were captured (arrows). (**e**) Clusters of CcNi-specific (green) and CcThau-specific (magenta) probes in the sponge mesohyl are highlighted in the merged color image by circles. CcPhy cells (cyan) did not specifically co-localize with CcNi or CcThau cells. Autofluorescence of the sponge tissue (light blue/cyan) served as a reference for the structure of the sponge mesohyl. Scale bars, 10 μm.

transcripts encoding for glycine amidinotransferase and creatine kinase. Although it is unknown whether sponge cells exchange creatine between different cells and tissues as described in higher animals (Wyss and Kaddurah-Daouk, 2000), it is conceivable that these compounds are accessible to the microbial community (Figure 1e). The possibility that creatine and creatinine are actively used by the microbiome is supported by the expression of genes able to degrade creatine to glycine by CcPhy and the encoded creatinine amidohydrolase in CcPhy and CcThau genomes. The degradation of these host metabolites by the symbionts is likely widespread, as inferred by the previous observation of related genes in the metagenome of six sponges, including *C. concentrica* (Fan *et al.*, 2012). Here we could assign this function to be actively used by specific members of the microbiome.

The metabolism of CcPhy, diatom, CcNi and CcThau are linked by the production and consumption of urea. CcPhy internally generates urea from creatine degradation, which can potentially accumulate and diffuse through the bacterial membrane (Figure 1f; Lodish *et al.*, 2000). This assumption is further supported by the fact that heterotrophic marine bacteria have been observed to be net producer of urea even in the presence of hydrolytic activity (Cho *et al.*, 1996; Berg and Jorgensen, 2006). The diatom symbiont is another potential source of urea as suggested by the expression of the urea cycle (Figure 1g). The *Nitrospira* population represented by CcNi may benefit directly from the urea in the extracellular milieu, as it abundantly expresses the genes related to the transport and degradation of urea. Despite the internal production of urea via L-arginine degradation, CcThau may also uptake urea via the amino acid/amide ABC transporter of the HAAT family. Additionally, urea can spontaneously dissociate to cyanate (Marier and Rose, 1964; Guilloton and Karst, 1985). Similarly, cyanate is formed from carbamoyl phosphate (Allen and Jones, 1964), which is an intermediate of the urea cycle in diatoms. Therefore, urea indirectly links CcPhy and the diatom symbiont to CcNi via cyanate (Figures 1h–j), which could be imported and decomposed to CO_2 and ammonia as indicated by the expression of cyanate lyase genes in CcNi.

Urease genes were also found in other sponge-associated microbial genomes and microbiomes (Hallam *et al.*, 2006; Siegl *et al.*, 2011; Bayer *et al.*, 2014; Liu *et al.*, 2016). Together with the phylogenetic diversity found for *ureC* genes and transcripts found in the sponge *Xestospongia testudinaria* (Su *et al.*, 2013), these data indicate that urea degradation is a common trait of sponge-associated microorganisms. Although urea can be found in benthic environments (Crandall and Teece, 2012), our data points to the possibility of urea being derived from host metabolites, that is, via bacterial metabolism of creatine and creatinine, and from intracellular metabolism of sponge symbionts, such as diatoms.

Pumping activity and host metabolism have been regarded as sources of ammonia in the sponge tissue (Ribes *et al.*, 2012; Figure 1k). Additionally, urea and cyanate are degraded by CcNi, which is likely a source of ammonia (Figure 1l; Koch *et al.*, 2015). Our analysis indicates that CcPhy takes up ammonium for nitrogen assimilation, while CcThau oxidizes ammonia to generate energy, releasing nitrite (Figure 1m). Nitrite in turn serves as the energy source for CcNi, which expressed the genes necessary for nitrite oxidation. Fluorescence *in situ* hybridization analysis showed that CcThau and CcNi are often localized in close proximity (Figure 7), supporting such a metabolic interaction. Nitrification, a process in which the oxidation of ammonia is coupled with the oxidation of nitrite, is a common

theme in sponge microbiology, being the subject of many studies (Taylor *et al.*, 2007). Based on the use of urea and cyanate as indirect sources of ammonia in nitrification carried out by co-cultures of *Nitrospira* and ammonia-oxidizing bacteria (Koch *et al.*, 2015; Palatinszky *et al.*, 2015) and the expression profile of CcNi and CcThau, we propose that these compounds should be considered when modeling nitrification in marine sponges.

The end product of the combined aerobic nitrification by CcThau and CcNi is nitrate, which would support anaerobic nitrate respiration by CcPhy (Figure 1n, see above). Such a coupling is possible if the two processes and their associated population are temporally and/or spatially separated by variations in oxygen concentration or redox potential, which have been described to occur in sponges (Schläppy *et al.*, 2010; Lavy *et al.*, 2016). The facultative nature of the CcPhy metabolism supports its temporal separation from the aerobic metabolisms CcThau and CcNi, while the observation that CcPhy rarely co-occured with the CcThau and CcNi cells would indicate also a spatial separation of their metabolisms (see Figure 7). The incomplete denitrification pathway of CcPhy would also yield nitrite (Figure 1o), which again could serve as an energy source for CcNi, thus creating a 'mini' N cycle at the interface of aerobic and anaerobic micro-habitats. An alternative path for the N cycle within *C. concentrica* is the nitrate assimilation by diatoms (Figure 1n).

Conclusion

We described the lifestyle of prominent members of *C. concentrica* sponge–microbe symbiosis, that is, associated prokaryotes, diatoms and the host, by analyzing their transcriptional activities. Although connected metabolic pathways are expected to occur based on the complexity of nutrient cycles within sponges (Hoffmann *et al.*, 2009), our study is unprecedented in modeling how the physiology of microbiome members are integrated. We thus predicted how and which members can generate, retain, recycle and compete for biochemical resources. In addition, we considered the gene expression of the sponge and diatoms, unveiling the nutritional basis for biological interactions within the sponge–microbe symbiosis. Finally, we demonstrated the power of a holistic approach to further our understanding of the complexity of animal–microbe symbioses.

Conflict of Interest

The authors declare no conflict of interest.

Acknowledgements

We acknowledge the financial support of the Betty and Gordon Moore Foundation and the Australian Research Council. We thank Dr Tamsin Peters and Jadranka Nappi for sample collection. We also thank Dr Ute Hentschel for hosting GB at the GEOMAR Helmholtz Centre for Ocean Research. MTJ was supported by grants of the German Excellence Initiative to the Graduate School of Life Sciences, University of Wuerzburg.

References

Alexander H, Jenkins BD, Rynearson TA, Dyhrman ST. (2015). Metatranscriptome analyses indicate resource partitioning between diatoms in the field. *Proc Natl Acad Sci USA* **112**: E2182–E2190.

Allen AE, Dupont CL, Obornik M, Horak A, Nunes-Nesi A, McCrow JP *et al.* (2011). Evolution and metabolic significance of the urea cycle in photosynthetic diatoms. *Nature* **473**: 203–207.

Allen CM, Jones ME. (1964). Decomposition of carbamylphosphate in aqueous solutions. *Biochemistry* **3**: 1238–1247.

Alonso-Saez L, Waller AS, Mende DR, Bakker K, Farnelid H, Yager PL *et al.* (2012). Role for urea in nitrification by polar marine Archaea. *Proc Natl Acad Sci USA* **109**: 17989–17994.

Anderson PM, Sung YC, Fuchs JA. (1990). The cyanase operon and cyanate metabolism. *FEMS Microbiol Rev* **7**: 247–252.

Aoshima M, Ishii M, Igarashi Y. (2004a). A novel enzyme, citryl-CoA synthetase, catalysing the first step of the citrate cleavage reaction in *Hydrogenobacter thermophilus* TK-6. *Mol Microbiol* **52**: 751–761.

Aoshima M, Ishii M, Igarashi Y. (2004b). A novel enzyme, citryl-CoA lyase, catalysing the second step of the citrate cleavage reaction in *Hydrogenobacter thermophilus* TK-6. *Mol Microbiol* **52**: 763–770.

Arp DJ, Chain PS, Klotz MG. (2007). The impact of genome analyses on our understanding of ammonia-oxidizing bacteria. *Annu Rev Microbiol* **61**: 503–528.

Bartossek R, Spang A, Weidler G, Lanzen A, Schleper C. (2012). Metagenomic analysis of ammonia-oxidizing archaea affiliated with the soil group. *Front Microbiol* **3**: 208.

Bayer B, Vojvoda J, Offre P, Alves RJ, Elisabeth NH, Garcia JA *et al.* (2016). Physiological and genomic characterization of two novel marine thaumarchaeal strains indicates niche differentiation. *ISME J* **10**: 1051–1063.

Bayer K, Moitinho-Silva L, Brummer F, Cannistraci CV, Ravasi T, Hentschel U. (2014). GeoChip-based insights into the microbial functional gene repertoire of marine sponges (high microbial abundance, low microbial abundance) and seawater. *FEMS Microbiol Ecol* **90**: 832–843.

Bazan JF, Weaver LH, Roderick SL, Huber R, Matthews BW. (1994). Sequence and structure comparison suggest that methionine aminopeptidase, prolidase, aminopeptidase P, and creatinase share a common fold. *Proc Natl Acad Sci USA* **91**: 2473–2477.

Bell JJ. (2008). The functional roles of marine sponges. *Estuar Coastal Shelf Sci* **79**: 341–353.

Berg GM, Jorgensen NOG. (2006). Purine and pyrimidine metabolism by estuarine bacteria. *Aquat Microb Ecol* **42**: 215–226.

Berg IA, Kockelkorn D, Buckel W, Fuchs G. (2007). A 3-hydroxypropionate/4-hydroxybutyrate autotrophic

carbon dioxide assimilation pathway in Archaea. *Science* **318**: 1782–1786.
Berg IA. (2011). Ecological aspects of the distribution of different autotrophic CO2 fixation pathways. *Appl Environ Microbiol* **77**: 1925–1936.
Bertero MG, Rothery RA, Palak M, Hou C, Lim D, Blasco F *et al.* (2003). Insights into the respiratory electron transfer pathway from the structure of nitrate reductase A. *Nat Struct Biol* **10**: 681–687.
Blainey PC, Mosier AC, Potanina A, Francis CA, Quake SR. (2011). Genome of a low-salinity ammonia-oxidizing archaeon determined by single-cell and metagenomic analysis. *PLoS ONE* **6**: e16626.
Cary SC, Giovannoni SJ. (1993). Transovarial inheritance of endosymbiotic bacteria in clams inhabiting deep-sea hydrothermal vents and cold seeps. *Proc Natl Acad Sci USA* **90**: 5695–5699.
Chen J-W, Dodia C, Feinstein SI, Jain MK, Fisher AB. (2000). 1-Cys peroxiredoxin, a bifunctional enzyme with glutathione peroxidase and phospholipase A2 activities. *J Biol Chem* **275**: 28421–28427.
Cho B, Park M, Shim J, Azam F. (1996). Significance of bacteria in urea dynamics in coastal surface waters. *Mar Ecol Prog Ser* **142**: 19–26.
Cho I, Blaser MJ. (2012). The human microbiome: at the interface of health and disease. *Nat Rev Genet* **13**: 260–270.
Coyte KZ, Schluter J, Foster KR. (2015). The ecology of the microbiome: networks, competition, and stability. *Science* **350**: 663–666.
Crandall JB, Teece MA. (2012). Urea is a dynamic pool of bioavailable nitrogen in coral reefs. *Coral Reefs* **31**: 207–214.
de Goeij JM, van den Berg H, van Oostveen MM, Epping EHG, van Duyl FC. (2008). Major bulk dissolved organic carbon (DOC) removal by encrusting coral reef cavity sponges. *Mar Ecol Prog Ser* **357**: 139–151.
de Goeij JM, van Oevelen D, Vermeij MJ, Osinga R, Middelburg JJ, de Goeij AF *et al.* (2013). Surviving in a marine desert: the sponge loop retains resources within coral reefs. *Science* **342**: 108–110.
Dethlefsen L, McFall-Ngai M, Relman DA. (2007). An ecological and evolutionary perspective on human-microbe mutualism and disease. *Nature* **449**: 811–818.
Díez-Vives C, Moitinho-Silva L, Nielsen S, Reynolds D, Thomas T. (2016). Expression of eukaryotic-like protein in the microbiome of sponges. *Mol Ecol*; e-pub ahead of print 30 December 2016; doi:10.1111/mec.14003.
Douglas AE, Werren JH. (2016). Holes in the hologenome: why host-microbe symbioses are not holobionts. *MBio* **7**: e02099.
Ellington WR. (2000). A dimeric creatine kinase from a sponge: implications in terms of phosphagen kinase evolution. *Comp Biochem Physiol B Biochem Mol Biol* **126**: 1–7.
Ellington WR, Suzuki T. (2007). Early evolution of the creatine kinase gene family and the capacity for creatine biosynthesis and membrane transport. *Subcell Biochem* **46**: 17–26.
Estelmann S, Hugler M, Eisenreich W, Werner K, Berg IA, Ramos-Vera WH *et al.* (2011). Labeling and enzyme studies of the central carbon metabolism in *Metallosphaera sedula*. *J Bacteriol* **193**: 1191–1200.
Esteves AI, Amer N, Nguyen M, Thomas T. (2016). Sample processing impacts the viability and cultivability of the sponge microbiome. *Front Microbiol* **7**: 499.
Evans MC, Buchanan BB, Arnon DI. (1966). A new ferredoxin-dependent carbon reduction cycle in a photosynthetic bacterium. *Proc Natl Acad Sci USA* **55**: 928–934.
Fan L, Reynolds D, Liu M, Stark M, Kjelleberg S, Webster NS *et al.* (2012). Functional equivalence and evolutionary convergence in complex communities of microbial sponge symbionts. *Proc Natl Acad Sci USA* **109**: E1878–E1887.
Freeman CJ, Thacker RW, Baker DM, Fogel ML. (2013). Quality or quantity: is nutrient transfer driven more by symbiont identity and productivity than by symbiont abundance? *ISME J* **7**: 1116–1125.
Furdui C, Ragsdale SW. (2000). The role of pyruvate ferredoxin oxidoreductase in pyruvate synthesis during autotrophic growth by the Wood-Ljungdahl pathway. *J Biol Chem* **275**: 28494–28499.
Gabel C, Maier RJ. (1993). Oxygen-dependent transcriptional regulation of cytochrome aa3 in *Bradyrhizobium japonicum*. *J Bacteriol* **175**: 128–132.
Garcia-Horsman JA, Barquera B, Rumbley J, Ma J, Gennis RB. (1994). The superfamily of heme-copper respiratory oxidases. *J Bacteriol* **176**: 5587–5600.
Gillan FT, Stoilov IL, Thompson JE, Hogg RW, Wilkinson CR, Djerassi C. (1988). Fatty acids as biological markers for bacterial symbionts in sponges. *Lipids* **23**: 1139–1145.
Gorres KL, Raines RT. (2010). Prolyl 4-hydroxylase. *Crit Rev Biochem Mol Biol* **45**: 106–124.
Guilloton M, Karst F. (1985). A spectrophotometric determination of cyanate using reaction with 2-aminobenzoic acid. *Anal Biochem* **149**: 291–295.
Hadas E, Shpigel M, Ilan M. (2009). Particulate organic matter as a food source for a coral reef sponge. *J Exp Biol* **212**: 3643–3650.
Hagerhall C. (1997). Succinate: quinone oxidoreductases. Variations on a conserved theme. *Biochim Biophys Acta* **1320**: 107–141.
Hallam SJ, Mincer TJ, Schleper C, Preston CM, Roberts K, Richardson PM *et al.* (2006). Pathways of carbon assimilation and ammonia oxidation suggested by environmental genomic analyses of marine Crenarchaeota. *PLoS Biol* **4**: e95.
Hoffmann F, Radax R, Woebken D, Holtappels M, Lavik G, Rapp HT *et al.* (2009). Complex nitrogen cycling in the sponge Geodia barretti. *Environ Microbiol* **11**: 2228–2243.
Hosie AH, Allaway D, Galloway CS, Dunsby HA, Poole PS. (2002). Rhizobium leguminosarum has a second general amino acid permease with unusually broad substrate specificity and high similarity to branched-chain amino acid transporters (Bra/LIV) of the ABC family. *J Bacteriol* **184**: 4071–4080.
Huson DH, Mitra S, Ruscheweyh HJ, Weber N, Schuster SC. (2011). Integrative analysis of environmental sequences using MEGAN4. *Genome Res* **21**: 1552–1560.
Imelfort M, Parks D, Woodcroft BJ, Dennis P, Hugenholtz P, Tyson GW. (2014). GroopM: an automated tool for the recovery of population genomes from related metagenomes. *PeerJ* **2**: e603.
Javelle A, Thomas G, Marini AM, Kramer R, Merrick M. (2005). *In vivo* functional characterization of the *Escherichia coli* ammonium channel AmtB: evidence for metabolic coupling of AmtB to glutamine synthetase. *Biochem J* **390**: 215–222.
Johnson WV, Anderson PM. (1987). Bicarbonate is a recycling substrate for cyanase. *J Biol Chem* **262**: 9021–9025.

Kamke J, Sczyrba A, Ivanova N, Schwientek P, Rinke C, Mavromatis K *et al.* (2013). Single-cell genomics reveals complex carbohydrate degradation patterns in poribacterial symbionts of marine sponges. *ISME J* **7**: 2287–2300.

Kikuchi Y, Hosokawa T, Fukatsu T. (2007). Insect-microbe mutualism without vertical transmission: a stinkbug acquires a beneficial gut symbiont from the environment every generation. *Appl Environ Microbiol* **73**: 4308–4316.

Kim JM, Shimizu S, Yamada H. (1986). Sarcosine oxidase involved in creatinine degradation in *Alcaligenes denitrificans* subsp *dentrificans* J9 and *Arthrobacter* spp J5 and J11. *Agric Biol Chem* **50**: 2811–2816.

Koch H, Lucker S, Albertsen M, Kitzinger K, Herbold C, Spieck E *et al.* (2015). Expanded metabolic versatility of ubiquitous nitrite-oxidizing bacteria from the genus *Nitrospira*. *Proc Natl Acad Sci USA* **112**: 11371–11376.

Konneke M, Bernhard AE, de la Torre JR, Walker CB, Waterbury JB, Stahl DA. (2005). Isolation of an autotrophic ammonia-oxidizing marine archaeon. *Nature* **437**: 543–546.

Konneke M, Schubert DM, Brown PC, Hugler M, Standfest S, Schwander T *et al.* (2014). Ammonia-oxidizing archaea use the most energy-efficient aerobic pathway for CO_2 fixation. *Proc Natl Acad Sci USA* **111**: 8239–8244.

Koopmans M, van Rijswijk P, Boschker HT, Marco H, Martens D, Wijffels RH. (2015). Seasonal variation of Fatty acids and stable carbon isotopes in sponges as indicators for nutrition: biomarkers in sponges identified. *Mar Biotechnol (NY)* **17**: 43–54.

Kozlowski JA, Stieglmeier M, Schleper C, Klotz MG, Stein LY. (2016). Pathways and key intermediates required for obligate aerobic ammonia-dependent chemolithotrophy in bacteria and Thaumarchaeota. *ISME J* **10**: 1836–1845.

Kraft B, Strous M, Tegetmeyer HE. (2011). Microbial nitrate respiration–genes, enzymes and environmental distribution. *J Biotechnol* **155**: 104–117.

Langmead B, Trapnell C, Pop M, Salzberg SL. (2009). Ultrafast and memory-efficient alignment of short DNA sequences to the human genome. *Genome Biol* **10**: R25.

Lavy A, Keren R, Yahel G, Ilan M. (2016). Intermittent hypoxia and prolonged suboxia measured in situ in a marine sponge. *Front Mar Sci* **3**: 263.

Lehtovirta-Morley LE, Ross J, Hink L, Weber EB, Gubry-Rangin C, Thion C *et al.* (2016). Isolation of '*Candidatus* Nitrosocosmicus franklandus', a novel ureolytic soil archaeal ammonia oxidiser with tolerance to high ammonia concentration. *FEMS Microbiol Ecol* **92**.

Li B, Ruotti V, Stewart RM, Thomson JA, Dewey CN. (2010). RNA-Seq gene expression estimation with read mapping uncertainty. *Bioinformatics* **26**: 493–500.

Li B, Dewey CN. (2011). RSEM: accurate transcript quantification from RNA-Seq data with or without a reference genome. *BMC Bioinformatics* **12**: 1–16.

Liu F, Li J, Feng G, Li Z. (2016). New genomic insights into 'Entotheonella' symbionts in *Theonella swinhoei*: mixotrophy, anaerobic adaptation, resilience, and interaction. *Front Microbiol* **7**: 1333.

Liu M, Fan L, Zhong L, Kjelleberg S, Thomas T. (2012). Metaproteogenomic analysis of a community of sponge symbionts. *ISME J* **6**: 1515–1525.

Liu MY, Kjelleberg S, Thomas T. (2011). Functional genomic analysis of an uncultured delta-proteobacterium in the sponge *Cymbastela concentrica*. *ISME J* **5**: 427–435.

Lodish H, Berk A, Zipursky SL, Matsudaira P, Baltimore D, Darnell J. (2000). *Section 15.1. Diffusion of Small Molecules Across Phospholipid Bilayers. Molecular Cell Biology*4th ednFreeman & Co.: New York, NY, USA, p1084.

Lu W, Du J, Schwarzer NJ, Wacker T, Andrade SL, Einsle O. (2013). The formate/nitrite transporter family of anion channels. *Biol Chem* **394**: 715–727.

Lucker S, Wagner M, Maixner F, Pelletier E, Koch H, Vacherie B *et al.* (2010). A Nitrospira metagenome illuminates the physiology and evolution of globally important nitrite-oxidizing bacteria. *Proc Natl Acad Sci USA* **107**: 13479–13484.

Lucker S, Nowka B, Rattei T, Spieck E, Daims H. (2013). The genome of nitrospina gracilis illuminates the metabolism and evolution of the major marine nitrite oxidizer. *Front Microbiol* **4**: 27.

Marier JR, Rose D. (1964). Determination of cyanate, and a study of its accumulation in aqueous solutions of urea. *Anal Biochem* **7**: 304–314.

Markowitz VM, Chen IM, Palaniappan K, Chu K, Szeto E, Pillay M *et al.* (2014). IMG 4 version of the integrated microbial genomes comparative analysis system. *Nucleic Acids Res* **42**: D560–D567.

Marta R, Rafel C, Josep-Maria G. (1999). Natural diet and grazing rate of the temperate sponge *Dysidea avara* (Demospongiae, Dendroceratida) throughout an annual cycle. *Mar Ecol Prog Ser* **176**: 179–190.

Martens EC, Heungens K, Goodrich-Blair H. (2003). Early colonization events in the mutualistic association between *Steinernema carpocapsae* nematodes and *Xenorhabdus nematophila* bacteria. *J Bacteriol* **185**: 3147–3154.

Moitinho-Silva L, Seridi L, Ryu T, Voolstra CR, Ravasi T, Hentschel U. (2014). Revealing microbial functional activities in the Red Sea sponge *Stylissa carteri* by metatranscriptomics. *Environ Microbiol* **16**: 3683–3698.

Morris RL, Schmidt TM. (2013). Shallow breathing: bacterial life at low O(2). *Nat Rev Microbiol* **11**: 205–212.

Palatinszky M, Herbold C, Jehmlich N, Pogoda M, Han P, von Bergen M *et al.* (2015). Cyanate as an energy source for nitrifiers. *Nature* **524**: 105–108.

Parks DH, Imelfort M, Skennerton CT, Hugenholtz P, Tyson GW. (2015). CheckM: assessing the quality of microbial genomes recovered from isolates, single cells, and metagenomes. *Genome Res* **25**: 1043–1055.

Peix A, Rivas R, Trujillo ME, Vancanneyt M, Velazquez E, Willems A. (2005). Reclassification of *Agrobacterium ferrugineum* LMG 128 as *Hoeflea marina* gen. nov., sp. nov. *Int J Syst Evol Microbiol* **55**: 1163–1166.

Preisig O, Zufferey R, Thony-Meyer L, Appleby CA, Hennecke H. (1996). A high-affinity cbb3-type cytochrome oxidase terminates the symbiosis-specific respiratory chain of *Bradyrhizobium japonicum*. *J Bacteriol* **178**: 1532–1538.

Qin W, Amin SA, Martens-Habbena W, Walker CB, Urakawa H, Devol AH *et al.* (2014). Marine ammonia-oxidizing archaeal isolates display obligate mixotrophy and wide ecotypic variation. *Proc Natl Acad Sci USA* **111**: 12504–12509.

Radax R, Rattei T, Lanzen A, Bayer C, Rapp HT, Urich T *et al.* (2012). Metatranscriptomics of the marine sponge Geodia barretti: tackling phylogeny and function of its microbial community. *Environ Microbiol* **14**: 1308–1324.

Ribes M, Jimenez E, Yahel G, Lopez-Sendino P, Diez B, Massana R *et al.* (2012). Functional convergence of microbes associated with temperate marine sponges. *Environ Microbiol* **14**: 1224–1239.

Ryu T, Seridi L, Moitinho-Silva L, Oates M, Liew YJ, Mavromatis C *et al.* (2016). Hologenome analysis of two marine sponges with different microbiomes. *BMC Genomics* **17**: 158.

Schläppy ML, Weber M, Mendola D, Hoffmann F, de Beer D. (2010). Heterogeneous oxygenation resulting from active and passive flow in two Mediterranean sponges, *Dysida avara* and *Chondrosia reniformis*. *Limnol Oceanogr* **55**: 1289–1300.

Schmitt S, Angermeier H, Schiller R, Lindquist N, Hentschel U. (2008). Molecular microbial diversity survey of sponge reproductive stages and mechanistic insights into vertical transmission of microbial symbionts. *Appl Environ Microbiol* **74**: 7694–7708.

Schmitt S, Tsai P, Bell J, Fromont J, Ilan M, Lindquist N *et al.* (2012). Assessing the complex sponge microbiota: core, variable and species-specific bacterial communities in marine sponges. *ISME J* **6**: 564–576.

Shaibe E, Metzer E, Halpern YS. (1985). Metabolic pathway for the utilization of L-arginine, L-ornithine, agmatine, and putrescine as nitrogen sources in *Escherichia coli* K-12. *J Bacteriol* **163**: 933–937.

Shimizu S, Kim J, Shinmen Y, Yamada H. (1986). Evaluation of two alternative metabolic pathways for creatinine degradation in microorganisms. *Arch Microbiol* **145**: 322–328.

Siegl A, Kamke J, Hochmuth T, Piel J, Richter M, Liang C *et al.* (2011). Single-cell genomics reveals the lifestyle of Poribacteria, a candidate phylum symbiotically associated with marine sponges. *ISME J* **5**: 61–70.

Solomon C, Collier J, Berg G, Glibert P. (2010). Role of urea in microbial metabolism in aquatic systems: a biochemical and molecular review. *Aquatic Microbial Ecol* **59**: 67–88.

Sona S, Suzuki T, Ellington WR. (2004). Cloning and expression of mitochondrial and protoflagellar creatine kinases from a marine sponge: implications for the origin of intracellular energy transport systems. *Biochem Biophys Res Commun* **317**: 1207–1214.

Spang A, Poehlein A, Offre P, Zumbragel S, Haider S, Rychlik N *et al.* (2012). The genome of the ammonia-oxidizing *Candidatus* Nitrososphaera gargensis: insights into metabolic versatility and environmental adaptations. *Environ Microbiol* **14**: 3122–3145.

Spieck E, Ehrich S, Aamand J, Bock E. (1998). Isolation and immunocytochemical location of the nitrite-oxidizing system in nitrospira moscoviensis. *Arch Microbiol* **169**: 225–230.

Spieck E, Bock E. (2005). The lithoautotrophic nitrite-oxidizing bacteriaIn:Brenner DJ, Krieg NR, Staley JT, Garrity GM, Boone DR, Vos PD *et al.* (eds). *Bergey's Manual of Systematic Bacteriology*. Springer Science +Business Media: New York, USA, pp 149–153.

Starkenburg SR, Chain PS, Sayavedra-Soto LA, Hauser L, Land ML, Larimer FW *et al.* (2006). Genome sequence of the chemolithoautotrophic nitrite-oxidizing bacterium *Nitrobacter winogradskyi* Nb-255. *Appl Environ Microbiol* **72**: 2050–2063.

Stieglmeier M, Alves RJE, Schleper C. (2014a). The Phylum ThaumarchaeotaIn:Rosenberg E, DeLong EF, Lory S, Stackebrandt E, Thompson F(eds). *The Prokaryotes: Other Major Lineages of Bacteria and the Archaea*4th edn.Springer-Verlag: Berlin, Heidelberg, Germany.

Stieglmeier M, Klingl A, Alves RJ, Rittmann SK, Melcher M, Leisch N *et al.* (2014b). *Nitrososphaera viennensis* gen. nov., sp. nov., an aerobic and mesophilic, ammonia-oxidizing archaeon from soil and a member of the archaeal phylum Thaumarchaeota. *Int J Syst Evol Microbiol* **64**: 2738–2752.

Su J, Jin L, Jiang Q, Sun W, Zhang F, Li Z. (2013). Phylogenetically diverse ureC genes and their expression suggest the urea utilization by bacterial symbionts in marine sponge *Xestospongia testudinaria*. *PLoS ONE* **8**: e64848.

Swem LR, Elsen S, Bird TH, Swem DL, Koch HG, Myllykallio H *et al.* (2001). The RegB/RegA two-component regulatory system controls synthesis of photosynthesis and respiratory electron transfer components in Rhodobacter capsulatus. *J Mol Biol* **309**: 121–138.

Tate Jr DJ, Miceli MV, Newsome DA. (1995). Phagocytosis and H2O2 induce catalase and metallothionein gene expression in human retinal pigment epithelial cells. *Invest Ophthalmol Vis Sci* **36**: 1271–1279.

Taylor MW, Schupp PJ, Dahllof I, Kjelleberg S, Steinberg PD. (2004). Host specificity in marine sponge-associated bacteria, and potential implications for marine microbial diversity. *Environ Microbiol* **6**: 121–130.

Taylor MW. (2005). *The ecology of marine sponge-associated bacteria* Ph.D. thesis The University of New South Wales: Sydney, Australia.

Taylor MW, Radax R, Steger D, Wagner M. (2007). Sponge-associated microorganisms: evolution, ecology, and biotechnological potential. *Microbiol Mol Biol Rev* **71**: 295–347.

Thomas T, Rusch D, DeMaere MZ, Yung PY, Lewis M, Halpern A *et al.* (2010). Functional genomic signatures of sponge bacteria reveal unique and shared features of symbiosis. *ISME J* **4**: 1557–1567.

Thomas T, Moitinho-Silva L, Lurgi M, Bjork JR, Easson C, Astudillo-Garcia C *et al.* (2016). Diversity, structure and convergent evolution of the global sponge microbiome. *Nat Commun* **7**: 11870.

van Kessel MA, Speth DR, Albertsen M, Nielsen PH, Op den Camp HJ, Kartal B *et al.* (2015). Complete nitrification by a single microorganism. *Nature* **528**: 555–559.

Wagner GP, Kin K, Lynch VJ. (2012). Measurement of mRNA abundance using RNA-seq data: RPKM measure is inconsistent among samples. *Theory Biosci* **131**: 281–285.

Walker CB, de la Torre JR, Klotz MG, Urakawa H, Pinel N, Arp DJ *et al.* (2010). Nitrosopumilus maritimus genome reveals unique mechanisms for nitrification and autotrophy in globally distributed marine crenarchaea. *Proc Natl Acad Sci USA* **107**: 8818–8823.

Webster NS, Thomas T. (2016). The sponge hologenome. *MBio* **7**: e00135-16.

Wetz MS, Wheeler PA. (2007). Release of dissolved organic matter by coastal diatoms. *Limnol Oceanogr* **52**: 798–807.

White D. (2007), The Physiology and Biochemistry of Prokaryotes. Oxford University Press: New York, NY, USA.

Willems A. (2014)The family Phyllobacteriaceae. In: Rosenberg E, DeLong EF, Lory S, Stackebrandt E, Thompson F(eds). *The Prokaryotes: Alphaproteobacteria and Betaproteobacteria*4th edn.Springer: Berlin, Germany, pp 355–418.

Wilson MC, Mori T, Ruckert C, Uria AR, Helf MJ, Takada K *et al.* (2014). An environmental bacterial taxon with a large and distinct metabolic repertoire. *Nature* **506**: 58–62.

Wulff J. (2012). Ecological interactions and the distribution, abundance, and diversity of sponges. *Adv Mar Biol* **61**: 273–344.

Wyss M, Kaddurah-Daouk R. (2000). Creatine and creatinine metabolism. *Physiol Rev* **80**: 1107–1213.

Yahel G, Sharp JH, Marie D, Hase C, Genin A. (2003). In situ feeding and element removal in the symbiont-bearing sponge *Theonella swinhoei*: bulk DOC is the major source for carbon. *Limnol Oceanogr* **48**: 141–149.

Zhalnina KV, Dias R, Leonard MT, Dorr de Quadros P, Camargo FA, Drew JC *et al.* (2014). Genome sequence of *Candidatus* Nitrososphaera evergladensis from group I.1b enriched from Everglades soil reveals novel genomic features of the ammonia-oxidizing archaea. *PLoS One* **9**: e101648.

Zheng H, Wisedchaisri G, Gonen T. (2013). Crystal structure of a nitrate/nitrite exchanger. *Nature* **497**: 647–651.

Supplementary Information accompanies this paper on The ISME Journal website (http://www.nature.com/ismej)

CHAPTER 6

SYMBIONT CONTRIBUTIONS TO DISSOLVED ORGANIC MATTER UPTAKE BY MARINE SPONGES

Rix L., Ribes M., Coma R., **Jahn, M.T.**, de Goeij J., van Oevelen, D., Escrig S., Meibom A., & Hentschel U

Manuscript in preparation

Symbiont contributions to dissolved organic matter uptake by marine sponges

Laura Rix[1,2]*, Marta Ribes[3], Rafel Coma[4], Martin T. Jahn[1], Jasper de Goeij[5], Dick van Oevelen[6], Stéphane Escrig[7], Anders Meibom[8], Ute Hentschel[1,9]

[1]RD3 Marine Symbioses, GEOMAR Helmholtz Centre for Ocean Research Kiel, Düsternbrooker Weg 20, 24105 Kiel, Germany

[2]School of Biological Sciences, University of Queensland, St. Lucia, QLD 4072, Australia

[3]Department of Marine Biology and Oceanography. Institute of Marine Science, CSIC, Barcelona, Spain

[4]Department of Marine Ecology, Centre for Advanced Studies, CSIC, Blanes, Spain

[5]Department of Freshwater and Marine Ecology, Institute for Biodiversity and Ecosystem Dynamics, University of Amsterdam, PO Box 94248, 1090 GE Amsterdam, The Netherlands

[6]Department of Estuarine and Delta Systems, NIOZ Royal Netherlands Institute for Sea Research, and Utrecht University, PO Box 140, 4400 AC Yerseke, The Netherlands

[7]Laboratory for Biological Geochemistry, School of Architecture, Civil and Environmental Engineering, Ecole Polytechnique Fédérale de Lausanne (EPFL), CH-1015, Lausanne, Switzerland

[8]Center for Advanced Surface Analysis, Institute of Earth Sciences, University of Lausanne, CH-1015, Lausanne, Switzerland

[9]Christian-Albrechts-University of Kiel (CAU), Kiel, Germany

*corresponding author

Keywords: DOM, HMA-LMA, sponge loop, animal-microbe symbiosis, stable isotope tracer, NanoSIMS

ABSTRACT

Sponges play a key role in the cycling of dissolved organic matter (DOM) in benthic marine ecosystems. The mechanisms enabling them to take up DOM are unknown, but the process is widely believed to be mediated by their diverse communities of symbiotic microbes. To quantify the role of sponge symbionts in DOM uptake, we combined stable isotope pulse-chase experiments and nanoscale secondary ion mass spectrometry to compare DOM processing in a high-microbial abundance (HMA) and low-microbial abundance (LMA) sponge. Contrary to expectations, we found that both microbial symbionts and host choanocyte cells were active in DOM uptake. All DOM sources (glucose, amino acids, algal DOM) were assimilated by both sponges, but higher microbial activity in the HMA sponge corresponded to an increased capacity to efficiently process a greater variety of dissolved compounds. Nevertheless, *in situ* feeding data demonstrated that DOM was the primary carbon source for both the LMA and HMA sponge, accounting for ~90% of the heterotrophic diet in both species. Overall, microbes accounted for the majority (63-87%) of DOM assimilated by the HMA sponge (and ~60% of its total heterotrophic diet) but <5% in the LMA sponge. We propose that HMA and LMA sponges have evolved different strategies to exploit DOM—the most abundant organic resource in the ocean.

INTRODUCTION

Sponges are amongst the ocean's most efficient filter feeders (1); they pump up to 10,000 times their own volume in seawater per day and remove bacteria and other small plankton with efficiencies reaching 99% (2, 3). In habitats where they are abundant, sponges can filter the entire water column in the order of days (3), transferring particulate organic matter (POM) to the benthos and regenerating inorganic nutrient to support new primary production. Due to their global distribution (4) and ancient origin (5, 6), in this way they have been modulating nutrient fluxes in the ocean for millions of years. However, despite this enormous capacity to retain POM, it was recently been discovered that sponges may play an even greater role in the cycling of dissolved organic matter (DOM) (7-14).

DOM is the largest reservoir of organic carbon in the ocean (15) but is largely inaccessible to most marine animals and is instead primarily utilized by heterotrophic microbes who recycle as much as 50% total marine productivity as DOM through the microbial loop (16). Sponges have long been hypothesized to utilize DOM (17-19), but only in the last 15 years has there been growing consensus that DOM accounts for a significant proportion (up to 90%) of the sponge diet (7-14). This is remarkable given DOM uptake in marine invertebrates is typically restricted to larval life stages (20) or low uptake of specific compounds (20-22) and no other multicellular animal is known to use DOM as their primary carbon source. The mechanisms enabling sponges to take up such large quantities of DOM remain unknown, but the key is believed to lie in their microbial symbionts.

The microbial communities associated with sponges are exceptionally diverse (23), forming stable and species-specific associations that can account for as much as 35% of the total sponge biomass (24, 25). These symbionts are not evenly distributed across species; intriguingly sponge can be categorized into two distinct groups with high microbial abundance (HMA) sponges harbouring densities of microbes 2–4 orders of magnitude higher than low microbial abundance (LMA) sponges (24, 26, 27). The evolutionary reasons for this dichotomy are unknown, but HMA and LMA sponges further differ in the type and diversity of their microbial symbionts (27), host physiology (28, 29), and nutrient processing (12, 30); and this dichotomy is also further believed to influence DOM uptake capacity. Since microbes are assumed to mediate sponge DOM uptake, it is widely hypothesized that HMA sponges are better adapted for DOM uptake than LMA sponges (28). Early studies proposed that only HMA sponges used DOM (18) but recent research has produced conflicting results; while some studies have conformed to this initial hypothesis (10, 13), others have found similar DOM uptake rates in both HMA and LMA sponges (7, 8, 12). Despite the growing recognition of the importance of sponge DOM uptake not only as a food source for the sponges, but also for DOM cycling at the ecosystem level (31-33), the contribution of microbial symbionts remains unknown.

To investigate the role of microbial symbionts in sponge DOM uptake, we performed stable isotope pulse-chase experiments to compare the processing of three dissolved food sources (glucose, amino acids, and algal DOM) and one particulate food source (bacteria) in the HMA sponge

Aplysina aerophoba and LMA sponge *Dysidea avara* (Fig. 1A-B). Host and symbiont contributions to the DOM were quantified through stable isotope analysis of (i) bulk sponge tissue, (ii) separated sponge and microbial cell fractions, and (iii) single cells using nanoscale secondary ion mass spectrometry (NanoSIMS). Manipulative stable isotope tracer experiments were complimented with *in situ* measurements of the natural sponge diet to determine the total heterotrophic contribution of sponge symbionts to the sponge diet. Finally, we quantified DOM turnover into sponge detritus to test if the two sponge species contribute to DOM cycling via the sponge loop pathway. Our findings show that microbial symbionts played a major role in DOM uptake only in the HMA, but despite this both sponges were able to efficiently utilize DOC due to dual uptake by both host and symbiont cells.

RESULTS

Microbial biomass and diversity is higher in the HMA compared to LMA sponge

The microbial communities of the two sponges were investigated by electron microscopy and 16S rRNA gene amplicon sequencing and counts of DAPI stained cell fractions. Consistent with the HMA-LMA status of the two species (26), microbial cells outnumbered sponge cells by 102:1 in the HMA sponge *A. aerophoba*, while the ratio of microbial to sponge cells in the LMA sponge *D. avara* was nearly two orders of magnitude lower (1.8:1). Microbial symbiont cells were larger in *A aerophoba* compared with *D. avara* (Fig. 1E, F), and this corresponded to higher average C and N content in the microbial cells of *A. aerophoba* (C: 135.0 ± 18.0 fg/cell; N 26.4 ± 6.0 fg/cell) compared with *D. avara* (C: 33.5±5.8 fg/cell; N: 3.4±0.5 fg/cell). The C and N content of the sponge cells in the two sponges were similar (C: 46.3±11.2 pg/cell; N: 10.2±2.8 pg/cell for *A. aerophoba* and C: 41.2±11.5 pg/cell; N: 4.0±1.7 pg for *D. avara*). Using the cellular CN contents and total cell counts, we calculate that microbial cells accounted for 25.2 ± 12.4% of the total cellular C biomass (and 25.3 ± 10.6% of the total cellular N biomass) in *A. aerophoba*, but <0.5% in *D. avara* (0.4 ± 0.6% for both C and N). The HMA sponges not only had higher microbial biomass but also a more diverse microbial community (Fig. 1G, H; Shannon index $p<0.05$).

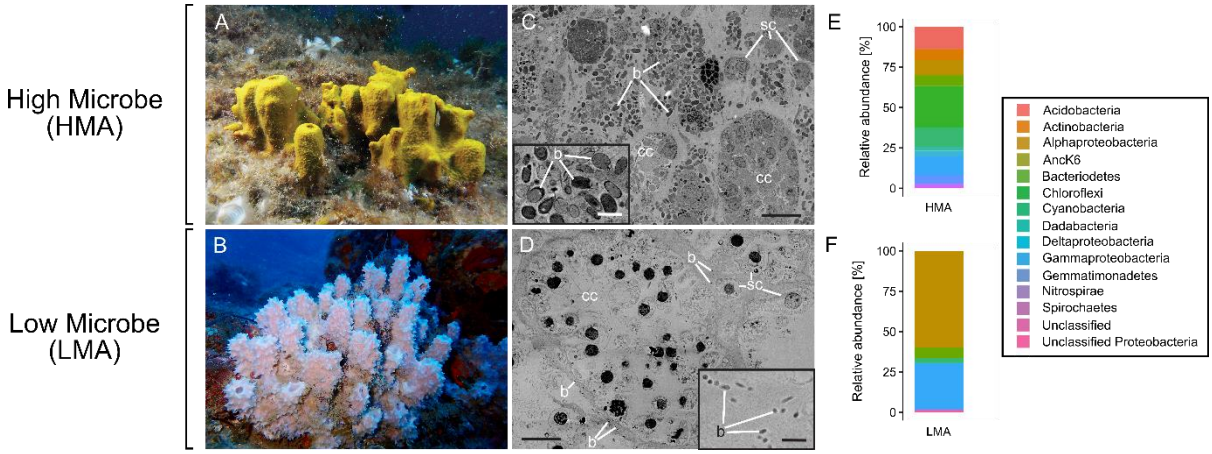

Figure 1. Comparative morphology and microbial diversity of the HMA sponge *Aplysina aerophoba* and LMA sponge *Dysidea avara*. (**A-B**) *In situ* photographs depicting the similar massive growth form of the two sponge species consisting of clumps of individual "chimneys" each containing a single osculum. (**C-D**) Scanning electron micrographs of the internal sponge morphology. The mesohyl of the HMA sponge *A. aerophoba* is more densely packed with bacteria and sponge cells and contains smaller choanocyte chambers compared to the LMA sponge *D. avara*, which has large choanocyte chambers and less dense tissue with sparse bacteria. Bacterial symbionts are larger and more abundant in the HMA sponge *A. aerophoba*. (**E-F**) Microbial community composition of the two sponges based on 16S rRNA gene data (n=6), showing that the HMA sponge *A. aerophoba* has a more diverse microbial community. Mesohyl (m), choanocyte chamber (cc) sponge cell (sc), bacteria (b). Scale bars: C-D 10 µm; E-F 1 µm.

Differential uptake of dissolved and particulate food by the HMA and LMA sponge

All four food sources (glucose, amino acids, algal DOM and bacteria) were assimilated by both sponge species during the isotope tracer experiments, but they exhibited significant differences in uptake rates (Fig. 2A-D). The HMA sponge *A. aerophoba* showed the highest uptake rate for amino acids, and both amino acids and algal-DOM were assimilated at a higher rate than the bacteria. By contrast, the LMA sponge *D. avara* showed highest assimilation rate for the particulate food source with bacteria assimilated at a rate at least 10x higher than for any of the dissolved food sources. When the two species were compared, *A. aerophoba* took up both the glucose and amino acids at a significantly higher rate (6 and 12 times higher, respectively) than *D. avara*, which took up bacteria at a rate 8 times higher than *A. aerophoba*. There were no significant differences in the uptake rates of algal DOM. Thus, while the HMA sponge was generally more efficient at taking up dissolved food, and the LMA sponge the particulate food, they were both able to take up algal DOM at a similar rate. The two species further differed in their preferences for dissolved compounds; algal DOM was incorporated at the highest rate by *D. avara*, while amino acids were assimilated most rapidly by *A. aerophoba*. For both species, glucose was taken up at the lowest rate, although the LMA sponge was particularly inefficient at utilizing glucose with uptake rates 7 times lower than for algal DOM and 70 times lower than for bacteria.

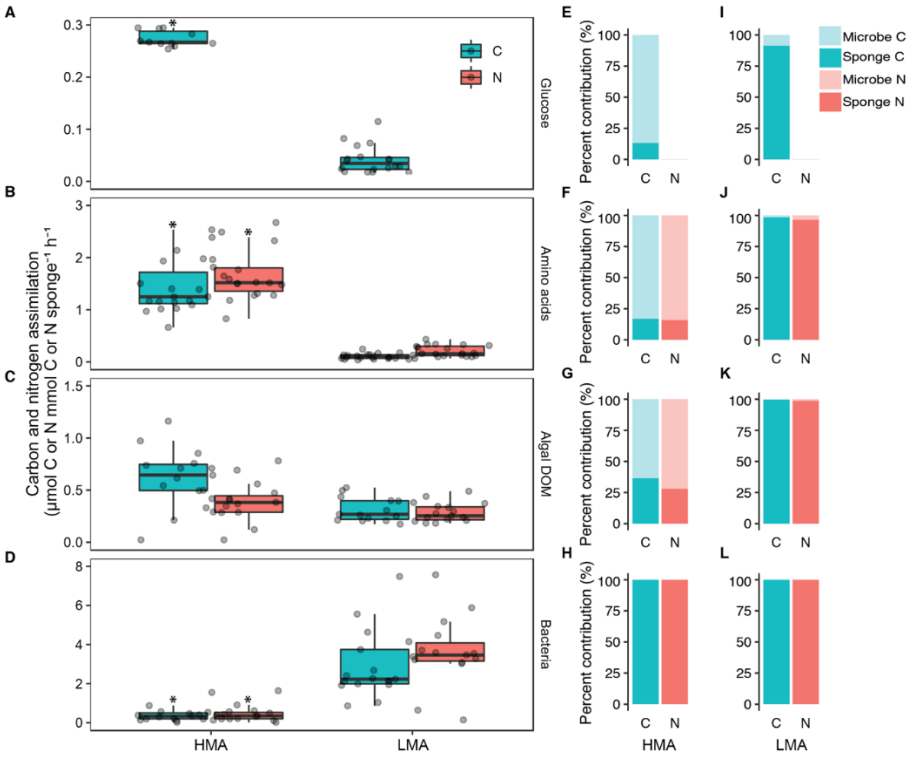

Figure 2. Total uptake of the four food sources and contribution of host and symbiont cells to total uptake. Rates of carbon (C) and nitrogen (N) assimilation of the four food sources (**A**) glucose, (**B**) amino acids, (**C**) algal DOM, and (**D**) bacteria into the bulk tissue of the HMA sponge *A. aerophoba* and LMA sponge *D. avara*. Rates presented as µmol C or N assimilated per mmol C or N sponge tissue per hour. Significant differences in C or N assimilation between the two sponge species are marked (*) for each food source (significance level $P_{(perm)} < 0.05$). Boxplots are overlaid with the raw data points (n=20). (**E-L**) Percent contribution of host sponge cells (dark colours) and microbial symbionts (light colours) to total assimilation of the four food sources for both carbon (green) and nitrogen (orange).

Single-cell NanoSIMS analysis reveals DOM is incorporated by both host and symbiont cells

The cell separation data showed significant isotopic enrichment in all sponge cell and bacterial cell fractions for all treatments (Fig. S1, Table S2) and this was supported at the single-cell level by the NanoSIMS data. For both the HMA and LMA sponge, the NanoSIMS images showed clear uptake of ^{13}C and ^{15}N from all dissolved food sources into both host and microbial cells (Fig. 3). The majority (64–97%) of microbial cells in both species showed uptake of amino acids and algal DOM and hotspots of enrichment for these DOM sources could be seen in host cells (Fig. 3). As observed in the bulk uptake rates (Fig. 2A), incorporation of glucose was low; ^{13}C enrichment was detected in fewer than 26% and 7% of microbes in the HMA and LMA sponge, respectively, and only at very low levels in host cells (Fig. 4A, E). For all food sources, both dissolved and particulate, hotspots of enrichment in host cells were limited to the choanocyte cells—the filtering cells that form the choanocyte chambers where food is captured by the host (Fig. 3). Enrichment was less frequently detected in amoebocyte cells in the sponge mesohyl and only when there was already high uptake in a large proportion of the choanocyte cells or microbial cells in the case of the HMA sponge (Fig. 4), suggesting mesohyl cells were not the initial uptake sites. Although other cell types can be involved in food uptake (34), choanocytes are known to transfer food vacuoles to amoebocytes for subsequent digestion (35). In both host and symbiont cells enrichment of C and N was generally co-localized; however, due to dilution of the C signal during sample resin embedding (36), the ^{13}C enrichment was always lower than the ^{15}N enrichment (Fig. 4). Consequently, cells that were enriched in ^{13}C were also enriched in ^{15}N > 70% of the time, while the opposite was not always the case.

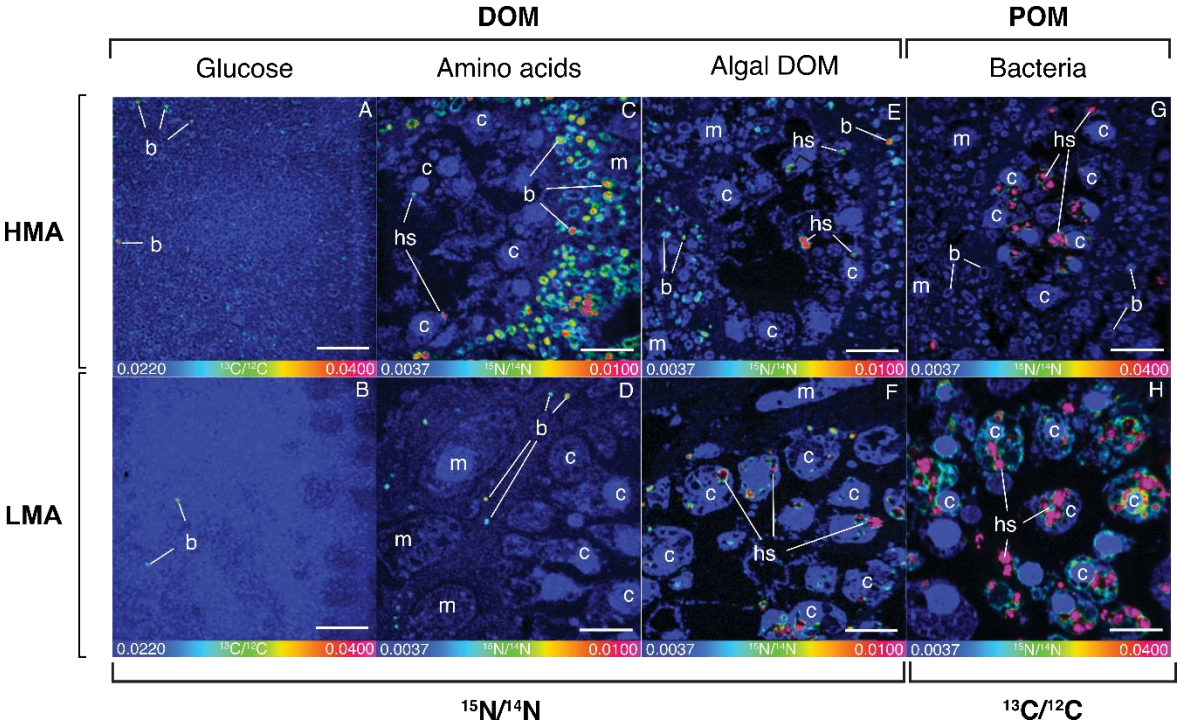

Figure 3. NanoSIMS visualization of ^{13}C or ^{15}N enrichment in sponge host and symbiont cells. *A. aerophoba* (HMA) and *D. avara* (LMA) tissue after the 3h isotopic pulse with the four ^{13}C and ^{15}N-labelled food sources: (**A-B**) glucose, (**C-D**) amino acids, (**E-F**), algal-DOM, (**G-H**) bacteria. Representative NanoSIMS ratio images showing the distribution of ^{13}C or ^{15}N within the sponge holobiont displayed as Hue Saturation Intensity. The rainbow scale ranges from natural abundance in blue shifting to pink with increasing ^{13}C or ^{15}N enrichment. Note the different scale for bacteria (G-H). DOM, dissolved organic matter; POM, particulate organic matter; c, host choanocyte cell, hs, hotspot of enrichment in host choanocyte cell; m, host mesophyll cell; b, symbiont bacteria. Scale bars are 5 µm.

The NanoSIMS data demonstrated clear differences in food processing by the HMA and LMA sponge. These differences were largely driven by the disparity in microbial abundances in the two species rather than distinct variations in cellular uptake rates between the two sponge species; this could be seen qualitatively in the NanoSIMS images (Fig. 3) but also quantitatively in the extracted data (Fig. 4). Enrichment of ^{13}C and ^{15}N in host cells and microbes were overall very similar in the HMA and LMA sponges with few significant differences detected in the specific enrichment of choanocyte cells or choanocyte hotspots and bacteria in between the two sponges (Fig. 4). In general, a higher proportion of microbial cells were enriched in the HMA sponge while a higher proportion of choanocyte cells tended to be enriched in the LMA sponge, but the differences tended to be small (Fig. 4, pie chart panels). Consequently, the differences in the overall uptake rates of the four food sources (Fig. 2A-D) appear to be largely driven by the substantial differences in host and symbiont biomass in the HMA and LMA sponge (Fig. 3) rather than differences in single-cell activities of the host and symbiont cells in the HMA versus LMA sponge (Fig. 4).

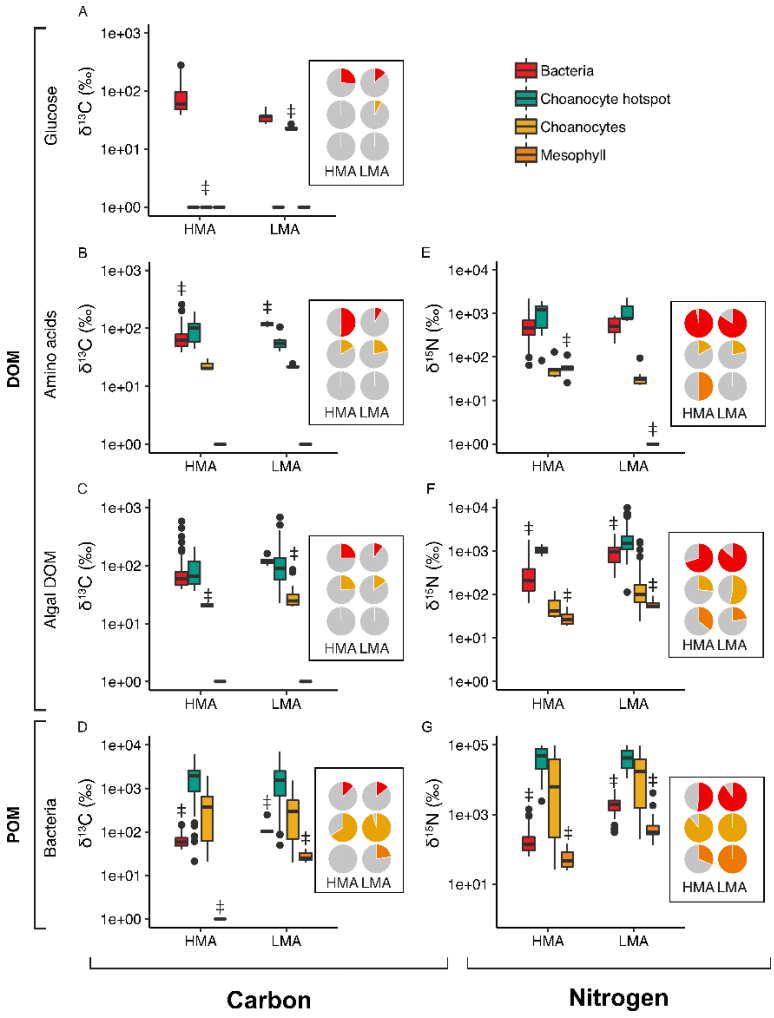

Figure 4. Single-cell quantification of δ^{13}carbon and δ^{15}nitrogen enrichment in the HMA sponge *A. aerophoba* and LMA sponge *D. avara*. Four regions of interest (ROIs) were analysed by NanoSIMS: 1) symbiont bacteria, 2) hotspots of enrichment in host choanocyte cells, 3) host choanocyte cells, and 4) host mesohyl cells. Measured was the mean enrichment (‰) of $\delta^{13}C$ (**A-D**) and $\delta^{15}N$ (**E-G**) for each ROI type after the 3h isotopic pulse with the four labelled food sources. A minimum of n=20 ROIs were analysed for each ROI type. Note the different log10 y-axis scales. Pie charts depicting the proportion of ROIs enriched in ^{13}C or ^{15}N (L-N) for each of the three cell types of interest (bacteria, choanocyte cells, mesohyl cells).

Contribution of symbiont cells to holobiont DOM uptake differs in the HMA and LMA sponge

To quantitatively determine host and symbiont contributions to DOM uptake rates (Fig. 2A-D), the ^{13}C and ^{15}N enrichment in the separated sponge and microbial cell fractions and their total cellular CN biomass was used to calculate the percent contributions of the two compartments to total holobiont uptake (Fig. 2E-L). The relative host and symbiont contributions differed substantially in the HMA and LMA sponge (Fig. 2E-L). Incorporation of DOM into microbial cells accounted for 67-89% of the dissolved C and 75-86% of the dissolved N assimilated by the HMA sponge *A. aerophoba*. By contrast, <5% of the dissolved C and N assimilated by the LMA sponge *D. avara* was incorporated into microbial cells with the majority of DOM being assimilated by host sponge cells (up to 99% for the algal DOM). Although the $\delta^{13}C$ and $\delta^{15}N$ values of separated cell fraction data were used to calculate the percentages presented in Figure 2, the NanoSIMS data produced remarkably similar results (Table S2). Thus, while microbial symbionts accounted for the majority of DOM uptake in the HMA sponge, the sponge host was responsible for most DOM taken up by the LMA sponge. In both sponge species, microbes assimilated a higher percentage of glucose and amino acids compared with algal DOM, which showed the highest incorporation into sponge cells (Fig. 2E-L).

Microbial contributions to total sponge heterotrophic diet are higher in the HMA sponge

Despite significant differences in DOM uptake rates between the two sponges in the isotope tracer experiments where food was supplied in excess of natural concentrations (Fig. 2A-D), we found that the natural diets of the two sponges were more similar when measured *in situ* under natural concentrations (Fig. 5). *In situ* measurements comparing the water inhaled and exhaled by the sponges, revealed that both species removed similar amounts particulate organic carbon (POC; measured as pico- and nanoplankton) (Fig. 5A). The HMA sponge *A. aerophoba* was more efficient at removing DOC, removing 12 µmol/L compared to 5 µmol/L for *D. avara* (Fig. 5A); but, since *D. avara* had a significantly higher pumping rate (Fig. 5B), filtration rates were actually slightly higher for both DOC and POC in the LMA sponge when normalized to pumping activity (Fig. 5C). For both species, DOM was the primary source of heterotrophic carbon (Fig. 5C). It accounted for 92.4 ± 4.4% of the total C and 88.7 ± 5.5% of the N consumed by *A. aerophoba*. Although DOM accounted for a similar proportion of the heterotrophic C of *D. avara* (87.3%), the LMA sponge exhibited net excretion of DON *in situ* (12). Using the host and symbionts percent contributions estimated for uptake of algal DOM—the DOM source most representative of the *in situ* DOM pool—we calculate that microbes account for 58.6 ± 2.8% and 63.9 ± 3.9% of the total heterotrophic C and N, respectively assimilated by *A. aerophoba.* In contrast, symbiotic microbes account for less than 0.5% of C assimilated by *D. avara* and made no contribution to net N uptake (Fig. 5D).

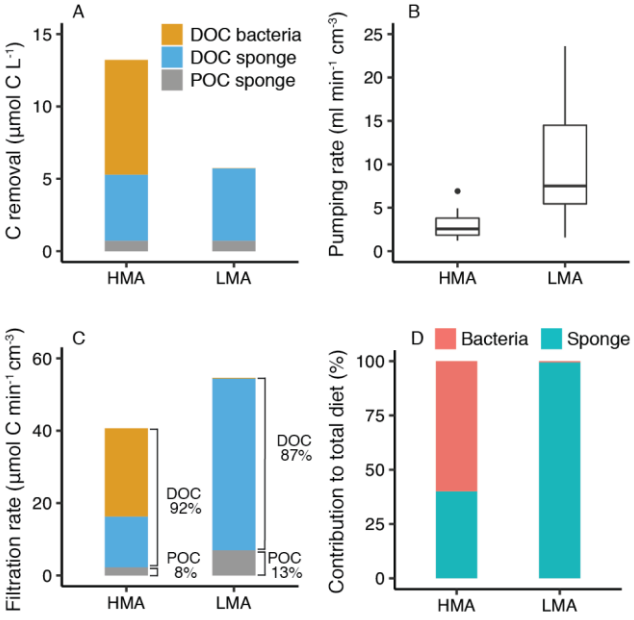

Figure 5. Natural diets of the HMA sponge *Aplysina aerophoba* and LMA sponge *Dysidea avara*. (**A**) Differential *in situ* measurements of the seawater inhaled and exhaled by the sponges using the VacuSIP technique. (**B**) Pumping rates of HMA and LMA sponges. (**C**) Filtration rate with carbon removal normalized to pumping rate (**D**) Microbes accounted for 58.6% of the total C (DOC + POC) filtered by the HMA sponge, but <1% in the LMA sponge. *D. avara* data from Morganti et al. 2017. DOC, dissolved organic carbon; POC, particulate organic carbon.

Translocation of C and N between symbiont and host cells

The separated cell fractions showed no evidence for translocation of microbial-assimilated C and N to the host sponge host within the 9h timeframe of the experiment as there was no significant increase in $\delta^{13}C$ or $\delta^{15}N$ values in the sponge cells between the end of the 3h isotopic pulse and 9h chase period (Fig. S1). However, we did observe host cells engulfing symbionts cells, suggesting a potential mechanism by which C and N could be transferred from the symbionts to host cells. There was a small but significant increase in $\delta^{13}C$ and/or $\delta^{15}N$ values in the microbial cell fractions of the HMA sponge between the pulse and chase periods in the glucose and amino acids treatments (Fig. S1), which could suggest transfer of C and N from host cells, although we did not observe a concurrent decrease in enrichment in the host cells. Interestingly, we detected ^{13}C and ^{15}N enrichment in microbial cells in the bacteria treatment in the NanoSIMS data after only 3h (Fig. 4D, K). Since food bacteria are phagocytosed by host choanocyte cells and either digested or transferred to mesohyl cells for digestion, this suggests host assimilated bacteria were rapidly digested and the processed C and N waste products readily made available to microbial symbionts in the mesohyl.

Turnover of assimilated DOM into sponge detritus

In order to determine if the two sponge species contribute to DOM recycling via the sponge loop, we measured the amount of incorporated DOM that was turned over as sponge detritus between the end of the 3h pulse period and the 6h chase period. Both sponge species produced detritus during all treatments, demonstrating detritus production occurred regardless of food source (Fig. 6A-D). However, there was significant turnover of assimilated C and N into sponge detritus only in the algal DOM and bacterial treatments, with turnover rates 1-2 orders of magnitude higher than in the glucose or amino acid treatments (Fig. 6D-H). The percentage of DOM that was turned over into sponge detritus between 3 and 6h was 2–7% for the algal DOM and 0.03–0.7% for the amino acids and glucose but was consistently higher (2–24 times) in the LMA sponge. Thus, despite consistency in detritus production rates, there was high variability in the turnover of ingested food into detritus reflecting differences in how the food sources were processed.

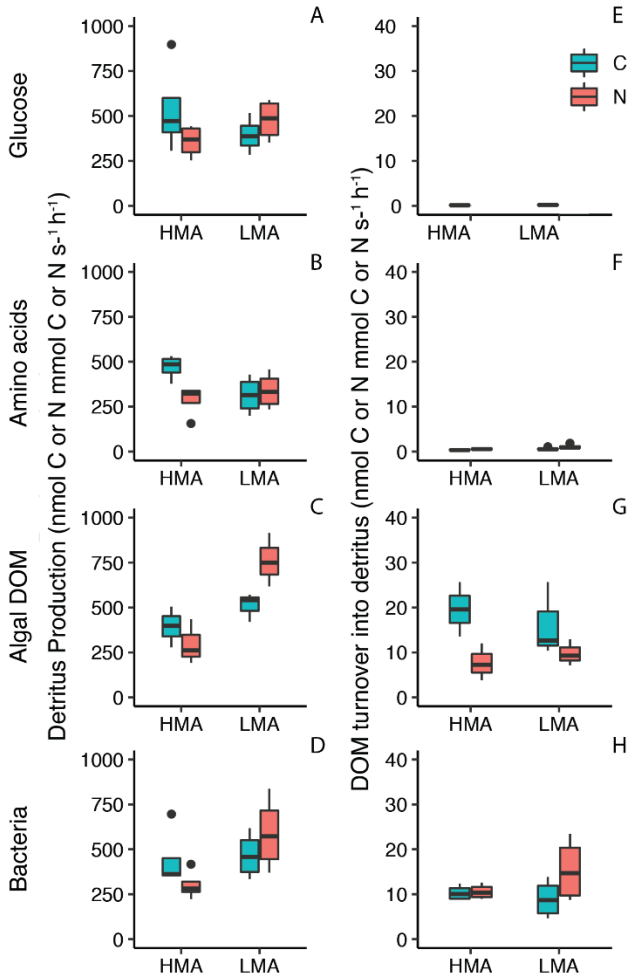

Figure 6. Total detritus production and turnover of DOM into detritus. Rates of total detritus production in the HMA sponge *A. aerophoba* and LMA sponge *D. avara*. (**A-D**) Rates at which the dissolved C and N assimilated by the two sponge species was subsequently released as detrital C and N (**E-H**) for each for the four dissolved and particulate food sources: glucose, amino acids, algal DOM, and bacteria. C, carbon; N, nitrogen.

DISCUSSION

DOM is assimilated by both host and symbiont cells. Contrary to prevailing hypotheses that sponge DOM uptake is exclusively mediated by symbiotic microbes, we found that both host sponge cells and microbial symbionts actively assimilate DOM. The restriction of ^{13}C and ^{15}N enrichment hotspots to the choanocyte cells in the host indicates that the same cells responsible for the capture and phagocytosis of bacterial food (34, 35, 37) are also the primary cells involved in the uptake of DOM. Choanocyte cells are unique to *Porifera* and their involvement in DOM uptake is likely an important factor for their high capacity for DOM uptake compared with other marine invertebrates. While the exact mechanisms by which DOM is taken up are not clear, DOM fed choanocytes exhibit similar spatial enrichment patterns as for those fed with food bacteria, with ^{13}C and ^{15}N localized within food vacuoles (Fig. 3). This suggests that DOM uptake may occur via endocytosis (34). Indeed, sponge choanocytes exhibit macropinocytotic activity (38) and high expression of genes involved in macropinocytosis (39, 40); nevertheless, membrane transporters may also play a role as reported in other marine invertebrates (39, 41).

Sponge-associated microbes possess diverse transporters for the uptake of organic compounds (42-45), but their extracellular location in the inner sponge mesohyl requires that these compounds first pass through the epithelia of the either pinacoderm or choanoderm before it is accessible. Dissolved substances may be transported across the membranes of choanocytes or the endopinacocytes lining the incurrent canals of the host aquiferous system (39) or pass through leaky cell junctions to enter the mesophyll directly (37, 46). Despite hosting distinct and diverse microbial communities (Fig. 1E, F), the majority of microbes in both sponges were enriched in ^{13}C or ^{15}N in the amino acids and algal DOM treatments (64-97%), indicating DOM utilization is a common feature of sponge-associated microbes. Indeed, diverse heterotrophic metabolic capabilities are a common feature in the genomes of sponge symbionts (42-45, 47-51) and widespread use of DOM by sponge-associated microbes could explain inability to link sponge DOM uptake to specific microbial phyla (52). Nevertheless, the DOM pool represents a diverse and heterogenous mixture of substances and differences in utilisation of our three DOM sources suggest that, similar to DOM compartmentalization by free-living seawater microbes (53), there is likely to be metabolic specialization within the sponge microbiome for certain dissolved compounds (42-44).

Despite the fact that both host and microbial cells were active in DOM uptake, host cells were more limited in their capacity to utilize a broad range of dissolved compounds. In contrast, microbial sponge symbionts were better able to effectively utilize the full range of dissolved compounds measured, particularly glucose and amino acids, which translated into significantly higher uptake rates of these compounds in the HMA compared to the LMA sponge. It has been proposed that sponge cells may utilize the colloidal fraction of DOM, while the associated microbes consume the truly dissolved material (18, 54). Although incorporation of amino acids into choanocytes demonstrates clear uptake

of true low-molecular DOM by host cells, it is possible that the higher uptake of the algal DOM is due higher colloidal content. The exact composition of algal DOM is unknown but consists of the complex mixture of compounds released during algal cell lysis. By expanding host access to a wider variety of compounds the sponge microbiome provides an important function analogous to the gut microbiomes of higher animals (55). Despite lacking a gut, sponges essentially function as efficient uptake systems and in fact represent an early multicellular uptake system (5). Dual uptake by host and symbionts cells likely increases the capacity of the sponge holobiont to take up DOM compared to either free-living microbes or other marine animals.

HMA and LMA sponges have different strategies for DOM uptake. Despite exhibiting significant differences in DOM uptake rates during *ex situ* isotope tracer experiments (Fig. 2), both the HMA and LMA sponge were well-adapted to taking up DOM *in situ*. DOC accounting for ~90% of the natural diet of both species (Fig. 5). However, the role of microbial symbionts in mediating DOM uptake was strikingly different in the two sponge types. The HMA sponge relied heavily on its microbial symbionts for DOM uptake with microbes accounting for the majority (67-89%). By comparison, symbiont microbes made a very low contribution to DOM uptake in the LMA sponge (<5%) and instead DOM was taken up almost entirely by host cells. Symbiotic microbes often provide their host with entirely novel functions (e.g. photosynthesis), but in this case the two sponges appear to have evolved two strategies —one largely microbial-mediated and the other host driven—for accomplishing the same function. One proposed explanation for the HMA-LMA dichotomy is that HMA sponges have evolved to while LMA sponges solely use particulate food to meet their energy demands (28), but our findings suggest this is not the case.

HMA sponges have been considered better adapted for DOM uptake due to: 1) higher symbiont densities and 2) slower pumping rates which increase the residence time of water in the sponge aquiferous system and therefore the contact time for to cells to access DOM (28). We found limited evidence for the latter as we consistently found similar enrichment in the choanocytes and microbes of the two sponges. The HMA sponge was more efficient at taking up DOC *in situ*, removing 12 µmol/L compared with 5µmol/L in the LMA sponge and this appeared to directly due to higher uptake by microbial symbionts resulting from its higher microbial biomass (Fig. 5A). However, the higher pumping rate in the LMA resulted in an overall higher DOC filtration rate in the LMA sponge (Fig. 5B, C). Thus, while microbes allow HMA sponges to more efficiently utilize a wider range of dissolved compounds, LMA sponges may able to compensate for decreased uptake efficiency by processing larger volumes of water (28). The capacity to efficiently utilize a greater variety of dissolved compounds could contribute to the fact that *in situ* HMA sponges often exhibit higher and more consistent DOM uptake compared to LMA sponges where DOM uptake tends to be much more variable, sometimes showing net excretion (10, 12, 13). These two strategies also likely contribute to trophic niche partitioning between HMA and LMA sponges (12), with HMA sponges able to capitalize on dissolved compounds

that are unavailable to LMA sponges. Niche partitioning is an important factor in enabling co-existence of species and is thought to play a role in explaining the high densities of HMA and LMA sponges (12). DOC is by far the most abundant source of organic carbon in the ocean (15), and it appears the two sponge types have evolved different strategies for to exploit DOM strongly suggesting that DOM utilization is a key factor in the success of marine sponges.

Symbiont contributions to the heterotrophic sponge diet. Microbes not only accounted for the majority of DOM uptake in the HMA sponge, but also accounted for most of the total heterotrophic C and N assimilated by the HMA sponge. Chemo- and photosynthetic microbes are known to provide the sponge host with autotrophically fixed C (56-62), but here we provide quantitative data demonstrating sponge symbionts also contribute to heterotrophic C. We calculate that microbial symbionts are responsible for more than half (~60%) of the total heterotrophic C and N assimilated by the HMA sponge. Although microbes were similarly active in the LMA sponge, due to their low numbers and high host activity, their contribution to total C and N assimilation was overall low. Nevertheless, even in LMA sponge heterotrophic microbes likely contribute to host nutrition through the provision of vitamins and essential amino acids (44, 51). Although symbiont contributions are likely to vary across species, we show they can make a major contribution to heterotrophic nutrient acquisition by the sponge holobiont through the assimilation of DOM.

We did not detect translocation of microbial-assimilated C and N to the sponge host, but the 9h timeframe may have been insufficient to detect potential nutrient transfer (56). Since we estimate that microbes assimilate ~60% of the total heterotrophic C and N assimilated by the HMA sponge but only account for ~25% of its biomass, there may be an imbalance in energy requirements if C and N were not transferred to the host. Symbiont-host nutrient transfer could occur through the translocation of small organic compounds (58, 63), as for many intracellular symbioses (64), or via phagocytosis of symbionts by host cells (65), or a combination of both through a "double translocation" system (66). There is evidence for translocation of low-molecular weight compounds (58, 63) and high rates of phagocytosis in the HMA sponge *Geodia barretti* are estimated to be sufficient to allow for a significant proportion of microbial-assimilated DOM to be transferred to the host (11). Indeed, we did observe host cells engulfing symbionts in the HMA sponge. However, it remains uncertain how dependent on microbial supplied DOM the sponge host is to meet its metabolic demand. In support of the complex recycling of nutrients believed to occur within the sponge holobiont (45, 67, 68) we did find evidence that symbionts rapidly recycle host processed C and N. Such internal nutrient recycling in other marine holobionts (e.g. corals) is believed to help these animals survive in oligotrophic marine environments (66).

Microbes may influence DOM turnover via the sponge loop. Through the rapid turnover of assimilated DOM into sponge detritus, sponges are thought to play an important role in recycling DOM in benthic food webs (31). However, it has been suggested that the sponge loop may simply be a

microbial loop occurring inside a host. Although both species produced detritus in all treatments, turnover of assimilated C and N into detritus only occurred for food sources that showed high uptake into sponge choanocyte cells (bacteria and algal DOM), while DOM sources that were largely taken up by microbes (glucose and amino acids) showed much lower turnover (<1%). This is consistent with the hypothesis that sponge detritus consists largely of shed host choanocyte cells (69, 70). However, this may also reflect differences in processing of the different food sources; incomplete digestion of bacteria and algal DOM may result in the excretion of detrital waste products (71), while glucose and amino acids are more rapidly respired (54) and assimilated into biomass (21), respectively, compared to algal DOM. Interestingly, this suggests that microbial-assimilated DOM may not contribute to rapid turnover of DOM into detritus via the sponge loop, at least through cell shedding; other processes such as excretion of undigested food and waste products (71) as well as mucus production (72, 73) also generate sponge detritus.

Overall, the percentages of algal DOM turnover were substantially lower (2–7%) in the two massive sponges compared to sponges with encrusting growth forms (~15–40%) (74-76). This supports the hypothesis that massive sponges likely allocate more resources into upward growth compared with encrusting sponges whose growth is limited by available substrate and may instead invest in high biomass turnover to rejuvenate their filtration system (10, 13, 77). However, while cell turnover can occur rapidly (<6h; (69, 70, 78), slower or more sporadic processes, may not have been captured within the 6h timeframe of the experiment but could still contribute to the sponge loop (72). These findings suggest that DOM composition, sponge growth form, and microbial abundance all impact how DOM is recycled via the sponge loop pathway. Importantly, while microbes influence both the uptake of DOM and how it is recycled, the host itself plays an active role in DOM cycling demonstrating that the sponge loop is not simply a host-associated microbial loop but is rather influenced by both host and symbiont activity.

CONCLUSION

Here we demonstrate that contrary to the widespread hypothesis that DOM uptake by sponges is mediated solely by symbiotic microbes, both symbionts and host cells are actively involved in DOM cycling. Consequently, both the HMA and LMA sponge were able to effectively utilize DOM. However, despite the fact the DOM accounted for a similar proportion of the natural sponge diet of both species (~90%), the HMA and LMA sponge used two different strategies for DOM uptake; Microbes accounted for the majority of DOM uptake in the HMA sponge but made a minimal contribution in the LMA sponge, which instead relied on uptake by host choanocyte cells. We thus propose that HMA and LMA sponges have different strategies for utilizing DOM. The increased microbial uptake in the HMA sponges allowed the HMA sponge to efficiently use dissolved compounds that were less available to LMA sponges. Despite lower uptake efficiencies, the LMA sponge may have been able to compensate

by pumping higher volumes of water. Thus, HMA and LMA sponges may be adapted to utilizing different types of DOM, allowing both sponge types to capitalize on the largest reservoir of organic carbon in the ocean. A complex interplay between DOM quality and quantity, host activity, and symbiont abundance is likely to influence DOM uptake in marine sponges. Overall, we estimate the microbial symbionts account for ~60% of the total heterotrophic C and N assimilated in the HMA sponge but make a negligible contribution (<0.5%) in the LMA sponge. This demonstrates that similar to phototrophic symbionts, heterotrophic symbionts can play an important role in nutrient acquisition in marine sponges. Further studies are needed to establish the exact mechanisms by which DOM is taken up, whether the host can regulate symbiont access to DOM, and the degree to which microbial assimilated C and N is translocated to the host. In addition to contributing to nutrient cycling within the holobiont, microbes may also influence DOM turnover via the sponge loop. Collectively this demonstrates that microbes play an integral role in influencing how DOM is cycled by the sponge holobiont with implications for DOM cycling at the ecosystem level.

METHODS

Organism collection

Specimens of *Aplysina aerophoba* and *Dysidea avara* (each n=20) were collected by SCUBA from the coast of Girona, Spain (42º 06' 55" N, 3º 10' 8" E) at depths of 3–15 m during April and May 2017. Sponges were transferred to the aquaria facilities at the Institute of Marine Sciences (ICM-CSIC) in Barcelona and maintained in individual 6 L aquaria supplied with fresh flowing seawater at a rate of ~30 L h^{-1}. Each sponge individual was divided into 5 fragments of a similar size, each with a single fully functional osculum, and attached to PVC plates. Sponges were acclimated for 5 days and only healthy, actively pumping individuals were used in experiments.

Stable isotope pulse-chase labelling experiments

Stable isotope pulse-chase experiments were conducted to test for the assimilation of three dissolved (^{13}C-glucose, ^{13}C- and ^{15}N-amino acids, ^{13}C- and ^{15}N- algal DOM) and one particulate food source (^{13}C- and ^{15}N-labelled bacteria). Details of the preparation of the four food sources and experimental procedures is described in (SI Appendix, SI Materials and Methods). Food sources were added to individual 6 L aquaria (1 sponge fragment per aquaria) at a concentration of ~80 µM C, approximately equivalent to the background concentrations of DOC in the surrounding seawater (60-120 µM). Total amounts C and N added and enrichment of the four food sources is listed in Table S1.

The experiment followed a pulse-chase design to follow incorporation over time and test for translocation of assimilated C and N between host and symbiont cells. Small aquaria pumps ensured water circulation during the 3h pulse incubation and aquaria were kept in a water bath of free-flowing seawater to ensure maintenance of ambient seawater temperature. Sponges were sampled at 5 time points: three pulse time-points (0.5h, 1h, and 3h) after which all remaining sponges were rinsed in label-free seawater and transferred without air exposure to label-free aquaria and sampled at two chase points (6h and 9h). Production of sponge detritus was measured during the chase period by stopping water flow to the aquaria to allow any detritus produced by the sponges to accumulate. Detritus was collected after the 6h chase point and water flow was resumed for the 9h chase point. Each time point consisted of 4 replicates with one fragment from each individual used in each time point (total of $n = 20$ replicates per treatment). Control samples were collected before ($n = 4$) and after ($n = 4$) the experiments.

At each sampling point sponge tissue samples were collected for 1) stable isotope analysis of bulk sponge tissue, 2) stable isotope analysis of separated sponge and microbial cell fractions, and 3) scanning electron microscopy (SEM) and NanoSIMS (details in SI Appendix, SI Materials and Methods). Samples for SEM and NanoSIMS were sampled with a 2 mm tissue biopsy punch and immediately fixed in 4% paraformaldehyde in PBS buffer for 12h at 4°C and then transferred to PBS and stored at 4°C until further processing. Samples for isotope analysis of the bulk sponge tissue (~1

cm^3) were rinsed in filtered seawater followed by a brief rinse with MilliQ water to remove excess salt and frozen at -80°C. The remainder of the sponge tissue was cut into small pieces and placed in ice-cold calcium- and magnesium-free artificial seawater with 10% EDTA (CMFASW+EDTA) at 4°C for 1h before separation into sponge cell and microbial cell fractions. To sample the detritus produced by the sponges, the seawater from the 6h chase was vacuum filtered onto pre-combusted GF/F filters. Filters were lyophilized and stored at -80°C until analysis.

Calculations of host and symbiont biomass

Sponge and microbial cell fractions were separated by centrifugation using methods adapted from Wehrl et al. 2007 (79) and Freeman et al. 2014 (57) (details in SI Appendix, SI Materials and Methods). To determine the number of sponge and microbial cells present in the initial homogenate and to test the purity of the sponge and microbial cell fractions, samples were taken from the initial 100 µm filtered homogenate and the purified sponge and microbial cell fractions (N=176 in total). These samples were fixed with 1% paraformaldehyde, vortexed, fixed at room temperature for 10 min, and frozen at -80°C until cell counts were performed. For the cell counts, the thawed samples were stained with DAPI (1µg/ml) and counted using a C-Chip Neubauer improved hemocytometer (Carl Roth, Germany) on an Axio Observer.Z1 microscope equipped with AxioCam 506 and Zen 2 version 2.0.0.0 software (Carl Zeiss Microscopy GmbH, Göttingen, Germany) at 40x magnification. Combined brightfield and DAPI signals were used to quantify stained cells according to the manufacturer instructions (C-Chip Neubauer improved, Carl Roth, Germany). All controls and samples from the 3h timepoint were counted (N=56). Purity of cell fractions was >99 % for the microbial cell fractions and >85 % for the sponge cell fractions.

To determine C and N content of the sponge and microbial cells for biomass calculations, known volumes of the separated cell fractions were filtered onto a pre-combusted GF/F filter for elemental CN analysis (n=16). Cell counts indicated that 99.5 % of the microbial cells were effectively captured on the filters. The C and N content of the filters was divided by number of cells filtered to calculate the mean C and N content per sponge and microbial cell for each of the two species. The mean C and N contents and total cell numbers in the initial homogenate were used to calculate the percent biomass of sponge and microbial C and N in the two sponge species.

Calculations host and symbiont percent contribution to DOM uptake

The CN biomass of sponge and microbial cells and the ^{13}C and ^{15}N enrichment of the two cell fractions (determined independently by both bulk isotope analysis of separated cell fractions and NanoSIMS) were used to calculate the percent contributions of host cells and microbial symbionts to the total uptake rates of the three dissolved food sources. It was assumed that host sponge cells were responsible for 100 % of the uptake of the particulate food source (bacteria) based on known mechanisms of sponge feeding (34, 35, 37).

SEM and NanoSIMS analysis

Samples for SEM and NanoSIMS were sampled with a 2 mm tissue biopsy punch and immediately fixed in 4% paraformaldehyde in PBS buffer for 12h at 4°C and then transferred to PBS and stored at 4°C until further processing. Fixed tissue samples from the pulse-chase experiment were dehydrated in a series of ethanol and embedded in LR white for SEM and NanoSIMS. Ultrathin tissue sections (~120 nm) were mounted onto silicon wafers and stained with uranyl acetate and lead citrate before imaging on a Zeiss Gemini 500 field emission variable pressure SEM equipped with energy selective backscatter detector and secondary ion detector at 5kv. Images with ~50x50 µm field of view containing cellular structures of interest were mapped for subsequent NanoSIMS analysis.

To examine ^{13}C and ^{15}N enrichment in the two sponges at single cell resolution, the selected areas mapped by SEM were analysed for ^{13}C and ^{15}N enrichment using a NanoSIMS 50L ion probe (CAMECA) at the Center for Advanced Surface Analysis (University of Lausanne). SEM sections on silicon wafers were gold-coated and bombarded with a 16 keV primary Cs+ ion beam with a spot size of ~150 nm. Raster scans of the areas of interest (10 layers) were performed at a resolution of 256x256 pixels with a beam dwell time of 5ms per pixel and an image size of 30x30 µm. The secondary ions $^{12}C_2$ (mass 24), $^{13}C^{12}C$ (mass 25), $^{12}C^{14}N$ (mass 26), $^{12}C^{15}N$ (mass 27), ^{31}P (mass 31), ^{32}S (mass 32), and ^{19}F (mass 19) were simultaneously collected using electron multipliers at a mass resolution (M/ΔM) of 9000. Unlabelled sponges were measured daily as controls.

NanoSIMS data were processed using the ImageJ plugin OpenMIMS in Fiji (National Resource for Imaging Mass Spectrometry, https:// github.com/BWHCNI/OpenMIMS/wiki). Maps of $^{13}C/^{12}C$ and $^{15}N/^{14}N$ enrichment were obtained by taking the ratio of the drift corrected and stacked $^{13}C^{12}C$ and $^{12}C_2$ or $^{12}C^{15}N$ and $^{12}C^{14}N$ images, respectively. Quantification of isotope ratios in the different cell types was achieved by manually drawing regions of interest (ROIs) on the $^{12}C^{14}N$-image using the corresponding SEM maps for reference. The analysis focused on three main cell types 1) symbiont microbes (0.2-2µm), 2) host choanocyte cells (3-10 µm), and 3) all other host cells in the sponge mesophyll, including ameobocytes, archeocytes, spherulous cells, and pinacocytes (7-30 µm). Additionally, hotspots of enrichment in the host choanocyte cells were measured separately. A total of 16 samples were analysed: two samples per species from each treatment (apart from the glucose treatment where enrichment was low and only one samples was measured) and two controls (one for each species). Approximately 4-8 images were obtained per sample in order to capture at a minimum of n=20 for each cell or region of interest (ROI) type. In total 4,562 ROIs were measured. ROIs were considered enriched if the extracted $\delta^{13}C$ or $\delta^{15}N$ values were greater than twice the standard deviation of the control ROIs.

In situ measurements the natural sponge diet

The natural diet of the two sponge species were measured *in situ* by SCUBA using the InEx VacuSIP technique (see Morganti et al. 2016 (80) for full methodological details). Sampling for *A. aerophoba* was conducted in May–June 2017 off the coast of Girona, Spain (42º 03' 34" N 3º 12' 51" E) between 5–15m water depth. Data for *D. avara* was taken from Morganti et al. 2017 (12). Briefly, net fluxes were determined by measuring concentration differences between the water inhaled (In) and exhaled (Ex) by the sponge. Exhalant water was sampled directly from the sponge osculum while inhalant water was measured a few cm away using a custom set-up using vacuum pressure to draw in water. The sampling rate (<1 mL min^{-1}) was kept sufficiently below the pumping rate of the sponge to avoid contamination of the exhaled sample with ambient of water. Samples were taken for dissolved organic carbon (DOC) and nitrogen (DON) to measure the DOM components of the diet and samples for pico- and nanoplankton were taken as the primary POM component of the sponge diet. Although some sponges can also consume detritus, this was not measured due to the long sampling time required (>8h) and because detritus is not an important food source for *D. avara* (81). Details of sample analysis in SI Appendix, SI Materials and Methods. The percent contribution of DOM to the total heterotrophic sponge diet and percent symbiont contribution to the uptake of algal DOM were used to calculate the symbiont contribution to total heterotrophic C and N uptake by the sponge holobiont. Values calculated for algal DOM were selected as it is the DOM source most representative of the natural DOM pool available *in situ*.

Statistical analyses

Statistical analyses were conducted in PRIMERv7 (82) with the PERMANOVA+ add-on (83). Univariate permutational analyses of variance (PERMANOVAs) were used to test for significant differences between groups. Dissimilarity matrices constructed using Euclidean distance and the $P_{(perm)}$ value was based on 9999 permutations. Type III (partial) sums of squares were used to account for the unbalanced design of the NanoSIMS data. Post-hoc comparisons were conducted when significant factor effects were found. Results were considered significant at the level $P_{(perm)}<0.05$.

REFERENCES

1. Gili JM & Coma R (1998) Benthic suspension feeders: their paramount role in littoral marine food webs. Trends Ecol Evol 13(8):316-321.
2. Pile AJ, Patterson MR, Savarese M, Chernykh VI, & Fialkov VA (1997) Trophic effects of sponge feeding within Lake Baikal's littoral zone .2. Sponge abundance, diet, feeding efficiency, and carbon flux. Limnol Oceanogr 42(1):178-184.
3. McMurray SE, Johnson ZI, Hunt DE, Pawlik JR, & Finelli CM (2016) Selective feeding by the giant barrel sponge enhances foraging efficiency. Limnol Oceanogr 61: 1271-1286.
4. Bell JJ (2008) The functional roles of marine sponges. Estuarine Coastal and Shelf Science 79(3):341-353.
5. Simion P, et al. (2017) A large and consistent phylogenomic dataset supports sponges as the sister group to all other animals. Curr Biol 27(7):958-967.

6. Yin Z, et al. (2015) Sponge grade body fossil with cellular resolution dating 60 Myr before the Cambrian. PNAS 112(12):E1453-E1460.
7. de Goeij JM, van den Berg H, van Oostveen MM, Epping EHG, & Van Duyl FC (2008) Major bulk dissolved organic carbon (DOC) removal by encrusting coral reef cavity sponges. Mar Ecol Prog Ser 357:139-151.
8. Mueller B, et al. (2014) Natural diet of coral-excavating sponges consists mainly of dissolved organic carbon (DOC). PloS One 9(2).
9. Archer SK, Stevens JL, Rossi RE, Matterson KO, & Layman CA (2017) Abiotic conditions drive significant variability in nutrient processing by a common Caribbean sponge, *Ircinia felix*. Limnol Oceanogr 62(4):1783-1793.
10. Hoer DR, Gibson PJ, Tommerdahl JP, Lindquist NL, & Martens CS (2018) Consumption of dissolved organic carbon by Caribbean reef sponges. Limnol Oceanogr 63(1):337-351.
11. Leys SP, Kahn AS, Fang JKH, Kutti T, & Bannister RJ (2018) Phagocytosis of microbial symbionts balances the carbon and nitrogen budget for the deep-water boreal sponge *Geodia barretti*. Limnol Oceanogr 63(1):187-202.
12. Morganti T, Coma R, Yahel G, & Ribes M (2017) Trophic niche separation that facilitates co-existence of high and low microbial abundance sponges is revealed by *in situ* study of carbon and nitrogen fluxes. Limnol Oceanogr 62(5):1963-1983.
13. McMurray SE, Stubler AD, Erwin PM, Finelli CM, & Pawlik JR (2018) A test of the sponge-loop hypothesis for emergent Caribbean reef sponges. Mar Ecol Prog Ser 588:1-14.
14. Yahel G, Sharp JH, Marie D, Hase C, & Genin A (2003) In situ feeding and element removal in the symbiont-bearing sponge *Theonella swinhoei*: Bulk DOC is the major source for carbon. Limnol Oceanogr 48(1):141-149.
15. Zhang C, et al. (2018) Evolving paradigms in biological carbon cycling in the ocean. National Science Review 5(4):481-499.
16. Azam F (1998) Microbial control of oceanic carbon flux: the plot thickens. Science 280(5364):694.
17. Putter AF (1914) Der Stoffwechsel der Kieselschwamme. Z. allg. Physiol 16:65-114.
18. Reiswig HM (1974) Water transport, respiration and energetics of 3 tropical marine sponges J Exp Mar Bio Ecol 14(3):231-249.
19. Jorgensen CB (1966) Biology of suspension feeding, Pergamon Press, Oxford.
20. Manahan DT (2015) Adaptations by invertebrate larvae for nutrient acquisition from seawater Integr Comp Biol 30(1):147-160.
21. Mueller CE, Larsson AI, Veuger B, Middelburg JJ, & van Oevelen D (2014) Opportunistic feeding on various organic food sources by the cold-water coral *Lophelia pertusa*. Biogeosciences 11(1):123-133.
22. Baines SB, Fisher NS, & Cole JJ (2005) Uptake of dissolved organic matter (DOM) and its importance to metabolic requirements of the zebra mussel, *Dreissena polymorpha*. Limnol Oceanogr 50(1):36-47.
23. Thomas T, et al. (2016) Diversity, structure and convergent evolution of the global sponge microbiome. Nat Com 7(1):11870.
24. Hentschel U, Usher KM, & Taylor MW (2006) Marine sponges as microbial fermenters. FEMS Microbiol Ecol 55(2):167-177.
25. Vacelet J (1975) Electron-microscope study of association between bacteria and sponges of genus *Verongia* (*Dictyoceratida*). Journal De Microscopie Et De Biologie Cellulaire 23(3):271-288.
26. Gloeckner V, et al. (2014) The HMA-LMA dichotomy revisited: an electron microscopical survey of 56 sponge species. Biol Bull 227(1):78-88.
27. Moitinho-Silva L, et al. (2017) Predicting the HMA-LMA status in marine sponges by machine learning. Front Microbiol 8(752).
28. Weisz JB, Lindquist N, & Martens CS (2008) Do associated microbial abundances impact marine demosponge pumping rates and tissue densities? Oecologia 155(2):367-376.
29. Poppell E, et al. (2014) Sponge heterotrophic capacity and bacterial community structure in high- and low-microbial abundance sponges. Marine Ecology 35(4):414-424.
30. Southwell MW, Weisz JB, Martens CS, & Lindquist N (2008) In situ fluxes of dissolved inorganic nitrogen from the sponge community on Conch Reef, Key Largo, Florida. Limnol Oceanogr 53(3):986-996.
31. de Goeij J, et al. (2013) surviving in a marine desert: the sponge loop retains resources within coral reefs. Science 342(6154):108-110.
32. Pawlik JR, Burkepile DE, & Thurber RV (2016) A vicious circle? altered carbon and nutrient cycling may explain the low resilience of caribbean coral reefs. Bioscience 66(6):470-476.

33. Mumby PJ & Steneck RS (2018) Paradigm lost: dynamic nutrients and missing detritus on coral reefs. BioScience 68(7):487-495.
34. Simpson TL (1984) The cell biology of sponges, Springer-Verlag, New York.
35. Imsiecke G (1993) Ingestion, digestion, and egestion in *Spongilla lacustris* (*Porifera*, *Spongillidae*) after pulse feeding with *Chlamydomonas reinhardtii* (*Volvocales*). Zoomorphology 113:233-244.
36. Musat N, Musat F, Weber PK, & Pett-Ridge J (2016) Tracking microbial interactions with NanoSIMS. Curr Opin Biotechnol 41:114-121.
37. Maldonado M, et al. (2010) Selective feeding by sponges on pathogenic microbes: a reassessment of potential for abatement of microbial pollution. Mar Ecol Prog Ser 403:75-89.
38. Laundon D, Larson BT, McDonald K, King N, & Burkhardt P (2019) The architecture of cell differentiation in choanoflagellates and sponge choanocytes. PLoS Biol. 17(4):e3000226.
39. Sogabe S, et al. (2019) Pluripotency and the origin of animal multicellularity. Nature 570(7762):519-522.
40. Musser JM, et al. (2019) Profiling cellular diversity in sponges informs animal cell type and nervous system evolution. bioRxiv:758276.
41. Wright SH & Manahan DT (1989) Integumental nutrient uptake by aquatic organisms. Annu Rev Physio 51:585-600.
42. Slaby BM, Hackl T, Horn H, Bayer K, & Hentschel U (2017) Metagenomic binning of a marine sponge microbiome reveals unity in defense but metabolic specialization. ISME J 11(11):2465-2478.
43. Bayer K, Jahn MT, Slaby BM, Moitinho-Silva L, & Hentschel U (2018) Marine sponges as chloroflexi hot spots: genomic insights and high-resolution visualization of an abundant and diverse symbiotic clade. mSystems 3(6):e00150-00118.
44. Gauthier M-EA, Watson JR, & Degnan SM (2016) Draft genomes shed light on the dual bacterial symbiosis that dominates the microbiome of the coral reef sponge *Amphimedon queenslandica*. Front Mar Sci 3(196).
45. Moitinho-Silva L, et al. (2017) Integrated metabolism in sponge–microbe symbiosis revealed by genome-centered metatranscriptomics. ISME J 11(7):1651-1666.
46. Leys SP & Riesgo A (2012) Epithelia, an evolutionary novelty of Metazoans. J Exp Zool B Mol Dev Evol 318(6):438-447.
47. Kamke J, et al. (2013) Single-cell genomics reveals complex carbohydrate degradation patterns in poribacterial symbionts of marine sponges. ISME J 7(12):2287-2300.
48. Horn H, et al. (2016) An enrichment of crispr and other defense-related features in marine sponge-associated microbial metagenomes. Front Microbio 7(1751).
49. Astudillo-Garcia C, et al. (2018) Phylogeny and genomics of SAUL, an enigmatic bacterial lineage frequently associated with marine sponges. Environ Microbiol 20(2):561-576.
50. Karimi E, et al. (2018) Metagenomic binning reveals versatile nutrient cycling and distinct adaptive features in alphaproteobacterial symbionts of marine sponges. FEMS Microbiol Ecol 94(6).
51. Fan L, et al. (2012) Functional equivalence and evolutionary convergence in complex communities of microbial sponge symbionts. PNAS 109(27):E1878-E1887.
52. Gantt SE, et al. (2019) Testing the relationship between microbiome composition and flux of carbon and nutrients in Caribbean coral reef sponges. Microbiome 7(1):124.
53. Teeling H, et al. (2012) Substrate-controlled succession of marine bacterioplankton populations induced by a phytoplankton bloom. Science 336(6081):608-611.
54. de Goeij JM, Moodley L, Houtekamer M, Carballeira NM, & van Duyl FC (2008) Tracing C-13-enriched dissolved and particulate organic carbon in the bacteria-containing coral reef sponge *Halisarca caerulea*: Evidence for DOM feeding. Limnol Oceanogr 53(4):1376-1386.
55. Stewart RD, et al. (2019) Compendium of 4,941 rumen metagenome-assembled genomes for rumen microbiome biology and enzyme discovery. Nat Biotechnol 37(8):953-961.
56. Achlatis M, et al. (2018) Single-cell measurement of ammonium and bicarbonate uptake within a photosymbiotic bioeroding sponge. ISME J 12(5):1308-1318.
57. Freeman CJ, Thacker RW, Baker DM, & Fogel ML (2013) Quality or quantity: is nutrient transfer driven more by symbiont identity and productivity than by symbiont abundance? ISME J 7(6):1116-1125.
58. Wilkinson CR (1979) Nutrient translocation from symbiontic cyanobacteria to coral reef sponges. Biologie des Spongiaires, eds Levi C & Boury-Esnault N (Coll. internat. CNRS, Paris), Vol 291, pp 373-380.
59. Rubin-Blum M, et al. (2019) Fueled by methane: deep-sea sponges from asphalt seeps gain their nutrition from methane-oxidizing symbionts. ISME J 13(5):1209-1225.
60. Freeman CJ, Baker DM, Easson CG, & Thacker RW (2015) Shifts in sponge-microbe mutualisms across an experimental irradiance gradient. Mar Ecol Prog Ser 526:41-53.

61. Achlatis M, et al. (2017) Sponge bioerosion on changing reefs: ocean warming poses physiological constraints to the success of a photosymbiotic excavating sponge. Sci Rep 7(1):10705.
62. Fang JK, Schonberg CH, Mello-Athayde MA, Hoegh-Guldberg O, & Dove S (2014) Effects of ocean warming and acidification on the energy budget of an excavating sponge. Glob Chang Biol 20(4):1043-1054.
63. Shih JL, et al. (2019) Trophic ecology of the tropical pacific sponge *mycale grandis* inferred from amino acid compound-specific isotopic analyses. Microb Ecol.
64. Venn AA, Loram JE, & Douglas AE (2008) Photosynthetic symbioses in animals. J Exp Bot 59(5):1069-1080.
65. Vacelet J & Donadey C (1977) Electron microscope study of the association between some sponges and bacteria. J Exp Mar Bio Ecol 30:301-314.
66. Tanaka Y, Suzuki A, & Sakai K (2018) The stoichiometry of coral-dinoflagellate symbiosis: carbon and nitrogen cycles are balanced in the recycling and double translocation system. ISME J 12(3):860-868.
67. Webster NS & Thomas T (2016) The sponge hologenome. mBio 7(2):e00135-00116.
68. Fiore CL, Labrie M, Jarettt JK, & Lesser MP (2015) transcriptional activity of the giant barrel sponge, *Xestospongia muta* holobiont: molecular evidence for metabolic interchange. Front Microbiol 6.
69. de Goeij JM, et al. (2009) Cell kinetics of the marine sponge *Halisarca caerulea* reveal rapid cell turnover and shedding. Journal of Experimental Biology 212(23):3892-3900.
70. Alexander BE, et al. (2014) Cell turnover and detritus production in marine sponges from tropical and temperate benthic ecosystems. PLoS One 9(10).
71. Maldonado M (2015) Sponge waste that fuels marine oligotrophic food webs: a re-assessment of its origin and nature. Mar Ecol.
72. Hammond LS & Wilkinson CR (1985) Exploitation of sponge exudates by coral reef holothuroids. J Exp Mar Bio Ecol 94:1-9.
73. McGrath EC, Smith DJ, Jompa J, & Bell JJ (2017) Adaptive mechanisms and physiological effects of suspended and settled sediment on barrel sponges. J Exp Mar Bio Ecol 496:74-83.
74. de Goeij JM, et al. (2013) Surviving in a marine desert: the sponge loop retains resources within coral reefs. Science 342(6154):108-110.
75. Rix L, et al. (2017) Differential recycling of coral and algal dissolved organic matter via the sponge loop. Funct Ecol 31(3):778-789.
76. Rix L, et al. (2016) Coral mucus fuels the sponge loop in warm- and cold-water coral reef ecosystems. Sci Rep 6:18715.
77. Pawlik JR & McMurray SE (2020) The Emerging Ecological and Biogeochemical Importance of Sponges on Coral Reefs. Ann Rev Mar Sci 12(1)
78. Kahn AS & Leys SP (2016) The role of cell replacement in benthic–pelagic coupling by suspension feeders. Royal Society Open Science 3(11):160484.
79. Wehrl M, Steinert M, & Hentschel U (2007) Bacterial uptake by the marine sponge *Aplysina aerophoba*. Microbial Ecology 53(2):355-365.
80. Morganti T, Yahel G, Ribes M, & Coma R (2016) VacuSIP, an improved inex method for *in situ* measurement of particulate and dissolved compounds processed by active suspension feeders. J Vis Exp (114):e54221.
81. Ribes M, Coma R, & Gili JM (1999) Natural diet and grazing rate of the temperate sponge *Dysidea avara* (*Demospongiae, Dendroceratida*) throughout an annual cycle. Mar Ecol Prog Ser 176:179-190.
82. Clarke KR & Gorley RN (2006) PRIMER version 6: user manual/tutorial. (PRIMER-E, Plymouth), p.192.
83. Anderson MJ, Gorley RN, & Clarke KR (2008) PERMANOVA+for PRIMER: guide to software and statistical methods, Primer-e.

SUPPLEMENTS

Supplementary Figures:

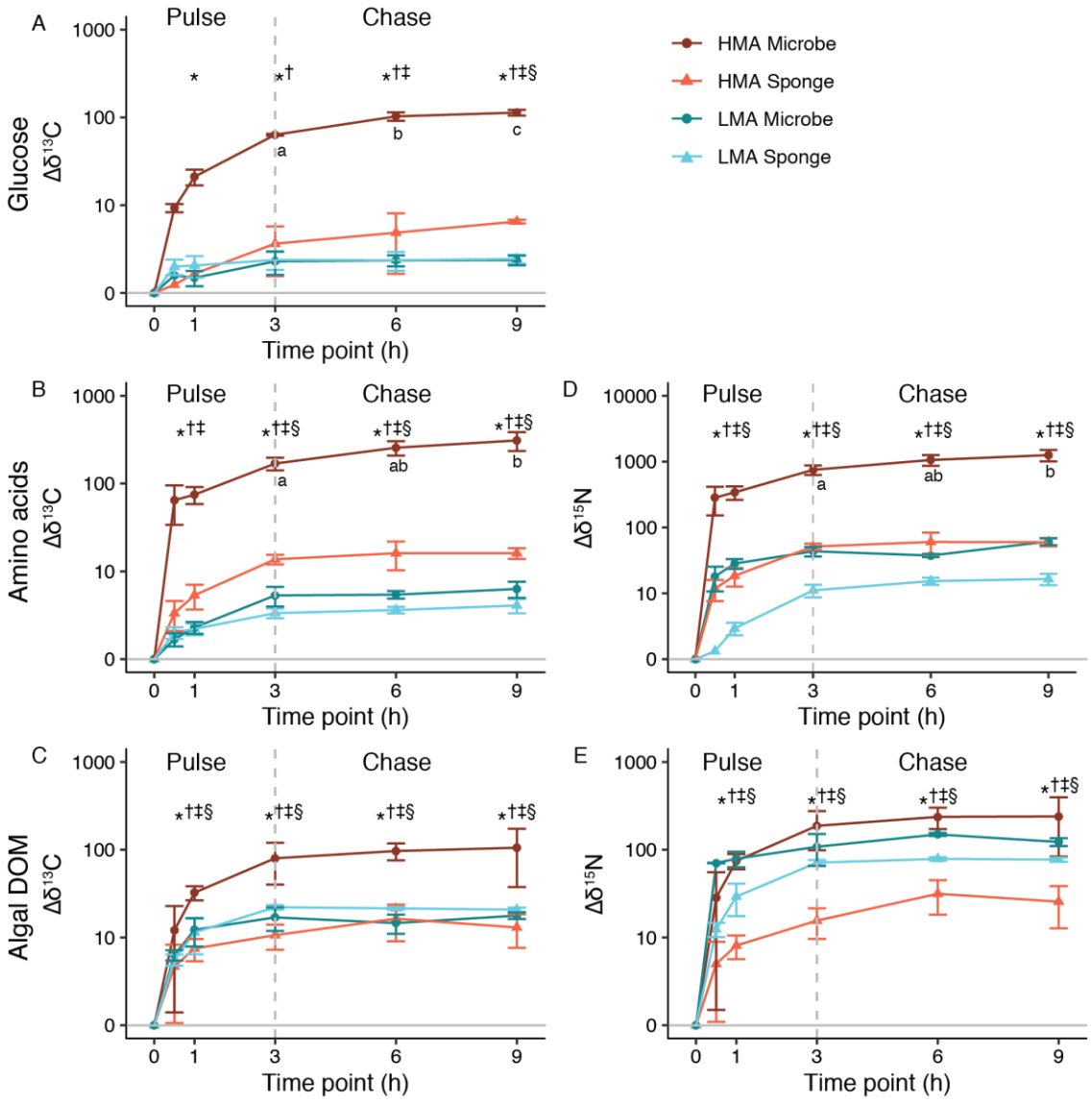

Figure S1. Above background enrichment of ^{13}C (A-C) and ^{15}N (D-E) in the separated sponge and microbial cell fractions for the three dissolved food sources: glucose (A), amino acids (B, D), and algal DOM (C, E) over the 6 time points in the pulse-chase experiments (0, 0.5, 1, 3, 6, 9h) in the HMA sponge *Aplysina aerophoba* and LMA sponge *Dysidea avara*. The vertical grey dashed line at 3h represents the end of the labelling pulse phase and start of the chase phase. Note the different y-axis scale in D. Markers denote significant enrichment compared to controls for HMA microbes*, HMA sponge cells†, LMA microbes‡, and LMA sponge cells§. Letters denote significant differences between the final pulse time point (3h) and the two chase time points (6h and 9h) within the individual cell fractions.

Supplementary Tables:

Table S1. Enrichment of ^{13}C and ^{15}N (atom %), concentration (µM) of carbon (C) and nitrogen (N), and total amounts (µmol) of the four food sources added to the stable isotope pulse-chase experiments.

	Carbon			Nitrogen		
Food source	Concentration (µM)	Total (µmol)	Atm^{13}C%	Concentration (µM)	Total (µM)	Atm^{15}N%
Glucose	81.8	491	99	-	-	-
Amino acids	79.7	478	99	20.0	120	99
Algal DOM	77.6	466	36	8.2	49	43
Bacteria	80	480	50	19.8	118	99

Table S2. Comparison of the percent contribution of host and symbiont cells to the uptake of the different DOM using the cell fraction data (CF) and NanoSIMS data (NS).

DOM source	HMA				LMA			
C	Symbiont (%)		Host (%)		Symbiont (%)		Host (%)	
Glucose	CF	NS	CF	NS	CF	NS	CF	NS
Amino acids	89	83	11	17	1	1	99	99
Algal DOM	85	60	15	40	2	1	98	99
N	67	61	33	39	0.4	1	99.5	99
Glucose	-	-	-	-	-	-	-	
Amino acids	86	89	14	11	5	9	95	91
Algal DOM	75	86	25	14	1	2	99	98

SI MATERIAL AND METHODS

Microbial community analysis.

Microbial community composition was assessed by Illumina sequencing of the 16S sRNA taxonomic gene from 6 individuals of each sponge species collected in June 2017. DNA was extracted from frozen tissue (~0.25 g) using the DNeasy Power Soil Kit (Qiagen) as per the manufacturer's instructions. DNA quantity and purity were measured using a NanoDrop spectrophotometer and gel electrophoresis after a polymerase chain reaction (PCR) with universal 16 rRNA gene primers. The V3 to V4 variable regions of the 16S rRNA gene were amplified using the primer pair 341F 5'-CCTACGGGAGGCAGCAG-3' & 806R 5'-GGACTACHVGGGTWTCTAAT-3' and amplicons were sequenced on a MiSeq platform (MiSeqFGx, Illumina). Sequences were processed using QIIME2 (version 2018.11) with default parameters. The DADA2 algorithm was applied on forward reads (truncated to 250nt) to generate Amplicon Sequence Variants (ASVs) which were phylogenetically classified based on the Silva 132 99% OTUs 16S database and unassigned sequences removed.

Preparation of ^{13}C- and ^{15}N-labelled food sources for stable isotope pulse-chase experiments. The glucose (99 atm% ^{13}C) and algal-derived amino acid mixture (>97 atm% ^{13}C and ^{15}N) were commercially available from Cambridge Isotopes. The algal-DOM and bacteria were produced as follows. The diatom *Skeletonema costatum* was cultured axenically in F/2 media containing 2.1 nM NaHCO3 and 0.9 mM NaNO3 (98 atm% ^{13}C and 99 atm% ^{15}N, respectively; Cambridge Isotopes) at 24°C on a 12h:12h light/dark cycle. Once the diatoms had reached stationary growth phase (~2 weeks), they were centrifuged for 5 min at 1500 rpm, rinsed three times in artificial seawater, frozen at -80°C, and lyophilized. To extract DOM, cells lysis was induced by the addition of MQ followed by 5 min of vortexing and 20 min ultrasonication. The suspension was centrifuged at 4000rpm to pellet any remaining particulate material and the supernatant filtered to 0.2 µm. The extracted DOM was then lyophilized and stored at -80°C until use in experiments. The diatom DOM was supplemented with DOM produced from commercially available cyanobacteria (98 atm% ^{13}C and ^{15}N; Cambridge Isotopes) extracted using the same method as the diatom DOM. This mixture was intended to replicate a more natural source of DOM as would be produced *in situ* by pelagic phytoplankton.

To generate ^{13}C and ^{15}N labelled bacteria, a naturally community of seawater bacteria obtained from 5 ml of Baltic seawater was added to 1L of modified M63 media containing 0.02 mol glucose (50 atm% ^{13}C, Cambridge Isotopes) and 0.01 mol ammonium chloride (99 atm% ^{15}N, Cambridge Isotopes) and cultured in the dark at 28°C on a shaker. After 3 days, once the cells had reached stationary phase, samples were taken for cell counts and elemental analysis and the bacteria were centrifuged at 4500 rpm, rinsed with label-free ASW, and frozen at -20°C until use in experiments. The isotope ratios and

C/N content of the algal DOM and bacteria were measured by EA-IRMS prior to use in experiment to determine the isotopic enrichment and total amounts of C and N added to experiments (Table S1).

Stable isotope analysis and calculations of food uptake rates

Bulk tissue samples were lyophilized, homogenized, and sub-samples weighed into silver (C) and tin (N) cups for stable isotope analysis of $\delta^{13}C$ and $\delta^{15}N$. Samples for $\delta^{13}C$ were decalcified with 0.4M HCl to obtain the organic carbon content. Separated cell fractions were lyophilized and weighed into tin cups for simultaneous $\delta^{13}C$ and $\delta^{15}N$ as test samples indicated that acidification was not required. Isotope ratios and C/N content were simultaneously measured using a Thermo FlashEA 1112 elemental analyser (EA) coupled to a Delta V isotope ratio mass spectrometer (IRMS). Standard deviations of C and N content are < x% of the concentrations analyzed and < x ‰ for repeated $\delta^{13}C$ and $\delta^{15}N$ measurements of standard material (peptone). Carbon and nitrogen stable isotope ratios are expressed in standard delta notation as:

$$\delta^{13}C \text{ or } \delta^{15}N(‰) = \left(\frac{R_{sample}}{R_{ref}} - 1\right) \times 1000 \quad (1)$$

where R is the ratio of $^{13}C/^{12}C$ or $^{15}N/^{14}N$ in the sample or reference material: Vienna Pee Dee Belemnite for C (R_{ref} = 0.01118) and atmospheric nitrogen for N (R_{ref} = 0.00368 N). The fractional abundance of ^{13}C or ^{15}N in the samples was calculated as:

$$F_{sample\ or\ bckgr} = \frac{^{13}C}{(^{13}C + ^{12}C)} \text{ or } \frac{^{15}N}{(^{15}N + ^{14}N)} = \frac{R_{sample\ or\ bckgr}}{(R_{sample\ or\ bckgr} + 1)} \quad (1)$$

and:

$$R_{sample\ or\ bckgr} = \left(\frac{\delta^{13}C \text{ or } \delta^{15}N}{1000 + 1}\right) \times R_{ref} \quad (2)$$

Sample enrichments (*E*) was calculated as the excess fractional abundance (*F*) of ^{13}C or ^{15}N compared to control samples:

$$E_{sample} = F_{sample} - F_{bckgr} \quad (3)$$

Total ^{13}C and ^{15}N incorporation (*I*) was calculated by multiplying the excess fractional abundance (E_{sample}) by the total C_{org} or N content (µmol) of the sample (*A*) divided by the fractional abundance of the different labelled food sources (F_{source}):

$$I = \frac{(E_{sample} \times A)}{E_{source}} \quad (4)$$

Values for E_{source} are presented in Table S1. Uptake rates (*Q*) were normalized to the sponge biomass (B_{sponge}) measured as the total sponge C_{org} or N content (mmol) and the labelling incubation time (*t*):

$$Q = \frac{I}{(B_{sponge} \times t)} \quad (5)$$

Q is presented as µmol C or N incorporated per mmol C or N of sponge biomass per h (i.e. µmol C or N mmol C or N_{sponge}^{-1} h^{-1}; Fig. 2). All time points from the pulse-chase experiment are included in Figure 2.

Separation of sponge and microbial cell fractions

Methods for separation of sponge tissue into sponge and microbial cell fractions were adapted from Wehrl et al. 2007 (79) and Freeman et al. 2013 (57). Tissue samples were incubated in CMFASW+EDTA for 1h at 4°C and transferred to a clean 50ml falcon tube with fresh ice-cold CMFASW+EDTA. All subsequent sampling steps were performed on ice or at 4°C. Tissue samples were homogenized with a mortar and pestle to gently dissociate the tissue while avoiding cell breakage and passed through 100um Nitex mesh to remove any undissociated tissue. The filtrate was resuspended in 50 ml CMFASW+EDTA in clean 50 ml falcon tubes, vortexed for 5 min, and centrifuged to separate the sponge and microbial cells. For optimal purity, *A. aerophoba* was centrifuged at 770xg for 4 min and *D. avara* for 1100xg for 4 min. The supernatant containing the microbial cells was pipetted into a new falcon tube, leaving the last 5 ml to prevent contamination with the sponge pellet. The final 5ml of supernatant was poured off and the pellet containing the sponge cells was resuspended in fresh CMFASW+EDTA, vortexed again for 5 min, and centrifuged for 4 min this time at 520g for *A. aerophoba* and 770g for *D. avara* to remove any final microbes. The supernatant was poured off and the pellet rinsed one more time in CMFASW and centrifuged at the first centrifugation speeds for 4 min. The initial supernatant containing the microbial cell fraction was first re-centrifuged at the initial speeds to remove any remaining sponge cells and the resulting supernatant containing the microbial cells was centrifuged at 2800g for 20 min followed by two rinsing steps; once in CMFASW+EDTA and once in CMFASW. The final sponge and microbial cell pellets were resuspended in 1ml CMFASW, transferred to 1.5ml Eppendorf tubes, and centrifuged at 1000g and 7000g, respectively, for 2 min. The remaining supernatant was removed and the pellet frozen at -80°C.

***In situ* InEx VacuSIP sampling to measure the natural sponge diet**

Samples for DOC (10 ml) were filtered *in situ* to 0.7 µm using in-line stainless steel filter holders with pre-combusted GF/F filters directly into pre-cleaned 40 ml EPA vials. Samples were brought to the surface and immediately fixed with 25% orthophosphoric acid (Ultrapure Sigma 79617) and stored in the dark at 4°C until analysis by high-temperature combustion on Shimadzu a TOC analyser later that day. Unfiltered triplicate samples for picoplankton (2 ml) were fixed with 1% paraformaldehyde and 0.5% electron microscopy grade glutaraldehyde, frozen in liquid nitrogen, and stored at -80°C until analysis by flow cytometry using standard methods (12, 80).

CHAPTER 7

A PHAGE PROTEIN AIDS BACTERIAL SYMBIONTS IN EUKARYOTE IMMUNE EVASION

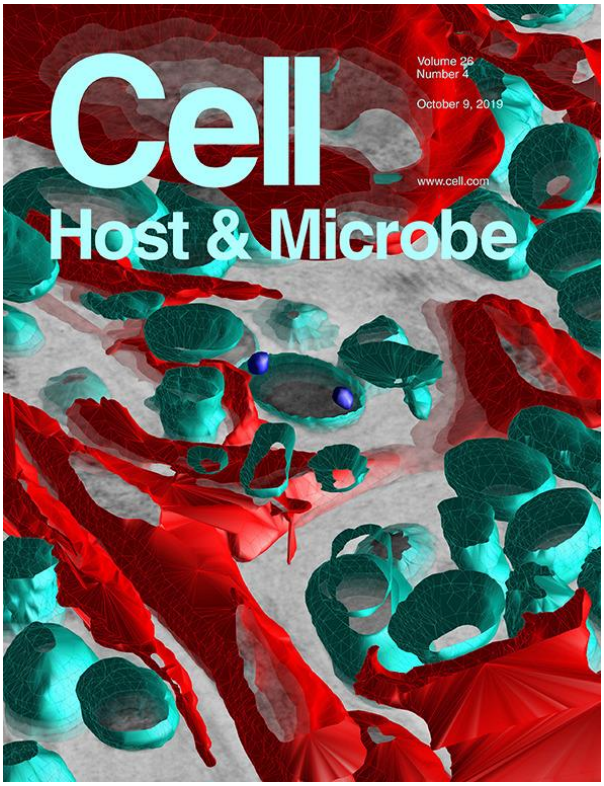

On the cover: Marine sponges are evolutionary basal animals that associate with dense and diverse microbial consortia. In this issue of Cell Host and Microbe, Jahn et al. report on the diversity and function of sponge-associated viruses. This study finds that symbiont phages encode a protein that downregulates sponge antibacterial immunity to foster host-microbe symbiosis. The cover is a three-dimensional reconstruction illustrating this intimate association between sponge host cells (red) and their associated microbiota (turquoise). Image created by Martin T. Jahn.

Jahn M.T., Arkhipova, K, Markert S.M., Stigloher C., Lachnit T., Pita L., Kupczok A., Ribes M., Stengel S.T., Rosenstiel P., Dutilh B.E., Hentschel U.

Cell Host & Microbe, 2019

doi: 10.1016/j.chom.2019.08.019

Short Article

Cell Host & Microbe

A Phage Protein Aids Bacterial Symbionts in Eukaryote Immune Evasion

Graphical Abstract

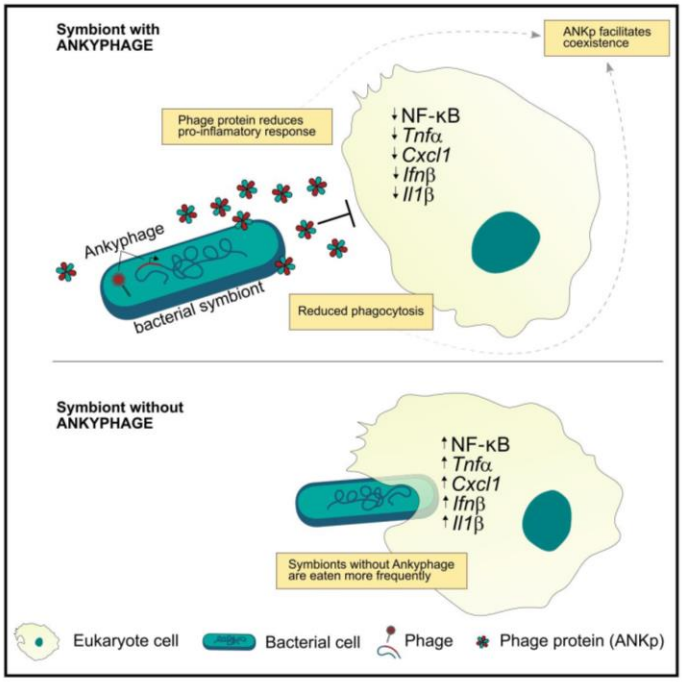

Authors

Martin T. Jahn, Ksenia Arkhipova, Sebastian M. Markert, ..., Philip Rosenstiel, Bas E. Dutilh, Ute Hentschel

Correspondence

mjahn@geomar.de (M.T.J.), uhentschel@geomar.de (U.H.)

In Brief

Jahn et al. find that sponges, although massively filtering seawater, host individually unique and species-specific viral communities. An abundant sponge bacteriophage encodes ankyrins that, upon bacterial expression, reduce the eukaryotic immune response and phagocytosis of bacteria. This suggests a mechanism of tripartite phage-bacterium-host interplay with the phage fostering host-microbe symbiosis.

Highlights

- Sponges, evolutionary basal animals, represent a reservoir of novel viral diversity
- Viromes of neighboring sponges are individually unique and species specific
- Phages encode ankyrins to aid bacteria in evading the eukaryotic immune system
- Such "Ankyphages" are widespread in host-associated environments, including humans

Jahn et al., 2019, Cell Host & Microbe *26*, 1–9
October 9, 2019
https://doi.org/10.1016/j.chom.2019.08.019

CellPress

Please cite this article in press as: Jahn et al., A Phage Protein Aids Bacterial Symbionts in Eukaryote Immune Evasion, Cell Host & Microbe (2019), https://doi.org/10.1016/j.chom.2019.08.019

Cell Host & Microbe
Short Article

CellPress

A Phage Protein Aids Bacterial Symbionts in Eukaryote Immune Evasion

Martin T. Jahn,[1,*] Ksenia Arkhipova,[2] Sebastian M. Markert,[3] Christian Stigloher,[3] Tim Lachnit,[4] Lucia Pita,[1] Anne Kupczok,[4] Marta Ribes,[5] Stephanie T. Stengel,[6] Philip Rosenstiel,[4,6] Bas E. Dutilh,[2] and Ute Hentschel[1,4,7,*]
[1]GEOMAR Helmholtz Centre for Ocean Research Kiel, Marine Symbioses, 24105 Kiel, Germany
[2]Theoretical Biology and Bioinformatics, Utrecht University, 3584 Utrecht, the Netherlands
[3]Imaging Core Facility, Biocenter, University of Würzburg, 97074 Würzburg, Germany
[4]Christian-Albrechts-University of Kiel, 24105 Kiel, Germany
[5]Institut de Ciències del Mar-CSIC, 08003 Barcelona, Spain
[6]Institute of Clinical Molecular Biology, University Hospital Schleswig-Holstein, 24105 Kiel, Germany
[7]Lead Contact
*Correspondence: mjahn@geomar.de (M.T.J.), uhentschel@geomar.de (U.H.)
https://doi.org/10.1016/j.chom.2019.08.019

SUMMARY

Phages are increasingly recognized as important members of host-associated microbiomes, with a vast genomic diversity. The new frontier is to understand how phages may affect higher order processes, such as in the context of host-microbe interactions. Here, we use marine sponges as a model to investigate the interplay between phages, bacterial symbionts, and eukaryotic hosts. Using viral metagenomics, we find that sponges, although massively filtering seawater, harbor species-specific and even individually unique viral signatures that are taxonomically distinct from other environments. We further discover a symbiont phage-encoded ankyrin-domain-containing protein, which is widely spread in phages of many host-associated contexts including human. We confirm in macrophage infection assays that the ankyrin protein (ANKp) modulates the eukaryotic host immune response against bacteria. We predict that the role of ANKp in nature is to facilitate coexistence in the tripartite interplay between phages, symbionts, and sponges and possibly many other host-microbe associations.

INTRODUCTION

Phages are the most abundant and diverse entities in the oceans (Gregory et al., 2019; Rohwer, 2003; Wommack and Colwell, 2000) and, along with their role as major bacterial killers, significantly impact global biochemical cycles (Breitbart et al., 2018; Suttle, 2007), bacterial fitness, and diversity (Betts et al., 2018; Marston et al., 2012). A plethora of fine-tuned defense and counter-defense mechanisms and lysogenic conversion factors have been discovered through research focusing on phage-bacteria interactions (Barrangou et al., 2007; Kronheim et al., 2018). Importantly, however, in host-associated microbial communities, a third player, the eukaryotic host, not only sets the stage but may also interact with both other parties in its own interest. Surprisingly little is, however, known about the tripartite interaction between phages, their bacterial hosts, and the animals that harbor the microbial communities (Barr et al., 2013; Keen and Dantas, 2018).

Marine sponges and their dense and diverse microbial symbiont communities are attractive models for the study of host-microbe-phage interactions (Thomas et al., 2016). As filter-feeding animals, sponges pump up to 24,000 liters of seawater through their system per day (Weisz et al., 2008), exposing them to up to an estimated $\sim 2.4 \times 10^{13}$ viruses daily. Interestingly, defense mechanisms (e.g., restriction modification and CRISPR-Cas) to selfish genetic elements (e.g., phages and plasmids) are clearly enriched in sponge symbiont genomes (Horn et al., 2016; Podell et al., 2019; Slaby et al., 2017).

While these features indicate phage resistance of bacterial sponge symbionts, the beneficial effects of phages on the sponge microbial community are largely unexplored. The first and only other sponge virome sequencing approach revealed species-specific viral signatures in Great Barrier Reef sponges, which shared low identity to known viral genomes (Laffy et al., 2018). Here, we generated nested viromes from Mediterranean sponges and identified specialized phage taxa and host-enriched phage functions. Importantly, we discovered and expressed an immunomodulatory phage protein that critically alters microbe-eukaryote interactions with potential implications in sponges and many other systems.

RESULTS

High Diversity and Novelty in Marine Sponge Viromes

We report the metagenomic analysis of marine sponge viromes that were sampled to cover the levels of sponge species, sponge individuals, and sponge tissues (outer layer "pinacoderm" and inner tissue "mesohyl matrix"). Viruses from nearby seawater, collected in immediate vicinity and at the same time, were used as controls. With 142 Gbp of sequencing data from 32 sponges (two tissues × 4 individuals × 4 species) and 4 seawater reference viromes, this represents the deepest sequencing effort performed on sponge viruses to date. The final assembly contained 4,484 curated viral contigs representing population-level genomes (≥5 kb, hereafter termed "BCvir"

Please cite this article in press as: Jahn et al., A Phage Protein Aids Bacterial Symbionts in Eukaryote Immune Evasion, Cell Host & Microbe (2019), https://doi.org/10.1016/j.chom.2019.08.019

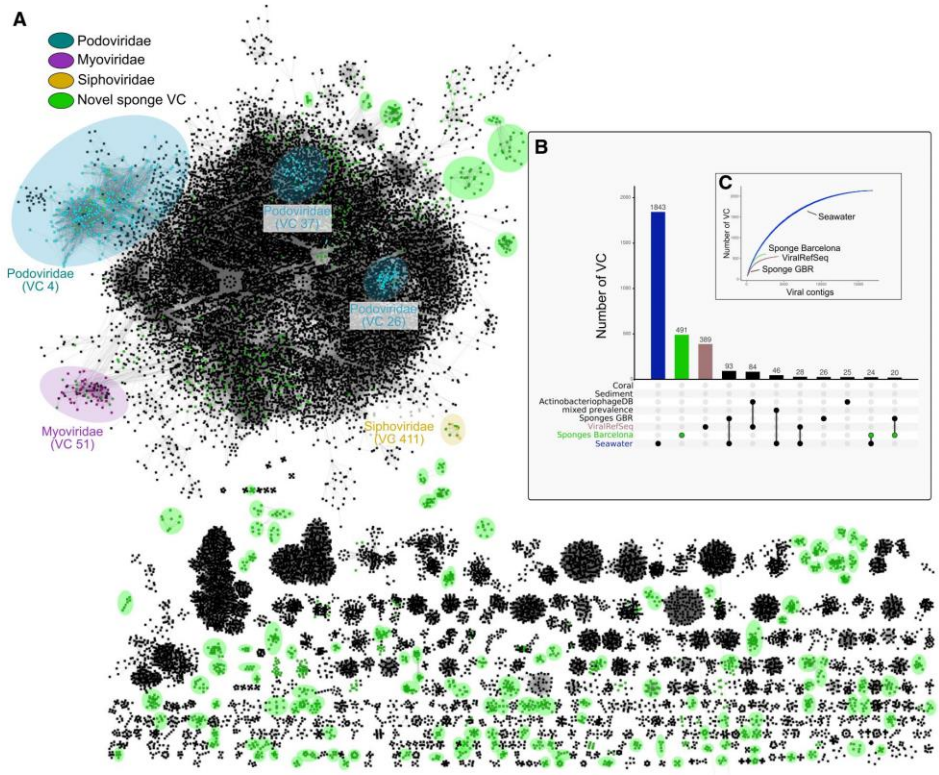

Figure 1. Diversity of Sponge Viruses in Relation to Known Viral Sequence Space

(A) The gene-sharing network associates identified sponge viral clusters in this study (VCs, green ovals) with a database of viral genomes that includes (i) assembled contigs from 130 marine viromes, (ii) the ActinophageDB, and (iii) ViralRefseq (black). Further, VCs containing the 5 most taxonomically assigned sponge viral genomes are highlighted. Network nodes are viral genomes and edges are significant similarities between them based on shared gene content. VCs with at least 5 genomes are shown (see detailed network statistics in Table S2 and raw data in Data S1).

(B) The matrix layout shows the number of VCs that are exclusive (one circle) or shared (multiple circles) between the eight different datasets used for clustering. Shown are the top intersections (≥20 members) as a vertical bar plot, sorted by size.

(C) Rarefaction curves for the most diverse datasets showing the accumulation of VCs as a function of sampled viral contigs (N).

for viral populations of the North Western Mediterranean Coast close to Barcelona), representing 51.4% of all the read-level data (Table S1; Figure S1). Of these, 101 were circular with matching ends and represent putatively complete viral genomes. The remaining contigs (of which 1,649 were ≥10 kb) were either putative linear genomes or genome fragments (Roux et al., 2019). To investigate how the 4,484 BCvir populations were positioned in the known viral sequence space, we clustered our sequences with an extended sequence space of 11,901 viral genome sequences obtained from viral Refseq and the ActinophageDB as well as 29,922 assembled contigs from 130 publicly available marine viral communities. This analysis was based on shared gene content and detected 3,218 viral clusters (VCs) (Figure 1A). The 4,484 BCvir populations partitioned into 813 VCs (green) representing 25.3% (n = 813 of 3,218 VCs) of the total viral diversity included in this extended database. Notably, most of the BCvir diversity consisted of viruses that were never detected before, as indicated by the fact that these VCs contained only BCvir contigs (n = 491 of 3,218 VCs; 15.3%) (Figure 1B), many of which shared no distant edge with other VCs. To ensure that this observation was not inflated by the shorter 5 kb contig length cutoff, which we had initially applied to capture shorter single-stranded DNA (ssDNA) viruses, we performed the same analysis again using a more stringent 10 kb length filter as suggested in Roux et al. (2017). With this approach, the 1,649 BCvir populations partitioned into 997 sponge VCs, of which 371 were uncharacterized (n = 371 of 1,304 VCs; 28.5%) in the extended sequence space. VCs delineate approximately genus-level taxonomy in known viruses (Lima-Mendez et al., 2008; Roux et al., 2015) with at least 371 sponge-derived VCs appear not to be part of the 803 viral genera currently listed by the International Committee on Taxonomy of Viruses ICTV (King et al., 2018) (via ViralRefseq; see Figure S2). Our virome dataset contained 3.9% BCvir

Please cite this article in press as: Jahn et al., A Phage Protein Aids Bacterial Symbionts in Eukaryote Immune Evasion, Cell Host & Microbe (2019), https://doi.org/10.1016/j.chom.2019.08.019

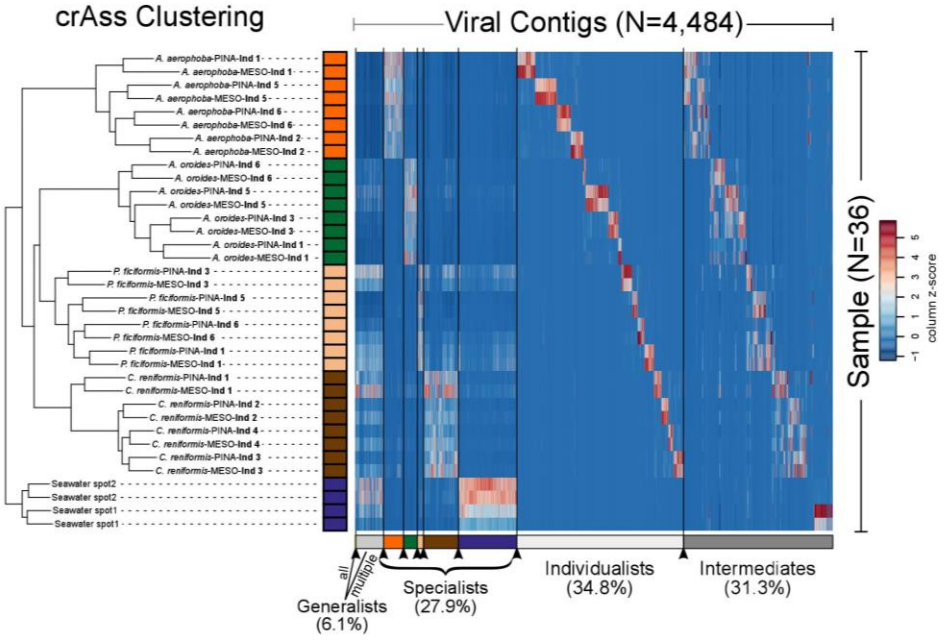

Figure 2. Iterative Cross-Assembly of Sponge-Associated Viromes

Clustering shows the distance between viral metagenomes based on the fraction of cross-assembled contigs between all sample pairs. Comparing topology against 1,000 random trees indicates significant separation of environments (sponge versus seawater) and sponge species (p value $\leq$ 0.001) but not sponge tissues (p value = 0.991). Heatmap shows the relative abundances of viral contigs and their grouping into prevalence groups as detailed in the STAR Methods section. Color scheme is based on *Z* score distribution across samples from low (blue) to high (red).

populations that could be annotated at the family level, representing mainly bacteriophages of the Caudovirales families, Siphoviridae, Myoviridae, and Podoviridae (Figure S2B). Rarefaction analysis indicated that more sponge viral diversity remains to be discovered, as the curve has not reached saturation (Figure 1C). These observations, combined with the limited taxonomic overlap with other marine environments (Figure 1C), led us to the conclusion that sponges represent distinct niches for viruses with potential for previously undescribed functions.

Unique Viromes in Neighboring Sponges

Viral communities of neighboring sponges were individually unique, host species specific, and different from environmental seawater (Figure 2). This is indicated by the fact that viral community profiles grouped per sponge species (p value < 0.001, consistency value = 0.907) and were distinct from adjacent viroplankton (p value < 0.001, consistency value = 0.973). Variation in viral community composition within a given sponge species was mainly on the level of sponge individuals (p value < 0.001, consistency value = 0.679), rather than tissue-specific signatures (p value = 0.991, consistency value = 0.534). These observations based on the fraction of cross contigs between the sample pairs (detailed in STAR Methods) showed high concordance with results from hierarchical clustering of abundance profiles (Figure S4). We further explored viral populations by conceptualizing viral prevalence groups (see STAR Methods for details). These were the generalists (prevalent in more than one sponge species or seawater), specialists (prevalent in one sponge species or seawater), individualists (detected in only one individual but both tissues), and intermediates (not falling into the above definitions) (Figure 2). Notably, even though we obtained the samples from neighboring sponges of each sponge species at the same time point, individualists, at 34.8% (1,560 of 4,484 BCvir contigs), represented the largest virome group in our study. Furthermore, individualists were the second most abundant prevalence group in the dataset, indicating that these were not rare members of the community. In contrast, a minor fraction of BCvir population contigs were generalists being prevalent in all (n = 10) or multiple (n = 262) sample types (species and/or seawater). Specialists, with prevalence in one of the sponge species or seawater, were 27.9% (1,249 of 4,484). The intermediates, although not further categorized, still contain a species-specific pattern. Because efforts were made to minimize environmental variations by sampling in close spatial and temporal proximity, we conclude that the sponge individuals each have a unique viral fingerprint.

Symbiont Phage Protein Aids Bacteria in Eukaryote Immune Evasion

To identify factors that might improve fitness of the phages, we queried BCvir populations for auxiliary genes (Roux et al.,

Please cite this article in press as: Jahn et al., A Phage Protein Aids Bacterial Symbionts in Eukaryote Immune Evasion, Cell Host & Microbe (2019), https://doi.org/10.1016/j.chom.2019.08.019

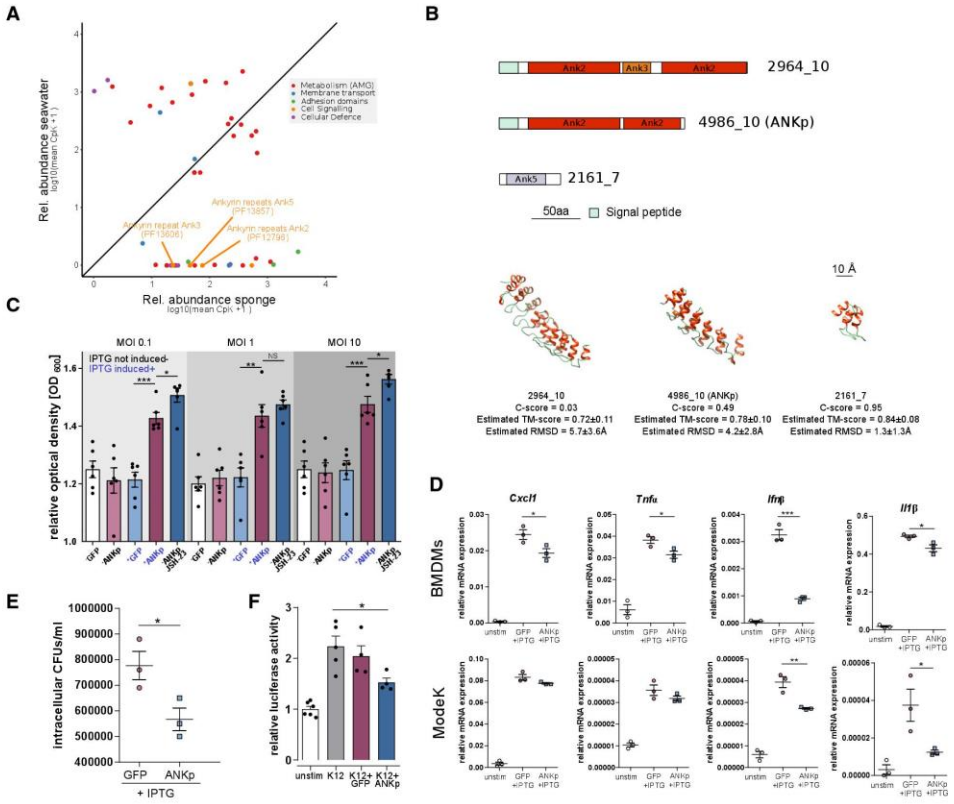

Figure 3. Symbiont Phage ANKp Reduces Phagocytosis and Immune Response of Eukaryote Cells toward Bacteria

(A) Relative abundance of auxiliary viral functions in sponge versus seawater (raw data and further host association factors available in Data S1).

(B) Domain architecture of ankyrin repeat encoding genes from sponge-enriched phages and representative protein models, approximated using I-TASSER. Template modeling (TM) score measures protein similarity and the confidence (C)-score prediction accuracy (Roy et al., 2010). RMSD indicates model root-mean-square deviation.

(C) Growth kinetics of *E. coli* K12 that are challenged with murine bone-marrow-derived macrophages (BMDMs) upon expression of recombinant ANKp. Plus^{+} and minus^{-} indicate treatments with and without IPTG induction of protein expression. Strains expressing GPF were used as the negative control and the NF-κB inhibitor JSH-23 was used as the positive control for immune inhibition. Data are presented as the mean ± SEM of three independent experiments (each with n = 6).

(D) Expression levels of pro-inflammatory cytokines in macrophages (BMDMs) and intestinal epithelial cells ModeK upon infection with ANKp expressing *E. coli*.

(E) Gentamycin protection assay reveals that ANKp expression leads to a reduced number of intracellular bacteria.

(F) NF-κB activation in ModeK with dual-luciferase assay.

Data are presented as the mean ± SEM of at least three independent experiments. Statistical significance between treatments was determined by two-tailed unpaired Student's t tests with *$p < 0.05$, **$p < 0.01$, and ***$p < 0.001$.

2016; Data S1). We then extended our search for cellular membrane transporters, adhesins, defense systems, and cellular signal molecules owing to their potential relevance in a symbiosis context. We were surprised to find Ankyrin repeat domains (ANKs), discussed modulators of eukaryote-prokaryote interaction (Nguyen et al., 2014), to be encoded on sponge-associated phages (Figure 3A). These ANK-encoding phages (BCvir 2964, BCvir 2161, and BCvir 4986), which we will call Ankyphage 1, 2, and 3 hereinafter (Data S1; Ankyphage annotation), recruited reads from 12 of 32 sponge viromes from both pinacoderm and mesohyl tissues but were absent in seawater. All three Ankyphages fall in the category "intermediates" (Figure 2). Furthermore, Ankyphages were in the top 75th percentile of most abundant viruses detected in *Aplysina* and *Chondrosia*. To ensure that Ankyphage sequences are indeed phage, we confirmed their phylogenetic placement among bacteriophages based on capsid alignments (Figures S3A and S3B) and ensured on the same contigs the presence of further phage domains (Figure S3C), such as phage terminase (PF03354), phage portal protein (PF04860), and phage P22 coat protein (PF11651). The presence of *ANK* in CsCl-purified virus particles was confirmed by Sanger sequencing. Notably, the domain architecture of two Ankyphage ANKs comprised N-terminal signal peptides but no transmembrane domains (Figure 3B). This suggests that

Please cite this article in press as: Jahn et al., A Phage Protein Aids Bacterial Symbionts in Eukaryote Immune Evasion, Cell Host & Microbe (2019), https://doi.org/10.1016/j.chom.2019.08.019

CellPress

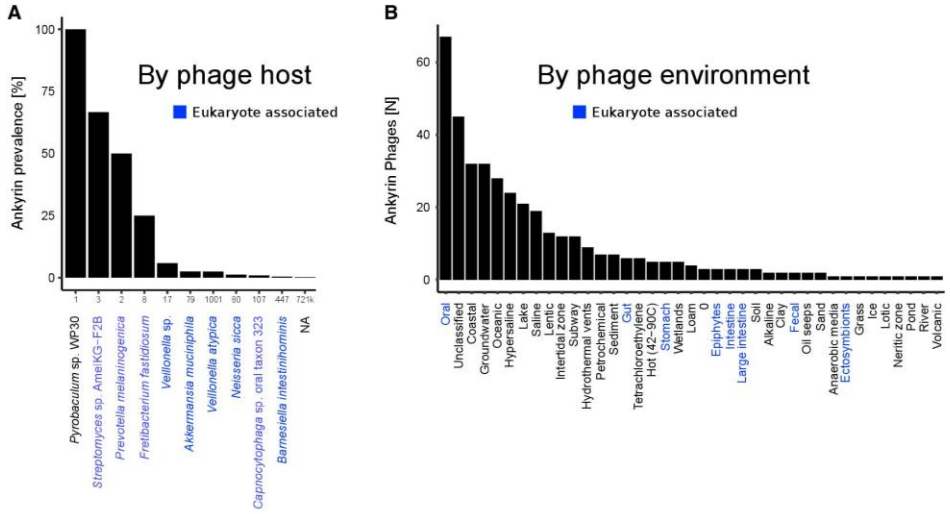

Figure 4. Global Distribution of Phage ANKs as Deposited in the IMGvr Database

(A) Prevalence of ankyrins in phages per predicted prokaryotic host (as deposited in IMGvr database metadata). Numbers on the x axis indicate the total size of phage genomes or contigs per host taxon.

(B) Number of phages with ANK domains per environment. Prokaryotes or environments with eukaryote host associations are highlighted in blue. The data are based on IMGvr database (Paez-Espino et al., 2019) screening for ankyrin Pfam signatures Ank (PF00023), Ank_2 (PF12796), Ank_3 (PF13606), Ank_4 (PF13637), and Ank_5 (PF13857) using InterPro (see STAR Methods).

these ANKs are secreted from a phage-infected bacterial cell where Ankyphages may be integrated as prophages or pseudolysogens with stable episome.

We then synthesized Ankyphage 3 ANK protein (ANKp) and assayed its impact on the interaction between bacteria and macrophages. Murine cell lines were chosen for the lack of an experimentally tractable model for sponge-microbe interactions (Pita et al., 2016). Murine macrophages functionally resemble certain sponge cells (archaeocytes) that are single, amoeboid, and phagocytotically active cells, which patrol throughout the sponge matrix. Notably, Ankyphages were found as well throughout all sponge tissues. Moreover, the major elements involved in mammalian immune signaling were found to be present in sponges (Pita et al., 2018; Riesgo et al., 2014). When *E. coli* was pre-incubated with purified ANKp, the bacterium survived in significantly higher abundances upon predatory pressure from murine macrophages than GFP controls (Figures S3F and S3D). This effect was dose dependent (1 μM > 100 nM ANKp) and reproducible for different bacteria to macrophage ratios (multiplicity of infection (MOI) 0.1, 1, and 10). Gentamycin protection assays, which allowed us to quantify the intracellular bacteria fraction, showed that increased survival of ANKp pre-incubated *E. coli* was paralleled with a decreased number of intracellular bacteria expressing the protein (p value = 0.0414, $t = 2.963$, and $df = 4$) (Figure 3E). This indicates that ANKp-mediated bacterial survival is facilitated by decreased macrophage phagocytosis rates. In support of these findings, when ANKp was directly expressed by *E.coli*, this resulted in a significantly increased survival rate of *E.coli* upon exposure to macrophages, showing that ANKp is functional when secreted (Figures 3C and S3E). To ensure that ANKp protein had no toxic effect on one of the players, we performed bacterial growth experiments in culture and on plates and for the eukaryotic cell line MTS assays upon protein exposure showing low cytotoxicity (Figures S3G–S3I). The same growth experiment exercised with pre-incubated *Bacillus subtilis*, a Gram-positive representative, was consistent with ANKp-mediated bacterial survival during macrophage challenge (Figure S3C).

On the side of the macrophage, ANKp synthesis by *E. coli* led to a reduced expression of pro-inflammatory cytokines upon bacterial exposure (Figure 3D). Specifically, this included a reduction in tumor necrosis factor alpha (*TNF-α*), *Cxcl1*, and *Ifn1*. To independently validate phage ANKp-mediated eukaryote immune suppression and to extend the analysis to a further eukaryotic cell type, we performed an NF-κB-dependent firefly luciferase assay on murine gut endothelial ModeK cells. In line with previous results, the NF-κB response, a central hub of eukaryote immunity (Li and Verma, 2002), was downregulated when ModeK cells were exposed to ANKp expressing *E. coli* (Figure 3F). In summary, this shows that ANKp modulates the eukaryote response to bacteria by downregulating pro-inflammatory signaling along with reduced phagocytosis rates.

To investigate whether phage ankyrins are more common in nature, we extended homology searches to various other viral databases including IMGvr (Paez-Espino et al., 2019) (July 2018 release). We identified an abundant ANK-encoding virus in the Great Barrier Reef sponge *Amphimedon queenslandica* (Laffy et al., 2018) (Data S1; Ankyphage annotation). Furthermore, we identified ANKs in 418 predicted phage contigs deposited in IMGvr (Paez-Espino et al., 2019) (Figure 4). Notably,

Please cite this article in press as: Jahn et al., A Phage Protein Aids Bacterial Symbionts in Eukaryote Immune Evasion, Cell Host & Microbe (2019), https://doi.org/10.1016/j.chom.2019.08.019

Ankyphages were obtained from host-associated environments such as the human oral cavity (n = 67 phages), gut (n = 6), stomach (n = 5), or rhizosphere (n = 4) but also from aquatic environments ranging from marine to groundwater.

DISCUSSION

We discovered an astonishingly intimate association between viruses and marine sponges. Altogether 491 yet unexplored VCs were identified in sponges that delineate genus-level taxonomy (Lima-Mendez et al., 2008; Roux et al., 2015). This compares to 1,843 VCs from the Tara Oceans and other large-scale expeditions focusing on viroplankton. Although the applied genome-based network clustering approach cannot replace well-curated taxonomy (King et al., 2018), the results of us and others (Paez-Espino et al., 2016) indicate that marine animals indeed represent distinct niches of viral diversity. Consequently, future efforts to capture more host-associated environments have high potential to add up to the increasingly understood planktonic virosphere of surface waters (Coutinho et al., 2017; Gregory et al., 2019; Roux et al., 2016). Because animal microbiomes are highly species specific (Hacquard et al., 2015; Moeller et al., 2016; Thomas et al., 2016) and the virome depends on the microbiome, we further expect species-specific viral communities to rule in nature. This is supported by our sympatric sponge species, each holding characteristic viral communities (Figure 2). Systematic studies in other sponges (Laffy et al., 2018) but also in *Hydra* (Grasis et al., 2014) and insects, where signatures of phylosymbiosis were observed (Leigh et al., 2018a), are supportive for species-specific viromes in animals.

An even higher level of association of viruses with their animal hosts was identified by our nested sampling approach (Figure 2). This revealed that a considerable part of the virome signatures was driven by viruses that were unique to sponge individuals but not to tissues (Figure 2). Inter-individual differences were also the largest source of variance in the viromes of humans (Abeles et al., 2014; Moreno-Gallego et al., 2019). Our report systematically extends individual virome signatures to marine sponges and adds to evidence of virome individuality in other marine animals (Leigh et al., 2018b; Orosco and Lluisma, 2017). The high degree of individuality in sponge viromes was surprising considering the constant filtration activity of sponges (Taylor et al., 2013). The diversifying forces accounting for individual viromes may be asynchronous temporal fluctuations between sponge individuals following delayed Lotka-Volterra-like dynamics (Parsons et al., 2012) or an independent diversification from a source pool (Enav et al., 2018). To resolve this, further studies capturing the temporal dynamics of environmental host-associated systems will provide valuable information.

The discovery of auxiliary ankyrin repeats (ANKs) in a previously undescribed group of sponge-associated phages, that we term Ankyphages, raised our special interest due to (1) their protein architecture, which indicates its secretion from the virocell; (2) their role as hubs of diverse protein-protein interactions, including functions in cellular signaling; and (3) their broader prevalence and abundance in the symbiotic context while lacking in nearby seawater. We reasoned that phage-encoded ANKs might increase the fitness of the carrying phages in the context of the sponge holobiont. ANK repeats are widespread in all domains of cellular life (Jernigan and Bordenstein, 2014), but reports of ANKs in the world of phages are rare. A notable exception is PRANC domains (Pox protein repeats of ankyrin CTD), which are ANK homologs of poxviruses discovered in prophages of Wolbachia (Bordenstein and Bordenstein, 2016; Wu et al., 2004). Its placement in a conserved eukaryote association module indicates its functioning in a eukaryotic context (Bordenstein and Bordenstein, 2016). In the bacterial world, ANKs were demonstrated to modulate interaction between species and even across kingdoms (Lambert et al., 2015; Wong et al., 2017). A notable example is a previous study on sponges, where chromosomally encoded ANKs from an uncultivated gammaproteobacterium seemed to modulate amoebal phagocytosis (Nguyen et al., 2014), even though the underlying mechanisms on the eukaryote side are largely unclear.

Our *in vitro* experiments show that phage ANKp undermined eukaryote immune response toward bacteria and facilitated bacteria-eukaryote coexistence by reduced phagocytosis rates. To the best of our knowledge, a secreted phage protein shown to downregulate eukaryote immune response has not been previously described. This finding has important implications from a symbiotic perspective. The reduction of predatory pressure from the eukaryote host represents a selective advantage for the symbiotic lifestyle of Ankyphage-infected bacteria as compared to strains missing this trait (see Graphical Abstract). Eukaryote immune evasion by phage-mediated lysogenic conversion is an emerging field of research that is currently best studied in opportunistic pathogens (Van Belleghem et al., 2018). Mechanisms range from phage-mediated reshaping of methicillin-resistant *Staphylococcus aureus* (MRSA) cell wall glycosylation to evade host immunity (Gerlach et al., 2018), to phage RNA of the *Pseudomonas aeruginosa* phage Pf4 that downregulates eukaryote inflammatory response and at the same time is taming for non-invasive infection (Secor et al., 2017; Sweere et al., 2019). We are aware that the choice for the experimentally more approachable murine model can only be a proxy for processes yet to be observed in sponges. However, consistent signals in *E. coli* and *B. subtilis* and the tested eukaryote cell type (macrophages and an epithelial cell line), might indicate a more widely distributed conserved mode of action. This is fueled by our public database screenings where we found phage-encoded ANKs in other eukaryote-associated environments, such as phages inhabiting human cavities (oral, stomach, or gut) representing a promising field for future research. In summary, our study highlights the novel diversity, intimate association, and tripartite interplay between phages, symbionts, and the eukaryote host. Importantly, we identify and characterize a phage-derived protein that can manipulate the immune interaction between eukaryotes and microbiota.

STAR★METHODS

Detailed methods are provided in the online version of this paper and include the following:

- KEY RESOURCES TABLE
- LEAD CONTACT AND MATERIALS AVAILABILITY

Please cite this article in press as: Jahn et al., A Phage Protein Aids Bacterial Symbionts in Eukaryote Immune Evasion, Cell Host & Microbe (2019), https://doi.org/10.1016/j.chom.2019.08.019

SUPPLEMENTAL INFORMATION

Supplemental Information can be found online at https://doi.org/10.1016/j.chom.2019.08.019.

ACKNOWLEDGMENTS

We acknowledge funding by the DFG CRC1182 to U.H. (TPB1), T.L. (TPA4), P.R. (TPC2), and A.K. (TPC3). M.T.J. was supported by a grant of the German Excellence Initiative to the Graduate School of Life Sciences, University of Würzburg, and the Young Investigator Award of CRC1182. S.M.M. was supported by the Studienstiftung des Deutschen Volkes. We thank Laura Rix (GEOMAR), Rafel Coma (CEAB-CSIC), and Berta Pintó for sponge sampling.

AUTHOR CONTRIBUTIONS

M.T.J. designed and performed the experiments, analyzed the data, prepared the figures and tables, and wrote the paper; L.P. and M.R. were involved in the planning and execution of the sponge field sampling; T.L. purified the viral particles and extracted the nucleotides; S.T.S. and P.R. performed cell culture experiments and immunoassays; M.T.J. and S.M.M. performed the microscopy under the supervision of C.S.; B.E.D., A.K., and K.A. advised the bioinformatic analyses and commented on the analysis strategy; U.H. helped in the experimental design and data interpretation and reviewed drafts of the paper. All authors edited and approved the final version of the manuscript.

DECLARATION OF INTERESTS

The authors declare no competing interests.

Received: May 8, 2019
Revised: July 22, 2019
Accepted: August 30, 2019
Published: September 24, 2019

REFERENCES

Abeles, S.R., Robles-Sikisaka, R., Ly, M., Lum, A.G., Salzman, J., Boehm, T.K., and Pride, D.T. (2014). Human oral viruses are personal, persistent and gender-consistent. ISME J. *8*, 1753–1767.

Barr, J.J., Auro, R., Furlan, M., Whiteson, K.L., Erb, M.L., Pogliano, J., Stotland, A., Wolkowicz, R., Cutting, A.S., Doran, K.S., et al. (2013). Bacteriophage adhering to mucus provide a non-host-derived immunity. Proc. Natl. Acad. Sci. USA *110*, 10771–10776.

Barrangou, R., Fremaux, C., Deveau, H., Richards, M., Boyaval, P., Moineau, S., Romero, D.A., and Horvath, P. (2007). CRISPR provides acquired resistance against viruses in prokaryotes. Science *315*, 1709–1712.

Betts, A., Gray, C., Zelek, M., MacLean, R.C., and King, K.C. (2018). High parasite diversity accelerates host adaptation and diversification. Science *360*, 907–911.

Bordenstein, S.R., and Bordenstein, S.R. (2016). Eukaryotic association module in phage WO genomes from Wolbachia. Nat. Commun. *7*, 13155.

Breitbart, M., Bonnain, C., Malki, K., and Sawaya, N.A. (2018). Phage puppet masters of the marine microbial realm. Nat. Microbiol. *3*, 754–766.

Conceição-Neto, N., Zeller, M., Lefrère, H., De Bruyn, P., Beller, L., Deboutte, W., Yinda, C.K., Lavigne, R., Maes, P., Van Ranst, M., et al. (2015). Modular approach to customise sample preparation procedures for viral metagenomics: a reproducible protocol for virome analysis. Sci. Rep. *5*, 16532.

Coutinho, F.H., Silveira, C.B., Gregoracci, G.B., Thompson, C.C., Edwards, R.A., Brussaard, C.P.D., Dutilh, B.E., and Thompson, F.L. (2017). Marine viruses discovered via metagenomics shed light on viral strategies throughout the oceans. Nat. Commun. *8*, 15955.

Dixon, P. (2003). VEGAN, a package of R functions for community ecology. J. Veg. Sci. *14*, 927–930.

Dutilh, B.E., Schmieder, R., Nulton, J., Felts, B., Salamon, P., Edwards, R.A., and Mokili, J.L. (2012). Reference-independent comparative metagenomics using cross-assembly: crAss. Bioinformatics *28*, 3225–3231.

Edwards, R.A., Vega, A.A., Norman, H.M., Ohaeri, M., Levi, K., Dinsdale, E.A., Cinek, O., Aziz, R.K., McNair, K., Barr, J.J., et al. (2019). Global phylogeography and ancient evolution of the widespread human gut virus crAssphage. Nat. Microbiol.

Enav, H., Kirzner, S., Lindell, D., Mandel-Gutfreund, Y., and Béjà, O. (2018). Adaptation to sub-optimal hosts is a driver of viral diversification in the ocean. Nat. Commun. *9*, 4698.

Enright, A.J., Van Dongen, S., and Ouzounis, C.A. (2002). An efficient algorithm for large-scale detection of protein families. Nucleic Acids Res. *30*, 1575–1584.

Eren, A.M., Esen, Ö.C., Quince, C., Vineis, J.H., Morrison, H.G., Sogin, M.L., and Delmont, T.O. (2015). Anvi'o: an advanced analysis and visualization platform for 'omics data. PeerJ *3*, e1319.

Erez, Z., Steinberger-Levy, I., Shamir, M., Doron, S., Stokar-Avihail, A., Peleg, Y., Melamed, S., Leavitt, A., Savidor, A., Albeck, S., et al. (2017). Communication between viruses guides lysis–lysogeny decisions. Nature *541*, 488–493.

Gerlach, D., Guo, Y., De Castro, C., Kim, S.H., Schlatterer, K., Xu, F.F., Pereira, C., Seeberger, P.H., Ali, S., Codée, J., et al. (2018). Methicillin-resistant Staphylococcus aureus alters cell wall glycosylation to evade immunity. Nature *563*, 705–709.

Grasis, J.A., Lachnit, T., Anton-Erxleben, F., Lim, Y.W., Schmieder, R., Fraune, S., Franzenburg, S., Insua, S., Machado, G., Haynes, M., et al. (2014). Species-specific viromes in the ancestral holobiont Hydra. PLoS One *9*, e109952.

Grazziotin, A.L., Koonin, E.V., and Kristensen, D.M. (2017). Prokaryotic Virus Orthologous Groups (pVOGs): a resource for comparative genomics and protein family annotation. Nucleic. Acids. Res. *45*, D491–D498.

Gregory, A.C., Zayed, A.A., Conceição-Neto, N., Temperton, B., Bolduc, B., Alberti, A., Ardyna, M., Arkhipova, K., Carmichael, M., Cruaud, C., et al. (2019). Marine DNA viral macro- and microdiversity from Pole to Pole. Cell *177*, 1109–1123.e14.

Gurevich, A., Saveliev, V., Vyahhi, N., and Tesler, G. (2013). QUAST: quality assessment tool for genome assemblies. Bioinformatics *29*, 1072–1075.

Hacquard, S., Garrido-Oter, R., González, A., Spaepen, S., Ackermann, G., Lebeis, S., McHardy, A.C., Dangl, J.L., Knight, R., Ley, R., et al. (2015). Microbiota and host nutrition across plant and animal kingdoms. Cell Host Microbe *17*, 603–616.

Horn, H., Slaby, B.M., Jahn, M.T., Bayer, K., Moitinho-Silva, L., Förster, F., Abdelmohsen, U.R., and Hentschel, U. (2016). An enrichment of CRISPR

Please cite this article in press as: Jahn et al., A Phage Protein Aids Bacterial Symbionts in Eukaryote Immune Evasion, Cell Host & Microbe (2019), https://doi.org/10.1016/j.chom.2019.08.019

and other defense-related features in marine sponge-associated microbial metagenomes. Front. Microbiol. *7*, 1751.

Hurwitz, B.L., Brum, J.R., and Sullivan, M.B. (2015). Depth-stratified functional and taxonomic niche specialization in the 'core' and 'flexible' pacific ocean virome. ISME J. *9*, 472–484.

Hyatt, D., Chen, G.L., LoCascio, P.F., Land, M.L., Larimer, F.W., and Hauser, L.J. (2010). Prodigal: prokaryotic gene recognition and translation initiation site identification. BMC Bioinformatics *11*, 119.

Jernigan, K.K., and Bordenstein, S.R. (2014). Ankyrin domains across the tree of life. PeerJ *2*, e264.

John, S.G., Mendez, C.B., Deng, L., Poulos, B., Kauffman, A.K.M., Kern, S., Brum, J., Polz, M.F., Boyle, E.A., and Sullivan, M.B. (2011). A simple and efficient method for concentration of ocean viruses by chemical flocculation. Environ. Microbiol. Rep. *3*, 195–202.

Jones, P., Binns, D., Chang, H.Y., Fraser, M., Li, W., McAnulla, C., McWilliam, H., Maslen, J., Mitchell, A., Nuka, G., et al. (2014). InterProScan 5: Genome-scale protein function classification. Bioinformatics *30*, 1236–1240.

Kaser, A., Lee, A.H., Franke, A., Glickman, J.N., Zeissig, S., Tilg, H., Nieuwenhuis, E.E., Higgins, D.E., Schreiber, S., Glimcher, L.H., et al. (2008). XBP1 links ER stress to intestinal inflammation and confers genetic risk for human inflammatory bowel disease. Cell *134* (5), 743–756.

Keen, E.C., and Dantas, G. (2018). Close encounters of three kinds: bacteriophages, commensal bacteria, and host immunity. Trends Microbiol. *26*, 943–954.

King, A.M.Q., Lefkowitz, E.J., Mushegian, A.R., Adams, M.J., Dutilh, B.E., Gorbalenya, A.E., Harrach, B., Harrison, R.L., Junglen, S., Knowles, N.J., et al. (2018). Changes to taxonomy and the International code of virus classification and nomenclature ratified by the international committee on taxonomy of viruses (2018). Arch. Virol. *163*, 2601–2631.

Krogh, A., Larsson, B., von Heijne, G., and Sonnhammer, E.L. (2001). Predicting transmembrane protein topology with a hidden Markov model: application to complete genomes. J. Mol. Biol. *305* (3), 567–580.

Kronheim, S., Daniel-Ivad, M., Duan, Z., Hwang, S., Wong, A.I., Mantel, I., Nodwell, J.R., and Maxwell, K.L. (2018). A chemical defence against phage infection. Nature *564*, 283–286.

Kurtz, S., Phillippy, A., Delcher, A.L., Smoot, M., Shumway, M., Antonescu, C., and Salzberg, S.L. (2004). Versatile and open software for comparing large genomes. Genome Biol. *5*, R12.

Lachnit, T., Thomas, T., and Steinberg, P. (2015). Expanding our understanding of the seaweed holobiont: RNA viruses of the red alga Delisea pulchra. Front. Microbiol. *6*, 1489.

Laffy, P.W., Wood-Charlson, E.M., Turaev, D., Jutz, S., Pascelli, C., Botté, E.S., Bell, S.C., Peirce, T.E., Weynberg, K.D., van Oppen, M.J.H., et al. (2018). Reef invertebrate viromics: diversity, host specificity and functional capacity. Environ. Microbiol. *20*, 2125–2141.

Lambert, C., Cadby, I.T., Till, R., Bui, N.K., Lerner, T.R., Hughes, W.S., Lee, D.J., Alderwick, L.J., Vollmer, W., Sockett, R.E., et al. (2015). Ankyrin-mediated self-protection during cell invasion by the bacterial predator Bdellovibrio bacteriovorus. Nat. Commun. *6*, 8884.

Leigh, B.A., Bordenstein, S.R., Brooks, A.W., Mikaelyan, A., and Bordenstein, S.R. (2018a). Finer-scale phylosymbiosis: insights from insect viromes. mSystems *3*, e00131-18.

Leigh, B.A., Djurhuus, A., Breitbart, M., and Dishaw, L.J. (2018b). The gut virome of the protochordate model organism, Ciona intestinalis subtype A. Virus Res. *244*, 137–146.

Letunic, I., and Bork, P. (2019). Interactive Tree of Life (iTOL) v4: recent updates and new developments. Nucleic Acids Res. *47*, W256–W259.

Li, Q., and Verma, I.M. (2002). NF-kappaB regulation in the immune system. Nat. Rev. Immunol. *2*, 725–734.

Lima-Mendez, G., Van Helden, J., Toussaint, A., and Leplae, R. (2008). Reticulate representation of evolutionary and functional relationships between phage genomes. Mol. Biol. Evol. *25*, 762–777.

López-Pérez, M., Haro-Moreno, J.M., Gonzalez-Serrano, R., Parras-Moltó, M., and Rodriguez-Valera, F. (2017). Genome diversity of marine phages recovered from Mediterranean metagenomes: size matters. PLoS Genet. *13*, e1007018.

Marston, M.F., Pierciey, F.J., Shepard, A., Gearin, G., Qi, J., Yandava, C., Schuster, S.C., Henn, M.R., and Martiny, J.B.H. (2012). Rapid diversification of coevolving marine Synechococcus and a virus. Proc. Natl. Acad. Sci. USA *109*, 4544–4549.

Moeller, A.H., Caro-Quintero, A., Mjungu, D., Georgiev, A.V., Lonsdorf, E.V., Muller, M.N., Pusey, A.E., Peeters, M., Hahn, B.H., and Ochman, H. (2016). Cospeciation of gut microbiota with hominids. Science *353*, 380–382.

Moreno-Gallego, J.L., Chou, S.P., Di Rienzi, S.C., Goodrich, J.K., Spector, T.D., Bell, J.T., Youngblut, N.D., Hewson, I., Reyes, A., and Ley, R.E. (2019). Virome diversity correlates with intestinal microbiome diversity in adult monozygotic twins. Cell Host Microbe *25*, 261–272.e5.

Nguyen, M.T., Liu, M., and Thomas, T. (2014). Ankyrin-repeat proteins from sponge symbionts modulate amoebal phagocytosis. Mol. Ecol. *23*, 1635–1645.

Nielsen, H. (2017). Predicting Secretory Proteins with SignalP. Methods Mol. Biol. *1611*, 59–73.

Nurk, S., Meleshko, D., Korobeynikov, A., and Pevzner, P.A. (2017). metaSPAdes: a new versatile metagenomic assembler. Genome Res. *27*, https://doi.org/10.1101/gr.213959.116.

Orosco, F.L., and Lluisma, A.O. (2017). Variation in virome diversity in wild populations of Penaeus monodon (Fabricius 1798) with emphasis on pathogenic viruses. Virusdisease *28*, 262–271.

Paez-Espino, D., Eloe-Fadrosh, E.A., Pavlopoulos, G.A., Thomas, A.D., Huntemann, M., Mikhailova, N., Rubin, E., Ivanova, N.N., and Kyrpides, N.C. (2016). Uncovering earth's virome. Nature *536*, 425–430.

Paez-Espino, D., Roux, S., Chen, I.A., Palaniappan, K., Ratner, A., Chu, K., Huntemann, M., Reddy, T.B.K., Pons, J.C., Llabrés, M., et al. (2019). IMG/VR v.2.0: an integrated data management and analysis system for cultivated and environmental viral genomes. Nucleic Acids Res. *47*, D678–D686.

Parsons, R.J., Breitbart, M., Lomas, M.W., and Carlson, C.A. (2012). Ocean time-series reveals recurring seasonal patterns of virioplankton dynamics in the northwestern Sargasso Sea. ISME J. *6*, 273–284.

Pita, L., Fraune, S., and Hentschel, U. (2016). Emerging sponge models of animal-microbe symbioses. Front. Microbiol. *7*, 2102.

Pita, L., Hoeppner, M.P., Ribes, M., and Hentschel, U. (2018). Differential expression of immune receptors in two marine sponges upon exposure to microbial-associated molecular patterns. Sci. Rep. *8*, 16081.

Podell, S., Blanton, J.M., Neu, A., Agarwal, V., Biggs, J.S., Moore, B.S., and Allen, E.E. (2019). Pangenomic comparison of globally distributed Poribacteria associated with sponge hosts and marine particles. ISME J. *13*, 468–481.

Riesgo, A., Farrar, N., Windsor, P.J., Giribet, G., and Leys, S.P. (2014). The analysis of eight transcriptomes from all Poriferan classes reveals surprising genetic complexity in sponges. Mol. Biol. Evol. *31*, 1102–1120.

Rohwer, F. (2003). Global phage diversity. Cell *113*, 141.

Roux, S., Adriaenssens, E.M., Dutilh, B.E., Koonin, E.V., Kropinski, A.M., Krupovic, M., Kuhn, J.H., Lavigne, R., Brister, J.R., Varsani, A., et al. (2019). Minimum information about an uncultivated virus genome (MIUViG). Nat. Biotechnol. *37*, 29–37.

Roux, S., Brum, J.R., Dutilh, B.E., Sunagawa, S., Duhaime, M.B., Loy, A., Poulos, B.T., Solonenko, N., Lara, E., Poulain, J., et al. (2016). Ecogenomics and potential biogeochemical impacts of globally abundant ocean viruses. Nature *537*, 689–693.

Roux, S., Emerson, J.B., Eloe-Fadrosh, E.A., and Sullivan, M.B. (2017). Benchmarking viromics: an in silico evaluation of metagenome-enabled estimates of viral community composition and diversity. PeerJ *5*, e3817.

Roux, S., Hallam, S.J., Woyke, T., and Sullivan, M.B. (2015). Viral dark matter and virus–host interactions resolved from publicly available microbial genomes. Elife *4*.

Roux, S., Krupovic, M., Debroas, D., Forterre, P., and Enault, F. (2013). Assessment of viral community functional potential from viral metagenomes

Please cite this article in press as: Jahn et al., A Phage Protein Aids Bacterial Symbionts in Eukaryote Immune Evasion, Cell Host & Microbe (2019), https://doi.org/10.1016/j.chom.2019.08.019

may be hampered by contamination with cellular sequences. Open Biol. *3*, 130160.

Roy, A., Kucukural, A., and Zhang, Y. (2010). I-TASSER: a unified platform for automated protein structure and function prediction. Nat. Protoc. *5*, 725–738.

Schloss, P.D., Westcott, S.L., Ryabin, T., Hall, J.R., Hartmann, M., Hollister, E.B., Lesniewski, R.A., Oakley, B.B., Parks, D.H., Robinson, C.J., et al. (2009). Introducing mothur: Open-Source, Platform-Independent, Community-Supported Software for Describing and Comparing Microbial Communities. Appl. Environ. Microbiol. *75* (23), 7537–7541.

Secor, P.R., Michaels, L.A., Smigiel, K.S., Rohani, M.G., Jennings, L.K., Hisert, K.B., Arrigoni, A., Braun, K.R., Birkland, T.P., Lai, Y., et al. (2017). Filamentous bacteriophage produced by Pseudomonas aeruginosa alters the inflammatory response and promotes noninvasive infection in vivo. Infect. Immun. *85*, e00648-16.

Shen, A., Lupardus, P.J., Morell, M., Ponder, E.L., Sadaghiani, A.M., Garcia, K.C., and Bogyo, M. (2009). Simplified, enhanced protein purification using an inducible, autoprocessing enzyme tag. PLoS One *4*, e8119.

Slaby, B.M., Hackl, T., Horn, H., Bayer, K., and Hentschel, U. (2017). Metagenomic binning of a marine sponge microbiome reveals unity in defense but metabolic specialization. ISME J. *11*, 2465–2478.

Suttle, C.A. (2007). Marine viruses–major players in the global ecosystem. Nat. Rev. Microbiol. *5*, 801–812.

Sweere, J.M., Van Belleghem, J.D., Ishak, H., Bach, M.S., Popescu, M., Sunkari, V., Kaber, G., Manasherob, R., Suh, G.A., Cao, X., et al. (2019). Bacteriophage trigger antiviral immunity and prevent clearance of bacterial infection. Science *363*.

Taylor, M.W., Tsai, P., Simister, R.L., Deines, P., Botte, E., Ericson, G., Schmitt, S., and Webster, N.S. (2013). 'Sponge-specific' bacteria are widespread (but rare) in diverse marine environments. ISME J. *7*, 438–443.

Thomas, T., Moitinho-Silva, L., Lurgi, M., Björk, J.R., Easson, C., Astudillo-García, C., Olson, J.B., Erwin, P.M., López-Legentil, S., Luter, H., et al. (2016). Diversity, structure and convergent evolution of the global sponge microbiome. Nat. Commun. *7*, 11870.

Thurber, R.V., Haynes, M., Breitbart, M., Wegley, L., and Rohwer, F. (2009). Laboratory procedures to generate viral metagenomes. Nat. Protoc. *4*, 470–483.

Van Belleghem, J.D., Dąbrowska, K., Vaneechoutte, M., Barr, J.J., and Bollyky, P.L. (2018). Interactions between bacteriophage, bacteria, and the mammalian immune system. Viruses *11*, 10.

Weisz, J.B., Lindquist, N., and Martens, C.S. (2008). Do associated microbial abundances impact marine demosponge pumping rates and tissue densities? Oecologia *155*, 367–376.

Wommack, K.E., and Colwell, R.R. (2000). Virioplankton: viruses in aquatic ecosystems. Microbiol. Mol. Biol. Rev. *64*, 69–114.

Wong, K., Perpich, J.D., Kozlov, G., Cygler, M., Abu Kwaik, Y., and Gehring, K. (2017). Structural mimicry by a bacterial F Box effector hijacks the host ubiquitin-proteasome system. Structure *25*, 376–383.

Wu, M., Sun, L.V., Vamathevan, J., Riegler, M., Deboy, R., Brownlie, J.C., McGraw, E.A., Martin, W., Esser, C., Ahmadinejad, N., et al. (2004). Phylogenomics of the reproductive parasite Wolbachia pipientis wMel: a streamlined genome overrun by mobile genetic elements. PLoS Biol. *2*, E69.

CellPress

Please cite this article in press as: Jahn et al., A Phage Protein Aids Bacterial Symbionts in Eukaryote Immune Evasion, Cell Host & Microbe (2019), https://doi.org/10.1016/j.chom.2019.08.019

STAR★METHODS

KEY RESOURCES TABLE

REAGENT or RESOURCE	SOURCE	IDENTIFIER
Antibodies		
D3I1O XP Rabbit mAb	Cell Signaling	Cat#12698; RRID: AB_2744546
Bacterial and Virus Strains		
Bacillus subtilis	DSMZ	DSM 10
Escherichia coli K12	DSMZ	DSM 498
BL21(DE3) *E. coli*	New England Biolabs	Cat#C2527I
Biological Samples		
Sponge: *Agelas oroides*	This manuscript	N/A
Sponge: *Aplysina aerophoba*	This manuscript	N/A
Sponge: *Chondrosia reniformis*	This manuscript	N/A
Sponge: *Petrosia ficiformis*	This manuscript	N/A
Chemicals, Peptides, and Recombinant Proteins		
Polyvinylpolypyrrolidone (PVPP)	Sigma-Aldrich	Cat#77627 CAS Number: 9003-39-8
Cesium chloride	Fisher Scientific	Cat#10648783 CAS Number: 7647-17-8
IPTG	Sigma-Aldrich	Cat#I6758 CAS Number: 367-93-1
JSH-23	Sigma-Aldrich	Cat#J4455CAS Number: 749886-87-1
Critical Commercial Assays		
FuGENE 6 Transfection Reagent	Promega	Cat#E2691
Maxima H Minus First Strand cDNA Synthesis kit	Thermo Scientific	Cat#K1682
Nextera XT DNA Library Preparation Kit	Illumina	Cat#FC-131-1096
pNF-κB-Luc	Clontech	N/A
Ni-NTA Fast Start Kit	Qiagen	Cat#30600
pRL-TK	Clontech	N/A
RNeasy Mini Kit	Qiagen	Cat#74106
TaqMan Gene Expression Master Mix	Applied Biosystems	Cat#4369016
Whole Transcriptome Amplification Kit 2	Sigma-Aldrich	Cat#WTA2-50RXN
Deposited Data		
Viromics raw data	This manuscript	BioProject: PRJNA522695
Microbiota 16S rDNA gene sequences	This manuscript	BioProject: PRJNA522695
Experimental Models: Cell Lines		
MODE-K cells	Kaser et al., 2008	N/A
Experimental Models: Organisms/Strains		
Mice: female C57BL/6	own breeding	N/A
Oligonucleotides		
Cxcl1	TaqMan Gene Expression Assays for mouse,Life Technologies	Mm00433859_m1
Gapdh	TaqMan Gene Expression Assays for mouse,Life Technologies	Mm99999915_g1
Ifnb1	TaqMan Gene Expression Assays for mouse,Life Technologies	Mm00439552_s1
Tnfα	TaqMan Gene Expression Assays for mouse,Life Technologies	Mm00443258_m1
Recombinant DNA		
pET22b-GFP-CPDSal	Shen et al., 2009	Addgene Cat# 38257 RRID:Addgene_38257
pET22b-ANKp	This manuscript	N/A

(*Continued on next page*)

Please cite this article in press as: Jahn et al., A Phage Protein Aids Bacterial Symbionts in Eukaryote Immune Evasion, Cell Host & Microbe (2019), https://doi.org/10.1016/j.chom.2019.08.019

Continued

REAGENT or RESOURCE	SOURCE	IDENTIFIER
Software and Algorithms		
Anvi'o v.2.1.1	Eren et al., 2015	http://merenlab.org/software/anvio/
BBMap v.37.7	Bushnell B.	https://sourceforge.net/projects/bbmap/
CAT	Bas E. Dutilh	https://github.com/dutilh/CAT
cluster_screener	This manuscript	https://github.com/MartinTJahn/cluster_screener
crAss-Tool	Dutilh et al., 2012	http://crass.sourceforge.net
Prism 6 software v.6	GraphPad	https://www.graphpad.com/scientific-software/prism/
Markov cluster algorithm (MCL)	Enright et al., 2002	https://micans.org/mcl/
QUAST v5.0.2	Gurevich et al., 2013	http://quast.sourceforge.net/quast.html
InterProScan v5.27-66.0	Jones et al., 2014	https://www.ebi.ac.uk/interpro/download.html
I-TASSER v.5.1	Roy et al., 2010	https://zhanglab.ccmb.med.umich.edu/I-TASSER/
iTOL v.4	Letunic and Bork, 2019	https://itol.embl.de/
LMCLUST	This manuscript	https://github.com/kseniaarkhipova/LMCLUST
metaSPAdes v.3.11.1	Nurk et al., 2017	https://github.com/ablab/spades/releases
mothur v.1.39.5	Schloss et al., 2009	https://www.mothur.org/wiki/Main_Page
PRODIGAL v2.6.3	Hyatt et al., 2010	https://github.com/hyattpd/Prodigal
RedRed	Ksenia Arkhipova	https://github.com/kseniaarkhipova/RedRed
SignalP v4.1f	Nielsen, 2017	http://www.cbs.dtu.dk/services/SignalP/
Tecan i-control v.1.9	Tecan	https://lifesciences.tecan.com/
TMHMM 2.0c	Krogh et al., 2001	http://www.cbs.dtu.dk/services/TMHMM/
treestats	Rob Edwards	https://github.com/linsalrob/crAssphage/tree/master/bin
VirSorter v.1.0.3	Roux et al., 2015	https://github.com/simroux/VirSorter
7900HT Fast Real-Time PCR Software v.2.4.1	Applied Biosystems	https://www.thermofisher.com

LEAD CONTACT AND MATERIALS AVAILABILITY

Further information and requests for resources and reagents should be directed to and will be fulfilled by the Lead Contact, Ute Hentschel (uhentschel@geomar.de). All unique reagents generated in this study are available from the Lead Contact without restriction.

EXPERIMENTAL MODEL AND SUBJECT DETAILS

Generation of Bone Marrow-Derived Macrophages (BMDMs)

C57BL/6 mice (10-14 weeks old) were killed, femur and tibia were dissected, and bone marrow was isolated under sterile conditions. Haematopoietic stem cells differentiated into BMDMs by incubating for 7 days in BMDM medium (1:1 SFM:DMEM, Gibco) supplemented with 10 % FCS (Biochrom), 1 % penicillin/streptomycin (Gibco), 1 % amphotericin B (Gibco), and 20 ng/mL macrophage colony-stimulating factor (mCSF, Immunotools). All animal experiments were approved by the Animal Investigation Committee of the University Hospital Schleswig-Holstein (Campus Kiel, Germany; acceptance no.: V242-7224.121-33) and were performed according the relevant guidelines and regulations.

ModeK Cells

ModeK cells were kindly provided by Arthur Kaser. ModeK cells were cultured in DMEM (DMEM Glutamax plus 10% FCS, non-essential amino acids and HEPES, Gibco). Cells were incubated at 37°C at 5% CO_2. All cell lines were authenticated by microscopic morphologic evaluation, characteristic growth curves and screening for mycoplasma.

Bacteria

The bacterial strains used in this study are listed on the Key Resources Table. *B. subtilis* (DSMZ, #10) and *E. coli*, strain K12 (DSMZ, #498) were cultured overnight at 37°C in LB medium. After adjustment to the desired density, serial dilutions of the inocula were plated on LB agar plates to verify the CFU.

Please cite this article in press as: Jahn et al., A Phage Protein Aids Bacterial Symbionts in Eukaryote Immune Evasion, Cell Host & Microbe (2019), https://doi.org/10.1016/j.chom.2019.08.019

CellPress

METHOD DETAILS

Nested Sampling Design

The high microbial abundance (HMA) sponge species *Petrosia ficiformis*, *Chondrosia reniformis*, and *Agelas oroides* (each n=4) were collected at the Mongrí Coast, Cala Foradada, 3°12'00.09''E, 42°04'56.97''N, Girona, Catalunya, Spain) close to Barcelona by snorkelling and scuba diving within a 20 m radius. We randomly sampled four individuals per species. *Aplysina aerophoba* (n=4) was collected at a different site 25 km south-west (see for metadata Table S3). Immediately after collection, sponge samples were rinsed in sterile artificial seawater, plunge frozen in liquid nitrogen, and stored at -80°C until further processing. Prior to sponge sampling, for each spot, 30 litres of seawater were collected from the sponge vicinity using cooled sterilised tanks. Viroplankton was enriched by $FeCl_3$ flocculation according to John et al. (2011). Briefly, the seawater was pre-filtered (Millipore, 0.22 μm,142mm, GPWP14250) and the virus fraction was incubated with $FeCl_3$ (2.9 mg/liter) for 1 hour. The virion-iron precipitates were then recovered on a filter (GE Polycarbonate Membrane filter, 1.0 μm, 142mm, K10CP14220) and resuspended in EDTA-ascorbate buffer (pH 6).

Sample Processing and Virome Sequencing

Deep frozen sponge individuals were dissected, separating the outer epithelial area (pinacoderm) from the inner mesohyl matrix. All samples, including seawater references, were then randomly shuffled for virus purification and DNA/RNA extraction to avoid batch effects during processing. Samples were thawed in preboiled ice-cold extraction buffer (artificial seawater with 10mM EDTA and 3% (w/v) PVPP) and were disintegrated using a blender on ice at 6,500 rpm (T25 digital ULTRA-TURRAX, IKA). Particle aggregation was reduced by vortexing the suspension 10 min on ice. Tissue debris, PVPP bound secondary metabolites and bacterial cells were removed by centrifugation (2x 4,600g; 30 min at 4°C; ThermoScientific Heraeus Multifuge 3SR). The cleared supernatant was filtered through a 0.45 μm filter (Conceição-Neto et al., 2015), and virions were pelleted using a Beckman SW-41-Ti swinging bucket rotor at 135,000 x g for 2 h. Virions were re-suspended in modified SM-buffer containing 0.01 M Na_2S overnight, purified by low speed centrifugation at 4,300g for 5 min, loaded onto a CsCl gradient (1.7/1.5/1.3/1.2/1.1) according Thurber et al. (2009) and separated at 135,000 x g for 2 h. Virion-containing layers (CsCl density 1.2-1.5) were retrieved using a syringe and confirmed for viral particles by epifluorescence and transmission electron microscopy. Notably, this purification method was shown to enrich for bacteriophages and negatively selects for groups of eukaryotic viruses (Thurber et al., 2009). The virions were diluted in SM-buffer, purified by low speed centrifugation as before and pelleted at 135,000 x g for 2 h. Upon overnight resuspension in Tris buffer, and removal of undissolved particles at 1000 g for 1 min, the supernatant was transferred to a fresh tube and incubated with benzonase for 2 h at 37°C to remove free nucleic acid contamination. Encapsulated viral DNA and RNA were extracted according to Thurber et al. (2009) and Lachnit et al. (2015). Viral nucleotides were randomly amplified using a modified version of the Whole Transcriptome Amplification Kit 2 (WTA2, Sigma Aldrich) as described in Conceição-Neto et al. (2015). This approach allows the capture of single-stranded and double-stranded DNA and RNA viruses with little amplification bias (as sequence reads represent viral genome copies). NexteraXT libraries were prepared and sequenced on a Hiseq2500 run with 2x250 bp paired end reads at IKMB Kiel (Data S1). From the same tissue as used for the viromes, V1V2+V3V4 of the 16S rRNA gene was amplified and sequenced as described in Thomas et al. (2016).

Metagenome Cross-Assembly and Curation

Illumina reads were quality trimmed and cleaned from adapters, primers and reads with Ns or an average Q-score below 15 using BBMap v37.75 (https://sourceforge.net/projects/bbmap/). This Q-score threshold was confirmed by trimming reads to either Q15 or Q25 and by comparing the assembly statistics for each library using QUAST v5.0.2. (Gurevich et al., 2013). This showed inferior Q25 assemblies compared to Q15 assemblies as indicated by fewer long contigs (> 5 kb; see Data S1). The reads were then assembled per library (n=36) and in random subsets of the total library pool (50x 0.01%, 12x 0.05%, 12x 0.10%) using metaSPAdes v3.11.1 with default parameters (https://github.com/MartinTJahn/Iter_assembly). This multistep assembly strategy was tested in pilot assemblies to improve the quality of the assemblies as described in more detail in Coutinho et al. (2017). Contigs from all assemblies were clustered using a custom script (https://github.com/kseniaarkhipova/RedRed) into populations with mummer3 (Kurtz et al., 2004) at ≥95% ANI across ≥80% of their lengths as inspired by (Roux et al., 2017). To filter for viral sequences and to remove remaining potential cellular contamination, population contigs were submitted to VirSorter 1.0.3 (using Virome Database and Virome decontamination options) and were additionally classified with the Contig Annotation Tool (CAT; https://github.com/dutilh/CAT). Contigs above 5 kb that were VirSorter classified and/or had superkingdom classification "Viruses" in CAT were used for downstream genome-centric analysis. For functional gene-centric analyses, we increased stringency against cellular sequence contamination by considering only contigs with at least two VirSorter hits for viral hallmark genes (i.e., "major capsid protein," "portal", "terminase large subunit," "spike", "tail," "virion formation" or "coat) or CAT "viral superfamily" annotation. In the next round of cellular decontamination, we screened against single-copy prokaryotic marker genes using Anvi'o v.2.1.1 workflow (Eren et al., 2015). A proportion of 6.19% (79 of 1276) of the contigs were hit by the single-copy prokaryotic marker database. Manual curation ensured that most of the hits were homologous to phage nucleotide replication machinery (DNA/RNA polymerases) and RecA, while there were no hits against any ribosomal RNA indicative of low remining contamination levels with cellular DNA/RNA (Roux et al., 2013). One contig with the ClpX C4-type zinc finger domain was removed from further analysis due to its unclear viral association. These in silico filtration steps ensured that no cellular signals should have been included in the functional analysis.

Please cite this article in press as: Jahn et al., A Phage Protein Aids Bacterial Symbionts in Eukaryote Immune Evasion, Cell Host & Microbe (2019), https://doi.org/10.1016/j.chom.2019.08.019

Gene Content-Based Viral Clustering

Evolutionary relationships between the viral genome (fragments) were inferred by implementing reticulate classification based on gene sharing as developed by Lima-Mendez et al. (2008). Briefly, we predicted 869,624 proteins from a set of 46,307 viral sequences (see details below) with PRODIGAL v2.6.3 (Hyatt et al., 2010) and detected pairwise similarities using all-by-all BLASTp, requiring a minimal bit score 50. Protein families were identified with the Markov cluster algorithm (MCL) using inflation factor 2 (Enright et al., 2002). All viral genomes were then compared to each other for shared protein family content, and the probability that similarity was by chance was estimated using a hypergeometric formula (Lima-Mendez et al., 2008). The resulting significance scores were corrected for multiple comparisons, and genome pairs with scores $\geq$ 0 were joined by an edge [see https://github.com/kseniaarkhipova/LMCLUST]. To define viral clusters (VCs) in the genome network, we determined 1.4 as the best MCL inflation factor based on ICCC (intracluster clustering coefficient) maximization as described in Roux et al. (2015). The curated viral contigs were clustered with well-characterized isolate genomes downloaded from the Actinobacteriophage database project (http://phagesdb.org/; January 2018) and ViralRefseq (January 2018). To investigate overlap with other marine environments, we also clustered with viral sequences from 130 environmental virome libraries. Specifically, 78 viromes cross-assembled from seawater (incl. Tara Oceans), corals and sediment (Coutinho et al., 2017), 24 viromes from a seawater transect throughout the Mediterranean Sea (López-Pérez et al., 2017) and all viromes from sponges known to date supplemented with corals (Laffy et al., 2018). Viral clusters were taxonomically classified based on the placement of ViralRefseq entries in the network using a custom script [https://github.com/MartinTJahn/cluster_screener]. For each taxonomic rank, clusters were screened for Viral RefSeq entries and classified according to the supermajority (3/4) of their taxonomic annotations.

Abundance Profiles

Relative abundance patterns of viral genomes in the different samples were assessed by mapping quality control reads from each library against the curated genome-centric catalogue using BBMap 37.75 (option ambiguous=random, ANI $\geq$ 99%). The resulting 36 x 4484 count matrix was normalised for contig/virus length and library size to yield counts per kbp (CpK, Equation 1):

$$CpK = \frac{count}{length} * scaling\ factor * 10^3 \quad with\ scaling\ factor = \left(mean\ library\ size / sample\ library\ size\right) \qquad \text{(Equation 1)}$$

Community and Prevalence Classification

Distances between viral metagenomes were computed with the reference-independent cross-assembly (crAss;(Dutilh et al., 2012)) tool. The resulting clustering was calculated based on the SHOT formula and was drawn with iTOL (Letunic and Bork, 2019). To infer significant clustering of sample categories (type, species, tissue), the leaf labels and associated sample categories were compared to N=1,000 trees where the leaf labels were randomized using a custom script [treestats.pl; https://github.com/linsalrob/crAssphage/tree/master/bin]. The observed patterns were validated independently by hierarchical clustering based on Bray-Curtis distances of community abundance signatures calculated in the R package vegan (Dixon, 2003).

Viral population enrichment for sample types was assessed using the population enrichment score (Equation 2)

$$Pop.enrichment\ score = \frac{mean(CpK_{sample})}{mean(CpK_{other\ samples})} \qquad \text{(Equation 2)}$$

with a $\geq$ 2-fold enrichment considered to be enriched.

Viral population contigs (BCvir) were defined as detected in a sample when at least 75% of its length was covered by read mapping as suggested by Roux et al. (2017). BCvir were considered prevalent based on the supermajority rule when detected in at least 75% of the samples in a sample category. "Individualists" were those BCvir that were detected in only one individual but both tissues. "Generalists" were prevalent in all or several sample categories, while "Specialists" were prevalent in only one sample type (Data S1).

Annotation and Auxiliary Gene Classification

Proteins were predicted from viral contigs that passed the stringent cellular contamination filter (n=1,275 BCvir contigs) and were searched against the PFAM database (v31) using InterProScan v5.27-66.0 (Jones et al., 2014). Identified PFAM domains were then classified into 8 functional categories: "metabolism", "lysis", "structural", "membrane transport, membrane-associated", "DNA replication, recombination, repair, nucleotide metabolism", "transcription, translation, protein synthesis", "other", and "unknown" as in (Hurwitz et al., 2015) and extended by (Roux et al., 2016). This PFAM classification catalogue was augmented with manual classification of 85 PFAM signatures that were novel compared to the seawater viromes in the present study. We realized that in addition to auxiliary functions involved in the hosts metabolism (AMG), further categories might be relevant in the tripartite system of phage-prokaryote-eukaryote (PPE-interaction, hereafter). Therefore, we manually reannotated category "others" into classes "signalling and protein-protein interaction", "cellular binding" and "cellular defence systems", based on the literature research and functional evidence. The final extended PFAM classification catalogue for phages is given in Data S1 and is open for further use in other systems. For abundance estimations, multiple identical PFAM motifs in one protein, such as by repeats, were counted as one to ensure that quantification is not biased towards repeat domains. Sequences were also annotated with Prokaryotic Virus Orthologous Groups (pVOGs; (Grazziotin et al., 2017)) through HMMER 3.1b2 (hmmscan -E 10^{-5}), SEED subsystems through MG-RAST (E 10^{-5}) and were matched to NCBI-nr database entries using Diamond (e-value 10^{-5} and identity $\geq$40%). Proteins

Please cite this article in press as: Jahn et al., A Phage Protein Aids Bacterial Symbionts in Eukaryote Immune Evasion, Cell Host & Microbe (2019), https://doi.org/10.1016/j.chom.2019.08.019

were screened for terminal signal peptides using SignalP v4.1f and for transmembrane domains using TMHMM 2.0c. The tertiary structure of phage ankyrin-containing proteins was approximated by I-TASSER (default settings) (Roy et al., 2010). All annotations are combined in Data S1.

ANKp Expression and Purification

The 568 nt ANKp encoding phage gene (BCvir 4986 ORF 10) was optimized for *E. coli* codon usage and then de-novo synthesized in collaboration with GenScript (Piscataway, NJ, USA). The sequence was then cloned into the pET-22b(+) vector using BamHi and XhoI restriction sites. The same pET22b construct encoding GFP (Addgene plasmid # 38257 pET22b-GFP-CPDSalI) was used as a negative control and was a gift from Matthew Bogyo & Aimee Shen (Shen et al., 2009). Plasmids were transformed into BL21(DE3)-competent *E. coli*. Heterologous protein expression was induced in *E. coli* with 0.4 mM IPTG, and cultures were grown for 3 h at 37°C. For the native purification of the His-tagged target proteins, the Ni-NTA Fast Start Kit (Qiagen) was applied according to the manufacturer's instructions.

ANKp Cell Exposure Assays

E. coli K12 (DSMZ, #498) or *B. subtilis* (DSMZ, #10) overnight Luria–Bertani (LB) medium cultures were harvested at 4,000g for 10 min at room temperature and were washed twice with PBS. The bacterial suspension was then either incubated with ANKp (0 nM, 100 nM, 1 μM purified protein) or GFP (0 nM, 100 nM, 1 μM purified protein) in PBS for 10 min at 4°C under mild agitation. Prior to infection, the medium of BMDM cell culture was replaced with fresh antibiotic-free BMDM medium, and the cells were then infected with the pre-incubated *E. coli* K12 with protein in their medium using a range of multiplicities of infection (MOIs). Optical density measurements at a wavelength of 600 nm were performed using a Tecan Infinite 200 plate reader in a 96-well plate as described in Erez et al. (2017). In addition to assays with purified protein we performed the BMDM experiment with recombinant *E.coli* (see ANKp expression) directly expressing the proteins. As positive control for immune suppression we added the NF-κB inhibitor JSH-23 (Sigma-Aldrich). All *in vitro* data is representative for three independent non-randomized experiments. Sample sizes varied between the experimental approach used and were selected based on previous experience about the expected magnitude and variance of the phenotype. If not otherwise stated in the figure legends, all experiments included at least 3 biological replicates.

RNA Extraction and Quantitative RealTime PCR

Total RNA was isolated from BMDM and ModeK cell culture 16 h post infection using the RNeasy kit (Qiagen) and reverse transcribed using the Maxima H Minus First Strand cDNA Synthesis kit (Thermo Scientific). Quantitative RealTime PCRs were performed with TaqMan Gene Expression Master Mix (Applied Biosystems) according to the manufacturer's instructions and were analysed on the 7900HT Fast Real Time PCR System (Applied Biosystems). The applied TaqMan assays for pro-inflammatory markers are: *Cxcl1* (TaqMan ID Mm00433859_m1), *Gapdh* (TaqMan ID Mm99999915_g1), *Ifnb1* (TaqMan ID Mm00439552_s1), *Tnfα* (TaqMan ID Mm00443258_m1).

NF-κB–Dependent Luciferase Assay

The dual-luciferase assay using an NF-κB–dependent firefly luciferase (pNF-κB-Luc; Clontech) and a Renilla luciferase driven by the thymidine kinase promoter (pRLTK; Clontech) was performed according to the manufacturer's instructions. Briefly, ModeK cells cultured in DMEM (DMEM Glutamax plus 10% FCS, non-essential amino acids and HEPES, Gibco) were transfected with 20 ng pNF-κB-Luc and 3 ng pRL-TK using FuGENE 6 (Roche). Transfected cells were incubated for 24 h (37°C, 5% CO2), lysed and the lysate was subjected to the dual-luciferase assay carried out on a Tecan 96-well microplate reader.

QUANTIFICATION AND STATISTICAL ANALYSIS

Sample Sizes

n represents the number of sponge individuals, seawater replicates or cell assay experiments as described in legends of each figure.

Statistical Analysis

Topology of the crAss clustering (Figure 2) was compared against 1,000 random trees as detailed in the methods section. The reported consistency values represent the average of frequencies of the most frequent metadata annotation in a branch (Edwards et al., 2019). Cell assay data are presented as the mean ± SEM of at least three independent experiments. Statistical significance between treatments was determined by two-tailed unpaired Student's t-tests with p values less than 0.05 that were considered statistically significant. Statistical tests were performed using GraphPad Prism 6.0 Software.

DATA AND CODE AVAILABILITY

The accession number for all sequencing libraries, the cross-assembly, of both the sponge viromes and seawater references, as well as microbial amplicon data reported in this paper is GenBank: BioProject: PRJNA522695). All custom code is available at GitHub as indicated in the methods section.

Cell Host & Microbe, Volume *26*

Supplemental Information

A Phage Protein Aids Bacterial Symbionts in Eukaryote Immune Evasion

Martin T. Jahn, Ksenia Arkhipova, Sebastian M. Markert, Christian Stigloher, Tim Lachnit, Lucia Pita, Anne Kupczok, Marta Ribes, Stephanie T. Stengel, Philip Rosenstiel, Bas E. Dutilh, and Ute Hentschel

Supplementary Figures

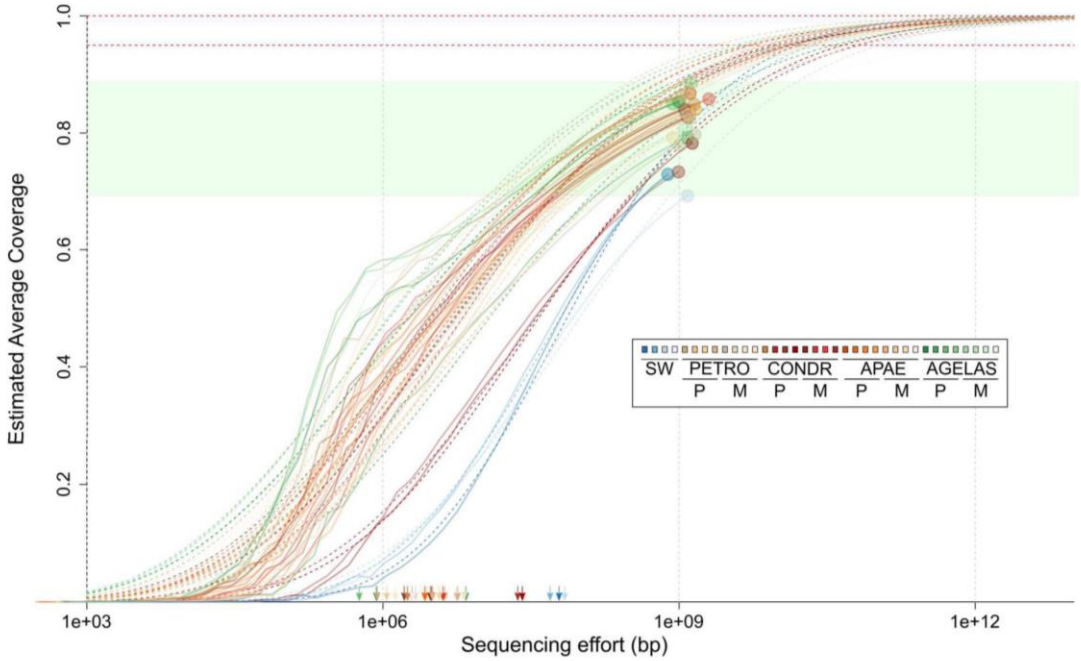

Figure S1: Community coverage of each metagenomic dataset was estimated using Nonpareil v3.301 with default parameters (Rodriguez et al., 2018), Related to Figure 1. The dashed lines indicate the fitted models of the Nonpareil curves (solid). Coloured circles are the estimated coverage for each sample, and the green area is the observed range for the samples. Horizontal dashed lines indicate 100 and 95% coverage. Coloured arrows indicate the needed sequencing effort to reach 50% coverage of the fitted model as a proxy for detected diversity. Abbreviations: SW = seawater, PETRO = *Petrosia*, CONDR = *Chondrosia*, APAE = *Aplysina*, AGELAS = *Agelas*, M = mesohyl, P = pinacoderm.

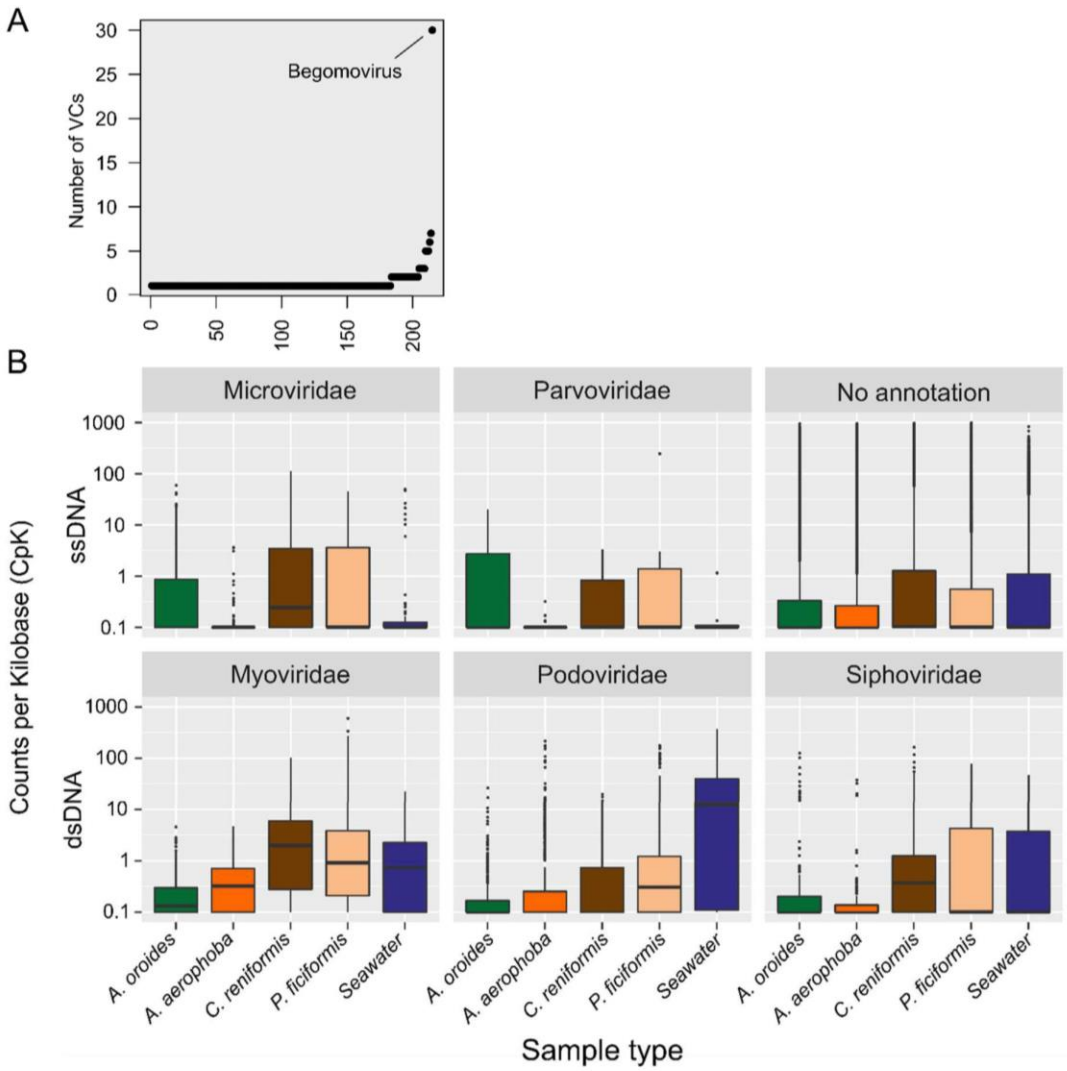

Figure S2, Related to Figure 2: (A) Quality of taxonomic assignments. Most ViralRefseq entries clustered in one cluster per given genus (index; 183 of 215 genera). Strongest exception was the genus Begomovirus, where genomes were distributed into 30 adjacent viral clusters. This is in line with reports stressing the need for new taxonomic demarcation criteria in this genus (Brown et al., 2015). Multiple genera per cluster were observed in 1.8% (59 of 3,218) of the VCs, representing a small minority where our approach may have been too inclusive. (**B**) **Taxonomic affiliation of viral population contigs**. Co-clustering with ViralRefseq allowed us to classify 1.2% (55/4,484) of BCvir populations on genus level and 3.9% (177/4,484) on family level. ssDNA and dsDNA bacteriophages were predominant. Specifically, tailed bacteriophages of the order Caudovirales (Podo-, Myo-, Siphoviridae) and Microviridae subfamily Gokushovirinae. Further detected ssDNA(+/-) Ambidensovirus, eukaryote viruses of the family Parvoviridae, in a majority of sponge individuals, which is consistent with observations from Australian reef sponges (Laffy et al., 2018).

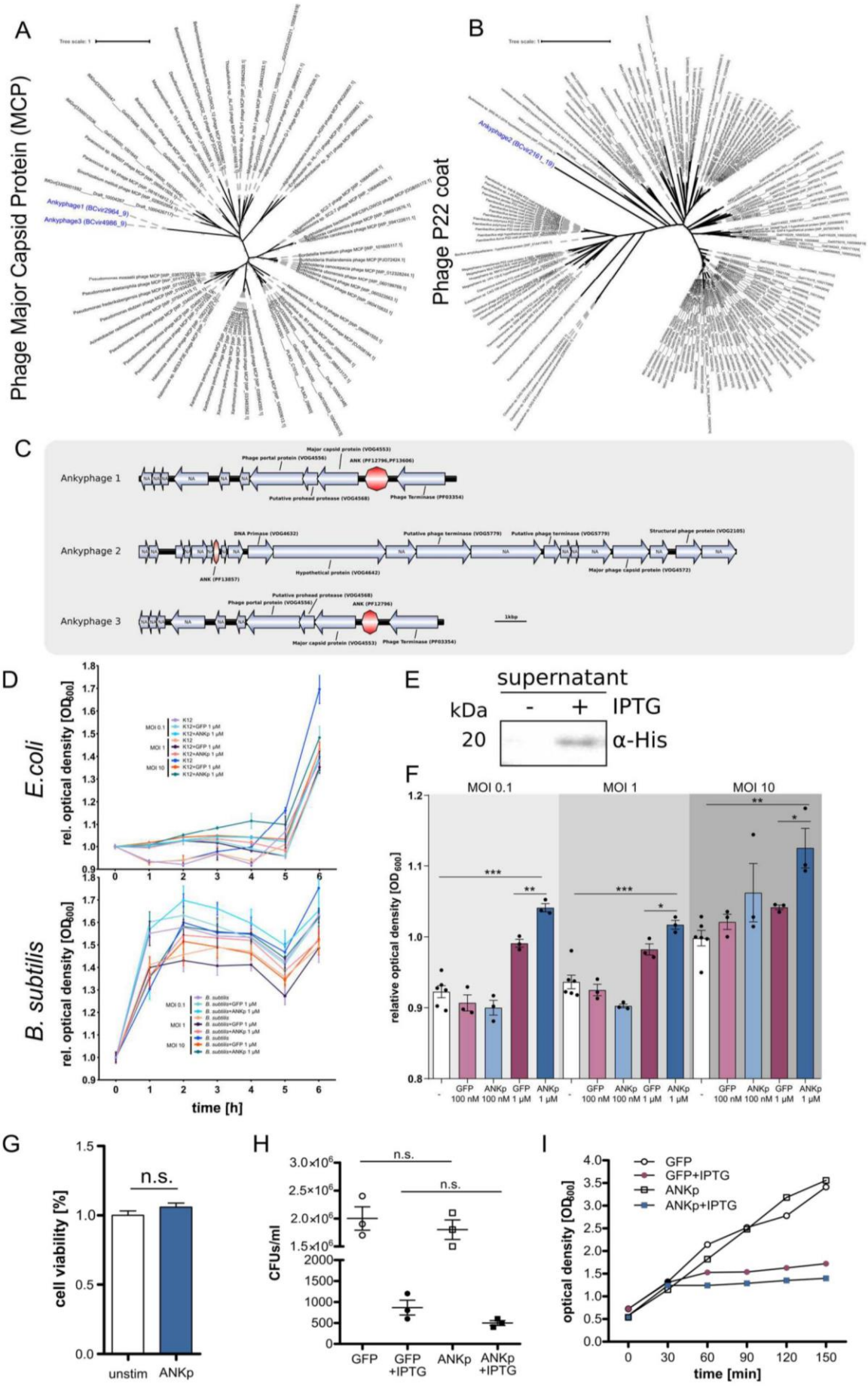
A
Phage Major Capsid Protein (MCP)
Ankyphage1 (BCvir2964_9)
Ankyphage3 (BCvir4986_9)
B
Phage P22 coat
Ankyphage2 (BCvir2181_19)
C
Ankyphage 1
Ankyphage 2
Ankyphage 3
Major capsid protein (VOG4553)
Phage portal protein (VOG4556)
ANK (PF12796,PF13606)
Putative prohead protease (VOG4568)
Phage Terminase (PF03354)
DNA Primase (VOG4632)
Putative phage terminase (VOG5779)
Structural phage protein (VOG2105)
ANK (PF13857)
Hypothetical protein (VOG4642)
Major phage capsid protein (VOG4572)
1kbp
D
E.coli
B. subtilis
rel. optical density [OD600]
time [h]
E
supernatant
kDa
IPTG
20
α-His
F
MOI 0.1
MOI 1
MOI 10
relative optical density [OD 600]
GFP 100 nM
ANKp 100 nM
GFP 1 µM
ANKp 1 µM
G
cell viability [%]
n.s.
unstim
ANKp
H
CFUs/ml
n.s.
GFP
GFP +IPTG
ANKp
ANKp +IPTG
I
GFP
GFP+IPTG
ANKp
ANKp+IPTG
optical density [OD600]
time [min]

Figure S3: Ankyphage phylogeny and ANKp control experiments, Related to Figure 3. Phylogenetic analysis of structural genes places Ankyphages among bacteriophages (A+B). Phylogenies were constructed based on (**A**) 401 aa of Phage major capsid protein (MCP) and (**B**) 382 aa of Phage P22 coat proteins with IQ-TREE (1,000 bootstraps). The protein set to compare with was identified by BLASTx searches against GenBank (v. April2018) and IMGVr (v. July2018) (e-value $\leq 10^{-5}$; coverage $\geq$ 33% MVC and 25% P22). The set was deduplicated with usearch v8.1.1861 at 100% ANI, aligned with MUSCLE, and alignment was curated using Guidance2 (column score >= 0.6). The best-fit model of protein evolution (LG+I+G+F for MVC, LG+R6 for P22) was identified with IQ-TREE. (**C**) G**enome architecture** of sponge derived Ankyphages. NAs are hypothetical genes; ANK are ankyrin repeat containing proteins in red; VOG identifiers indicate annotations for Prokaryotic Virus Orthologous Groups (pVOGs) (**D**) **Growth kinetics** of *E. coli* K12 and *B. subtilis* on macrophages (BMDMs) upon ANKp treatment. Optical density (OD) was normalised to the start value at the beginning of the experiment (t_0). The multiplicity of infection (MOI) denotes the microbe:macrophage ratio set at t_0. Data are presented as the mean ± SEM from 4 independent replicates. **(E) Detection of secreted ANKp** in the supernatant of *E.coli* expressing recombinant ANKp upon induction with IPTG. **(F)**Growth of *E. coli* K12 that are challenged with murine bone marrow-derived macrophages (BMDMs) upon exposure with GFP and ANKp at 100 nM or 1 µM. MOI refers to multiplicity of infection. The white bars indicate unstimulated (-) controls. Data are presented as the mean ± SEM of at least three independent experiments. **ANKp cytotoxicity controls (G-I).** (**G**) BMDM cell viability was measured with an MTS assay. Data are presented as the mean ± SEM from 4 replicates each. (**H**) *E. coli* viability on agar plates was measured by counting colony forming units with and without IPTG induction of ANKp expression. Data are presented as the mean ± SEM of 3 independent experiments. (**I**) *E. coli* viability in liquid LB-medium was measured by following optical density over time with and without IPTG induction. Statistical significance between treatments was determined by two-tailed unpaired Student´s *t*-tests with *p < 0.05, **p < 0.01 and ***p < 0.001.

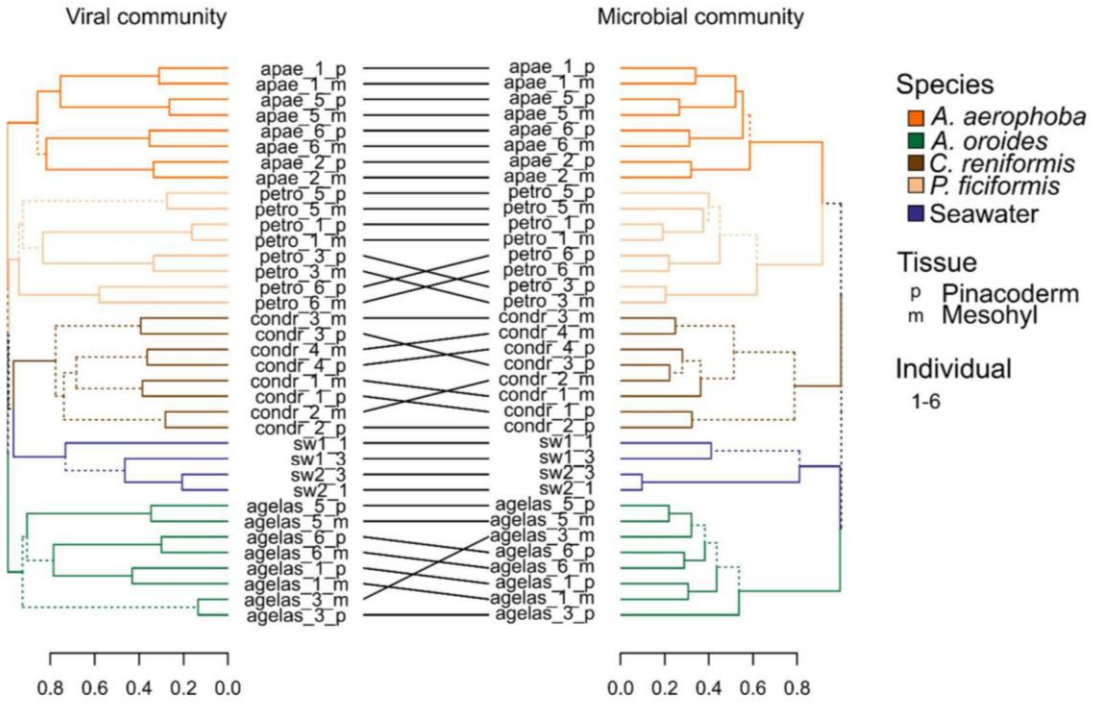

Figure S4: Hclust analysis supplementing CrAss and comparison to microbial community profiles, Related to Figure 2. Relative abundance profiles of (left) BCvir population contigs and (right) co-extracted prokaryotic 16S rRNA gene sequences, hierarchically clustered (complete linkage) with the Bray-Curtis similarity. Cladograms are compared with the tanglegram function (R dendextend package). Dashed lines indicate differences in tree topologies. Sample IDs indicate the following: apae, agelas, petro, condr are the sponge species *Aplysina aerophoba*, *Agelas oroides*, *Petrosia ficiformis*, *Chondrosia reniformis*. sw indicates seawater. _m and _p indicate mesohyl and pinacoderm tissues. _#_ is the individual identifier.

Supplementary Tables

Table S1. Cross-Assembly statistics, Related to Figure 1.

Criterium	Parameter
Assembly tool(s) used	metaSPAdes; 3.11.0; default parameters
Number of assembled contigs (> 5000)	7,105
Total bases assembled (bp)	72,419,424
Contig N50	10,746
Largest contig (bp)	155,600
% of Sequences assembled	62.47% of the reads mapped back to whole cross assembly 51.41% of the reads mapped back to filtered viral contigs

Table S2. Statistics of gene sharing network, Related to Figure 2.

Statistic	Value
Number of nodes	27,278
Number of viral clusters (VC)	3,218
Clustering coefficient	0.639
Avg. number of neighbors	24.044
Network heterogenity	1.584
Avg. cluster size	8.477
Maximal cluster size	776
Minimal cluster size	2
Number of nodes by source	3,579 BCvir (this study) 14,951 Marine viromes(Coutinho et al., 2017) 1,311 Planktonic virome (López-Pérez et al., 2017) 2,318 ActinophageDB (Russell and Hatfull, 2016) 4,335 RefSeqABVir (Brister et al., 2015) (v. December 2017) 785 GBR sponge (Laffy et al., 2018)

Table S3. Sampling metadata, Related to Star Methods, section Nested sampling design.

species	used for	location	date	time	temperature	depth	lat	long
A. aerophoba	virome	Port Lligat	12. July 2016	noon	23.3°C	3m	42°17'50.8"N	3°17'20.4"E
P. ficiformis	virome	Reserva Natural de Montgrí, Illes Medes i Baix Ter	18. July 2016	noon	21°C	15m	42°04'56.97"N	3°12'00.09"E
C. reniformis	virome	Reserva Natural de Montgrí, Illes Medes i Baix Ter	18. July 2016	noon	21°C	15m	42°04'56.97"N	3°12'00.09"E
A. oroides	virome	Reserva Natural de Montgrí, Illes Medes i Baix Ter	18. July 2016	noon	21°C	15m	42°04'56.97"N	3°12'00.09"E

CHAPTER 8

GENERAL DISCUSSION OF KEY FINDINGS

8.1 Integrative symbiont physiology

This PhD thesis contributed to a more detailed understanding of the functional activity and interplay of sponge symbionts (CHAPTER 3, CHAPTER 4) and established a set of integrative approaches to study microbial symbionts within the sponge matrix (see: microbial ecology toolset 2.1). In the following paragraphs, the key results and overarching themes from the Chapters 3-6 are discussed, with an emphasis on understudied spatial-functional characteristics.

8.1.1 Structural cell biology of *Poribacteria*

Beyond genomic information, little is known about the phenotypes of specific symbionts in the sponge host context (Webster and Thomas, 2016). However, various cases in microbiology show that structural features of microbes can be important descriptors for function (Yang et al., 2016, Kerfeld et al., 2018). This becomes apparent by striking examples such as *Pseudoalteromonas luteoviolacea*'s contractile injection system injecting tubeworms metamorphosis factors into host cells (Ericson et al., 2019, Shikuma et al., 2014), or even basic mechanisms of sporulation (Khanna et al., 2019), which, functionally, would have been hardly understood by genomic evidence alone. CHAPTER 3 provided the first clear evidence that supports the long standing hypothesis of cell compartmentation (Fieseler et al., 2004, Kamke et al., 2014) in a lineage of sponge endemic *Poribacteria* (Podell et al., 2019, Steinert et al., 2018a, Lafi et al., 2009). This revealed that the poribacterial cell structure is more complex than previously thought. Specifically, I discovered bacterial microcompartments (BMCs) and bipolar storage polymers as common structural features of poribacterial cells:

BMCs

Over 20 bacterial phyla have been reported to encode BMCs, highly structured membrane-bound compartments packed with specialised enzymes (Axen et al., 2014). Among BMCs encoding microbes are frequently pathogens such as *Salmonella* (Bobik et al., 1999) but also symbionts such as found in termite guts (*Acetonema longum;* (Tocheva et al., 2014)), where they can be detrimental virulence/symbiosis factors to occupy their host niche (Thiennimitr et al., 2011, Bertin et al., 2011). Mechanistically, diverse types of BMCs are described (Chowdhury et al., 2014, Axen et al., 2014) that collectively allow their carriers to process otherwise inaccessible nutrients by enclosing toxic/volatile metabolic intermediates (i.e. metabolosomes; (Kerfeld and Erbilgin, 2015)) or by optimising oxygen sensitive reactions in aerobic environments (e.g. cyanobacterial CO_2-fixing carboxysomes; Rae et al. (2013)).

Poribacterial BMCs, previously suggested by genomic evidence (Kamke et al., 2014), act most likely in 1,2-propanediol (1,2-PD) degradation pathways (CHAPTER 3) enclosing cytotoxic aldehyde intermediates (Sampson and Bobik, 2008). But where is 1,2-PD coming from in sponges? Interestingly, 1,2-PD arises from the anaerobic breakdown of sugars such as fucose or rhamnose (Huff, 1961, Saxena et al., 2010) which has two prominent sources in the sponge holobiont: Firstly, fucose is a main component of sponge glycosaminoglycans (GAGs), a component of the sponge extracellular matrix (Misevic et al., 1987, Zierer and Mourao, 2000). Secondly, fucose is a dominant sugar in dissolved organic matter (DOM) (Borch and

Kirchman, 1997, Repeta et al., 2002), a critical food source to the sponge holobiont (discussed in 8.1.3). Ultimately, the availability of 1,2-PD is supported by the presence of 1,2 propanediol generating pathways among sponge microbiota genes (see Appendix B3) and assays on sponge isolates (Santavy et al., 1990). Therefore, combining my data with previous genomic evidence (Kamke et al., 2014), I hypothesise that *Poribacteria* BMCs represent structural adaptations to efficiently degrade sponge extracellular matrix components or DOM - both expected to be rich nutritional sources within the sponge holobiont. While further sources and sinks symbiont metabolism will be discussed in more detail below, it seems likely that *Poribacteria* adapted to feed on a diversity of holobiont supplied food sources depending on internal (sponge matrix) and external (DOM) food availability.

BIPOLAR COMPARTMENTATION

Besides BMCs, our results indicate that bipolar compartments represent additional elements of poribacterial morphotypes (CHAPTER 3, CHAPTER 4). Amongst the studied *A. aerophoba* microbiota these bipolar compartments seem to be unique features to *Poribacteria* (Table 1) indicating an element of morphological specialization. Combining morphological and genomic evidence (CHAPTER 3), I expect the bipolar compartments most likely to represent carbon-rich storage polymers such as poly-β-hydroxybutyrate or glycogen. This is in contrast to Podell et al. (2018) who suggest that the bipolar compartments are endospores based on our images (CHAPTER 3). Several arguments point against this latter interpretation: First, electron micrographs reveal a crystalline appearance whilst lacking typical endospore characteristics such as spore sheath (CHAPTER 3). Second, it seems unlikely that the vast majority of poribacterial cells throughout hosts, time and in geographically distant locations engage synchronized in bipolar spore formation. Third, as the authors indicate, clear genomic evidence for spore formation is missing in Poribacter*ia* genomes (Podell et al., 2018) questioning the genomic basis. Therefore, I suggest that the bipolar compartments are storage polymers although future studies, such as with targeted staining's and energy dispersive X-ray spectroscopy combined with electron microscopy, will help to further our knowledge about their composition.

Energetically, the widespread stockpiling of nutrients by *Poribacteria* is an interesting finding considering the limited storage physiology of their sponge hosts. Unlike many other metazoans, sponges do not possess dedicated tissue scale storage structures (e.g. adipose tissue) and are limited to a few specialised cell types (L. Simpson, 1984). Therefore, potent *Poribacteria* heterotrophy might be coupled with their function as storage units potentially buffering the holobiont for nutrient input shortcomings (Coma and Ribes, 2003, Coma et al., 2000).

Collectively, these findings extend the genomic evidence for a pronounced heterotrophic carbon metabolism in *Poribacteria* (Kamke et al., 2013, Kamke et al., 2014) with structural adaptations to potentially process and store such compounds. From a symbiosis perspective, this is of interest as such carbon rich compounds are likely retrieved in the interplay with the sponge holobiont.

8.1.2 Comparative symbiont morphology & physiology

With my established FISH-CLEM approach in combination with novel probe design, I was able to visualise the ultrastructures of dominant sponge symbiont clades for the first time (CHAPTER 3, CHAPTER 4). This clearly showed that each of the assayed symbiont clades consists of a distinct morphotype that is compiled in Table 1. Consequently, clade-specific morphologies open an exciting future perspective for morphotype-based symbiont identification although the generalizability requires validation across an extended collection spectrum (i.e. different geographic locations). Interestingly, the comparative integration of genomic information with symbiont ultrastructure (CHAPTER 3, CHAPTER 4) in *A. aerophoba* revealed correlation between a carbon-directed heterotrophic genotype and electron-lucent halos surrounding such cells (Table 1; arrowheads). In contrast, such halos were not evident for SAR202 cells with a metabolism tailored for amino acid utilization (CHAPTER 4) and other unstained morphotypes (CHAPTER 3, CHAPTER 4). These electron-lucent halos may either represent bacterial capsules or digestion zones, resulting from the extracellular symbiont digestion of the host matrix. As the halo structures strictly follow cell shapes, it is less probable that they represent digestion zones of the surrounding mesohyl as such digestion zones are generally less confined and more diffuse in appearance (Personal communication Prof. Akos T. Kovacs). In this scenario, the C-directed heterotrophic metabolism of *Poribacteria*, *Anaerolinea* and *Caldilinea* lineages (CHAPTER 3,CHAPTER 4, (Kamke et al., 2013)) might provide excess C compounds for investment in polysaccharide rich capsule (Roberts, 1996) while this is not the case for SAR202. Due to the well-established role of bacterial capsules to resist host immunity (Surana and Kasper, 2012, Nanra et al., 2013, de Vos et al., 2015) it will be an exciting field of future research to systematically investigate the impact of symbiont encapsulation in sponge microbe symbiosis.

Table 1 Key physiological features of dominant *A. aerophoba* symbionts.

	Poribacteria	*Anaerolinea*	*Caldilinea*	SAR202
Morphotype	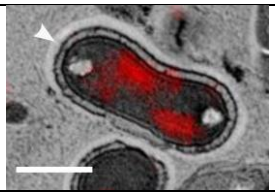	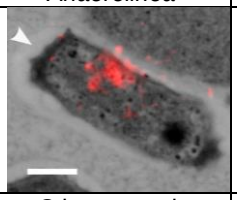	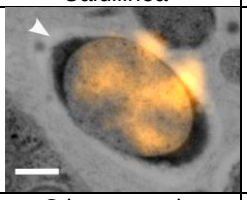	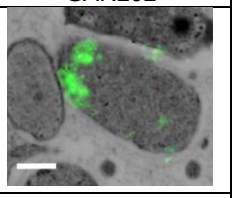
Metabolism type	C heterotroph	C heterotroph	C heterotroph	AA heterotroph
Halo/ Capsule	**YES**	**YES**	**YES**	**NO**
Capsular genes	+ EPS capsules	unclear evidence	unclear evidence	unclear evidence
Flagella	**NO**	**NO**	**NO**	**NO**
Subcellular compartment	Bipolar granules, BMCs			
Image Source/ Reference	CHAPTER 3, (Kamke et al., 2013, Kamke et al., 2014)	CHAPTER 4	CHAPTER 4	CHAPTER 4

Scale bars 500nm; AA abbreviates amino acid; C abbreviates carbon; arrowheads indicate halo position

8.1.3 Trophic links in the sponge holobiont

Nutrients are considered as a key currency in many symbioses (Wein et al., 2019) making it critical to determine what specific symbionts feed on in order to understand nutritional interplay within the holobiont. To this end, the new genomes representing six symbiont clades obtained in the framework of this thesis provide new insights into common and clade-specific metabolic features (CHAPTER 4, CHAPTER 5).

A common theme among these genomes is that symbionts seem to widely engage in the synthesis and degradation of fatty acids (FA, hereafter). This was the case for all studied sponge associated *Chloroflexi* clades (CHAPTER 4), *Poribacteria* (CHAPTER 3) as well as *Phyllobacteriaceae* from *Cymbastela concentrica* (CcPhy; CHAPTER 5). While FA were described as components of sponge tissues before (Koopmans et al., 2015), these findings attribute for the first time heterotrophic fatty acid-based metabolism to specific sponge symbionts. Independent results suggest the relevance of the FA metabolism in the sponge microbe symbiosis. For example, a final product of the BMC encapsulated 1,2-PD degradation (discussed above) is propionate, a short-chain fatty acids (SCFA), which was reported to stimulate physiological effects such as intestinal gluconeogenesis in eukaryotes (De Vadder et al., 2014). Further, carnitine, which was previously suggested to be degraded by sponge symbionts (Slaby et al., 2017), was reported to function as a FA carrier across mitochondrial membranes (Bremer, 1983) and therefore potentially engages in FA metabolism on the sponge host side. In recent years, SCFAs have attracted much attention in microbial symbiosis research as links between microbial- and animal host physiology. SCFA impact animal hosts by modulating innate and inflammatory responses (Schulthess et al., 2019), lead to metabolic reprogramming (Kelly et al., 2015), and are even assumed to alter gut–brain communication (reviewed in Dalile et al. (2019)). Though, much of this work focussed on mammalian gut models and it is tempting to speculate about the impact of FA on basal invertebrate host microbe interactions such as in sponges predestined via (temporarily) anoxic conditions for fermentation.

Detailed genomic signatures that were identified as "nutritional guilds" (Slaby et al., 2017) indicate that each of the studied genotypes likely occupies a distinct metabolic niche in the sponge holobiont. For instance, while most of the studied symbionts encode and express elements for ammonium uptake and assimilation, they differ in other aspects of their metabolism such as in the food spectrum of carbohydrates or amino acids as we described in *A. aerophoba* (i.e. *Poribacteria* CHAPTER 3), *Chloroflexi* CHAPTER 4) and *C. concentrica* (i.e. CcPhy, CcNi and CcThau; CHAPTER 5). Such metabolic mosaicism between symbionts leads to unique ensemble physiologies what ultimately allows them to occupy distinct metabolic niches in the same holobiont. This is further highlighted by the fact that symbionts with similar predicted nutrient spectra (e.g. *Caldilinea* & *Anaerolinea*) co-occur in spatially overlapping regions (CHAPTER 4). Hence, nutritional resource partitioning and metabolic

interplay (next paragraph) rather than spatial separation seem conceivable sponge symbiont strategies in order to avoid competitive exclusion. My conceptual working model for spatial sponge holobiont organisation is that cross-feeding microbes would spatially associate (Figure 9A) whereas symbionts feeding on the same metabolites could lower competitive exclusion by inhabiting different spatial niches (Figure 9B). Ultimately, spatial principles, which are increasingly understood in *in vitro* systems (Momeni et al., 2013, Mitri et al., 2016, Liu et al., 2019), could provide key explanations for how sponges, a spatially confined setting, can host such extraordinary microbial diversity and are therefore exciting routes of future research.

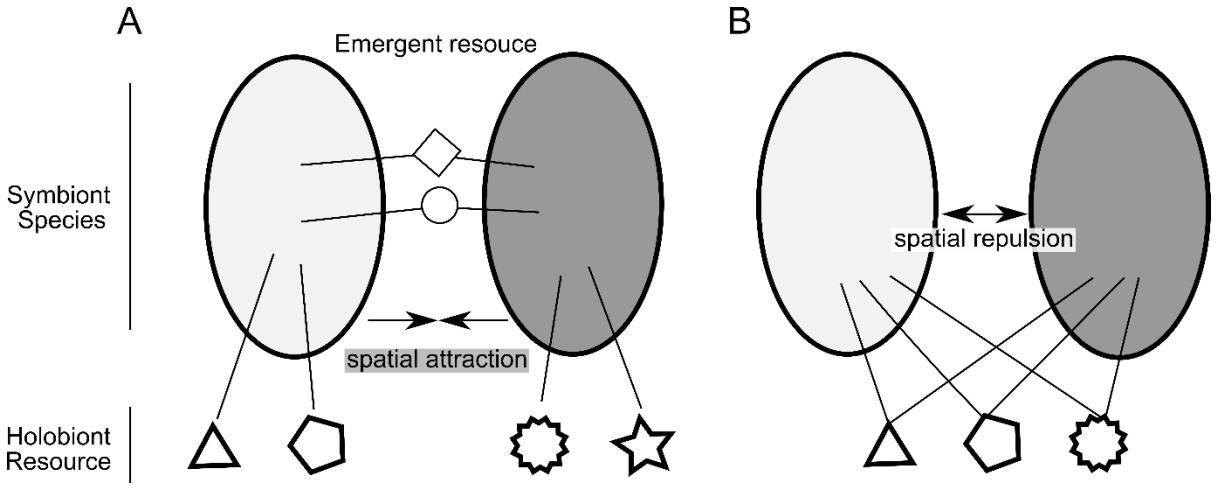

Figure 9: Hypothetical model on the relation between metabolic interaction and spatial association in sponges. (A) Symbionts assemble in distinct metabolic niches characterised by metabolic interplay**. (B)** Symbionts with overlapping food spectra establish distinct spatial niches facilitating co-occurrence by reduced competitive exclusion. Layout inspired by Levy and Borenstein (2013) and supplemented with the aspect of space.

Studies from various symbiosis systems showed that metabolic interactions strongly shape the structure of microbial communities (Zelezniak et al., 2015, Ren et al., 2015, Pande et al., 2014) and drive emergent properties (Lykidis et al., 2011, Medlock et al., 2018). While genomic approaches of this thesis (CHAPTER 4, CHAPTER 5) and of others (Slaby et al., 2017, Burgsdorf et al., 2019, Podell et al., 2018, Karimi et al., 2018, Burgsdorf et al., 2015, Kamke et al., 2014, Kamke et al., 2013, Hentschel et al., 2012, Rubin-Blum et al., 2019) have contributed to a growing genomic catalogue of sponge symbiont metabolisms, the next frontier is to identify how symbionts are metabolically connected via cross-feeding and how this may affect overall holobiont function. Metabolic reconstructions of CHAPTER 5 allowed for the first time to comprehensively predict in the LMA sponge *C. concentrica* how symbiont physiologies interconnect. This revealed many instances of complementary metabolism among symbionts where one lacks the ability the that another one has, indicting the presence of nutritional interplay (i.e. syntrophy). Further, the framework predicts pronounced metabolic fluxes of key nutrients (e.g. DOM, urea, creatine) across bacterial species within the holobiont via sequential cross-feeding. The importance of syntrophies may also be derived from further data where auxotrophies are reported for sponges (Fiore et al., 2015, Srivastava et al., 2010), but also its symbionts (Lackner et

al., 2017). Second, symbionts seem to stably enrich diverse transporter systems compared to planktonic microbes (CHAPTER 4, CHAPTER 5; (Moeller et al., 2019, Fan et al., 2012, Webster and Thomas, 2016, Hentschel et al., 2012)) which indicate vivid nutritional interplay within sponges. Collectively, these findings reveal the need, the machinery and the predicted nutrient fluxes for nutritional interplay among symbionts which is likely critical for holobiont stability and function.

8.1.4 Microbial participation in the sponge loop

Exciting findings of the past years have shown the decisive role of sponges in the biochemical cycles of marine benthic ecosystems (de Goeij et al., 2013, Maldonado et al., 2012). A key observation was that sponges can metabolize large quantities of DOM, which they transform into detritus, that is then passed on to higher trophic levels instead of being diluted into the open ocean - a pathway termed as sponge loop (see 1.3.1 Sponges). In this context, one theory states that sponge symbionts, analogous to the microbial loop in seawater (Azam et al., 1983), enable sponges to metabolize DOM. Indeed, the genomic data of several sponge symbionts generated in the framework of this thesis (CHAPTER 4, CHAPTER 5) and elsewhere (Astudillo-Garcia et al., 2018) suggest their potential capacity to metabolize DOM. However, despite this, and initial evidence (Rix et al., 2017b, Shih et al., 2019, de Goeij et al., 2008), comprehensive quantitative data was lacking on whether DOM is taken up by the sponge host or by its microbial symbionts. Therefore, CHAPTER 6 applied an integrative approach to quantify DOM processing for prokaryotic- and host cells each in an HMA and LMA sponge system. In collaboration with Dr. Rix, my contribution to this study was to develop the visualisation protocol that allowed us to combine SEM with nanoscale secondary ion mass spectrometry (NanoSIMS). This integration together with stable isotope pulse-chase experiments enabled us to map the metabolic contribution of cell types (i.e. sponge cells versus prokaryotes) in DOM cycling *in situ*. Interestingly, this revealed clearly dichotomous strategies between the studied HMA (*Aplysina aerophoba*) and LMA (*Dysidea avara*) sponge species. In the HMA sponge, symbionts significantly contribute to total heterotrophic DOM cycling (67-89 %; CHAPTER 6) whilst efficiently widening DOM nutrient spectrum of the holobiont. In the LMA sponge species on the other hand the lack of microbial abundance was compensated by excessive DOM uptake by host cells (>99 %). Overall, these results highlight divergent nutritional strategies following the HMA/LMA dichotomy and that sponge symbiont assimilation seems to impact DOM turnover via the sponge loop. Future studies identifying the specific symbiont clades involved in DOM recycling will help to correlate DOM processing capability with genomic evidence and thus to better understand its molecular basis. Practically, this can be approached by combining FISH with NanoSIMS (Dekas et al., 2015, Musat et al., 2014), by applying spectral Raman imaging (Wang et al., 2016), or by combining DNA/RNA stable-isotope probing with sequencing (Coyotzi et al., 2016, Whiteley et al., 2007). This will allow to disentangle individual symbiont contributions in critical sponge-driven biochemical cycles of marine ecosystems.

8.2. Sponge virology

Phages are key modulators of the structure and evolution of marine microbial communities (reviewed in Breitbart et al. (2018)). While, much of this knowledge and the paradigms derived are based on planktonic viruses (Gregory et al., 2019b, Roux et al., 2016, Wilhelm and Suttle, 1999, Lara et al., 2017, Paez-Espino et al., 2016, Guidi et al., 2016), the diversity and function of viruses that associate with marine animals remain understudied (Leigh et al., 2018b, Li et al., 2011, Laffy et al., 2018, Weynberg et al., 2017). CHAPTER 7 and Appendix A, demonstrate an astonishingly intimate association between viruses and sponges across ecological scales (host tissue, individual, species) highlighting unique individual fingerprints with potentially holobiont tailored functions. In the following paragraphs, I will set what we learned about the diversity, lifestyle and function of sponge-associated viruses into the broader context of holobiont virology whilst focusing on phages.

8.2.1. Diversity

My findings clearly demonstrate that sponges host a high degree of taxonomically distinct and novel viral diversity (CHAPTER 7). Specifically, more than half of the sponge-associated viral genera (i.e. 491 VCs) were newly discovered in this work, consistent with the genomic distance of viruses from Great Barrier Reef (GBR) sponges to viral references (Laffy et al., 2018). Here, the gene sharing network approach (CHAPTER 7), originally established by Lima-Mendez et al. (2008), was instrumental to test novelty against an extensive environmental dataset based on whole genome information. Notably, the entire viral diversity at genus level, which we have discovered in four sponge species (CHAPTER 7; 813 VCs), already fell within the range of large-scale sequencing initiatives such as the global Tara oceans and Malaspina research expeditions of viroplankton (Roux et al., 2016, Gregory et al., 2019b) or the human intestinal virus database (Gregory et al., 2019a) as summarized in **Table 2**:

Table 2: Comparison of Diversity estimates from different virome studies.

Study approach	Reference	Study design	Diversity Viral populations | Genera | Novel genera		
Sponge Mediterranean Sea	CHAPTER 7	32 viromes	4,484	813	491
Sponge Great Barrier Reef	(Laffy et al., 2018), CHAPTER 7	15 viromes	N/A	208	N/A
Human Gut	GVD database (Gregory et al., 2019a)	648 viromes & microbial metagenomes	13,203	957	702
Planktonic; Tara Oceans	GOV 1 (Roux et al., 2016)	104 viromes	15,222	867	658
Planktonic; Tara Oceans	GOV 2 (Gregory et al., 2019b)	145 viromes	195,728	N/A	N/A
ICTV	(King et al., 2018)	Taxonomy database	N/A	867	N/A

N/A indicates not determined in cited study; note that diversity estimates are influenced by sequencing effort and analysis.

The high-taxonomic-rank diversity, which seems to characterize sponge viromes, becomes further evident by comparison of genera to species ratios (i.e. VCs/population) across datasets. In sponges, this ratio was one order of magnitude higher (0.18 VCs/population) than in seawater (0.07 VCs/population; (Roux et al., 2016)). Therefore, with relatively few viral populations, sponge associated viruses already covered about one fourth of the total genus-level diversity of the applied global gene sharing network described in CHAPTER 7. Together, my findings indicate that sponges represent a rich resource of yet unexplored viral diversity.

Bacteriophages dominated the taxonomically classified fraction of our sponge viromes both in diversity and relative abundance (CHAPTER 7). This is not surprising as bacteria represent the largest and most diverse pool of cellular targets for viral infection in HMA sponge holobionts (Gloeckner et al., 2014b, Thomas et al., 2016). Such phage-dominated viromes are common and agree with signatures from GBR sponges (Laffy et al., 2018), corals (Weynberg et al., 2017, Wood-Charlson et al., 2015, Laffy et al., 2018), and seawater (Coutinho et al., 2017). Indeed, *in silico* host predictions showed that sponge associated phages infect sponge-associated symbionts (Appendix Figure A1-I). Amongst others, this comprised phages predicted to infect cosmopolitan core symbionts such as *Poribacteria* (see CHAPTER 3), *Chloroxlexi* (see CHAPTER 4), or *Cyanobacteria*. Yet, it is likely that our phage-bacteria infection network is far from being comprehensive considering a high fraction of phages without any host prediction. This is in line with the fact that to date no more that 5 % of uncultivated viruses are linked to any specific host (Roux, 2019) as deposited in the largest viral genome repository (IMG/VR v.2.0; Paez-Espino et al. (2018)). Since these types of host predictions depend on the availability of symbiont genomes, or at least classified metagenomic contigs (Edwards et al., 2016b, Coutinho et al., 2017), upcoming symbiont genomes will increase the sensitivity of future host predictions. While our findings represent the first links between sponge phages and their microbial hosts (CHAPTER 7, Appendix Figure A1-I), these assignments provide important baseline data for a more detailed investigation on the impact of phages on specific symbiont groups.

But how can this relatively high viral diversity in sponges be explained? One possible explanation might lie in our approach that captured both ss/ds DNA and RNA viruses (CHAPTER 7) while conventional virome sequencing approaches typically focus on dsDNA viruses. Genomically, RNA viruses, known to be highly diverse, display remarkable genomic flexibility, and were reported to be more prominent in invertebrates than in vertebrates (Li et al., 2015, Shi et al., 2016). Therefore, although eukaryotic RNA viruses were not my study focus, the data might provide valuable information for future investigations tailored to uncover the sponge RNA virosphere with potentially sponge host infecting viruses. Such endeavour might be motivated by recent findings showing that sponge viromes of thermally stressed sponges experience a drastic expansion of retro-transcribing viruses of *Caulimorviridae* and *Retroviridae* families (Laffy et al., 2019). Besides, we also detected ssDNA viruses (i.e. *Ambidensovirus*) in sponges. These were widespread in 75 % of the sponge species we

analysed from the Mediterranean Sea (CHAPTER 7), and in same proportion in GBR sponges (Laffy et al., 2018). Notably, *Densovirinae*, a related sub-family within *Parvoviridae*, are the reported top candidate to cause the devastating star wasting syndrome (Hewson et al., 2014). Therefore, while the infectivity and pathology of sponge associated viruses needs to be validated in sponges they bear the possibility for exciting new insights into evolution and origin of animal viruses (Zhang et al., 2018).

Another scenario explaining the viral diversity is that sponges function as natural bio-collectors enriching environmental phages, similar as described recently for environmental DNA (eDNA) (Mariani et al., 2019). However, the specificities for host species (see 8.2.2. Specificity) and taxonomically distinct viral signatures (CHAPTER 7) make unselective enrichment unlikely. In contrast, our data supports the assumption that viral diversity in sponges correlates with their diverse microbial host pool as sponge phages are predicted to infect sponge symbionts (Appendix Figure A1-I) and viral communities largely mirror microbial sponge community compositions (CHAPTER 7). For either scenario, the findings indicate that much viral diversity in the oceans remains to be discovered and that sponges represent a promising reservoir of novel viral diversity with high potential for novel auxiliary functions.

8.2.2. Specificity

The specificity of viruses for their environment is a key descriptor for their sphere of influence and provides evidence for potential transmission routes. While species-specific prokaryotic communities are becoming an established paradigm for many animals (Hacquard et al., 2015, Thomas et al., 2016, Moeller et al., 2016) we are just scratching the surface how this is reflected in viral communities. Landmark studies such as in *Hydra* (Grasis et al., 2014), birds (Wille et al., 2019) and insects (Leigh et al., 2018a) demonstrated that, alike the microbiomes, viromes tend to be species-specific. Traditionally, a large part of virome studies has focused on the role of viruses as an etiological agent by correlating viruses with disease phenotypes exemplified in corals (Soffer et al., 2013, Marhaver et al., 2008, Vega Thurber et al., 2008, Weynberg et al., 2015, Correa et al., 2016, Thurber et al., 2017). In contrast, comparatively understudied is the specificity and function of the "healthy virome" in unchallenged marine animals as they occur in nature. This gap motivated our nested sampling design to systematically study virome specificity at the level of a natural sponge host community, its sponge populations and tissues (Figure 10, CHAPTER 7).

SPONGE COMMUNITY SIGNATURES

Consistent with previous literature (Laffy et al., 2018), the results of my PhD thesis show that sponges do have species specific viral communities (Figure 10) that are different from the surrounding seawater (Figure 10). This adds further support to the notion (see 8.2.1. Diversity) that sponges represent distinct viral niches. These findings bear an important message for animal virology as they indicate defined non-pathogenic viral communities with potential for co-evolutionary dynamics in early branching animals (CHAPTER 7; (Grasis et al., 2014)).

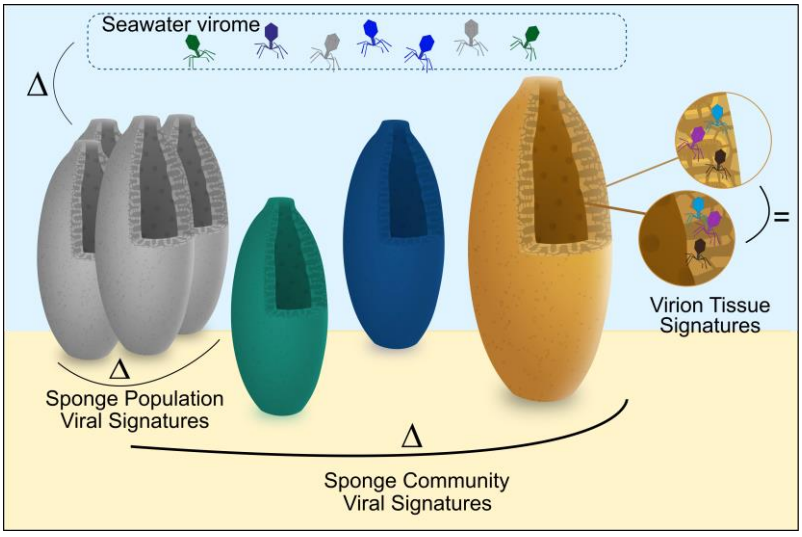

Figure 10: Summarized nested sampling design. Viral composition in sponges investigated on the scales of host community (4 species), population (4 individuals/species) and tissue (outside/inside) compared to seawater. Δ indicates levels with different virome signatures, = denotes similar viral communities as identified in CHAPTER 7. Sponge body modified from K. Song, Creative Commons licence CC BY-SA 3.0.

INDIVIDUAL & INTRA-INDIVIDUAL SIGNATURES

Within species, sponges display a striking individuality in viral community composition as I could resolve with my nested sampling design (Figure 10; 34.8 % individualists). The reproducibility of this pattern for the examined tissues as well as the fact that individualists were unlikely biased by the detection limit supports this finding. Individual virome signatures were reported in humans (23.4 % individualist, Moreno-Gallego et al. (2019)), the protochordate model *Ciona intestinalis* (Leigh et al., 2018b) or the crustacean *Penaeus monodon* (Orosco and Lluisma, 2017). In sponges, however, individual viromes are surprising and against my initial expectation considering that: (i) sponges can retain a relatively large fraction (~23.3 %) of external viruses by filtration (Hadas et al., 2006), the individuals were sampled next to each other (iii) and HMA sponge individuals generally display relatively low intraspecific variation (Erwin et al., 2015a). That this is not the case could either mean that transmission rates between nearby individuals are little or at least that rates do not keep pace with diversifying forces.

Collectively, this raises the question on the mechanisms how the species specificity and individuality we observe can be explained. Therefore, **Table 3** non-exhaustively summarizes a few conceivable explanatory models and suggests methodical approaches to verify or disproof them in future studies.

Table 3: Explanatory models for the observed specificity of sponge viromes.

Individuality	Species specificity
Dynamic viral community fluctuations asynchronous between individuals	**Species specific virion adhesion (see 8.2.4.)**
Mechanism: Lotka–Volterra dynamics such as kill the winner (Thingstad et al., 2014)	**Mechanism**: Sponge viruses do have structural features that allow attachment to sponge species specific targets in analogy to the Bacteriophage Adhering to Mucus model (Barr et al., 2013)
Experiment: Analysing viral abundance dynamics within host populations by strain-specific qPCR	**Experiment**: Virion binding assay for sponge matrix compounds
Virus & prokaryote selection imposed by host genetic variation (Griffiths et al., 2019)	**Virome specificity follows microbiome specificity**
Mechanism: Individual immune repertoire	**Mechanism**: Narrow viral host range
Experiment: Quantitative Trait Locus (QTL) analysis mapping host genotype and "viro-type"	**Experiment**: Comprehensive virome to microbiome correlation e.g. with deep metagenomics
Viral community divergence over lifetime	**Host feeding physiology**
Mechanism: Viral genomic plasticity, viral extinction, viral immigration	**Mechanism**: The sponge host may foster virome specificity by degrading external virions: 1st line defence choanocytes, 2nd line archaeocytes.
Experiment: Comparative viromics of sponge reproductive stages and resulting adults	**Experiment**: targeted localisation of non-community virions by ePhageFISH

Notably, while the sponge viromes were specific at all tested inter-individual scales (i.e. sponge community and population) the pattern within sponge individuals between tissues was more homogeneous (CHAPTER 7). This trend for viral tissue homogeneity was independently confirmed by automated *in situ* quantification of ePhageFISH signals (Appendix Figure A3-II) showing that viral abundances do not significantly differ between the outer, more exposed pinacoderm layer and the inner mesohyl matrix. This is surprising, as I anticipated that bacteriophage communities vary in different parts of the sponge together with its microbial content along the autotroph-heterotroph gradient (Achlatis et al., 2018, Wilkinson, 1978). In other words, patterns such as more cyanophages at surface and more *Poribacteria* (heterotroph) phages inside to cause tissue specific viral community patterns. Besides, the more exposed pinacoderm layer would have a higher change to be in contact with the external virus pool. Based on my data, it can be only speculated why this is not the case in sponges. One possibility is that virion populations in the tissue mix by regular body contractions of the host (Nickel, 2004) with virions being more mobile than bacteria. Secondly, the phototroph-heterotroph gradient might not weight enough on community scale to stratify viral community signatures. For future experiments this indicates, for the assayed sponges, that either tissue is representative for the holobiont viral composition.

Altogether, these findings show that although sponges are massively filtering on their environment, they retain species-specific yet individually-unique viromes. These results emphasize that small-scale collections of animals might easily underestimate true viral diversity by missing the abundant pool of individualist viruses present only on certain individuals. While different mechanisms (**Table 3**) are conceivable to facilitate virome specificity the patterns we observe likely result from a variety of factors.

VIROME SPECIFICITY ALONG THE HMA-LMA DICHOTOMY

When comparing sponge virome data from different systems (CHAPTER 7; (Laffy et al., 2018, Laffy et al., 2016, Laffy et al., 2019)), there seems to be an interesting distinction between HMA and LMA sponge viromes. Specifically, in *Rhopaloeides odorabile*, the viral communities of this HMA sponge, were more distinct from seawater (Laffy et al., 2018). This is consistent with the virome signature of our studied HMA sponges from the Mediterranean Sea with low overlap to seawater (CHAPTER 7). In contrast, the viromes of the studied LMA sponge species (i.e. *Amphimedon queenslandica*, *Xestospongia testudinaria*, *Ianthella basta*) were less distinct from ambient seawater which resembles what has been described for their microbial communities (Erwin et al., 2015a). Although we are still in the pioneering phase of sponge virology, this observation indicates that the HMA-LMA dichotomy is also reflected in the viral community signatures. Therefore, comparative virome studies investigating HMA and LMA sponges are an interesting avenue for future research to reveal the impact of microbiome complexity on viral community structure.

8.2.3. Insights into the lifestyle of sponge-associated phages

Identifying the bacterial hosts of the discovered phages is crucial to define their role in the sponge microbiome. Hence, we established the first connections between sponge-associated phages (CHAPTER 7) and the specific prokaryotes they infect (Appendix Figure A1-I; 8.2.2. Specificity). Collectively, the obtained infection-network in sponges indicated the trend for a modular topology (Appendix Figure A1-I). This means that some phages are predicted to infect multiple prokaryotic hosts and also hosts to be infected by multiple phages. This is surprising, as theory predicts that diverse (as for sponges; (Thomas et al., 2016)) and phage-defensive (case for sponges; (Horn et al., 2016, Fan et al., 2012), CHAPTER 4) microbiomes favour the emergence of phages with narrow host range (Weitz, 2015). Phage infectivity is generally considered limited to host species or even strains (Sullivan et al., 2003). In contrast, other authors indicate that broad-host-range phages are more widespread than previously thought suggesting a variety of host ranges to be common in natural systems (de Jonge et al., 2019, Kauffman et al., 2018). In this context, interesting observations were specificities of *Chondrosia* and *Petrosia* associated phages for typical planktonic microbes (e.g. *Candidatus* Pelagibacter). Although this is speculative it might impose a scenario where phages use sponges as a hunter's stall to forage for planktonic microbes. Yet, it needs to be highlighted that these findings are based on *in silico* predictions which might be skewed towards the available prokaryotic genomes. Therefore, high throughput screening strategies such as by viral tagging (Deng et al., 2014, Džunková et al., 2019) or proximity ligation assays (Marbouty et al., 2017) will be instrumental to validate and complement phage-microbe pairings from sponges. These data will provide a valuable basis to assay phage-microbe population dynamics in order to decipher the regulatory role of phage in host-associated microbiota.

Lysogenic replication (Figure 6) seems to be the preferred replication mode of sponge associated phages based on our predictions (Appendix A2). Notably, this prevalence of phages predicted for the lysogenic lifestyle was detected in our virome data capturing viral particles not lysogens. Therefore, since great care was taken to minimise sampling derived stress induction, I suggest that lytic events were widespread in all sponge individuals under basal conditions. In general, prophages are so widespread that they have been found in nearly half of the sequenced bacterial genomes (46 %; (Touchon et al., 2016)) and have also been reported to be widespread in other host-associated systems such as the murine gut (Kim and Bae, 2018). In sponges, several factors might favour lysogenic strategies. First, lysogeny is favoured in situations when external virion decay rates are high (Weitz, 2015), consistent with the pronounced virion phagocytosis by sponge archaeocytes I detected by ePhageFISH (Appendix Figure A3-II). Second, the prevalence of lysogens would be consistent with the Piggyback-the-Winner model (Knowles et al., 2016) for a system with high microbial densities, HMA sponges are. Ultimately, widespread lysogeny of sponge-associated phages offers a high genomic potential for lysogenic conversion, which will be discussed in the next chapter.

8.2.4. Tripartite phage-prokaryote- sponge interplay

In the following section, I will argue that sponge symbiont phages engage in tripartite phage-prokaryote-eukaryote (PPE) interactions with possible consequences on the stability, integrity and function of sponge holobionts (Figure 11). Therefore, I will integrate our findings (CHAPTER 7, Appendix A) with the current literature as a basis to derive hypothetical models on PPE interactions in sponges.

While phages are rightly seen as important bacterial killers in the oceans, estimated to lyse 20–50 % of marine surface bacteria per day (Fuhrman, 1999), bets change for bacteria when phages integrate into their genome and their fate is linked as a lysogen. Importantly, in this case, the phage then benefits from enhancing the host fitness to multiply together with its bacterial host (Weitz, 2015, Howard-Varona et al., 2017). Therefore, mechanisms that improve the fitness of their bacterial hosts should represent a selective advantage to prophages- a perspective that significantly extends their role as bacterial killers. Exciting examples show that prophages can indeed enhance the metabolism of their hosts such as by providing photosystem-II elements in cyanophages (Hevroni et al., 2015) or by providing virulence factors to pathogens (e.g. Shiga toxins; (Herold et al., 2004)) extending their host niches. In contrast, knowledge is limited about phages carrying symbiosis effectors that foster symbiont performance in the context of animal hosts.

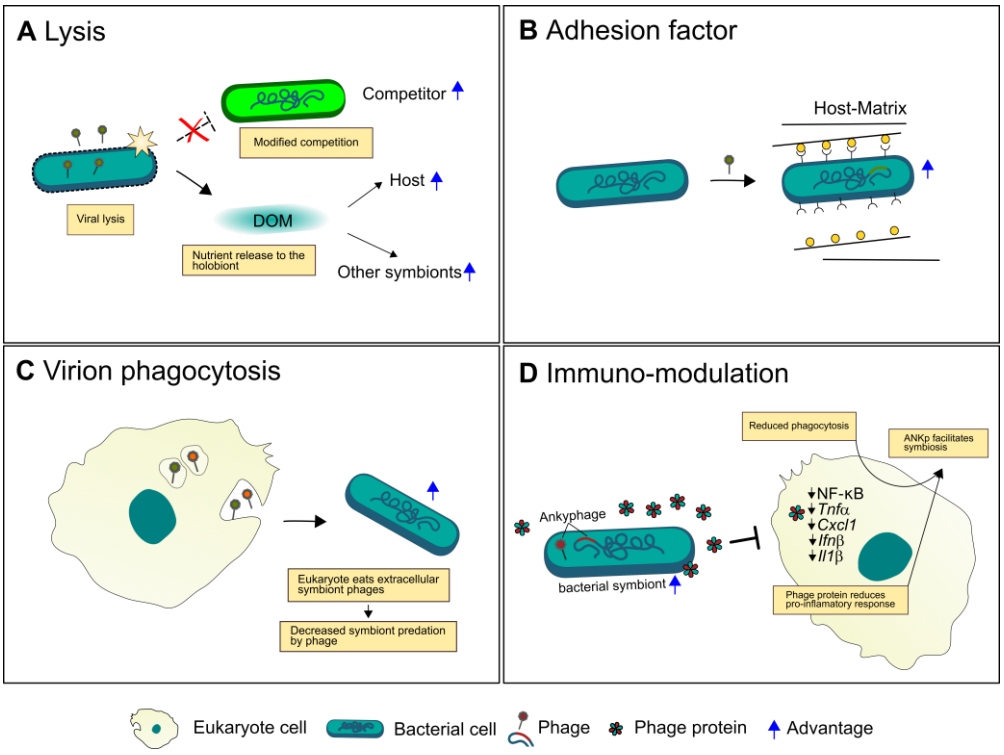

Figure 11: Overview of hypothetical models for tripartite phage- prokaryote-sponge interplay. (A) Lysis of specific symbionts potentially aids niche competitors whilst releasing dissolved organic matter (DOM) to other members of the holobiont. **(B)** Prophages encode adhesion domains that foster bacterial attachment via lysogenic conversion. **(C)** Sponge cells phagocytise virion particles from the mesohyl thereby modulating phage predation rates on symbionts. **(D)** Symbiont phage encoded Ankyrin proteins aid bacterial symbionts in eukaryote immune evasion.

ANKP MEDIATED IMMUNE EVASION

In the course of this PhD thesis, I discovered a novel symbiont phage-encoded protein, ANKp, that modulates eukaryote-bacterium interaction by altering the eukaryotes' response to bacteria (CHAPTER 7). To the best of my knowledge, ANKp represents the first secreted phage effector protein that downregulates eukaryote immune response facing bacteria. This is of high relevance to the host-microbe symbiosis field given that this indicates a mechanism of tripartite PPE interplay potentially stabilising symbiotic association (Figure 11).

Chromosomally encoded bacterial ankyrins were previously suggested to facilitate intracellular survival of sponge symbionts (Nguyen, Liu et al. 2014). However, the specific mechanisms involved on the sponge host side remained unclear. Ankyrin-mediated intracellular survival was described for a range of intracellular pathogens such as *Legionella pneumophila* (Al-Khodor et al., 2008), *Anaplasma phagocytophilum* (Park et al., 2004, Garcia-Garcia et al., 2009), or *Coxiella burnetii* (Lührmann et al., 2010). Yet, while ankyrin-mediated intracellular survival as a mode of action would fit to intracellular sponge symbionts, not all bacterial sponge symbionts with ANK domains occur intracellularly. This is best exemplified by a recent comparative study on sponge-associated *Synechococcus* species *(Ca*. Synechococcus feldmannii versus *Ca*. Synechococcus spongiarum*)*. Both species were shown to encode ankyrins but one occurs intra- and the other extracellularly, respectively (Burgsdorf et al., 2019). While we found Ankyphages to be common in many host-associated environments including humans an exciting line of research will be insofar ANKp immune modulation represents a blueprint for the widespread chromosomally-encoded symbiont ankyrins (Jernigan and Bordenstein, 2014). Given the versatility of protein-protein interactions mediated via ankyrins (reviewed in Voronin and Kiseleva (2008)), further modes of action, besides facilitating intracellular survival of symbionts, seem conceivable to be at play.

But what is the molecular mechanism behind phage ANKp mediated immune modulation? NF-κB signalling is widespread from sponges (Williams et al., 2019, Srivastava et al., 2010) to humans (Sen and Baltimore, 1986) where it is a central regulatory pathway to integrate various immune stimuli into a proinflammatory immune response (Liu et al., 2017). Upon stimulation, such as by pattern recognition receptor TLR4 (Toll-like receptor 4) via bacterial lipopolysaccharides, the transcription factor NF-κB translocates into the nucleus where it initiates the transcription of proinflammatory cytokines, chemokines and additional inflammatory mediators (Liu et al., 2017). This renders NF-κB to a central hub of the eukaryotic proinflammatory immune response. Without immune stimulation, NF-κB translocation into nucleus is inhibited by a group of IκBs (Inhibitor of κB) that mask nuclear localization signals (NLS) required for translocation (Jacobs and Harrison, 1998). Most notably, IκBs are characterised by the presence of ankyrin repeat domains (Sachdev et al., 1998), much like our identified ANKp protein from Ankyphage 3 (CHAPTER 7). Indeed, Phyre2 3D modelling (Kelley et al., 2015)

of ANKp revealed now with high confidence similarity to the crystal structure of an IκBβ/NF-κB p65 homodimer complex (Appendix B4, unpublished data). Therefore, I hypothesize that the mode of phage ANKp action might be to mimic eukaryotic IκBs, to prevent NF-κB translocation into the nucleus thus inactivating NF-κB mediated eukaryotic proinflammaty immune response. Although, this hypothesis is speculative at this stage, it would be consistent with our eukaryote *in vitro* expression data upon ANKp exposure (CHAPTER 7). While such mechanism is not yet described for phages it is consistent with reports from eukaryote viruses that feature a broad repertoire of effector proteins to inhibit NF-κB signalling (Lu et al., 2008, Benedict et al., 2003, Zhao et al., 2015). A striking example are ANK proteins from Poxviruses that bind the SCF ubiquitin ligase complex thereby preventing IκBs degradation and inhibiting NF-κB signalling (Sonnberg et al., 2008, Chang et al., 2009). Overall, given the central role of NF-κB in immune signalling, the NF-κB transcription factor represents a conceivable molecular target of ANKp function. Yet, open questions remain such as on the delivery mode of ANKp into the cytosol of eukaryotic immune cells, the reproducibility of the ANKp effect *in vivo* and its cellular origin. Informative follow-up experiments will be to test the binding affinity of ANKp to NF-κB using immunoprecipitation assays based on our established ANKp-HIS tag construct (CHAPTER 7; Appendix B5 Plasmid map).

While phages have recently had a comeback due to re-discovered phage therapy applications (McCallin et al., 2019), yet little knowledge exists (Keen and Dantas, 2018) and much is speculated (Van Belleghem et al., 2018) about mechanistic interactions between phages and the eukaryotic immune system. Though, recent studies provide first mechanisms such as a *Pseudomonas aeruginosa* phage effector RNA, that subverts the eukaryotic immune response and leads to reduced pathogen clearance (Sweere et al., 2019). In this context, we contribute here a protein and a potential mechanism to the emerging paradigm that phages can modulate the eukaryote immune system via tailored effectors.

BI-PARTITE INTERPLAY & THE HOLOBIONT

Although I deliberately focus here on tripartite PPE interplay, I would like to remark that also classical bipartite interactions likely have cascading effects on the whole holobiont (see Figure 11 a,c). First, the observed phage particle phagocytosis by sponge cells (Appendix Figure A3-II) reduces the pool of free phages in the holobiont system, thereby modulating the infection dynamics between phages and their bacterial hosts (Weitz, 2015, Weitz et al., 2013). Second, lysis of specific bacterial symbionts (CHAPTER 7) was described to favour the surviving competitors (Duerkop et al., 2012, Howard-Varona et al., 2017, Li et al., 2017). Via kill the winner dynamics (Thingstad et al., 2014, Thingstad, 2000) this can facilitate microbiome diversity (Morella et al., 2018). Third, while lysis derived release of DOM is well described in planktonic ecosystems to redirect vast nutrient fluxes via the viral shunt (Wilhelm and Suttle, 1999) similar mechanisms might impact the physiology within holobionts-altogether representing exciting routes for further research.

MATRIX ADHESION

The interaction between phage particles and the host supplied matrix was suggested to be detrimental for the extent to which bacteria and phages can co-exist in natural environments (Simmons et al., 2018, Barr et al., 2015, Barr et al., 2013). This renders the over 200-fold enrichment of adhesion domains in sponge-associated phages compared to ambient seawater (Appendix B6; not discussed in CHAPTER 7) to an interesting observation. Specifically, sponge symbiont phage adhesion domains comprised "link domains" (i.e. hyaluronan binding; (Kohda et al., 1996, Barta et al., 1993), YadA (i.e. collagens, laminin, fibronectin binding; (El Tahir and Skurnik, 2001)) and Ig-like domains (i.e. glycan binding domains; (Barr et al., 2013))- altogether potentially binding molecules that are present in the sponge matrix (L. Simpson, 1984, Hooper and Van Soest, 2002). These adhesion domains might either function as a binding structure on the virion or improve bacterial adhesion to the sponge matrix via lysogenic conversion of phage infected symbiont cells. Notably, for phage proteins with YadA-like membrane anchor domains we detected signal peptides and mainly transmembrane domains (CHAPTER 7, supplement). Therefore, I hypothesize that sponge associated phages might enable their prokaryotic hosts to better stick to sponge matrix. Although this is yet only supported by *in silico* data it would represent a further route of tripartite interaction where symbiont phages may provide adhesion domains to enable their bacterial host to expand their niche towards a symbiont lifestyle. In contrast, link- and Ig-like domain containing proteins were lacking detectable signal peptides indicative that they rather function in viral particle adhesion.

The enrichment of phages in mucosal surfaces compared to non-mucosal environments was reported in a wide range of animals such as in corals, humans and fish (Barr et al., 2013, Nguyen-Kim et al., 2015, Nguyen-Kim et al., 2014). Its implications were previously framed in the Bacteriophage Adherence to Mucus (BAM)-model, in which phages provide non-host-derived immunity by questing in the host interface for intruders (Barr et al., 2013). While the BAM model is explicitly stated for mucus adhesion, our results might justify an extension for further host-associated matrixes such as the extracellular matrix of sponges (CHAPTER 7).

In summary, these findings suggest that phages are not only to be regarded as killers, or accessory, but are central elements of microbial symbiosis and sponge holobiont function.

8.2.5. Future perspectives

Combining metabolic modelling with spatial cell localisation

CHAPTER 5 provides qualitative evidence for spatial nitrification clusters in the LMA sponge *Cymbastela concentrica*. Extending such analyses by a combination of metabolic modelling and spatial statistics has high potential to deepen our understanding of the nutritional ecology within the sponge holobiont. Practically, sponge symbiont genomic information, generated in the framework of this thesis and elsewhere, will provide a valuable basis for *in silico* metabolic modelling of the holobiont. This will allow to identify nutritional networks in the holobiont and to predict metabolic fluxes within e.g. via inter-genomic flux balance analyses (Orth et al., 2010) spanning symbiont clades. FISH-CLEM (CHAPTER 3) will provide the spatial resolution to correlate predicted syntropies or niche exclusion with the spatial organisation in the holobiont. Ultimately, this will provide a more detailed view of the basic organisation principles of the sponge holobiont.

Study host genome reduction along the HMA/LMA dichotomy

A promising, yet not immediately obvious route of further research will be to follow up on the physiological consequences of the diverging strategies between HMA and LMA sponges we observed in CHAPTER 6. A working hypothesis might be that HMA sponges outsource the genomic repertoire for heterotrophic DOM processing to their microbiome while in LMA sponges this set of genes is encoded in their own eukaryotic genomes. In this context, a highly interesting observation is that HMA sponges seem to have smaller genomes sizes compared to LMA sponges (Ryu et al., 2016). Although, the number of available sponge genomes is still limited, this might indicate genome streamlining on the host side what would shift the genome streamlining paradigm, that is, yet, typically described for the microbial symbiont side. Practically, this interesting research can be approached by systematic genome size estimations and comparative genomics of the host heterotrophic gene repertoire along the HMA/LMA dichotomy.

Bacteria-phage abundance dynamics & the impact of phages in holobiont composition

While our viral study design comprehensively captured community signatures the addition of the time dimension in longitudinal studies will provide valuable information on ongoing phage- prokaryote dynamics (Shkoporov et al., 2019). In case the microbial diversity in the sponge holobiont is maintained by phage regulating mechanisms such as “kill the winner” dynamics, I would expect oscillating abundance patterns of phages and their respective hosts over time. Besides, analogous to Lotka–Volterra dynamics that explain predator–prey population dynamics, lagged abundance shifts between phages and their host would be expected. Therefore, fitting the observed abundance dynamics, captured via strain specific qPCR, into mathematical models will be instrumental to infer the regulatory role of phages in the sponge holobiont.

Exploring the lysogenic symbiont conversion space

The ubiquity of lysogeny in natural systems (Touchon et al., 2016) raises the question on the dimension of further yet undiscovered mechanisms that modulate symbiotic interaction via lysogenic conversion in tripartite interplay. Here, a common misconception is that phages, when integrated into bacterial genomes, are dormant. Therefore, studying the gene expression of prophages (Owen et al., 2019, Howard-Varona et al., 2017) when integrated into symbionts might pinpoint new genes of interest acting on lysogens. I expect ANKp only to be the beginning and future work in different systems will reveal more phage encoded effector proteins that impact animals via symbiont bacteria providing selective advantage for these symbionts for successful host colonisation.

Validation of molecular ANKp mode of action and its relevance *in vivo*

Consequential follow-up work in relation to Ankyphages will be to confirm the molecular mechanism of eukaryote host cell manipulation. As previously indicated, the identification of the binding partner, hypothetically NF-κB itself, represents the logical next step. Notably, this can be done also in sponge cell homogenates and will complement our results in murine cell lines. Further, it will be exciting to screen the function of the many other identified Ankyphage ankyrins with our cell assays. Here, I identify Ankyphages infecting the human gut commensal *Akkermansia muciniphila* as well as human oral symbionts as highly promising targets with high clinical relevance. This new research direction will tackle the important question of how widespread phage immune modulation in symbiosis is in nature.

8.2.6. Final Conclusions

The sponge holobiont is an interacting ecosystem. The studies presented in the first parts of this PhD thesis (CHAPTER 3-5) suggest that sponge symbionts do not act alone but rather assemble syntrophic metabolic networks channelling nutrients through the holobiont. Novel approaches to environmental microbiology gave insights into the cell biology of key sponge symbionts by integrating activity and ultrastructure. This confirms extensive heterotrophy as common theme among sponge symbionts but provides now the detail to suggest clade specific nutritional niche partitioning. Ultimately, specialised symbiont repertoires would facilitate vivid nutritional interplay between symbiont species whilst improving the heterotrophic capacity of sponges.

Symbiont action impacts the environment. The study presented in the middle part of this PhD thesis (CHAPTER 6) demonstrates that HMA sponge symbionts engage in the sponge loop by equipping the holobiont with the heterotrophic repertoire to cycle DOM- the most abundant organic C source in the oceans. In this scenario, HMA sponge symbionts would drive the transformation of DOM to POM thereby increasing the carrying capacity of the ecosystem for higher trophic levels (e.g. fish) by providing access to particulate food. This connects heterotrophic sponge symbioses with the big picture of DOM-driven biochemical cycles of benthic ecosystems.

Importance of tripartite phage-prokaryote-eukaryote interplay. The studies presented in the final part of this PhD thesis (CHAPTER 7) demonstrate an astonishingly intimate tie between sponges and its associated viruses. Findings highlight sponges as reservoir of considerable novel viral diversity with highly individual, yet species-specific viral communities that are clearly distinct to the ambient seawater. Considering the high global diversity and abundance of *Porifera*, it becomes evident that sponges may represent a significant pool of novel viral diversity in the oceans. Within sponge viral communities we identify mechanisms of symbiont phages to improve their stand in the holobiont such as by adhesion and eukaryote immune modulation. This bears an important message to the field of animal-microbe symbiosis research to take lysogenic conversion by symbiont phages into account. Collectively, the discovered specificity and functions, establish viruses as integral elements of the sponge holobiont. Based on our findings, I expect therefore exciting new insights into viral mediated processes that beneficially shape holobionts in the years to come.

REFERENCES

introduction & discussion

ACHLATIS, M., PERNICE, M., GREEN, K., GUAGLIARDO, P., KILBURN, M. R., HOEGH-GULDBERG, O. & DOVE, S. 2018. Single-cell measurement of ammonium and bicarbonate uptake within a photosymbiotic bioeroding sponge. *ISME J,* 12**,** 1308-1318.

AL-KHODOR, S., PRICE, C. T., HABYARIMANA, F., KALIA, A. & ABU KWAIK, Y. 2008. A Dot/Icm-translocated ankyrin protein of Legionella pneumophila is required for intracellular proliferation within human macrophages and protozoa. *Mol Microbiol,* 70**,** 908-23.

ALEX, A. & ANTUNES, A. 2019. Whole-genome comparisons among the genus *Shewanella r*eveal the enrichment of genes encoding ankyrin-repeats containing proteins in sponge-associated bacteria. *Front Micrbiol,* 10.

AMATO, K. R., G. SANDERS, J., SONG, S. J., NUTE, M., METCALF, J. L., THOMPSON, L. R., MORTON, J. T., AMIR, A., J. MCKENZIE, V., HUMPHREY, G., GOGUL, G., GAFFNEY, J., L. BADEN, A., A.O. BRITTON, G., P. CUOZZO, F., DI FIORE, A., J. DOMINY, N., L. GOLDBERG, T., GOMEZ, A., KOWALEWSKI, M. M., J. LEWIS, R., LINK, A., L. SAUTHER, M., TECOT, S., A. WHITE, B., E. NELSON, K., M. STUMPF, R., KNIGHT, R. & R. LEIGH, S. 2019. Evolutionary trends in host physiology outweigh dietary niche in structuring primate gut microbiomes. *ISME J,* 13**,** 576-587.

ARPAIA, N., CAMPBELL, C., FAN, X., DIKIY, S., VAN DER VEEKEN, J., DEROOS, P., LIU, H., CROSS, J. R., PFEFFER, K., COFFER, P. J. & RUDENSKY, A. Y. 2013. Metabolites produced by commensal bacteria promote peripheral regulatory T-cell generation. *Nature,* 504**,** 451-5.

ASTUDILLO-GARCIA, C., SLABY, B. M., WAITE, D. W., BAYER, K., HENTSCHEL, U. & TAYLOR, M. W. 2018. Phylogeny and genomics of SAUL, an enigmatic bacterial lineage frequently associated with marine sponges. *Environ Mico,* 20**,** 561-576.

AUGUSTIN, R., SCHRÖDER, K., MURILLO RINCÓN, A. P., FRAUNE, S., ANTON-ERXLEBEN, F., HERBST, E.-M., WITTLIEB, J., SCHWENTNER, M., GRÖTZINGER, J., WASSENAAR, T. M. & BOSCH, T. C. G. 2017. A secreted antibacterial neuropeptide shapes the microbiome of *Hydra*. *Nat Commun,* 8**,** 698.

ÁVILA, E. & BRICEÑO-VERA, A. E. 2018. A reciprocal inter-habitat transplant reveals changes in the assemblage structure of macroinvertebrates associated with the sponge *Halichondria melanadocia*. *Estuaries Coast,* 41**,** 1397-1409.

ÁVILA, E. & ORTEGA-BASTIDA, A. L. 2015. Influence of habitat and host morphology on macrofaunal assemblages associated with the sponge *Halichondria melanadocia* in an estuarine system of the southern Gulf of Mexico. *Mar Ecol,* 36**,** 1345-1353.

AXEN, S. D., ERBILGIN, O. & KERFELD, C. A. 2014. A taxonomy of bacterial microcompartment loci constructed by a novel scoring method. *PLoS Comput Biol,* 10**,** e1003898.

AZAM, F., FENCHEL, T., FIELD, J., GREY, J., MEYER-REIL, L. & THINGSTAD, F. 1983. The ecological role of water-column microbes. *Mar Ecol Prog Ser,* 10**,** 257-263.

BARR, J. J., AURO, R., FURLAN, M., WHITESON, K. L., ERB, M. L., POGLIANO, J., STOTLAND, A., WOLKOWICZ, R., CUTTING, A. S., DORAN, K. S., SALAMON, P., YOULE, M. & ROHWER, F. 2013. Bacteriophage adhering to mucus provide a non-host-derived immunity. *PNAS,* 110**,** 10771-6.

BARR, J. J., AURO, R., SAM-SOON, N., KASSEGNE, S., PETERS, G., BONILLA, N., HATAY, M., MOURTADA, S., BAILEY, B., YOULE, M., FELTS, B., BALJON, A., NULTON, J., SALAMON, P. & ROHWER, F. 2015. Subdiffusive motion of bacteriophage in mucosal surfaces increases the frequency of bacterial encounters. *PNAS,* 112**,** 13675-80.

BARTA, E., DEÁK, F. & KISS, I. 1993. Evolution of the hyaluronan-binding module of link protein. *Biochem J,* 292**,** 947-949.

BAYER, K., KAMKE, J. & HENTSCHEL, U. 2014. Quantification of bacterial and archaeal symbionts in high and low microbial abundance sponges using real-time PCR. *FEMS Microbiol Ecol,* 89**,** 679-690.

BAYER, K., SCHMITT, S. & HENTSCHEL, U. 2008. Physiology, phylogeny and in situ evidence for bacterial and archaeal nitrifiers in the marine sponge *Aplysina aerophoba*. *Environ Mico,* 10**,** 2942-2955.

BELL, J. J. & BARNES, D. K. A. 2001. Sponge morphological diversity: a qualitative predictor of species diversity? *Aquat Conserv,* 11**,** 109-121.

BENEDICT, C. A., BANKS, T. A. & WARE, C. F. 2003. Death and survival: viral regulation of TNF signaling pathways. *Current Opinion in Immunology,* 15**,** 59-65.

BERTIN, Y., GIRARDEAU, J. P., CHAUCHEYRAS-DURAND, F., LYAN, B., PUJOS-GUILLOT, E., HAREL, J. & MARTIN, C. 2011. Enterohaemorrhagic Escherichia coli gains a competitive advantage by using ethanolamine as a nitrogen source in the bovine intestinal content. *Environmental Microbiology,* 13**,** 365-377.

BIGGS, B. C. 2013. Harnessing natural recovery processes to improve restoration outcomes: An experimental assessment of sponge-mediated coral reef restoration. *PLoS One,* 8**,** e64945.

BISWAS, A., GAGNON, J. N., BROUNS, S. J., FINERAN, P. C. & BROWN, C. M. 2013. CRISPRTarget: bioinformatic prediction and analysis of crRNA targets. *RNA Biol,* 10**,** 817-27.

BJÖRK, J. R., DÍEZ-VIVES, C., ASTUDILLO-GARCÍA, C., ARCHIE, E. A. & MONTOYA, J. M. 2019. Vertical transmission of sponge microbiota is inconsistent and unfaithful. *Nat Ecol Evol,* 3**,** 1172-1183.

BOARDMAN, G. D., STARBUCK, S. M., HUDGINS, D. B., LI, X. & KUHN, D. D. 2004. Toxicity of ammonia to three marine fish and three marine invertebrates. *Environmental Toxicology,* 19**,** 134-142.

BOBIK, T. A., HAVEMANN, G. D., BUSCH, R. J., WILLIAMS, D. S. & ALDRICH, H. C. 1999. The propanediol utilization (pdu) operon *of Salmonella enterica* serovar Typhimurium LT2 includes genes necessary for formation of polyhedral organelles involved in coenzyme B(12)-dependent 1, 2-propanediol degradation. *J Bacteriol,* 181**,** 5967-75.

BORCH, N. H. & KIRCHMAN, D. L. 1997. Concentration and composition of dissolved combined neutral sugars (polysaccharides) in seawater determined by HPLC-PAD. *Mar Chem,* 57**,** 85-95.

BORDENSTEIN, S. R. & THEIS, K. R. 2015. Host biology in light of the microbiome: ten principles of holobionts and hologenomes. *PLoS Biol,* 13**,** e1002226.

BRANDT, M. E., OLINGER, L. K., CHAVES-FONNEGRA, A., OLSON, J. B. & GOCHFELD, D. J. 2019. Coral recruitment is impacted by the presence of a sponge community. *Mar Biol,* 166**,** 49.

BREITBART, M., BONNAIN, C., MALKI, K. & SAWAYA, N. A. 2018. Phage puppet masters of the marine microbial realm. *Nat Microbiol***,** 1-13.

BREMER, J. 1983. Carnitine--metabolism and functions. *Physiol Rev,* 63**,** 1420-1480.

BRUCK, W. M., SENNETT, S. H., POMPONI, S. A., WILLENZ, P. & MCCARTHY, P. J. 2008. Identification of the bacterial symbiont *Entotheonella* sp. in the mesohyl of the marine sponge *Discodermia* sp. *ISME J,* 2**,** 335-339.

BRUCKER, R. M. & BORDENSTEIN, S. R. 2013. The hologenomic basis of speciation: gut bacteria cause hybrid lethality in the genus *Nasonia*. *Science,* 341**,** 667-669.

BRUNE, A. 2014. Symbiotic digestion of lignocellulose in termite guts. *Nat Rev Microbiol,* 12**,** 168.

BURGSDORF, I., HANDLEY, K. M., BAR-SHALOM, R., ERWIN, P. M. & STEINDLER, L. 2019. Life at home and on the roam: genomic adaptions reflect the dual lifestyle of an intracellular, facultative symbiont. *mSystems,* 4**,** e00057-19.

BURGSDORF, I., SLABY, B. M., HANDLEY, K. M., HABER, M., BLOM, J., MARSHALL, C. W., GILBERT, J. A., HENTSCHEL, U. & STEINDLER, L. 2015. Lifestyle evolution in cyanobacterial symbionts of sponges. *MBio,* 6**,** e00391-15.

BURSTEIN, D., HARRINGTON, L. B., STRUTT, S. C., PROBST, A. J., ANANTHARAMAN, K., THOMAS, B. C., DOUDNA, J. A. & BANFIELD, J. F. 2016. New CRISPR–Cas systems from uncultivated microbes. *Nature,* 542**,** 237.

CARRILLO-ARAUJO, M., TAŞ, N., ALCÁNTARA-HERNÁNDEZ, R. J., GAONA, O., SCHONDUBE, J. E., MEDELLÍN, R. A., JANSSON, J. K. & FALCÓN, L. I. 2015. Phyllostomid bat microbiome composition is associated to host phylogeny and feeding strategies. *Front Micrbiol,* 6**,** 447.

CHANG, S. J., HSIAO, J. C., SONNBERG, S., CHIANG, C. T., YANG, M. H., TZOU, D. L., MERCER, A. A. & CHANG, W. 2009. Poxvirus host range protein CP77 contains an F-box-like domain that is necessary to suppress NF-kappaB activation by tumor necrosis factor alpha but is independent of its host range function. *J Virol,* 83**,** 4140-52.

CHEN, I. A., CHU, K., PALANIAPPAN, K., PILLAY, M., RATNER, A., HUANG, J., HUNTEMANN, M., VARGHESE, N., WHITE, J. R., SESHADRI, R., SMIRNOVA, T., KIRTON, E., JUNGBLUTH, S. P., WOYKE, T., ELOE-FADROSH, E. A., IVANOVA, N. N. & KYRPIDES, N. C. 2019. IMG/M v.5.0: an integrated data management and comparative analysis system for microbial genomes and microbiomes. *Nucleic Acids Res,* 47**,** D666-d677.

CHIN, C. R., PERREIRA, J. M., SAVIDIS, G., PORTMANN, J. M., AKER, A. M., FEELEY, E. M., SMITH, M. C. & BRASS, A. L. 2015. Direct visualization of HIV-1 replication intermediates shows that capsid and CPSF6 modulate HIV-1 intra-nuclear invasion and integration. *Cell Rep,* 13**,** 1717-31.

CHOWDHURY, C., SINHA, S., CHUN, S., YEATES, T. O. & BOBIK, T. A. 2014. Diverse bacterial microcompartment organelles. *Microbiol Mol Biol Rev.,* 78**,** 438-468.

CIMINO, G., DE ROSA, S., DE STEFANO, S., SPINELLA, A. & SODANO, G. 1984. The zoochrome of the sponge *Verongia aerophoba* ("Uranidine"). *Tetrahedron Letters,* 25**,** 2925-2928.

CLARK, M. A., MORAN, N. A., BAUMANN, P. & WERNEGREEN, J. J. 2000. Cospeciation between bacterial endosymbionts (*Buchnera*) and a recent radiation of aphids (Uroleucon) and pitfalls of testing for phylogenetic congruence. *Evolution,* 54**,** 517-525.

CLAY, K. 2014. Defensive symbiosis: a microbial perspective. *Functional Ecology,* 28**,** 293-298.

CLEARY, D. F. R., POLÓNIA, A. R. M., BECKING, L. E., DE VOOGD, N. J., PURWANTO, GOMES, H. & GOMES, N. C. M. 2018. Compositional analysis of bacterial communities in seawater, sediment, and sponges in the Misool coral reef system, Indonesia. *Mar Biod,* 48**,** 1889-1901.

CLEARY, D. F. R., SWIERTS, T., COELHO, F. J. R. C., POLÓNIA, A. R. M., HUANG, Y. M., FERREIRA, M. R. S., PUTCHAKARN, S., CARVALHEIRO, L., VAN DER ENT, E., UENG, J.-P., GOMES, N. C. M. & DE VOOGD, N. J. 2019. The sponge microbiome within the greater coral reef microbial metacommunity. *Nat Commun,* 10**,** 1644.

COHEN, S. N., CHANG, A. C., BOYER, H. W. & HELLING, R. B. 1973. Construction of biologically functional bacterial plasmids *in vitro*. *PNAS,* 70**,** 3240-3244.

COMA, R. & RIBES, M. 2003. Seasonal energetic constraints in Mediterranean benthic suspension feeders: effects at different levels of ecological organization. *Oikos,* 101**,** 205-215.

COMA, R., RIBES, M., GILI, J.-M. & ZABALA, M. 2000. Seasonality in coastal benthic ecosystems. *Trends Ecol Evol,* 15**,** 448-453.

CORREA, A. M. S., AINSWORTH, T. D., ROSALES, S. M., THURBER, A. R., BUTLER, C. R. & VEGA THURBER, R. L. 2016. Viral Outbreak in Corals Associated with an In Situ Bleaching Event: Atypical Herpes-Like Viruses and a New Megavirus Infecting Symbiodinium. *Frontiers in Microbiology,* 7.

COUTINHO, F. H., SILVEIRA, C. B., GREGORACCI, G. B., THOMPSON, C. C., EDWARDS, R. A., BRUSSAARD, C. P. D., DUTILH, B. E. & THOMPSON, F. L. 2017. Marine viruses discovered via metagenomics shed light on viral strategies throughout the oceans. *Nat Commun,* 8**,** 15955.

COYOTZI, S., PRATSCHER, J., MURRELL, J. C. & NEUFELD, J. D. 2016. Targeted metagenomics of active microbial populations with stable-isotope probing. *Current Opinion in Biotechnology,* 41**,** 1-8.

DALILE, B., VAN OUDENHOVE, L., VERVLIET, B. & VERBEKE, K. 2019. The role of short-chain fatty acids in microbiota–gut–brain communication. *Nat Rev Gastroenterol Hepatol,* 16**,** 461-478.

DAVIES, E. V., JAMES, C. E., WILLIAMS, D., O'BRIEN, S., FOTHERGILL, J. L., HALDENBY, S., PATERSON, S., WINSTANLEY, C. & BROCKHURST, M. A. 2016. Temperate phages both mediate and drive adaptive evolution in pathogen biofilms. *PNAS,* 113**,** 8266-8271.

DE BARY, A. 1879. *Die erscheinung der symbiose,* Strassburg, Verlag von Karl J. Trübner.

DE GOEIJ, J. M., DE KLUIJVER, A., VAN DUYL, F. C., VACELET, J., WIJFFELS, R. H., DE GOEIJ, A. F. P. M., CLEUTJENS, J. P. M. & SCHUTTE, B. 2009. Cell kinetics of the marine sponge *Halisarca caerulea* reveal rapid cell turnover and shedding. *J Exp Biol,* 212**,** 3892-3900.

DE GOEIJ, J. M., MOODLEY, L., HOUTEKAMER, M., CARBALLEIRA, N. M. & VAN DUYL, F. C. 2008. Tracing 13C-enriched dissolved and particulate organic carbon in the bacteria-containing coral reef sponge *Halisarca caerulea*: evidence for DOM-feeding. *Limnol Oceanogr,* 53**,** 1376-1386.

DE GOEIJ, J. M. & VAN DUYL, F. C. 2007. Coral cavities are sinks of dissolved organic carbon (DOC). *Limnol Oceanogr,* 52**,** 2608-2617.

DE GOEIJ, J. M., VAN OEVELEN, D., VERMEIJ, M. J., OSINGA, R., MIDDELBURG, J. J., DE GOEIJ, A. F. & ADMIRAAL, W. 2013. Surviving in a marine desert: the sponge loop retains resources within coral reefs. *Science,* 342**,** 108-10.

DE JONGE, P. A., NOBREGA, F. L., BROUNS, S. J. J. & DUTILH, B. E. 2019. Molecular and Evolutionary Determinants of Bacteriophage Host Range. *Trends in Microbiology,* 27**,** 51-63.

DE MARES, M. C., JIMENEZ, D. J., PALLADINO, G., GUTLEBEN, J., LEBRUN, L. A., MULLER, E. E. L., WILMES, P., SIPKEMA, D. & VAN ELSAS, J. D. 2018. Expressed protein profile of a Tectomicrobium and other microbial symbionts in the marine sponge Aplysina aerophoba as evidenced by metaproteomics. *Sci Rep,* 8.

DE VADDER, F., KOVATCHEVA-DATCHARY, P., GONCALVES, D., VINERA, J., ZITOUN, C., DUCHAMPT, A., BACKHED, F. & MITHIEUX, G. 2014. Microbiota-generated metabolites promote metabolic benefits via gut-brain neural circuits. *Cell,* 156**,** 84-96.

DE VOS, A. F., DESSING, M. C., LAMMERS, A. J. J., DE PORTO, A. P. N. A., FLORQUIN, S., DE BOER, O. J., DE BEER, R., TERPSTRA, S., BOOTSMA, H. J., HERMANS, P. W., VAN 'T VEER, C. & VAN DER POLL, T. 2015. The Polysaccharide Capsule of Streptococcus pneumonia Partially Impedes MyD88-Mediated Immunity during Pneumonia in Mice. *PLOS ONE,* 10**,** e0118181.

DEKAS, A. E., CONNON, S. A., CHADWICK, G. L., TREMBATH-REICHERT, E. & ORPHAN, V. J. 2015. Activity and interactions of methane seep microorganisms assessed by parallel transcription and FISH-NanoSIMS analyses. *The Isme Journal,* 10**,** 678.

DENG, L., IGNACIO-ESPINOZA, J. C., GREGORY, A. C., POULOS, B. T., WEITZ, J. S., HUGENHOLTZ, P. & SULLIVAN, M. B. 2014. Viral tagging reveals discrete populations in *Synechococcus* viral genome sequence space. *Nature,* 513**,** 242-245.

DIEZ-VIVES, C., MOITINHO-SILVA, L., NIELSEN, S., REYNOLDS, D. & THOMAS, T. 2017. Expression of eukaryotic-like protein in the microbiome of sponges. *Mol Ecol,* 26**,** 1432-1451.

DOOLITTLE, W. F. & BOOTH, A. 2017. It's the song, not the singer: an exploration of holobiosis and evolutionary theory. *Biology & Philosophy,* 32**,** 5-24.

DOSSE, G. 1939. Bakterien- und Pilzbefunde sowie pathologische und Fäulnisvorgänge in Meeres- und Süsswasserschwämmen. *Zeitschrift für Parasitenkunde,* 11**,** 331-356.

DOUGLAS, A. E. 1998. Nutritional interactions in insect-microbial symbioses: aphids and their symbiotic bacteria *Buchnera*. *Annu Rev Entomol,* 43**,** 17-37.

DOUGLAS, A. E. & PROSSER, W. A. 1992. Synthesis of the essential amino acid tryptophan in the pea aphid (*Acyrthosiphon pisum*) symbiosis. *J Insect Physiol,* 38**,** 565-568.

DOUGLAS, A. E. & WERREN, J. H. 2016. Holes in the hologenome: Why host-microbe symbioses are not holobionts. *MBio,* 7**,** e02099.

DUBILIER, N., BERGIN, C. & LOTT, C. 2008. Symbiotic diversity in marine animals: the art of harnessing chemosynthesis. *Nat Rev Microbiol,* 6**,** 725.

DUERKOP, B. A., CLEMENTS, C. V., ROLLINS, D., RODRIGUES, J. L. M. & HOOPER, L. V. 2012. A composite bacteriophage alters colonization by an intestinal commensal bacterium. *PNASs,* 109**,** 17621-17626.

DŽUNKOVÁ, M., LOW, S. J., DALY, J. N., DENG, L., RINKE, C. & HUGENHOLTZ, P. 2019. Defining the human gut host–phage network through single-cell viral tagging. *Nat Microbiol*.

EDWARDS, R. A., MCNAIR, K., FAUST, K., RAES, J. & DUTILH, B. E. 2016a. Computational approaches to predict bacteriophage-host relationships. *FEMS Microbiol Rev,* 40**,** 258-72.

EDWARDS, R. A., MCNAIR, K., FAUST, K., RAES, J. & DUTILH, B. E. 2016b. Computational approaches to predict bacteriophage—host relationships. *FEMS Microbiol Rev,* 40.

EL TAHIR, Y. & SKURNIK, M. 2001. YadA, the multifaceted Yersinia adhesin. *International Journal of Medical Microbiology,* 291**,** 209-218.

ENTICKNAP, J. J., KELLY, M., PERAUD, O. & HILL, R. T. 2006. Characterization of a culturable alphaproteobacterial symbiont common to many marine sponges and evidence for vertical transmission via sponge larvae. *Appl Environ Microbiol,* 72**,** 3724-32.

ERICSON, C. F., EISENSTEIN, F., MEDEIROS, J. M., MALTER, K. E., CAVALCANTI, G. S., ZELLER, R. W., NEWMAN, D. K., PILHOFER, M. & SHIKUMA, N. J. 2019. A contractile injection system stimulates tubeworm metamorphosis by translocating a proteinaceous effector. *eLife,* 8**,** e46845.

ERWIN, P. M., COMA, R., LOPEZ-SENDINO, P., SERRANO, E. & RIBES, M. 2015a. Stable symbionts across the HMA-LMA dichotomy: low seasonal and interannual variation in sponge-associated bacteria from taxonomically diverse hosts. *FEMS Microbiol Ecol,* 91.

ERWIN, P. M., COMA, R., LÓPEZ-SENDINO, P., SERRANO, E. & RIBES, M. 2015b. Stable symbionts across the HMA-LMA dichotomy: low seasonal and interannual variation in sponge-associated bacteria from taxonomically diverse hosts. *FEMS Microbiol Ecol,* 91.

ERWIN, P. M., COMA, R., LÓPEZ-SENDINO, P., SERRANO, E. & RIBES, M. 2015c. Stable symbionts across the HMA-LMA dichotomy: low seasonal and interannual variation in sponge-associated bacteria from taxonomically diverse hosts. *FEMS Microbiology Ecology,* 91.

ERWIN, P. M., PITA, L., LOPEZ-LEGENTIL, S. & TURON, X. 2012. Stability of sponge-associated bacteria over large seasonal shifts in temperature and irradiance. *Appl Environ Microbiol,* 78**,** 7358-7368.

FAN, L., REYNOLDS, D., LIU, M., STARK, M., KJELLEBERG, S., WEBSTER, N. S. & THOMAS, T. 2012. Functional equivalence and evolutionary convergence in complex communities of microbial sponge symbionts. *PNAS,* 109**,** E1878-87.

FERNÁNDEZ, L., RODRÍGUEZ, A. & GARCÍA, P. 2018. Phage or foe: an insight into the impact of viral predation on microbial communities. *The ISME Journal,* 12**,** 1171-1179.

FIESELER, L., HORN, M., WAGNER, M. & HENTSCHEL, U. 2004. Discovery of the novel candidate phylum "*Poribacteria*" in marine sponges. *Appl Environ Microbiol,* 70**,** 3724-3732.

FINLAY, B. B. & MCFADDEN, G. 2006. Anti-immunology: evasion of the host immune system by bacterial and viral pathogens. *Cell,* 124**,** 767-782.

FIORE, C. L., LABRIE, M., JARETT, J. K. & LESSER, M. P. 2015. Transcriptional activity of the giant barrel sponge, *Xestospongia muta h*olobiont: molecular evidence for metabolic interchange. *Front Micrbiol,* 6.

FISHER, R. M., HENRY, L. M., CORNWALLIS, C. K., KIERS, E. T. & WEST, S. A. 2017a. The evolution of host-symbiont dependence. *Nat Commun,* 8**,** 15973.

FISHER, R. M., HENRY, L. M., CORNWALLIS, C. K., KIERS, E. T. & WEST, S. A. 2017b. The evolution of host-symbiont dependence. *Nat Commun,* 8**,** 15973.

FOSTER, K. R., SCHLUTER, J., COYTE, K. Z. & RAKOFF-NAHOUM, S. 2017. The evolution of the host microbiome as an ecosystem on a leash. *Nature,* 548**,** 43-51.

FRANZENBURG, S., WALTER, J., KÜNZEL, S., WANG, J., BAINES, J. F., BOSCH, T. C. G. & FRAUNE, S. 2013. Distinct antimicrobial peptide expression determines host species-specific bacterial associations. *PNAS,* 110**,** E3730-E3738.

FREILICH, S., ZARECKI, R., EILAM, O., SEGAL, E. S., HENRY, C. S., KUPIEC, M., GOPHNA, U., SHARAN, R. & RUPPIN, E. 2011. Competitive and cooperative metabolic interactions in bacterial communities. *Nat Commun,* 2**,** 589.

FRIEDRICH, A. B., MERKERT, H., FENDERT, T., HACKER, J., PROKSCH, P. & HENTSCHEL, U. 1999. Microbial diversity in the marine sponge *Aplysina cavernicola* (formerly Verongia cavernicola) analyzed by fluorescence *in situ* hybridization (FISH). *Mar Biol,* 134**,** 461-470.

FRITH, D. W. 1976. Animals associated with sponges at North Hayling, Hampshire. *Zool J Linn Soc,* 58**,** 353-362.

FUHRMAN, J. A. 1999. Marine viruses and their biogeochemical and ecological effects. *Nature,* 399**,** 541-548.

FUNAYAMA, N. 2013. The stem cell system in demosponges: suggested involvement of two types of cells: archeocytes (active stem cells) and choanocytes (food-entrapping flagellated cells). *Development Genes and Evolution,* 223**,** 23-38.

GANTT, S. E., LÓPEZ-LEGENTIL, S. & ERWIN, P. M. 2017. Stable microbial communities in the sponge Crambe crambe from inside and outside a polluted Mediterranean harbor. *FEMS Microbiol Lett,* 364.

GAO, E. B., HUANG, Y. & NING, D. 2016. Metabolic Genes within Cyanophage Genomes: Implications for Diversity and Evolution. *Genes,* 7**,** 80.

GAO, Z.-M., WANG, Y., TIAN, R.-M., WONG, Y. H., BATANG, Z. B., AL-SUWAILEM, A. M., BAJIC, V. B. & QIAN, P.-Y. 2014. Symbiotic adaptation drives genome streamlining of the cyanobacterial sponge Symbiont *Candidatus* Synechococcus spongiarum". *MBio,* 5**,** e00079-14.

GARCIA-GARCIA, J. C., RENNOLL-BANKERT, K. E., PELLY, S., MILSTONE, A. M. & DUMLER, J. S. 2009. Silencing of host cell CYBB gene expression by the nuclear effector AnkA of the intracellular pathogen Anaplasma phagocytophilum. *Infect Immun,* 77**,** 2385-91.

GARRABOU, J. & ZABALA, M. 2001. Growth dynamics in four Mediterranean demosponges. *Estuar Coast Shelf Sci,* 52**,** 293-303.

GAUTHIER, M.-E. A., WATSON, J. R. & DEGNAN, S. M. 2016. Draft genomes shed light on the dual bacterial symbiosis that dominates the microbiome of the coral reef sponge *Amphimedon queenslandica*. *Front Mar Sci,* 3.

GERÇE, B., SCHWARTZ, T., VOIGT, M., RÜHLE, S., KIRCHEN, S., PUTZ, A., PROKSCH, P., OBST, U., SYLDATK, C. & HAUSMANN, R. 2009. Morphological,bacterial, and secondary metabolite changes of *Aplysina aerophoba* upon long-lerm maintenance under artificial conditions. *Microb Ecol,* 58**,** 865.

GILBERT, S. F., BOSCH, T. C. G. & LEDON-RETTIG, C. 2015. Eco-Evo-Devo: developmental symbiosis and developmental plasticity as evolutionary agents. *Nat Rev Genet,* 16**,** 611-622.

GLASL, B., SMITH, C. E., BOURNE, D. G. & WEBSTER, N. S. 2018. Exploring the diversity-stability paradigm using sponge microbial communities. *Sci Rep,* 8**,** 8425.

GLOECKNER, V., WEHRL, M., MOITINHO-SILVA, L., GERNERT, C., SCHUPP, P., PAWLIK, J. R., LINDQUIST, N. L., ERPENBECK, D., WOERHEIDE, G. & HENTSCHEL, U. 2014a. The HMA-LMA dichotomy revisited: an electron microscopical Survey of 56 sponge species. *Biol Bull,* 227**,** 78-88.

GLOECKNER, V., WEHRL, M., MOITINHO-SILVA, L., GERNERT, C., SCHUPP, P., PAWLIK, J. R., LINDQUIST, N. L., ERPENBECK, D., WORHEIDE, G. & HENTSCHEL, U. 2014b. The HMA-LMA dichotomy revisited: an electron microscopical Survey of 56 sponge species. *Biol Bull,* 227**,** 78-88.

GODEFROY, N., LE GOFF, E., MARTINAND-MARI, C., BELKHIR, K., VACELET, J. & BAGHDIGUIAN, S. 2019. Sponge digestive system diversity and evolution: filter feeding to carnivory. *Cell Tissue Res*.

GRASIS, J. A., LACHNIT, T., ANTON-ERXLEBEN, F., LIM, Y. W., SCHMIEDER, R., FRAUNE, S., FRANZENBURG, S., INSUA, S., MACHADO, G., HAYNES, M., LITTLE, M., KIMBLE, R., ROSENSTIEL, P., ROHWER, F. L. & BOSCH, T. C. 2014. Species-specific viromes in the ancestral holobiont *Hydra*. *PLoS One,* 9**,** e109952.

GREGORY, A. C., ZABLOCKI, O., HOWELL, A., BOLDUC, B. & SULLIVAN, M. B. 2019a. The human gut virome database. *bioRxiv***,** 655910.

GREGORY, A. C., ZAYED, A. A., CONCEICAO-NETO, N., TEMPERTON, B., BOLDUC, B., ALBERTI, A., ARDYNA, M., ARKHIPOVA, K., CARMICHAEL, M., CRUAUD, C., DIMIER, C., DOMINGUEZ-HUERTA, G., FERLAND, J., KANDELS, S., LIU, Y., MAREC, C., PESANT, S., PICHERAL, M., PISAREV, S., POULAIN, J., TREMBLAY, J. E., VIK, D., BABIN, M., BOWLER, C., CULLEY, A. I., DE VARGAS, C., DUTILH, B. E., IUDICONE, D., KARP-BOSS, L., ROUX, S., SUNAGAWA, S., WINCKER, P. & SULLIVAN, M. B. 2019b. Marine DNA viral macro- and microdiversity from Pole to Pole. *Cell*.

GRIFFITHS, S. M., ANTWIS, R. E., LENZI, L., LUCACI, A., BEHRINGER, D. C., BUTLER IV, M. J. & PREZIOSI, R. F. 2019. Host genetics and geography influence microbiome composition in the sponge Ircinia campana. *Journal of Animal Ecology,* 0.

GROUSSIN, M., MAZEL, F., SANDERS, J. G., SMILLIE, C. S., LAVERGNE, S., THUILLER, W. & ALM, E. J. 2017. Unraveling the processes shaping mammalian gut microbiomes over evolutionary time. *Nat Commun,* 8**,** 14319.

GUIDI, L., CHAFFRON, S., BITTNER, L., EVEILLARD, D., LARHLIMI, A., ROUX, S., DARZI, Y., AUDIC, S., BERLINE, L., BRUM, J. R., COELHO, L. P., ESPINOZA, J. C. I., MALVIYA, S., SUNAGAWA, S., DIMIER, C., KANDELS-LEWIS, S., PICHERAL, M., POULAIN, J., SEARSON, S., TARA OCEANS CONSORTIUM, C., STEMMANN, L., NOT, F., HINGAMP, P., SPEICH, S., FOLLOWS, M., KARP-BOSS, L., BOSS, E., OGATA, H., PESANT, S., WEISSENBACH, J., WINCKER, P., ACINAS, S. G., BORK, P., DE VARGAS, C., IUDICONE, D., SULLIVAN, M. B., RAES, J., KARSENTI, E., BOWLER, C. & GORSKY, G. 2016. Plankton networks driving carbon export in the oligotrophic ocean. *Nature,* 532**,** 465.

GÜNDÜZ, E. A. & DOUGLAS, A. E. 2009. Symbiotic bacteria enable insect to use a nutritionally inadequate diet. *PNAS,* 276**,** 987-991.

HAAS, A. F., FAIROZ, M. F. M., KELLY, L. W., NELSON, C. E., DINSDALE, E. A., EDWARDS, R. A., GILES, S., HATAY, M., HISAKAWA, N., KNOWLES, B., LIM, Y. W., MAUGHAN, H., PANTOS, O., ROACH, T. N. F., SANCHEZ, S. E., SILVEIRA, C. B., SANDIN, S., SMITH, J. E. & ROHWER, F. 2016. Global microbialization of coral reefs. *Nat Microbiol,* 1**,** 16042.

HACQUARD, S., GARRIDO-OTER, R., GONZALEZ, A., SPAEPEN, S., ACKERMANN, G., LEBEIS, S., MCHARDY, A. C., DANGL, J. L., KNIGHT, R., LEY, R. & SCHULZE-LEFERT, P. 2015. Microbiota and host nutrition across plant and animal kingdoms. *Cell Host Microbe,* 17**,** 603-16.

HADAS, E., MARIE, D., SHPIGEL, M. & ILAN, M. 2006. Virus predation by sponges is a new nutrient-flow pathway in coral reef food webs. *Limnol Oceanogr,* 51**,** 1548-1550.

HADAS, E., SHPIGEL, M. & ILAN, M. 2009. Particulate organic matter as a food source for a coral reef sponge. *J Exp Biol,* 212**,** 3643-50.

HARDOIM, C. C., CARDINALE, M., CUCIO, A. C., ESTEVES, A. I., BERG, G., XAVIER, J. R., COX, C. J. & COSTA, R. 2014. Effects of sample handling and cultivation bias on the specificity of bacterial communities in keratose marine sponges. *Front Microbiol,* 5**,** 611.

HATCHER, B. G. 1990. Coral reef primary productivity. A hierarchy of pattern and process. *Trends Ecol Evol,* 5**,** 149-155.

HENTSCHEL, U., HOPKE, J., HORN, M., FRIEDRICH, A. B., WAGNER, M., HACKER, J. & MOORE, B. S. 2002. Molecular Evidence for a Uniform Microbial Community in Sponges from Different Oceans. *Applied and Environmental Microbiology,* 68**,** 4431-4440.

HENTSCHEL, U., PIEL, J., DEGNAN, S. M. & TAYLOR, M. W. 2012. Genomic insights into the marine sponge microbiome. *Nat Rev Microbiol,* 10**,** 641-654.

HENTSCHEL, U., USHER, K. M. & TAYLOR, M. W. 2006. Marine sponges as microbial fermenters. *FEMS Microbiol Ecol,* 55**,** 167-177.

HEROLD, S., KARCH, H. & SCHMIDT, H. 2004. Shiga toxin-encoding bacteriophages – genomes in motion. *International Journal of Medical Microbiology,* 294**,** 115-121.

HESTER, E. R., BAROTT, K. L., NULTON, J., VERMEIJ, M. J. A. & ROHWER, F. L. 2015. Stable and sporadic symbiotic communities of coral and algal holobionts. *ISME J,* 10**,** 1157.

HEVRONI, G., ENAV, H., ROHWER, F. & BÉJÀ, O. 2015. Diversity of viral photosystem-I psaA genes. *The ISME Journal,* 9**,** 1892-1898.

HEWSON, I., BUTTON, J. B., GUDENKAUF, B. M., MINER, B., NEWTON, A. L., GAYDOS, J. K., WYNNE, J., GROVES, C. L., HENDLER, G., MURRAY, M., FRADKIN, S., BREITBART, M., FAHSBENDER, E., LAFFERTY, K. D., KILPATRICK, A. M., MINER, C. M., RAIMONDI, P., LAHNER, L., FRIEDMAN, C. S., DANIELS, S., HAULENA, M., MARLIAVE, J., BURGE, C. A., EISENLORD, M. E. & HARVELL, C. D. 2014. Densovirus associated with sea-star wasting disease and mass mortality. *PNAS,* 111**,** 17278-17283.

HOER, D. R., GIBSON, P. J., TOMMERDAHL, J. P., LINDQUIST, N. L. & MARTENS, C. S. 2018. Consumption of dissolved organic carbon by Caribbean reef sponges. *Limnology and Oceanography,* 63**,** 337-351.

HOFFMANN, F., LARSEN, O., THIEL, V., RAPP, H. T., PAPE, T., MICHAELIS, W. & REITNER, J. 2005. An anaerobic world in sponges. *Geomicrobiology Journal,* 22**,** 1-10.

HOFFMANN, F., RADAX, R., WOEBKEN, D., HOLTAPPELS, M., LAVIK, G., RAPP, H. T., SCHLÄPPY, M.-L., SCHLEPER, C. & KUYPERS, M. M. M. 2009. Complex nitrogen cycling in the sponge *Geodia barretti*. *Environ Mico,* 11**,** 2228-2243.

HOFFMANN, F., RØY, H., BAYER, K., HENTSCHEL, U., PFANNKUCHEN, M., BRÜMMER, F. & DE BEER, D. 2008. Oxygen dynamics and transport in the Mediterranean sponge *Aplysina aerophoba*. *Mar Biol,* 153**,** 1257-1264.

HOOPER, J. A. & VAN SOEST, R. M. 2002. Systema *Porifera*. A guide to the classification of sponges. *In:* HOOPER, J. A., VAN SOEST, R. M. & WILLENZ, P. (eds.) *Systema Porifera.* New York: Springer US.

HOOPER, J. N., HALL, K. A., EKINS, M., ERPENBECK, D., WORHEIDE, G. & JOLLEY-ROGERS, G. 2013. Managing and sharing the escalating number of sponge "unknowns": the SpongeMaps project. *Integr Comp Biol,* 53**,** 473-81.

HORN, H., SLABY, B. M., JAHN, M. T., BAYER, K., MOITINHO-SILVA, L., FORSTER, F., ABDELMOHSEN, U. R. & HENTSCHEL, U. 2016. An enrichment of CRISPR and other defense-related features in marine sponge-associated microbial metagenomes. *Front Microbiol,* 7**,** 1751.

HOWARD-VARONA, C., HARGREAVES, K. R., ABEDON, S. T. & SULLIVAN, M. B. 2017. Lysogeny in nature: mechanisms, impact and ecology of temperate phages. *The ISME journal,* 11**,** 1511-1520.

HUFF, E. 1961. The metabolism of 1,2-propanediol. *Biochimica et Biophysica Acta,* 48**,** 506-517.

HURWITZ, B. L., HALLAM, S. J. & SULLIVAN, M. B. 2013. Metabolic reprogramming by viruses in the sunlit and dark ocean. *Genome Biology,* 14**,** R123.

IBRAHIM, D., NAZARI, T. F., KASSIM, J. & LIM, S.-H. 2014. Prodigiosin-an antibacterial red pigment produced by *Serratia marcescens* IBRL USM 84 associated with a marine sponge *Xestospongia testudinaria*. *J Appl Pharm Sci,* 4**,** 1-6.

JACOBS, M. D. & HARRISON, S. C. 1998. Structure of an IκBα/NF-κB complex. *Cell,* 95**,** 749-758.

JAHN, M. T., MARKERT, S. M., RYU, T., RAVASI, T., STIGLOHER, C., HENTSCHEL, U. & MOITINHO-SILVA, L. 2016. Shedding light on cell compartmentation in the candidate phylum Poribacteria by high resolution visualisation and transcriptional profiling. *Sci Rep,* 6**,** 35860.

JERNIGAN, K. K. & BORDENSTEIN, S. R. 2014. Ankyrin domains across the tree of life. *PeerJ,* 2**,** e264.

JIMÉNEZ, E. & RIBES, M. 2007. Sponges as a source of dissolved inorganic nitrogen: Nitrification mediated by temperate sponges. *Limnol Oceanogr,* 52**,** 948-958.

JOHNSON, K. V. A. & FOSTER, K. R. 2018. Why does the microbiome affect behaviour? *Nat Rev Microbiol,* 16**,** 647-655.

KAMKE, J., RINKE, C., SCHWIENTEK, P., MAVROMATIS, K., IVANOVA, N., SCZYRBA, A., WOYKE, T. & HENTSCHEL, U. 2014. The candidate phylum *Poribacteria* by single-cell genomics: new insights into phylogeny, cell-compartmentation, eukaryote-like repeat proteins, and other genomic features. *PLoS One,* 9.

KAMKE, J., SCZYRBA, A., IVANOVA, N., SCHWIENTEK, P., RINKE, C., MAVROMATIS, K., WOYKE, T. & HENTSCHEL, U. 2013. Single-cell genomics reveals complex carbohydrate degradation patterns in poribacterial symbionts of marine sponges. *ISME J,* 7**,** 2287-2300.

KARIMI, E., SLABY, B. M., SOARES, A. R., BLOM, J., HENTSCHEL, U. & COSTA, R. 2018. Metagenomic binning reveals versatile nutrient cycling and distinct adaptive features in alphaproteobacterial symbionts of marine sponges. *FEMS Microbiol Ecol,* 94.

KAUFFMAN, K. M., HUSSAIN, F. A., YANG, J., AREVALO, P., BROWN, J. M., CHANG, W. K., VANINSBERGHE, D., ELSHERBINI, J., SHARMA, R. S., CUTLER, M. B., KELLY, L. & POLZ, M. F. 2018. A major lineage of non-tailed dsDNA viruses as unrecognized killers of marine bacteria. *Nature,* 554**,** 118.

KEEN, E. C. & DANTAS, G. 2018. Close encounters of three kinds: bacteriophages, commensal bacteria, and host immunity. *Trends Microbiol,* 26**,** 943-954.

KELLEY, L. A., MEZULIS, S., YATES, C. M., WASS, M. N. & STERNBERG, M. J. E. 2015. The Phyre2 web portal for protein modeling, prediction and analysis. *Nature Protocols,* 10**,** 845.

KELLY, CALEB J., ZHENG, L., CAMPBELL, ERIC L., SAEEDI, B., SCHOLZ, CARSTEN C., BAYLESS, AMANDA J., WILSON, KELLY E., GLOVER, LOUISE E., KOMINSKY, DOUGLAS J., MAGNUSON, A., WEIR, TIFFANY L., EHRENTRAUT, STEFAN F., PICKEL, C., KUHN, KRISTINE A., LANIS, JORDI M., NGUYEN, V., TAYLOR, CORMAC T. & COLGAN, SEAN P. 2015. Crosstalk between microbiota-derived short-chain fatty acids and intestinal epithelial HIF augments tissue barrier function. *Cell Host Microbe,* 17**,** 662-671.

KERFELD, C. A., AUSSIGNARGUES, C., ZARZYCKI, J., CAI, F. & SUTTER, M. 2018. Bacterial microcompartments. *Nat Rev Microbiol,* 16**,** 277.

KERFELD, C. A. & ERBILGIN, O. 2015. Bacterial microcompartments and the modular construction of microbial metabolism. *Trends Microbiol,* 23**,** 22-34.

KHANNA, K., LOPEZ-GARRIDO, J., ZHAO, Z., WATANABE, R., YUAN, Y., SUGIE, J., POGLIANO, K. & VILLA, E. 2019. The molecular architecture of engulfment during Bacillus subtilis sporulation. *eLife,* 8**,** e45257.

KIM, M.-S. & BAE, J.-W. 2018. Lysogeny is prevalent and widely distributed in the murine gut microbiota. *The ISME Journal,* 12**,** 1127-1141.

KING, A. M. Q., LEFKOWITZ, E. J., MUSHEGIAN, A. R., ADAMS, M. J., DUTILH, B. E., GORBALENYA, A. E., HARRACH, B., HARRISON, R. L., JUNGLEN, S., KNOWLES, N. J., KROPINSKI, A. M., KRUPOVIC, M., KUHN, J. H., NIBERT, M. L., RUBINO, L., SABANADZOVIC, S., SANFACON, H., SIDDELL, S. G., SIMMONDS, P., VARSANI, A., ZERBINI, F. M. & DAVISON, A. J. 2018. Changes to taxonomy and the International code of virus classification and nomenclature ratified by the international committee on taxonomy of viruses. *Arch Virol*.

KING, N. & ROKAS, A. 2017. Embracing uncertainty in reconstructing early animal evolution. *Curr Biol,* 27**,** R1081-R1088.

KNOWLES, B., SILVEIRA, C. B., BAILEY, B. A., BAROTT, K., CANTU, V. A., COBIÁN-GÜEMES, A. G., COUTINHO, F. H., DINSDALE, E. A., FELTS, B., FURBY, K. A., GEORGE, E. E., GREEN, K. T., GREGORACCI, G. B., HAAS, A. F., HAGGERTY, J. M., HESTER, E. R., HISAKAWA, N., KELLY, L. W., LIM, Y. W., LITTLE, M., LUQUE, A., MCDOLE-SOMERA, T., MCNAIR, K., DE OLIVEIRA, L. S., QUISTAD, S. D., ROBINETT, N. L., SALA, E., SALAMON, P., SANCHEZ, S. E., SANDIN, S., SILVA, G. G. Z., SMITH, J., SULLIVAN, C., THOMPSON, C., VERMEIJ, M. J. A., YOULE, M., YOUNG, C., ZGLICZYNSKI, B., BRAINARD, R., EDWARDS, R. A., NULTON, J., THOMPSON, F. & ROHWER, F. 2016. Lytic to temperate switching of viral communities. *Nature,* 531**,** 466.

KOHDA, D., MORTON, C. J., PARKAR, A. A., HATANAKA, H., INAGAKI, F. M., CAMPBELL, I. D. & DAY, A. J. 1996. Solution structure of the link module: a hyaluronan-binding domain involved in extracellular matrix stability and cell migration. *Cell,* 86**,** 767-75.

KOOPMANS, M., VAN RIJSWIJK, P., BOSCHKER, H. T., MARCO, H., MARTENS, D. & WIJFFELS, R. H. 2015. Seasonal variation of fatty acids and stable carbon isotopes in sponges as indicators for nutrition: biomarkers in sponges identified. *Mar Biotechnol (NY),* 17**,** 43-54.

KREMER, N., KOCH, E. J., EL FILALI, A., ZHOU, L., HEATH-HECKMAN, E. A. C., RUBY, E. G. & MCFALL-NGAI, M. J. 2018. Persistent interactions with bacterial symbionts direct mature-host cell morphology and gene expression in the Squid-Vibrio symbiosis. *mSystems,* 3**,** e00165-18.

KUNDU, P., BLACHER, E., ELINAV, E. & PETTERSSON, S. 2017. Our gut microbiome: the evolving inner self. *Cell,* 171**,** 1481-1493.

L. SIMPSON, T. 1984. The cell biology of sponges.

LACKNER, G., PETERS, E. E., HELFRICH, E. J. N. & PIEL, J. 2017. Insights into the lifestyle of uncultured bacterial natural product factories associated with marine sponges. *PNAS,* 114**,** E347-E356.

LAFFY, P. W., BOTTÉ, E. S., WOOD-CHARLSON, E. M., WEYNBERG, K. D., RATTEI, T. & WEBSTER, N. S. 2019. Thermal stress modifies the marine sponge virome. *Environ Microbiol Rep,* 0.

LAFFY, P. W., WOOD-CHARLSON, E. M., TURAEV, D., JUTZ, S., PASCELLI, C., BOTTE, E. S., BELL, S. C., PEIRCE, T. E., WEYNBERG, K. D., VAN OPPEN, M. J. H., RATTEI, T. &

WEBSTER, N. S. 2018. Reef invertebrate viromics: diversity, host specificity and functional capacity. *Environ Microbiol,* Epub ahead of print.

LAFFY, P. W., WOOD CHARLSON, E., TURAEV, D., WEYNBERG, K. D., BOTTE, E., VAN OPPEN, M. J., WEBSTER, N. & RATTEI, T. 2016. HoloVir: a workflow for investigating the diversity and function of viruses in invertebrate holobionts. *Front Microbiol,* 7.

LAFI, F. F., FUERST, J. A., FIESELER, L., ENGELS, C., GOH, W. W. L. & HENTSCHEL, U. 2009. Widespread distribution of *Poribacteria* in *Demospongiae*. *Appl Environ Microbiol,* 75**,** 5695-5699.

LAJEUNESSE, T. C., PARKINSON, J. E., GABRIELSON, P. W., JEONG, H. J., REIMER, J. D., VOOLSTRA, C. R. & SANTOS, S. R. 2018. Systematic revision of *Symbiodiniaceae h*ighlights the antiquity and diversity of coral endosymbionts. *Curr Biol,* 28**,** 2570-2580.e6.

LARA, E., VAQUÉ, D., SÀ, E. L., BORAS, J. A., GOMES, A., BORRULL, E., DÍEZ-VIVES, C., TEIRA, E., PERNICE, M. C., GARCIA, F. C., FORN, I., CASTILLO, Y. M., PEIRÓ, A., SALAZAR, G., MORÁN, X. A. G., MASSANA, R., CATALÁ, T. S., LUNA, G. M., AGUSTÍ, S., ESTRADA, M., GASOL, J. M. & DUARTE, C. M. 2017. Unveiling the role and life strategies of viruses from the surface to the dark ocean. *Science Advances,* 3**,** e1602565.

LAVY, A., KEREN, R., YAHEL, G. & ILAN, M. 2016. Intermittent hypoxia and prolonged suboxia measured *In situ* in a marine sponge. *Front Mar Sci,* 3**,** 263.

LEIGH, B. A., BORDENSTEIN, S. R., BROOKS, A. W., MIKAELYAN, A. & BORDENSTEIN, S. R. 2018a. Finer-scale phylosymbiosis: insights from insect viromes. *mSystems,* 3**,** e00131-18.

LEIGH, B. A., DJURHUUS, A., BREITBART, M. & DISHAW, L. J. 2018b. The gut virome of the protochordate model organism, *Ciona intestinalis* subtype A. *Virus Res,* 244**,** 137-146.

LÉVI, C. & PORTE, A. 1962. Etude au microscope électronique de l'éponge *Oscarella lobularis* Schmidt et de sa larve amphiblastula. *Cahiers de Biologie Marine,* 3**,** 307-315.

LEVY, R. & BORENSTEIN, E. 2013. Metabolic modeling of species interaction in the human microbiome elucidates community-level assembly rules. *PNAS,* 110**,** 12804-12809.

LEY, R. E., HAMADY, M., LOZUPONE, C., TURNBAUGH, P. J., RAMEY, R. R., BIRCHER, J. S., SCHLEGEL, M. L., TUCKER, T. A., SCHRENZEL, M. D., KNIGHT, R. & GORDON, J. I. 2008. Evolution of mammals and their gut microbes. *Science,* 320**,** 1647.

LEYS, S. P. & DEGNAN, B. M. 2001. cytological basis of photoresponsive behavior in a sponge Larva. *Biol Bull,* 201**,** 323-338.

LEYS, S. P., KAHN, A. S., FANG, J. K. H., KUTTI, T. & BANNISTER, R. J. 2018. Phagocytosis of microbial symbionts balances the carbon and nitrogen budget for the deep-water boreal sponge *Geodia barretti*. *Limnol Oceanogr,* 63**,** 187-202.

LHOCINE, N., RIBEIRO, P. S., BUCHON, N., WEPF, A., WILSON, R., TENEV, T., LEMAITRE, B., GSTAIGER, M., MEIER, P. & LEULIER, F. 2008. PIMS modulates immune tolerance by negatively regulating *Drosophila i*nnate immune signaling. *Cell Host Microbe,* 4**,** 147-158.

LI, C.-X., SHI, M., TIAN, J.-H., LIN, X.-D., KANG, Y.-J., CHEN, L.-J., QIN, X.-C., XU, J., HOLMES, E. C. & ZHANG, Y.-Z. 2015. Unprecedented genomic diversity of RNA viruses in arthropods reveals the ancestry of negative-sense RNA viruses. *eLife,* 4**,** e05378.

LI, L., SHAN, T., WANG, C., COTE, C., KOLMAN, J., ONIONS, D., GULLAND, F. M. & DELWART, E. 2011. The fecal viral flora of California sea lions. *J Virol,* 85**,** 9909-17.

LI, X.-Y., LACHNIT, T., FRAUNE, S., BOSCH, T. C. G., TRAULSEN, A. & SIEBER, M. 2017. Temperate phages as self-replicating weapons in bacterial competition. *Journal of The Royal Society Interface,* 14**,** 20170563.

LIMA-MENDEZ, G., VAN HELDEN, J., TOUSSAINT, A. & LEPLAE, R. 2008. Reticulate representation of evolutionary and functional relationships between phage genomes. *Mol Biol Evol,* 25**,** 762-77.

LIU, M., FAN, L., ZHONG, L., KJELLEBERG, S. & THOMAS, T. 2012. Metaproteogenomic analysis of a community of sponge symbionts. *ISME J,* 6**,** 1515-1525.

LIU, M. Y., KJELLEBERG, S. & THOMAS, T. 2011. Functional genomic analysis of an uncultured δ-*proteobacterium* in the sponge *Cymbastela concentrica*. *ISME J,* 5**,** 427-435.

LIU, T., ZHANG, L., JOO, D. & SUN, S.-C. 2017. NF-κB signaling in inflammation. *Signal transduction and targeted therapy,* 2**,** 17023.

LIU, W., JACQUIOD, S., BREJNROD, A., RUSSEL, J., BURMØLLE, M. & SØRENSEN, S. J. 2019. Deciphering links between bacterial interactions and spatial organization in multispecies biofilms. *The ISME Journal*.

LOPEZ-ACOSTA, M., LEYNAERT, A., CHAVAUD, L., AMICE, E., BIHANNIC, I., LE BEC, T. & MALDONADO, M. 2019. *In situ* determination of Si, N, and P utilization by the demosponge *Tethya citrina*: A benthic-chamber approach. *PLoS One,* 14**,** e0218787.

LOWE, T. M. & CHAN, P. P. 2016. tRNAscan-SE On-line: integrating search and context for analysis of transfer RNA genes. *Nucleic Acids Res,* 44**,** W54-7.

LU, F., WEIDMER, A., LIU, C.-G., VOLINIA, S., CROCE, C. M. & LIEBERMAN, P. M. 2008. Epstein-Barr Virus-Induced miR-155 Attenuates NF-κB Signaling and Stabilizes Latent Virus Persistence. *Journal of Virology,* 82**,** 10436-10443.

LUDEMAN, D. A., FARRAR, N., RIESGO, A., PAPS, J. & LEYS, S. P. 2014. Evolutionary origins of sensation in metazoans: functional evidence for a new sensory organ in sponges. *BMC Evol Biol,* 14**,** 3.

LÜHRMANN, A., NOGUEIRA, C. V., CAREY, K. L. & ROY, C. R. 2010. Inhibition of pathogen-induced apoptosis by a *Coxiella burnetii* type IV effector protein. *PNAS,* 107**,** 18997-19001.

LYKIDIS, A., CHEN, C.-L., TRINGE, S. G., MCHARDY, A. C., COPELAND, A., KYRPIDES, N. C., HUGENHOLTZ, P., MACARIE, H., OLMOS, A., MONROY, O. & LIU, W.-T. 2011. Multiple syntrophic interactions in a terephthalate-degrading methanogenic consortium. *ISME J,* 5**,** 122-130.

MALDONADO, M., RIBES, M. & VAN DUYL, F. C. 2012. Chapter three - nutrient fluxes through sponges: biology, budgets, and ecological implications. *In:* MIKEL A. BECERRO, M. J. U. M. M. & XAVIER, T. (eds.) *Advances in Marine Biology*. Academic Press.

MALDONADO, M., ZHANG, X., CAO, X., XUE, L., CAO, H. & ZHANG, W. 2010. Selective feeding by sponges on pathogenic microbes: a reassessment of potential for abatement of microbial pollution. *Mar Ecol Prog Ser,* 403**,** 75-89.

MALOOF, A. C., ROSE, C. V., BEACH, R., SAMUELS, B. M., CALMET, C. C., ERWIN, D. H., POIRIER, G. R., YAO, N. & SIMONS, F. J. 2010. Possible animal-body fossils in pre-marinoan limestones from South Australia. *Nat Geosci,* 3**,** 653.

MANCONI, R. & PRONZATO, R. 2008. Global diversity of sponges (*Porifera*: *Spongillina*) in freshwater. *Hydrobiologia,* 595**,** 27-33.

MARBOUTY, M., BAUDRY, L., COURNAC, A. & KOSZUL, R. 2017. Scaffolding bacterial genomes and probing host-virus interactions in gut microbiome by proximity ligation (chromosome capture) assay. *Sci Adv,* 3**,** e1602105.

MARGULIS, L. 1998. *Symbiotic planet : a new look at evolution,* New York, Basic Books.

MARGULIS, L. & FESTER, R. 1991. *Symbiosis as a source of evolutionary innovation: speciation and morphogenesis,* Cambridge, Mass MIT Press.

MARHAVER, K. L., EDWARDS, R. A. & ROHWER, F. 2008. Viral communities associated with healthy and bleaching corals. *Environmental Microbiology,* 10**,** 2277-2286.

MARIANI, S., BAILLIE, C., COLOSIMO, G. & RIESGO, A. 2019. Sponges as natural environmental DNA samplers. *Current Biology,* 29**,** R401-R402.

MARK WELCH, J. L., ROSSETTI, B. J., RIEKEN, C. W., DEWHIRST, F. E. & BORISY, G. G. 2016. Biogeography of a human oral microbiome at the micron scale. *PNAS,* 113**,** E791-E800.

MARKERT, S. M., BRITZ, S., PROPPERT, S., LANG, M., WITVLIET, D., MULCAHY, B., SAUER, M., ZHEN, M., BESSEREAU, J. L. & STIGLOHER, C. 2016. Filling the gap: adding super-resolution to array tomography for correlated ultrastructural and molecular identification of electrical synapses at the C. elegans connectome. *Neurophotonics,* 3**,** 041802.

MÁRQUEZ, L. M., REDMAN, R. S., RODRIGUEZ, R. J. & ROOSSINCK, M. J. 2007. A virus in a fungus in a plant: three-way symbiosis required for thermal tolerance. *Science,* 315**,** 513-515.

MATEO, L. Â. P.-V., SVEN, Z. & ERNESTO, W. 2006. Competition for space between encrusting excavating Caribbean sponges and other coral reef organisms. *Mar Ecol Prog Ser,* 312**,** 113-121.

MCCALLIN, S., SACHER, J. C., ZHENG, J. & CHAN, B. K. 2019. Current State of Compassionate Phage Therapy. *Viruses,* 11**,** 343.

MCCUTCHEON, J. P. & MORAN, N. A. 2011. Extreme genome reduction in symbiotic bacteria. *Nat Rev Microbiol,* 10**,** 13.

MCFALL-NGAI, M. 2008. Hawaiian bobtail squid. *Curr Biol,* 18**,** R1043-R1044.

MCFALL-NGAI, M., HADFIELD, M. G., BOSCH, T. C., CAREY, H. V., DOMAZET-LOSO, T., DOUGLAS, A. E., DUBILIER, N., EBERL, G., FUKAMI, T. & GILBERT, S. F. 2013. Animals in a bacterial world, a new imperative for the life sciences. *PNAS,* 110.

MCMURDIE, P. J. & HOLMES, S. 2013. phyloseq: An R Package for Reproducible Interactive Analysis and Graphics of Microbiome Census Data. *PLOS ONE,* 8**,** e61217.

MCMURRAY, S. E., JOHNSON, Z. I., HUNT, D. E., PAWLIK, J. R. & FINELLI, C. M. 2016. Selective feeding by the giant barrel sponge enhances foraging efficiency. *Limnol Oceanogr,* 61**,** 1271-1286.

MCMURRAY, S. E., PAWLIK, J. R. & FINELLI, C. M. 2014. Trait-mediated ecosystem impacts: how morphology and size affect pumping rates of the Caribbean giant barrel sponge. *Aquat Biol,* 23**,** 1-13.

MCMURRAY, S. E., STUBLER, A. D., ERWIN, P. M., FINELLI, C. M. & PAWLIK, J. R. 2018. A test of the sponge-loop hypothesis for emergent Caribbean reef sponges. *Mar Ecol Prog Ser,* 588**,** 1-14.

MCNAIR, K., BAILEY, B. A. & EDWARDS, R. A. 2012. PHACTS, a computational approach to classifying the lifestyle of phages. *Bioinformatics,* 28**,** 614-8.

MEDLOCK, G. L., CAREY, M. A., MCDUFFIE, D. G., MUNDY, M. B., GIALLOUROU, N., SWANN, J. R., KOLLING, G. L. & PAPIN, J. A. 2018. Inferring metabolic mechanisms of interaction within a defined gut microbiota. *Cell Sys,* 7**,** 245-257.e7.

MICHEVA, K. D. & SMITH, S. J. 2007. Array tomography: a new tool for imaging the molecular architecture and ultrastructure of neural circuits. *Neuron,* 55**,** 25-36.

MILLER, E. T., SVANBACK, R. & BOHANNAN, B. J. M. 2018. Microbiomes as metacommunities: understanding host-associated microbes through metacommunity *Trends Ecol Evol,* 33**,** 926-935.

MISEVIC, G. N., FINNE, J. & BURGER, M. M. 1987. Involvement of carbohydrates as multiple low affinity interaction sites in the self-association of the aggregation factor from the marine sponge Microciona prolifera. *Journal of Biological Chemistry,* 262**,** 5870-5877.

MITRI, S., CLARKE, E. & FOSTER, K. R. 2016. Resource limitation drives spatial organization in microbial groups. *The ISME Journal,* 10**,** 1471-1482.

MOELLER, A. H., CARO-QUINTERO, A., MJUNGU, D., GEORGIEV, A. V., LONSDORF, E. V., MULLER, M. N., PUSEY, A. E., PEETERS, M., HAHN, B. H. & OCHMAN, H. 2016. Cospeciation of gut microbiota with hominids. *Science,* 353**,** 380-2.

MOELLER, F. U., WEBSTER, N. S., HERBOLD, C. W., BEHNAM, F., DOMMAN, D., ALBERTSEN, M., MOOSHAMMER, M., MARKERT, S., TURAEV, D., BECHER, D., RATTEI, T., SCHWEDER, T., RICHTER, A., WATZKA, M., NIELSEN, P. H. & WAGNER, M. 2019. Characterization of a thaumarchaeal symbiont that drives incomplete nitrification in the tropical sponge *Ianthella basta*. *Environ Mico,* 21**,** 3831-3854.

MOHAMED, N. M., SAITO, K., TAL, Y. & HILL, R. T. 2009. Diversity of aerobic and anaerobic ammonia-oxidizing bacteria in marine sponges. *ISME J,* 4**,** 38.

MOITINHO-SILVA, L., BAYER, K., CANNISTRACI, C. V., GILES, E. C., RYU, T., SERIDI, L., RAVASI, T. & HENTSCHEL, U. 2014a. Specificity and transcriptional activity of microbiota associated with low and high microbial abundance sponges from the Red Sea. *Mol Ecol,* 23**,** 1348-63.

MOITINHO-SILVA, L., NIELSEN, S., AMIR, A., GONZALEZ, A., ACKERMANN, G. L., CERRANO, C., ASTUDILLO-GARCIA, C., EASSON, C., SIPKEMA, D., LIU, F., STEINERT, G., KOTOULAS, G., MCCORMACK, G. P., FENG, G., BELL, J. J., VICENTE, J., BJÖRK, J. R., MONTOYA, J. M., OLSON, J. B., REVEILLAUD, J., STEINDLER, L., PINEDA, M.-C., MARRA, M. V., ILAN, M., TAYLOR, M. W., POLYMENAKOU, P., ERWIN, P. M., SCHUPP, P. J., SIMISTER, R. L., KNIGHT, R., THACKER, R. W., COSTA, R., HILL, R. T., LOPEZ-LEGENTIL, S., DAILIANIS, T., RAVASI, T., HENTSCHEL, U., LI, Z., WEBSTER, N. S. & THOMAS, T. 2017a. The sponge microbiome project. *GigaScience,* 6.

MOITINHO-SILVA, L., SERIDI, L., RYU, T., VOOLSTRA, C. R., RAVASI, T. & HENTSCHEL, U. 2014b. Revealing microbial functional activities in the Red Sea sponge *Stylissa carteri* by metatranscriptomics. *Environ Microbiol,* 16**,** 3683-98.

MOITINHO-SILVA, L., STEINERT, G., NIELSEN, S., HARDOIM, C. C. P., WU, Y.-C., MCCORMACK, G. P., LOPEZ-LEGENTIL, S., MARCHANT, R., WEBSTER, N., THOMAS, T. & HENTSCHEL, U. 2017b. Predicting the HMA-LMA status in marine sponges by machine learning. *Front Micrbiol,* 8.

MOMENI, B., BRILEYA, K. A., FIELDS, M. W. & SHOU, W. 2013. Strong inter-population cooperation leads to partner intermixing in microbial communities. *eLife,* 2**,** e00230.

MORAN, N. A. & SLOAN, D. B. 2015. The Hologenome concept: helpful or hollow? *PLoS Biol,* 13**,** e1002311-e1002311.

MORELLA, N. M., GOMEZ, A. L., WANG, G., LEUNG, M. S. & KOSKELLA, B. 2018. The impact of bacteriophages on phyllosphere bacterial abundance and composition. *Molecular Ecology,* 27**,** 2025-2038.

MORENO-GALLEGO, J. L., CHOU, S.-P., DI RIENZI, S. C., GOODRICH, J. K., SPECTOR, T. D., BELL, J. T., YOUNGBLUT, N. D., HEWSON, I., REYES, A. & LEY, R. E. 2019. Virome Diversity Correlates with Intestinal Microbiome Diversity in Adult Monozygotic Twins. *Cell Host & Microbe,* 25**,** 261-272.e5.

MORGANTI, T., COMA, R., YAHEL, G. & RIBES, M. 2017. Trophic niche separation that facilitates co-existence of high and low microbial abundance sponges is revealed by *in situ* study of carbon and nitrogen fluxes. *Limnol Oceanogr,* 62**,** 1963-1983.

MOYA, A., PERETÓ, J., GIL, R. & LATORRE, A. 2008. Learning how to live together: genomic insights into prokaryote–animal symbioses. *Nat Rev Genet,* 9**,** 218.

MURILLO-RINCON, A. P., KLIMOVICH, A., PEMÖLLER, E., TAUBENHEIM, J., MORTZFELD, B., AUGUSTIN, R. & BOSCH, T. C. G. 2017. Spontaneous body contractions are modulated by the microbiome of *Hydra*. *Sci Rep,* 7**,** 15937.

MUSAT, N., STRYHANYUK, H., BOMBACH, P., ADRIAN, L., AUDINOT, J.-N. & RICHNOW, H. H. 2014. The effect of FISH and CARD-FISH on the isotopic composition of 13C- and 15N-labeled Pseudomonas putida cells measured by nanoSIMS. *Systematic and Applied Microbiology,* 37**,** 267-276.

NANRA, J. S., BUITRAGO, S. M., CRAWFORD, S., NG, J., FINK, P. S., HAWKINS, J., SCULLY, I. L., MCNEIL, L. K., ASTE-AMÉZAGA, J. M., COOPER, D., JANSEN, K. U. & ANDERSON, A. S. 2013. Capsular polysaccharides are an important immune evasion mechanism for Staphylococcus aureus. *Human Vaccines & Immunotherapeutics,* 9**,** 480-487.

NGUYEN-KIM, H., BETTAREL, Y., BOUVIER, T., BOUVIER, C., DOAN-NHU, H., NGUYEN-NGOC, L., NGUYEN-THANH, T., TRAN-QUANG, H. & BRUNE, J. 2015. Coral Mucus Is a Hot Spot for Viral Infections. *Applied and Environmental Microbiology,* 81**,** 5773-5783.

NGUYEN-KIM, H., BOUVIER, T., BOUVIER, C., DOAN-NHU, H., NGUYEN-NGOC, L., ROCHELLE-NEWALL, E., BAUDOUX, A.-C., DESNUES, C., REYNAUD, S., FERRIER-PAGES, C. & BETTAREL, Y. 2014. High occurrence of viruses in the mucus layer of scleractinian corals. *Environmental Microbiology Reports,* 6**,** 675-682.

NGUYEN, M. T., LIU, M. & THOMAS, T. 2014. Ankyrin-repeat proteins from sponge symbionts modulate amoebal phagocytosis. *Mol Ecol,* 23**,** 1635-45.

NICHOLS, S. A., ROBERTS, B. W., RICHTER, D. J., FAIRCLOUGH, S. R. & KING, N. 2012. Origin of metazoan cadherin diversity and the antiquity of the classical cadherin/β-catenin complex. *PNAS,* 109**,** 13046-13051.

NICKEL, M. 2004. Kinetics and rhythm of body contractions in the sponge Tethya wilhelma (Porifera: Demospongiae). *J Exp Biol,* 207**,** 4515-24.

NIELSEN, L. T., ASADZADEH, S. S., DOLGER, J., WALTHER, J. H., KIORBOE, T. & ANDERSEN, A. 2017. Hydrodynamics of microbial filter feeding. *PNAS,* 114**,** 9373-9378.

NISHIGUCHI, M. K., RUBY, E. G. & MCFALL-NGAI, M. J. 1998. Competitive dominance among strains of luminous bacteria provides an unusual form of evidence for parallel evolution in Sepiolid Squid-*Vibrio* Symbioses. *Appl Environ Microbiol,* 64**,** 3209-3213.

NYHOLM, S. V. & MCFALL-NGAI, M. 2004. The winnowing: establishing the squid–vibrio symbiosis. *Nat Rev Microbiol,* 2**,** 632-642.

O'BRIEN, P. A., WEBSTER, N. S., MILLER, D. J. & BOURNE, D. G. 2019. Host-microbe coevolution: applying evidence from model systems to complex marine invertebrate holobionts. *MBio,* 10**,** e02241-18.

OROSCO, F. L. & LLUISMA, A. O. 2017. Variation in virome diversity in wild populations of *Penaeus monodon* (Fabricius 1798) with emphasis on pathogenic viruses. *Virus disease,* 28**,** 262-271.

ORTH, J. D., THIELE, I. & PALSSON, B. Ø. 2010. What is flux balance analysis? *Nature Biotechnology,* 28**,** 245.

OWEN, S. V., CANALS, R., WENNER, N., HAMMARLÖF, D. L., KRÖGER, C. & HINTON, J. C. D. 2019. A window into lysogeny: Revealing temperate phage biology with transcriptomics. *bioRxiv***,** 787010.

PAEZ-ESPINO, D., ELOE-FADROSH, E. A., PAVLOPOULOS, G. A., THOMAS, A. D., HUNTEMANN, M., MIKHAILOVA, N., RUBIN, E., IVANOVA, N. N. & KYRPIDES, N. C. 2016. Uncovering Earth's virome. *Nature,* 536**,** 425.

PAEZ-ESPINO, D., ROUX, S., CHEN, I.-MIN A., PALANIAPPAN, K., RATNER, A., CHU, K., HUNTEMANN, M., REDDY, T B K., PONS, JOAN C., LLABRÉS, M., ELOE-FADROSH, EMILEY A., IVANOVA, NATALIA N. & KYRPIDES, NIKOS C. 2018. IMG/VR v.2.0: an integrated data management and analysis system for cultivated and environmental viral genomes. *Nucleic Acids Research,* 47**,** D678-D686.

PAN, X., LÜHRMANN, A., SATOH, A., LASKOWSKI-ARCE, M. A. & ROY, C. R. 2008. Ankyrin repeat proteins comprise a diverse family of bacterial Type IV effectors. *Science,* 320**,** 1651-1654.

PANDE, S., MERKER, H., BOHL, K., REICHELT, M., SCHUSTER, S., DE FIGUEIREDO, L. F., KALETA, C. & KOST, C. 2014. Fitness and stability of obligate cross-feeding interactions that emerge upon gene loss in bacteria. *ISME J,* 8**,** 953-962.

PARK, J., KIM, K. J., CHOI, K.-S., GRAB, D. J. & DUMLER, J. S. 2004. Anaplasma phagocytophilum AnkA binds to granulocyte DNA and nuclear proteins. *Cellular Microbiology,* 6**,** 743-751.

PASCELLI, C., LAFFY, P. W., KUPRESANIN, M., RAVASI, T. & WEBSTER, N. S. 2018. Morphological characterization of virus-like particles in coral reef sponges. *PeerJ,* 6**,** e5625-e5625.

PAUL-GILLOTEAUX, P., HEILIGENSTEIN, X., BELLE, M., DOMART, M. C., LARIJANI, B., COLLINSON, L., RAPOSO, G. & SALAMERO, J. 2017. eC-CLEM: flexible multidimensional registration software for correlative microscopies. *Nat Methods,* 14**,** 102-103.

PILE, A. J., PATTERSON, M. R., SAVARESE, M., CHERNYKH, V. I. & FIALKOV, V. A. 1997. Trophic effects of sponge feeding within Lake Baikal's littoral zone. 2. Sponge abundance, diet, feeding efficiency, and carbon flux. *Limnol Oceanogr,* 42**,** 178-184.

PILE, A. J., PATTERSON, M. R. & WITMAN, J. D. 1996. *In situ* grazing on plankton < 10 μm by the boreal sponge *Mycale lingua*. *Mar Ecol Prog Ser,* 141**,** 95-102.

PITA, L., HOEPPNER, M. P., RIBES, M. & HENTSCHEL, U. 2018a. Differential expression of immune receptors in two marine sponges upon exposure to microbial-associated molecular patterns. *Sci Rep,* 8.

PITA, L., RIX, L., SLABY, B. M., FRANKE, A. & HENTSCHEL, U. 2018b. The sponge holobiont in a changing ocean: from microbes to ecosystems. *Microbiome,* 6.

PITA, L., TURON, X., LOPEZ-LEGENTIL, S. & ERWIN, P. M. 2013. Host rules: spatial stability of bacterial communities associated with marine sponges (*Ircinia* spp.) in the Western Mediterranean Sea. *FEMS Microbiol Ecol,* 86**,** 268-76.

PODELL, S., BLANTON, J. M., NEU, A., AGARWAL, V., BIGGS, J. S., MOORE, B. S. & ALLEN, E. E. 2018. Pangenomic comparison of globally distributed *Poribacteria* associated with sponge hosts and marine particles. *ISME J*.

PODELL, S., BLANTON, J. M., NEU, A., AGARWAL, V., BIGGS, J. S., MOORE, B. S. & ALLEN, E. E. 2019. Pangenomic comparison of globally distributed *Poribacteria* associated with sponge hosts and marine particles. *ISME J,* 13**,** 468-481.

POLLOCK, F. J., MCMINDS, R., SMITH, S., BOURNE, D. G., WILLIS, B. L., MEDINA, M., THURBER, R. V. & ZANEVELD, J. R. 2018. Coral-associated bacteria demonstrate phylosymbiosis and cophylogeny. *Nat Commun,* 9**,** 4921.

PRICE, C. T. D., AL-KHODOR, S., AL-QUADAN, T. & ABU KWAIK, Y. 2010. Indispensable role for the eukaryotic-like ankyrin domains of the ankyrin B effector of *Legionella pneumophila* within macrophages and amoebae. *Infect Immun,* 78**,** 2079-2088.

QUELLER, D. C. & STRASSMANN, J. E. 2016. Problems of multi-species organisms: endosymbionts to holobionts. *Biology & Philosophy,* 31**,** 855-873.

RADAX, R., RATTEI, T., LANZEN, A., BAYER, C., RAPP, H. T., URICH, T. & SCHLEPER, C. 2012. Metatranscriptomics of the marine sponge *Geodia barretti*: tackling phylogeny and function of its microbial community. *Environ Microbiol,* 14**,** 1308-1324.

RAE, B. D., LONG, B. M., BADGER, M. R. & PRICE, G. D. 2013. Functions, compositions, and evolution of the two types of carboxysomes: polyhedral microcompartments that facilitate CO2 fixation in cyanobacteria and some proteobacteria. *Microbiology and molecular biology reviews : MMBR,* 77**,** 357-379.

REISWIG, H. M. 1971. Particle feeding in natural populations of three marine demosponges. *Biol Bull,* 141**,** 568-&.

REISWIG, H. M. 1974. Water transport, respiration and energetics of three tropical marine sponges. *J Exp Mar Bio Ecol,* 14**,** 231-249.

REISWIG, H. M. 1981. Partial Carbon and Energy Budgets of the Bacteriosponge Verohgia fistularis (*Porifera*: *Demospongiae*) in Barbados. *Mar Ecol,* 2**,** 273-293.

REN, D., MADSEN, J. S., SØRENSEN, S. J. & BURMØLLE, M. 2015. High prevalence of biofilm synergy among bacterial soil isolates in cocultures indicates bacterial interspecific cooperation. *ISME J,* 9**,** 81-89.

REPETA, D. J., QUAN, T. M., ALUWIHARE, L. I. & ACCARDI, A. 2002. Chemical characterization of high molecular weight dissolved organic matter in fresh and marine waters. *Geochim Cosmochim Acta,* 66**,** 955-962.

REVEILLAUD, J., MAIGNIEN, L., EREN, A. M., HUBER, J. A., APPRILL, A., SOGIN, M. L. & VANREUSEL, A. 2014. Host-specificity among abundant and rare taxa in the sponge microbiome. *ISME J,* 8**,** 1198.

REYES, M. L., LAUGHTON, A. M., PARKER, B. J., WICHMANN, H., FAN, M., SOK, D., HRČEK, J., ACEVEDO, T. & GERARDO, N. M. 2019. The influence of symbiotic bacteria on reproductive strategies and wing polyphenism in pea aphids responding to stress. *J Anim Ecol,* 88**,** 601-611.

REYNOLDS, D. & THOMAS, T. 2016. Evolution and function of eukaryotic-like proteins from sponge symbionts. *Mol Ecol,* 25**,** 5242-5253.

RIBES, M., COMA, R. & GILI, J. M. 1999. Natural diet and grazing rate of the temperate sponge *Dysidea avara* (Demospongiae, Dendroceratida) throughout an annual cycle. *Mar Ecol Prog Ser,* 176**,** 179-190.

RIESGO, A., FARRAR, N., WINDSOR, P. J., GIRIBET, G. & LEYS, S. P. 2014. The analysis of eight transcriptomes from all poriferan classes reveals surprising genetic complexity in sponges. *Mol Biol Evol,* 31**,** 1102-1120.

RIX, L., DE GOEIJ, J. M., MUELLER, C. E., STRUCK, U., MIDDELBURG, J. J., VAN DUYL, F. C., AL-HORANI, F. A., WILD, C., NAUMANN, M. S. & VAN OEVELEN, D. 2016. Coral mucus fuels the sponge loop in warm- and cold-water coral reef ecosystems. *Sci Rep,* 6**,** 18715.

RIX, L., DE GOEIJ, J. M., VAN OEVELEN, D., STRUCK, U., AL-HORANI, F. A., WILD, C. & NAUMANN, M. S. 2017a. Differential recycling of coral and algal dissolved organic matter via the sponge loop. *Funct Ecol,* 31**,** 778-789.

RIX, L., DE GOEIJ, J. M., VAN OEVELEN, D., STRUCK, U., AL-HORANI, F. A., WILD, C. & NAUMANN, M. S. 2017b. Differential recycling of coral and algal dissolved organic matter via the sponge loop. *Functional Ecology,* 31**,** 778-789.

ROBERTS, I. S. 1996. THE BIOCHEMISTRY AND GENETICS OF CAPSULAR POLYSACCHARIDE PRODUCTION IN BACTERIA. *Annual Review of Microbiology,* 50**,** 285-315.

ROSENBERG, E., KOREN, O., RESHEF, L., EFRONY, R. & ZILBER-ROSENBERG, I. 2007. The role of microorganisms in coral health, disease and evolution. *Nat Rev Microbiol,* 5**,** 355.

ROSS, A. A., MÜLLER, K. M., WEESE, J. S. & NEUFELD, J. D. 2018. Comprehensive skin microbiome analysis reveals the uniqueness of human skin and evidence for phylosymbiosis within the class Mammalia. *PNAS,* 115**,** E5786-E5795.

ROTHSCHILD, D., WEISSBROD, O., BARKAN, E., KURILSHIKOV, A., KOREM, T., ZEEVI, D., COSTEA, P. I., GODNEVA, A., KALKA, I. N., BAR, N., SHILO, S., LADOR, D., VILA, A. V., ZMORA, N., PEVSNER-FISCHER, M., ISRAELI, D., KOSOWER, N., MALKA, G., WOLF, B. C., AVNIT-SAGI, T., LOTAN-POMPAN, M., WEINBERGER, A., HALPERN, Z., CARMI, S., FU, J., WIJMENGA, C., ZHERNAKOVA, A., ELINAV, E. & SEGAL, E. 2018. Environment dominates over host genetics in shaping human gut microbiota. *Nature,* 555**,** 210.

ROUX, S. 2019. A viral ecogenomics framework to uncover the secrets of nature's "microbe whisperers". *mSystems,* 4**,** e00111-19.

ROUX, S., BRUM, J. R., DUTILH, B. E., SUNAGAWA, S., DUHAIME, M. B., LOY, A., POULOS, B. T., SOLONENKO, N., LARA, E., POULAIN, J., PESANT, S., KANDELS-LEWIS, S., DIMIER, C., PICHERAL, M., SEARSON, S., CRUAUD, C., ALBERTI, A., DUARTE, C. M., GASOL, J. M., VAQUÉ, D., TARA OCEANS, C., BORK, P., ACINAS, S. G., WINCKER, P. & SULLIVAN, M. B. 2016. Ecogenomics and potential biogeochemical impacts of globally abundant ocean viruses. *Nature,* 537**,** 689.

RUBIN-BLUM, M., ANTONY, C. P., SAYAVEDRA, L., MARTÍNEZ-PÉREZ, C., BIRGEL, D., PECKMANN, J., WU, Y.-C., CARDENAS, P., MACDONALD, I., MARCON, Y., SAHLING, H., HENTSCHEL, U. & DUBILIER, N. 2019. Fueled by methane: deep-sea sponges from asphalt seeps gain their nutrition from methane-oxidizing symbionts. *ISME J,* 13**,** 1209-1225.

RUDMAN, S. M., GREENBLUM, S., HUGHES, R. C., RAJPUROHIT, S., KIRATLI, O., LOWDER, D. B., LEMMON, S. G., PETROV, D. A., CHASTON, J. M. & SCHMIDT, P. 2019. Microbiome composition shapes rapid genomic adaptation of *Drosophila melanogaster*. *PNAS***,** 201907787.

RUSSELL, C. W., BOUVAINE, S., NEWELL, P. D. & DOUGLAS, A. E. 2013. Shared metabolic pathways in a coevolved insect-bacterial symbiosis. *Appl Environ Microbiol,* 79**,** 6117-6123.

RYU, T., SERIDI, L., MOITINHO-SILVA, L., OATES, M., LIEW, Y. J., MAVROMATIS, C., WANG, X., HAYWOOD, A., LAFI, F. F., KUPRESANIN, M., SOUGRAT, R., ALZAHRANI, M. A., GILES, E., GHOSHEH, Y., SCHUNTER, C., BAUMGARTEN, S., BERUMEN, M. L., GAO, X., ARANDA, M., FORET, S., GOUGH, J., VOOLSTRA, C. R., HENTSCHEL, U. & RAVASI, T. 2016. Hologenome analysis of two marine sponges with different microbiomes. *BMC Genomics,* 17**,** 1-11.

SACHDEV, S., HOFFMANN, A. & HANNINK, M. 1998. Nuclear localization of IkappaB alpha is mediated by the second ankyrin repeat: the IkappaB alpha ankyrin repeats define a novel class of cis-acting nuclear import sequences. *Mol Cell Biol,* 18**,** 2524-34.

SALEM, H., BAUER, E., KIRSCH, R., BERASATEGUI, A., CRIPPS, M., WEISS, B., KOGA, R., FUKUMORI, K., VOGEL, H., FUKATSU, T. & KALTENPOTH, M. 2017. Drastic genome reduction in an herbivore's pectinolytic symbiont. *Cell,* 171**,** 1520-1531.e13.

SAMPSON, E. M. & BOBIK, T. A. 2008. Microcompartments for B12-dependent 1,2-propanediol degradation provide protection from DNA and cellular damage by a reactive metabolic intermediate. *J Bacteriol,* 190**,** 2966-71.

SANGER, F., BROWNLEE, G. G. & BARRELL, B. G. 1965. A two-dimensional fractionation procedure for radioactive nucleotides. *J Mol Biol,* 13**,** 373-98.

SANTAVY, D. L., WILLENZ, P. & COLWELL, R. R. 1990. Phenotypic study of bacteria associated with the caribbean sclerosponge, *Ceratoporella nicholsoni*. *Appl Environ Microbiol,* 56**,** 1750-1762.

SAXENA, R. K., ANAND, P., SARAN, S., ISAR, J. & AGARWAL, L. 2010. Microbial production and applications of 1,2-propanediol. *Indian J Microbiol,* 50**,** 2-11.

SCHLÄPPY, M.-L., WEBER, M., MENDOLA, D., HOFFMANN, F. & DE BEER, D. 2010. Heterogeneous oxygenation resulting from active and passive flow in two Mediterranean sponges, *Dysida avara* and *Chondrosia reniformis*. *Limnol Oceanogr,* 55**,** 1289-1300.

SCHMITT, S., ANGERMEIER, H., SCHILLER, R., LINDQUIST, N. & HENTSCHEL, U. 2008. Molecular microbial diversity survey of sponge reproductive stages and mechanistic insights into vertical transmission of microbial symbionts. *Appl Environ Microbiol,* 74**,** 7694-708.

SCHMITT, S., DEINES, P., BEHNAM, F., WAGNER, M. & TAYLOR, M. W. 2011. *Chloroflexi* bacteria are more diverse, abundant, and similar in high than in low microbial abundance sponges. *FEMS Microbiol Ecol,* 78**,** 497-510.

SCHMITT, S., TSAI, P., BELL, J., FROMONT, J., ILAN, M., LINDQUIST, N., PEREZ, T., RODRIGO, A., SCHUPP, P. J., VACELET, J., WEBSTER, N., HENTSCHEL, U. & TAYLOR, M. W. 2012. Assessing the complex sponge microbiota: core, variable and species-specific bacterial communities in marine sponges. *ISME J,* 6**,** 564-576.

SCHÖNBERG, C. H. L., FANG, J. K.-H. & CARBALLO, J. L. 2017. Bioeroding sponges and the future of coral reefs. *In:* CARBALLO, J. L. & BELL, J. J. (eds.) *Climate change, ocean acidification and sponges: impacts across multiple levels of organization.* Cham: Springer International Publishing.

SCHRETTER, C. E., VIELMETTER, J., BARTOS, I., MARKA, Z., MARKA, S., ARGADE, S. & MAZMANIAN, S. K. 2018. A gut microbial factor modulates locomotor behaviour in *Drosophila*. *Nature,* 563**,** 402-406.

SCHULTHESS, J., PANDEY, S., CAPITANI, M., RUE-ALBRECHT, K. C., ARNOLD, I., FRANCHINI, F., CHOMKA, A., ILOTT, N. E., JOHNSTON, D. G. W., PIRES, E., MCCULLAGH, J., SANSOM, S. N., ARANCIBIA-CARCAMO, C. V., UHLIG, H. H. & POWRIE, F. 2019. The short chain fatty acid butyrate imprints an antimicrobial program in macrophages. *Immunity,* 50**,** 432-445.e7.

SEN, R. & BALTIMORE, D. 1986. Multiple nuclear factors interact with the immunoglobulin enhancer sequences. *Cell,* 46**,** 705-16.

SHABAT, S. K. B., SASSON, G., DORON-FAIGENBOIM, A., DURMAN, T., YAACOBY, S., BERG MILLER, M. E., WHITE, B. A., SHTERZER, N. & MIZRAHI, I. 2016. Specific microbiome-dependent mechanisms underlie the energy harvest efficiency of ruminants. *ISME J,* 10**,** 2958.

SHAPIRA, M. 2016. Gut microbiotas and host evolution: scaling up symbiosis. *Trends Ecol Evol,* 31**,** 539-549.

SHI, M., LIN, X.-D., TIAN, J.-H., CHEN, L.-J., CHEN, X., LI, C.-X., QIN, X.-C., LI, J., CAO, J.-P., EDEN, J.-S., BUCHMANN, J., WANG, W., XU, J., HOLMES, E. C. & ZHANG, Y.-Z. 2016. Redefining the invertebrate RNA virosphere. *Nature,* 540**,** 539.

SHIH, J. L., SELPH, K. E., WALL, C. B., WALLSGROVE, N. J., LESSER, M. P. & POPP, B. N. 2019. Trophic ecology of the tropical pacific sponge *Mycale grandis i*nferred from amino acid compound-specific isotopic analyses. *Microb Ecol*.

SHIKUMA, N. J., PILHOFER, M., WEISS, G. L., HADFIELD, M. G., JENSEN, G. J. & NEWMAN, D. K. 2014. Marine tubeworm metamorphosis induced by arrays of bacterial phage tail–like structures. *Science,* 343**,** 529-533.

SHKOPOROV, A. N., CLOONEY, A. G., SUTTON, T. D. S., RYAN, F. J., DALY, K. M., NOLAN, J. A., MCDONNELL, S. A., KHOKHLOVA, E. V., DRAPER, L. A., FORDE, A., GUERIN, E., VELAYUDHAN, V., ROSS, R. P. & HILL, C. 2019. The human gut virome is highly diverse, stable, and individual specific. *Cell Host Microbe,* 26**,** 527-541.e5.

SHROPSHIRE, J. D. & BORDENSTEIN, S. R. 2019. Two-by-one model of cytoplasmic incompatibility: Synthetic recapitulation by transgenic expression of cifA and cifB in *Drosophila*. *PLoS Genet,* 15**,** e1008221.

SIEGL, A., KAMKE, J., HOCHMUTH, T., PIEL, J., RICHTER, M., LIANG, C., DANDEKAR, T. & HENTSCHEL, U. 2011. Single-cell genomics reveals the lifestyle of *Poribacteria*, a candidate phylum symbiotically associated with marine sponges. *ISME J,* 5**,** 61-70.

SIMISTER, R. L., DEINES, P., BOTTÉ, E. S., WEBSTER, N. S. & TAYLOR, M. W. 2012. Sponge-specific clusters revisited: a comprehensive phylogeny of sponge-associated microorganisms. *Environmental Microbiology,* 14**,** 517-524.

SIMMONS, M., DRESCHER, K., NADELL, C. D. & BUCCI, V. 2018. Phage mobility is a core determinant of phage–bacteria coexistence in biofilms. *The ISME Journal,* 12**,** 531-543.

SIMMONS, T. L., COATES, R. C., CLARK, B. R., ENGENE, N., GONZALEZ, D., ESQUENAZI, E., DORRESTEIN, P. C. & GERWICK, W. H. 2008. Biosynthetic origin of natural products isolated from marine microorganism–invertebrate assemblages. *PNAS*, 105**,** 4587-4594.

SIMONET, P., GAGET, K., BALMAND, S., RIBEIRO LOPES, M., PARISOT, N., BUHLER, K., DUPORT, G., VULSTEKE, V., FEBVAY, G., HEDDI, A., CHARLES, H., CALLAERTS, P. & CALEVRO, F. 2018. Bacteriocyte cell death in the pea aphid *Buchnera* symbiotic system. *PNAS*, 115**,** E1819-E1828.

SIMONSEN, A. K., DINNAGE, R., BARRETT, L. G., PROBER, S. M. & THRALL, P. H. 2017. Symbiosis limits establishment of legumes outside their native range at a global scale. *Nat Commun*, 8**,** 14790.

SIMPSON, T. L. 1984. *The cell biology of sponges*, New York, Springer-Verlag.

SLABY, B. M., HACKL, T., HORN, H., BAYER, K. & HENTSCHEL, U. 2017. Metagenomic binning of a marine sponge microbiome reveals unity in defense but metabolic specialization. *ISME J*, 11**,** 2465.

SOFFER, N., BRANDT, M. E., CORREA, A. M. S., SMITH, T. B. & THURBER, R. V. 2013. Potential role of viruses in white plague coral disease. *The Isme Journal*, 8**,** 271.

SOGABE, S., HATLEBERG, W. L., KOCOT, K. M., SAY, T. E., STOUPIN, D., ROPER, K. E., FERNANDEZ-VALVERDE, S. L., DEGNAN, S. M. & DEGNAN, B. M. 2019. Pluripotency and the origin of animal multicellularity. *Nature*, 570**,** 519-522.

SONNBERG, S., SEET, B. T., PAWSON, T., FLEMING, S. B. & MERCER, A. A. 2008. Poxvirus ankyrin repeat proteins are a unique class of F-box proteins that associate with cellular SCF1 ubiquitin ligase complexes. *Proceedings of the National Academy of Sciences*, 105**,** 10955-10960.

SOUTHWELL, M. W., POPP, B. N. & MARTENS, C. S. 2008. Nitrification controls on fluxes and isotopic composition of nitrate from Florida Keys sponges. *Mar Chem*, 108**,** 96-108.

SRIVASTAVA, M., SIMAKOV, O., CHAPMAN, J., FAHEY, B., GAUTHIER, M. E. A., MITROS, T., RICHARDS, G. S., CONACO, C., DACRE, M. & HELLSTEN, U. 2010. The *Amphimedon queenslandica* genome and the evolution of animal complexity. *Nature*, 466.

STEIDINGER, B. S., CROWTHER, T. W., LIANG, J., VAN NULAND, M. E., WERNER, G. D. A., REICH, P. B., NABUURS, G., DE-MIGUEL, S., ZHOU, M., PICARD, N., HERAULT, B., ZHAO, X., ZHANG, C., ROUTH, D., PEAY, K. G., ABEGG, M., ADOU YAO, C. Y., ALBERTI, G., ALMEYDA ZAMBRANO, A., ALVAREZ-DAVILA, E., ALVAREZ-LOAYZA, P., ALVES, L. F., AMMER, C., ANTÓN-FERNÁNDEZ, C., ARAUJO-MURAKAMI, A., ARROYO, L., AVITABILE, V., AYMARD, G., BAKER, T., BAŁAZY, R., BANKI, O., BARROSO, J., BASTIAN, M., BASTIN, J.-F., BIRIGAZZI, L., BIRNBAUM, P., BITARIHO, R., BOECKX, P., BONGERS, F., BOURIAUD, O., BRANCALION, PEDRO H. S., BRANDL, S., BREARLEY, F. Q., BRIENEN, R., BROADBENT, E., BRUELHEIDE, H., BUSSOTTI, F., CAZZOLLA GATTI, R., CESAR, R., CESLJAR, G., CHAZDON, R., CHEN, H. Y. H., CHISHOLM, C., CIENCIALA, E., CLARK, C. J., CLARK, D., COLLETTA, G., CONDIT, R., COOMES, D., CORNEJO VALVERDE, F., CORRAL-RIVAS, J. J., CRIM, P., CUMMING, J., DAYANANDAN, S., DE GASPER, A. L., DECUYPER, M., DERROIRE, G., DEVRIES, B., DJORDJEVIC, I., IÊDA, A., DOURDAIN, A., OBIANG, N. L. E., ENQUIST, B., EYRE, T., FANDOHAN, A. B., FAYLE, T. M., FELDPAUSCH, T. R., FINÉR, L., FISCHER, M., FLETCHER, C., FRIDMAN, J., FRIZZERA, L., GAMARRA, J. G. P., GIANELLE, D., GLICK, H. B., HARRIS, D., HECTOR, A., HEMP, A., HENGEVELD, G., HERBOHN, J., HEROLD, M., HILLERS, A., HONORIO CORONADO, E. N., HUBER, M., HUI, C., CHO, H., IBANEZ, T., JUNG, I., IMAI, N., JAGODZINSKI, A. M., et al. 2019. Climatic controls of decomposition drive the global biogeography of forest-tree symbioses. *Nature*, 569**,** 404-408.

STEINDLER, L., SCHUSTER, S., ILAN, M., AVNI, A., CERRANO, C. & BEER, S. 2007. Differential gene expression in a marine sponge in relation to its symbiotic state. *Mar Biotechnol (NY)*, 9**,** 543-549.

STEINERT, G., GUTLEBEN, J., ATIKANA, A., WIJFFELS, R. H., SMIDT, H. & SIPKEMA, D. 2018a. Coexistence of poribacterial phylotypes among geographically widespread and phylogenetically divergent sponge hosts. *Environ Microbiol Rep*, 10**,** 80-91.

STEINERT, G., GUTLEBEN, J., ATIKANA, A., WIJFFELS, R. H., SMIDT, H. & SIPKEMA, D. 2018b. Coexistence of poribacterial phylotypes among geographically widespread and phylogenetically divergent sponge hosts. *Environmental Microbiology Reports,* 10**,** 80-91.

STEINERT, G., TAYLOR, M. W., DEINES, P., SIMISTER, R. L., DE VOOGD, N. J., HOGGARD, M. & SCHUPP, P. J. 2016. In four shallow and mesophotic tropical reef sponges from Guam the microbial community largely depends on host identity. *PeerJ,* 4**,** e1936.

SULLIVAN, M. B., WATERBURY, J. B. & CHISHOLM, S. W. 2003. Cyanophages infecting the oceanic cyanobacterium Prochlorococcus. *Nature,* 424**,** 1047-1051.

SURANA, N. K. & KASPER, D. L. 2012. The yin yang of bacterial polysaccharides: lessons learned from B. fragilis PSA. *Immunological Reviews,* 245**,** 13-26.

SWEERE, J. M., VAN BELLEGHEM, J. D., ISHAK, H., BACH, M. S., POPESCU, M., SUNKARI, V., KABER, G., MANASHEROB, R., SUH, G. A., CAO, X., DE VRIES, C. R., LAM, D. N., MARSHALL, P. L., BIRUKOVA, M., KATZNELSON, E., LAZZARESCHI, D. V., BALAJI, S., KESWANI, S. G., HAWN, T. R., SECOR, P. R. & BOLLYKY, P. L. 2019. Bacteriophage trigger antiviral immunity and prevent clearance of bacterial infection. *Science,* 363**,** eaat9691.

TAYLOR, M. W., RADAX, R., STEGER, D. & WAGNER, M. 2007. Sponge-associated microorganisms: Evolution, ecology, and biotechnological potential. *Microbiol Mol Biol Rev.,* 71**,** 295-+.

TAYLOR, M. W., TSAI, P., SIMISTER, R. L., DEINES, P., BOTTE, E., ERICSON, G., SCHMITT, S. & WEBSTER, N. S. 2013. 'Sponge-specific' bacteria are widespread (but rare) in diverse marine environments. *ISME J,* 7**,** 438-43.

THACKER, R. W., HILL, A. L., HILL, M. S., REDMOND, N. E., COLLINS, A. G., MORROW, C. C., SPICER, L., CARMACK, C. A., ZAPPE, M. E., POHLMANN, D., HALL, C., DIAZ, M. C. & BANGALORE, P. V. 2013. Nearly complete 28S rRNA gene sequences confirm new hypotheses of sponge evolution. *Integr Comp Biol,* 53**,** 373-387.

THEIS, K. R., DHEILLY, N. M., KLASSEN, J. L., BRUCKER, R. M., BAINES, J. F., BOSCH, T. C. G., CRYAN, J. F., GILBERT, S. F., GOODNIGHT, C. J., LLOYD, E. A., SAPP, J., VANDENKOORNHUYSE, P., ZILBER-ROSENBERG, I., ROSENBERG, E. & BORDENSTEIN, S. R. 2016. Getting the hologenome concept right: an eco-evolutionary framework for hosts and their microbiomes. *mSystems,* 1**,** e00028-16.

THIENNIMITR, P., WINTER, S. E., WINTER, M. G., XAVIER, M. N., TOLSTIKOV, V., HUSEBY, D. L., STERZENBACH, T., TSOLIS, R. M., ROTH, J. R. & BAUMLER, A. J. 2011. Intestinal inflammation allows Salmonella to use ethanolamine to compete with the microbiota. *Proc Natl Acad Sci U S A,* 108**,** 17480-5.

THINGSTAD, T. F. 2000. Elements of a theory for the mechanisms controlling abundance, diversity, and biogeochemical role of lytic bacterial viruses in aquatic systems. *Limnology and Oceanography,* 45**,** 1320-1328.

THINGSTAD, T. F., VAGE, S., STORESUND, J. E., SANDAA, R. A. & GISKE, J. 2014. A theoretical analysis of how strain-specific viruses can control microbial species diversity. *PNAS,* 111**,** 7813-8.

THOMAS, T., MOITINHO-SILVA, L., LURGI, M., BJORK, J. R., EASSON, C., ASTUDILLO-GARCIA, C., OLSON, J. B., ERWIN, P. M., LOPEZ-LEGENTIL, S., LUTER, H., CHAVES-FONNEGRA, A., COSTA, R., SCHUPP, P. J., STEINDLER, L., ERPENBECK, D., GILBERT, J., KNIGHT, R., ACKERMANN, G., VICTOR LOPEZ, J., TAYLOR, M. W., THACKER, R. W., MONTOYA, J. M., HENTSCHEL, U. & WEBSTER, N. S. 2016. Diversity, structure and convergent evolution of the global sponge microbiome. *Nat Commun,* 7**,** 11870.

THOMAS, T., RUSCH, D., DEMAERE, M. Z., YUNG, P. Y., LEWIS, M., HALPERN, A., HEIDELBERG, K. B., EGAN, S., STEINBERG, P. D. & KJELLEBERG, S. 2010. Functional genomic signatures of sponge bacteria reveal unique and shared features of symbiosis. *ISME J,* 4**,** 1557.

THOMPSON, L. R., SANDERS, J. G., MCDONALD, D., AMIR, A., LADAU, J., LOCEY, K. J., PRILL, R. J., TRIPATHI, A., GIBBONS, S. M., ACKERMANN, G., NAVAS-MOLINA, J. A., JANSSEN, S., KOPYLOVA, E., VÁZQUEZ-BAEZA, Y., GONZÁLEZ, A., MORTON, J. T., MIRARAB, S., ZECH XU, Z., JIANG, L., HAROON, M. F., KANBAR, J., ZHU, Q., JIN

SONG, S., KOSCIOLEK, T., BOKULICH, N. A., LEFLER, J., BRISLAWN, C. J., HUMPHREY, G., OWENS, S. M., HAMPTON-MARCELL, J., BERG-LYONS, D., MCKENZIE, V., FIERER, N., FUHRMAN, J. A., CLAUSET, A., STEVENS, R. L., SHADE, A., POLLARD, K. S., GOODWIN, K. D., JANSSON, J. K., GILBERT, J. A., KNIGHT, R., THE EARTH MICROBIOME PROJECT, C., RIVERA, J. L. A., AL-MOOSAWI, L., ALVERDY, J., AMATO, K. R., ANDRAS, J., ANGENENT, L. T., ANTONOPOULOS, D. A., APPRILL, A., ARMITAGE, D., BALLANTINE, K., BÁRTA, J. Í., BAUM, J. K., BERRY, A., BHATNAGAR, A., BHATNAGAR, M., BIDDLE, J. F., BITTNER, L., BOLDGIV, B., BOTTOS, E., BOYER, D. M., BRAUN, J., BRAZELTON, W., BREARLEY, F. Q., CAMPBELL, A. H., CAPORASO, J. G., CARDONA, C., CARROLL, J., CARY, S. C., CASPER, B. B., CHARLES, T. C., CHU, H., CLAAR, D. C., CLARK, R. G., CLAYTON, J. B., CLEMENTE, J. C., COCHRAN, A., COLEMAN, M. L., COLLINS, G., COLWELL, R. R., CONTRERAS, M., CRARY, B. B., CREER, S., CRISTOL, D. A., CRUMP, B. C., CUI, D., DALY, S. E., DAVALOS, L., DAWSON, R. D., DEFAZIO, J., DELSUC, F., DIONISI, H. M., DOMINGUEZ-BELLO, M. G., DOWELL, R., DUBINSKY, E. A., DUNN, P. O., ERCOLINI, D., ESPINOZA, R. E., et al. 2017. A communal catalogue reveals Earth's multiscale microbial diversity. *Nature,* 551**,** 457.

THURBER, R. V., PAYET, J. P., THURBER, A. R. & CORREA, A. M. S. 2017. Virus–host interactions and their roles in coral reef health and disease. *Nature Reviews Microbiology,* 15**,** 205.

TIAN, R. M., WANG, Y., BOUGOUFFA, S., GAO, Z. M., CAI, L., BAJIC, V. & QIAN, P. Y. 2014. Genomic analysis reveals versatile heterotrophic capacity of a potentially symbiotic sulfur-oxidizing bacterium in sponge. *Environ Microbiol,* 16**,** 3548-61.

TOCHEVA, E. I., MATSON, E. G., CHENG, S. N., CHEN, W. G., LEADBETTER, J. R. & JENSEN, G. J. 2014. Structure and Expression of Propanediol Utilization Microcompartments in *Acetonema longum*. *J. Bacteriol,* 196**,** 1651-1658.

TOUCHON, M., BERNHEIM, A. & ROCHA, E. P. 2016. Genetic and life-history traits associated with the distribution of prophages in bacteria. *ISME J,* 10**,** 2744-2754.

TRINDADE-SILVA, A. E., RUA, C., SILVA, G. G. Z., DUTILH, B. E., MOREIRA, A. P. B., EDWARDS, R. A., HAJDU, E., LOBO-HAJDU, G., VASCONCELOS, A. T., BERLINCK, R. G. S. & THOMPSON, F. L. 2012. Taxonomic and Functional Microbial Signatures of the Endemic Marine Sponge Arenosclera brasiliensis. *PLOS ONE,* 7**,** e39905.

TULLY, B. J., SACHDEVA, R., GRAHAM, E. D. & HEIDELBERG, J. F. 2017. 290 metagenome-assembled genomes from the Mediterranean Sea: a resource for marine microbiology. *PeerJ,* 5**,** e3558.

USHER, K. M., SUTTON, D. C., TOZE, S., KUO, J. & FROMONT, J. 2005. Inter-generational transmission of microbial symbionts in the marine sponge *Chondrilla australiensis* (*Demospongiae*). *Mar Freshw Res,* 56**,** 125-131.

VACELET, J. 1970. Description de cellules a bactéries intranucléaires chez des éponges *Verongia*. *J Microsc,* 9**,** 333-346.

VACELET, J. 1975a. *Electron microscope study of the association between bacteria and sponges of the genus Verongia (Dictyoceratida)*.

VACELET, J. 1975b. Étude en microscopie électronique de l'association entre bactéries et spongiaires du genre *Verongia* (Dictyoceratida). *Journal Microscroscopy Biological Cell,* 23**,** 271-288.

VACELET, J. & DONADEY, C. 1977a. Electron microscope study of the association between some sponges and bacteria. *J Exp Mar Bio Ecol,* 30**,** 301-314.

VACELET, J. & DONADEY, C. 1977b. Electron microscope study of the association between some sponges and bacteria. *Journal of Experimental Marine Biology and Ecology,* 30**,** 301-314.

VACELET, J. & GALLISSIAN, M.-F. 1978. Virus-like particles in cells of the sponge *Verongia cavernicola* (demospongiae, dictyoceratida) and accompanying tissues changes. *J Invertebr Pathol,* 31**,** 246-254.

VALA, F., EGAS, M., BREEUWER, J. A. J. & SABELIS, M. W. 2004. *Wolbachia* affects oviposition and mating behaviour of its spider mite host. *J Evol Biol,* 17**,** 692-700.

VALENTINE, M. M. & BUTLER, M. I. 2019. Sponges structure water-column characteristics in shallow tropical coastal ecosystems. *Mar Ecol Prog Ser,* 608**,** 133-147.

VAN BELLEGHEM, J., DĄBROWSKA, K., VANEECHOUTTE, M., BARR, J. & BOLLYKY, P. 2018. Interactions between bacteriophage, bacteria, and the mammalian immune system. *Viruses,* 11**,** 10.

VAN OPSTAL, E. J. & BORDENSTEIN, S. R. 2019. Phylosymbiosis impacts adaptive traits in *Nasonia* wasps. *MBio,* 10**,** e00887-19.

VAN SOEST, R. W. M., BOURY-ESNAULT, N., HOOPER, J. N. A., RÜTZLER, K., DE VOOGD, N. J., ALVAREZ, B., HAJDU, E., PISERA, A. B., MANCONI, R., SCHÖNBERG, C., KLAUTAU, M., PICTON, B., KELLY, M., VACELET, J., DOHRMANN, M., DÍAZ, M.-C., CÁRDENAS, P., CARBALLO, J. L., RÍOS, P. & DOWNEY, R. 2019. World porifera database.

VAN SOEST, R. W. M., BOURY-ESNAULT, N., VACELET, J., DOHRMANN, M., ERPENBECK, D., DE VOOGD, N. J., SANTODOMINGO, N., VANHOORNE, B., KELLY, M. & HOOPER, J. N. A. 2012. Global diversity of sponges (*Porifera*). *PLoS One,* 7**,** e35105-e35105.

VAN VLIET, S. & DOEBELI, M. 2019. The role of multilevel selection in host microbiome evolution. *Proceedings of the National Academy of Sciences***,** 201909790.

VASCONCELLOS, V., WILLENZ, P., ERESKOVSKY, A. & LANNA, E. 2019. Comparative ultrastructure of the spermatogenesis of three species of *Poecilosclerida* (*Porifera, Demospongiae*). *Zoomorphology,* 138**,** 1-12.

VEGA THURBER, R. L., BAROTT, K. L., HALL, D., LIU, H., RODRIGUEZ-MUELLER, B., DESNUES, C., EDWARDS, R. A., HAYNES, M., ANGLY, F. E., WEGLEY, L. & ROHWER, F. L. 2008. Metagenomic analysis indicates that stressors induce production of herpes-like viruses in the coral <em>Porites compressa</em&gt. *Proceedings of the National Academy of Sciences,* 105**,** 18413.

VENN, A. A., LORAM, J. E. & DOUGLAS, A. E. 2008. Photosynthetic symbioses in animals. *J Exp Bot,* 59**,** 1069-1080.

VILANOVA, E., COUTINHO, C. C. & MOURAO, P. A. 2009. Sulfated polysaccharides from marine sponges (*Porifera*): an ancestor cell-cell adhesion event based on the carbohydrate-carbohydrate interaction. *Glycobiology,* 19**,** 860-7.

VORONIN, D. A. & KISELEVA, E. V. 2008. Functional role of proteins containing ankyrin repeats. *Cell and Tissue Biology,* 2**,** 1-12.

WAGNER, D. & KELLEY, C. D. 2017. The largest sponge in the world? *Mar Biod,* 47**,** 367-368.

WANG, Y., HUANG, W. E., CUI, L. & WAGNER, M. 2016. Single cell stable isotope probing in microbiology using Raman microspectroscopy. *Current Opinion in Biotechnology,* 41**,** 34-42.

WATTAM, A. R., DAVIS, J. J., ASSAF, R., BOISVERT, S., BRETTIN, T., BUN, C., CONRAD, N., DIETRICH, E. M., DISZ, T., GABBARD, J. L., GERDES, S., HENRY, C. S., KENYON, R. W., MACHI, D., MAO, C., NORDBERG, E. K., OLSEN, G. J., MURPHY-OLSON, D. E., OLSON, R., OVERBEEK, R., PARRELLO, B., PUSCH, G. D., SHUKLA, M., VONSTEIN, V., WARREN, A., XIA, F., YOO, H. & STEVENS, R. L. 2017. Improvements to PATRIC, the all-bacterial Bioinformatics Database and Analysis Resource Center. *Nucleic Acids Res,* 45**,** D535-d542.

WEBB, A. E., POMPONI, S. A., VAN DUYL, F. C., REICHART, G.-J. & DE NOOIJER, L. J. 2019. ph regulation and tissue coordination pathways promote calcium carbonate bioerosion by excavating *Sci Rep,* 9**,** 758.

WEBSTER, N. S., TAYLOR, M. W., BEHNAM, F., LUCKER, S., RATTEI, T., WHALAN, S., HORN, M. & WAGNER, M. 2010. Deep sequencing reveals exceptional diversity and modes of transmission for bacterial sponge symbionts. *Environ Mico,* 12**,** 2070-2082.

WEBSTER, N. S. & THOMAS, T. 2016. The sponge hologenome. *MBio,* 7**,** e00135-16.

WEBSTER, N. S., WILSON, K. J., BLACKALL, L. L. & HILL, R. T. 2001. Phylogenetic diversity of bacteria associated with the marine sponge *Rhopaloeides odorabile*. *Appl Environ Microbiol,* 67**,** 434-44.

WEHRL, M., STEINERT, M. & HENTSCHEL, U. 2007. Bacterial uptake by the marine sponge *Aplysina aerophoba*. *Microb Ecol,* 53**,** 355-365.

WEIN, T., ROMERO PICAZO, D., BLOW, F., WOEHLE, C., JAMI, E., REUSCH, T. B. H., MARTIN, W. F. & DAGAN, T. 2019. Currency, Exchange, and Inheritance in the Evolution of Symbiosis. *Trends in Microbiology,* 27**,** 836-849.

WEISZ, J. B., LINDQUIST, N. & MARTENS, C. S. 2008. Do associated microbial abundances impact marine demosponge pumping rates and tissue densities? *Oecologia,* 155**,** 367-376.

WEITZ, J. S. 2015. *Quantitative Viral Ecology*

Dynamics of Viruses and Their Microbial Hosts, Princeton University Press.

WEITZ, J. S., POISOT, T., MEYER, J. R., FLORES, C. O., VALVERDE, S., SULLIVAN, M. B. & HOCHBERG, M. E. 2013. Phage–bacteria infection networks. *Trends Microbiol,* 21**,** 82-91.

WEITZ, J. S., STOCK, C. A., WILHELM, S. W., BOUROUIBA, L., COLEMAN, M. L., BUCHAN, A., FOLLOWS, M. J., FUHRMAN, J. A., JOVER, L. F., LENNON, J. T., MIDDELBOE, M., SONDEREGGER, D. L., SUTTLE, C. A., TAYLOR, B. P., FREDE THINGSTAD, T., WILSON, W. H. & ERIC WOMMACK, K. 2015. A multitrophic model to quantify the effects of marine viruses on microbial food webs and ecosystem processes. *The Isme Journal,* 9**,** 1352.

WESTHEIDE, W., RIEGER, R., WESTHEIDE, W., RIEGER, G. & LAY, M. 2013. *Spezielle Zoologie. Teil 1: Einzeller und Wirbellose Tiere,* Springer Berlin Heidelberg.

WEYNBERG, K. D., LAFFY, P. W., WOOD-CHARLSON, E. M., TURAEV, D., RATTEI, T., WEBSTER, N. S. & VAN OPPEN, M. J. H. 2017. Coral-associated viral communities show high levels of diversity and host auxiliary functions. *PeerJ,* 5**,** e4054.

WEYNBERG, K. D., VOOLSTRA, C. R., NEAVE, M. J., BUERGER, P. & VAN OPPEN, M. J. H. 2015. From cholera to corals: Viruses as drivers of virulence in a major coral bacterial pathogen. *Scientific Reports,* 5**,** 17889.

WHITELEY, A. S., THOMSON, B., LUEDERS, T. & MANEFIELD, M. 2007. RNA stable-isotope probing. *Nature Protocols,* 2**,** 838-844.

WIENS, M., KORZHEV, M., KRASKO, A., THAKUR, N. L., PEROVIC-OTTSTADT, S., BRETER, H. J., USHIJIMA, H., DIEHL-SEIFERT, B., MULLER, I. M. & MULLER, W. E. 2005. Innate immune defense of the sponge Suberites domuncula against bacteria involves a MyD88-dependent signaling pathway. Induction of a perforin-like molecule. *J Biol Chem,* 280**,** 27949-59.

WILHELM, S. W. & SUTTLE, C. A. 1999. Viruses and Nutrient Cycles in the Sea: Viruses play critical roles in the structure and function of aquatic food webs. *BioScience,* 49**,** 781-788.

WILKINSON, C. R. 1978. Microbial associations in sponges. III. Ultrastructure of the in situ associations in coral reef sponges. *Mar Biol,* 49**,** 177-185.

WILKINSON, C. R., GARRONE, R., VACELET, J. & SMITH DAVID, C. 1984. Marine sponges discriminate between food bacteria and bacterial symbionts: electron microscope radioautography and in situ evidence. *PNAS,* 220**,** 519-528.

WILLE, M., SHI, M., KLAASSEN, M., HURT, A. C. & HOLMES, E. C. 2019. Virome heterogeneity and connectivity in waterfowl and shorebird communities. *The ISME Journal,* 13**,** 2603-2616.

WILLENZ, P. 1980. Kinetic and morphological aspects of particle ingestion by the freshwater sponge *Ephydatia fluviatilis* l. *In:* SMITH, D. C. & TIFFON, Y. (eds.) *Nutrition in the Lower Metazoa.* Pergamon.

WILLIAMS, L. M., INGE, M. M., MANSFIELD, K. M., RASMUSSEN, A., AFGHANI, J., AGRBA, M., ALBERT, C., ANDERSSON, C., BABAEI, M., BABAEI, M., BAGDASARYANTS, A., BONILLA, A., BROWNE, A., CARPENTER, S., CHEN, T., CHRISTIE, B., CYR, A., DAM, K., DULOCK, N., ERDENE, G., ESAU, L., ESONWUNE, S., HANCHATE, A., HUANG, X., JENNINGS, T., KASABWALA, A., KEHOE, L., KOBAYASHI, R., LEE, M., LEVAN, A., LIU, Y., MURPHY, E., NAMBIAR, A., OLIVE, M., PATEL, D., PAVESI, F., PETTY, C. A., SAMOFALOVA, Y., SANCHEZ, S., STEJSKAL, C., TANG, Y., YAPO, A., CLEARY, J. P., YUNES, S. A., SIGGERS, T. & GILMORE, T. D. 2019. Transcription factor NF-κB in a basal metazoan, the sponge, has conserved and unique sequences, activities, and regulation. *bioRxiv***,** 691097.

WILSON, A. C. C. & DUNCAN, R. P. 2015. Signatures of host/symbiont genome coevolution in insect nutritional endosymbioses. *PNAS,* 112**,** 10255-10261.

WINTER, C., BOUVIER, T., WEINBAUER, M. G. & THINGSTAD, T. F. 2010. Trade-offs between competition and defense specialists among unicellular planktonic organisms: the "killing the winner" hypothesis revisited. *Microbiology and molecular biology reviews : MMBR,* 74**,** 42-57.

WOMMACK, K. E. & COLWELL, R. R. 2000. Virioplankton: viruses in aquatic ecosystems. *Microbiol Mol Biol Rev.,* 64**,** 69-114.

WOOD-CHARLSON, E. M., WEYNBERG, K. D., SUTTLE, C. A., ROUX, S. & VAN OPPEN, M. J. 2015. Metagenomic characterization of viral communities in corals: mining biological signal from methodological noise. *Environ Microbiol,* 17**,** 3440-9.

WOOSTER, M. K., MCMURRAY, S. E., PAWLIK, J. R., MORÁN, X. A. G. & BERUMEN, M. L. 2019. Feeding and respiration by giant barrel sponges across a gradient of food abundance in the Red Sea. *Limnol Oceanogr,* 0.

WULFF, J. L. 1984. Sponge-mediated coral reef growth and rejuvenation. *Coral Reefs,* 3**,** 157-163.

WULFF, J. L. 2006. Resistance vs recovery: morphological strategies of coral reef sponges. *Funct Ecol,* 20**,** 699-708.

YAHEL, G., SHARP, J. H., MARIE, D., HÄSE2, C. & GENIN, A. 2003. *In situ* feeding and element removal in the symbiont-bearing sponge *Theonella swinhoei*: Bulk DOC is the major source for carbon. *Limnol Oceanogr,* 48**,** 141-149.

YANG, D. C., BLAIR, K. M. & SALAMA, N. R. 2016. Staying in shape: the impact of cell shape on bacterial survival in diverse environments. *Microbiol Mol Biol Rev.,* 80**,** 187.

YARNOLD, J. E., HAMILTON, B. R., WELSH, D. T., POOL, G. F., VENTER, D. J. & CARROLL, A. R. 2012. High resolution spatial mapping of brominated pyrrole-2-aminoimidazole alkaloids distributions in the marine sponge *Stylissa flabellata* via MALDI-mass spectrometry imaging. *Mol Biosyst,* 8**,** 2249-59.

YIN, Z., ZHU, M., DAVIDSON, E. H., BOTTJER, D. J., ZHAO, F. & TAFFOREAU, P. 2015. Sponge grade body fossil with cellular resolution dating 60 Myr before the Cambrian. *PNAS,* 112**,** E1453-E1460.

ZAN, J., LI, Z., TIANERO, M. D., DAVIS, J., HILL, R. T. & DONIA, M. S. 2019. A microbial factory for defensive kahalalides in a tripartite marine symbiosis. *Science,* 364**,** eaaw6732.

ZÉLÉ, F., MAGALHÃES, S., KÉFI, S. & DUNCAN, A. B. 2018. Ecology and evolution of facilitation among symbionts. *Nat Commun,* 9**,** 4869.

ZELEZNIAK, A., ANDREJEV, S., PONOMAROVA, O., MENDE, D. R., BORK, P. & PATIL, K. R. 2015. Metabolic dependencies drive species co-occurrence in diverse microbial communities. *PNAS,* 112**,** 6449-6454.

ZHANG, Y.-Z., SHI, M. & HOLMES, E. C. 2018. Using Metagenomics to Characterize an Expanding Virosphere. *Cell,* 172**,** 1168-1172.

ZHAO, J., HE, S., MINASSIAN, A., LI, J. & FENG, P. 2015. Recent advances on viral manipulation of NF-κB signaling pathway. *Current opinion in virology,* 15**,** 103-111.

ZIERER, M. S. & MOURAO, P. A. 2000. A wide diversity of sulfated polysaccharides are synthesized by different species of marine sponges. *Carbohydr Res,* 328**,** 209-16.

ZILBER-ROSENBERG, I. & ROSENBERG, E. 2008. Role of microorganisms in the evolution of animals and plants: the hologenome theory of evolution. *FEMS Microbiol Rev,* 32**,** 723-735.

ZIVKOVIC, A. M., GERMAN, J. B., LEBRILLA, C. B. & MILLS, D. A. 2011. Human milk glycobiome and its impact on the infant gastrointestinal microbiota. *PNAS,* 108**,** 4653-4658.

ABSTRACTS OF RELATED PUBLICATIONS

ATF6 executes ER stress-dependent inflammatory signals in intestinal epithelial cells

Stengel S.T, Lipinski S., **Jahn M.T**, Aden K., Ito G., Fazio A., Wottawa F., Kuiper J.W., Coleman O.I., Tran F., Bordoni D., Bernardes J.P., Jentzsch M., Luzius A., Bierwirth S., Messner B., Henning A., Welz L., Kakavand N., Schreiber S., Kaser A., Blumberg R.S., Haller D., Rosenstiel P.

Abstract

Excessive, unresolved ER stress in intestinal epithelial cells has been shown to drive intestinal inflammation, but the upstream pro-inflammatory signalling events are still only partially understood. We here aim to assess the upstream regulatory network of ATF6 signaling as a potential executioner of such pro-inflammatory signals. Using a systematic siRNA screening approach, we identify and validate 15 suppressors and 7 activators of ATF6α signaling, including the regulatory subunit of casein kinase 2 (CSNK2B) and acyl-CoA synthetase long chain family member 1 (ACSL1), which both co-activate the ATF6α pathway. We demonstrate that hyper-active signals in murine organoids overexpressing a constitutively active form of ATF6α can be abolished by pharmacological inhibition of ACSL1 and CSNK2B. Targeting these two co-activators alleviates ER stress and pro-inflammatory signals associated with genetically impaired autophagy and ER stress in Atg16l1- deficient intestinal organoids and in a murine in vivo ER stress model (tunicamycin injection). Finally, we demonstrate that inhibition of ATF6α signaling attenuates the pro-inflammatory profile in human organoids from inflammatory bowel disease (IBD) patients upon ER stress induction. The findings point to the regulatory ATF6α network as a promising therapeutic target to ameliorate inflammatory responses associated with disturbed ER homeostasis in intestinal epithelial cells in IBD.

Submitted to: *Gastroenterology*

Comparative analysis of amplicon and metagenomic sequencing methods reveals key features in the evolution of animal metaorganisms

Rausch, P., Rühlemann, M., Hermes, B. M., Doms, S., Dagan, T., Dierking, K., Domin, H., Fraune, S., von Frieling, J., Hentschel, U., Heinsen, F.-A., Höppner, M., **Jahn, M. T**., Jaspers, C., Kissoyan, K. A. B., Langfeldt, D., Rehman, A., Reusch, T. B. H., Roeder, T., Schmitz, R. A., Schulenburg, H., Soluch, R., Sommer, F., Stukenbrock, E., Weiland-Bräuer, N., Rosenstiel, P., Franke, A., Bosch, T. and Baines, J. F.

Abstract

Background The interplay between hosts and their associated microbiome is now recognized as a fundamental basis of the ecology, evolution, and development of both players. These interdependencies inspired a new view of multicellular organisms as "metaorganisms." The goal of the Collaborative Research Center "Origin and Function of Metaorganisms" is to understand why and how microbial communities form long-term associations with hosts from diverse taxonomic groups, ranging from sponges to humans in addition to plants.

Methods In order to optimize the choice of analysis procedures, which may differ according to the host organism and question at hand, we systematically compared the two main technical approaches for profiling microbial communities, 16S rRNA gene amplicon and metagenomic shotgun sequencing across our panel of ten host taxa. This includes two commonly used 16S rRNA gene regions and two amplification procedures, thus totaling five different microbial profiles per host sample.

Conclusion While 16S rRNA gene-based analyses are subject to much skepticism, we demonstrate that many aspects of bacterial community characterization are consistent across methods. The resulting insight facilitates the selection of appropriate methods across a wide range of host taxa. Overall, we recommend single- over multi-step amplification procedures, and although exceptions and trade-offs exist, the V3 V4 over the V1 V2 region of the 16S rRNA gene. Finally, by contrasting taxonomic and functional profiles and performing phylogenetic analysis, we provide important and novel insight into broad evolutionary patterns among metaorganisms, whereby the transition of animals from an aquatic to a terrestrial habitat marks a major event in the evolution of host-associated microbial composition.

Published: *Microbiome* 2019 Sep 14;7(1):133. doi: 10.1186/s40168-019-0743-1.

Marine Sponge Holobionts in Health and Disease

Slaby B.M., Franke A, Rix L, Pita L, Bayer K, **Jahn M.T**., Hentschel U

Abstract

Sponges—like all multicellular organisms—are holobionts, complex ecosystems comprising the host and its microbiota. The symbiosis of sponges with their microbial communities is a highly complex system, requiring interaction mechanisms and adaptation on both sides. The microbiome seems to rely on eukaryotic-like protein domains, such as ankyrins, modifications of the lipopolysaccharide structure, CRISPR-Cas, toxin-antitoxin, and restriction-modification systems, as well as secondary metabolism to communicate with the host and within the microbial community, evade phagocytosis, and defend itself against foreign DNA. Secondary metabolites produced by certain symbionts may even defend the entire holobiont against predators. On the other hand, the immune system of the sponge itself has evolved to discriminate not only between self and nonself but also between its associated microbiota and foreign microbes, such as food bacteria. Sponge holobionts are inextricably dependent on the surrounding environmental conditions due to their sessile nature. Thus, we discuss the link between environmental stress and sponge disease and dysbiosis, with a particular focus on the holobiont's response to ongoing global change. While some species may be the "winners of climate change," other species are adversely affected, e.g., by metabolic and immune suppression, as well as microbiome shifts resulting in loss of symbiotic functions. Hence, a much better understanding of sponge holobionts and the underlying molecular mechanisms of host-microbe interaction is required before the fate of sponge holobionts in a changing ocean can finally be validated.

Published as a book chapter in Symbiotic Microbiomes of Coral Reefs Sponges and Corals (2019) Ed Li Z. *Springer Netherlands*, pp. 81-104.

Antibiotics-induced monodominance of a novel gut bacterial order

Hildebrand F, Moitinho-Silva L, Blasche S, **Jahn M.T.**, Gossmann T.I., Heuerta-Cepas J, Hercog R, Luetge M, Bahram M, Pryszlak A, Alves R.J., Waszak S.M., Zhu A, Ye L, Costea P.I., Aalvink S, Belzer C, Forslund S.K., Sunagawa S, Hentschel U, Merten C, Patil K.R., Benes V, Bork P

Abstract

Objective The composition of the healthy human adult gut microbiome is relatively stable over prolonged periods, and representatives of the most highly abundant and prevalent species have been cultured and described. However, microbial abundances can change on perturbations, such as antibiotics intake, enabling the identification and characterisation of otherwise low abundant species.

Design Analysing gut microbial time-series data, we used shotgun metagenomics to create strain level taxonomic and functional profiles. Community dynamics were modelled postintervention with a focus on conditionally rare taxa and previously unknown bacteria.

Results In response to a commonly prescribed cephalosporin (ceftriaxone), we observe a strong compositional shift in one subject, in which a previously unknown species, ^{U} *Borkfalki ceftriaxensis*, was identified, blooming to 92 % relative abundance. The genome assembly reveals that this species (1) belongs to a so far undescribed order of Firmicutes, (2) is ubiquitously present at low abundances in at least one third of adults, (3) is opportunistically growing, being ecologically similar to typical probiotic species and (4) is stably associated to healthy hosts as determined by single nucleotide variation analysis. It was the first coloniser after the antibiotic intervention that led to a long-lasting microbial community shift and likely permanent loss of nine commensals.

Conclusion The bloom of ^{U} *B. ceftriaxensis* and a subsequent one of *Parabacteroides distasonis* demonstrate the existence of monodominance community states in the gut. Our study points to an undiscovered wealth of low abundant but common taxa in the human gut and calls for more highly resolved longitudinal studies, in particular on ecosystem perturbations.

Published: *Gut*. 2019 Oct;68(10):1781-1790. doi: 10.1136/gutjnl-2018-317715

Landscape structure affects the prevalence and distribution of a tick-borne zoonotic pathogen

Millins C, Dickinson E. R., Isakovic P, Gilbert L, Wojciechowska A, Paterson V, Tao F, Jahn M.T., Kilbride E, Birtles R, Johnson R, Biek R

Abstract

Background Landscape structure can affect pathogen prevalence and persistence with consequences for human and animal health. Few studies have examined how reservoir host species traits may interact with landscape structure to alter pathogen communities and dynamics. Using a landscape of islands and mainland sites we investigated how natural landscape fragmentation affects the prevalence and persistence of the zoonotic tick-borne pathogen complex *Borrelia burgdorferi* (*sensu lato*), which causes Lyme borreliosis. We hypothesized that the prevalence of *B. burgdorferi* (*s.l.*) would be lower on islands compared to the mainland and *B. afzelii*, a small mammal specialist genospecies, would be more affected by isolation than bird-associated *B. garinii* and *B. valaisiana* and the generalist *B. burgdorferi* (*sensu stricto*).

Methods Questing (host-seeking) nymphal *I. ricinus* ticks (n = 6567) were collected from 12 island and 6 mainland sites in 2011, 2013 and 2015 and tested for *B. burgdorferi* (*s.l.*). Deer abundance was estimated using dung transects.

Result: The prevalence of *B. burgdorferi* (*s.l.*) was significantly higher on the mainland (2.5 %, 47/1891) compared to island sites (0.9 %, 44/4673) (P < 0.01). While all four genospecies of *B. burgdorferi* (*s.l.*) were detected on the mainland, bird-associated species *B. garinii* and *B. valaisiana* and the generalist genospecies *B. burgdorferi* (*s.s.*) predominated on islands.

Conclusion We found that landscape structure influenced the prevalence of a zoonotic pathogen, with a lower prevalence detected among island sites compared to the mainland. This was mainly due to the significantly lower prevalence of small mammal-associated *B. afzelii*. Deer abundance was not related to pathogen prevalence, suggesting that the structure and dynamics of the reservoir host community underpins the observed prevalence patterns, with the higher mobility of bird hosts compared to small mammal hosts leading to a relative predominance of the bird-associated genospecies *B. garinii* and generalist genospecies *B. burgdorferi* (*s.s.*) on islands. In contrast, the lower prevalence of *B. afzelii* on islands may be due to small mammal populations there exhibiting lower densities, less immigration and stronger population fluctuations. This study suggests that landscape fragmentation can influence the prevalence of a zoonotic pathogen, dependent on the biology of the reservoir host.

Published: *Parasites & Vectors.* 2018 Dec 4;11(1):621. doi: 10.1186/s13071-018-3200-2.

An enrichment of CRISPR and other defense-related features in marine sponge-associated microbial metagenomes

Horn H, Slaby B, **Jahn M.T.**, Bayer K, Moitinho-Silva L, Förster F, Abdelmohsen U.R., Hentschel U

Abstract

Many marine sponges are populated by dense and taxonomically diverse microbial consortia. We employed a metagenomics approach to unravel the differences in the functional gene repertoire among three Mediterranean sponge species, *Petrosia ficiformis*, *Sarcotragus foetidus*, *Aplysina aerophoba* and seawater. Different signatures were observed between sponge and seawater metagenomes with regard to microbial community composition, GC content, and estimated bacterial genome size. Our analysis showed further a pronounced repertoire for defense systems in sponge metagenomes. Specifically, clustered regularly interspaced short palindromic repeats, restriction modification, DNA phosphorothioation and phage growth limitation systems were enriched in sponge metagenomes. These data suggest that defense is an important functional trait for an existence within sponges that requires mechanisms to defend against foreign DNA from microorganisms and viruses. This study contributes to an understanding of the evolutionary arms race between viruses/phages and bacterial genomes and it sheds light on the bacterial defenses that have evolved in the context of the sponge holobiont.

Published: *Frontiers in Microbiology* 2016 Nov 8;7:1751. doi: 10.3389/fmicb.2016.01751

APPENDICES

Appendix A

This appendix provides additional information related to Chapter 7 on the lifestyle of sponge symbiont phages by host prediction and microscopy.

Appendix A1

Viral host prediction- Method:

Hosts of sponge phages were predicted by a combination of the most prognostic approaches that are (a) CRISPR-spacer- (b) homology- and (d) tRNA- matching as reviewed in (Edwards et al., 2016a). First, we created a custom database of microbial sequences representing the potential host pool (X2, hereafter). This comprised three Mediterranean sponge microbial metagenomes (*Petrosia ficiformis*, *Sarcotragus foetidus*, *Aplysina aerophoba*; (Horn et al., 2016)), 37 high quality bins from *A. aerophoba* (Slaby et al., 2017), 13 single-cell genomes and assembled microbial metatranscriptomes (*Xestospongia muta*, *Xestospongia testudinaria*). This set was extended with 290 Tara Oceans metagenome-assembled genomes from the Mediterranean Sea (Tully et al., 2017) and all 97,941 bacterial genomes available in PATRIC as of 2017-06-14. CRISPR-match. The X2 database was searched for CRISPR spacers using CRISPRDetect_2.2 (-array_quality_score_cutoff 3 -q 1). The identified spacers were assigned to BCvir contigs by BLASTn search (-dust no -gapopen 10 -gapextend 10 -penalty -1 -e-value 1 -word_size 7) as suggested by (Biswas et al., 2013). Hits were allowed a maximum of 1 mismatch over full spacer length to increase precision/stringency against false positive classification(Burstein et al., 2016). Homology match. To search for homologous signatures of mVCs in the microbial X2 database, such as lysogen viral contigs, were searched against the X2 database through BLASTn. The best hits from this search below an e-value threshold of 10^{-5} were considered a match when they aligned with more than 80% sequence identity over at least 1 kb. tRNA match. tRNA sequences predicted in BCvir contigs using tRNAscan-SE v.1.23 (Lowe and Chan, 2016) using default settings and searched against X2 using BLASTn keeping only best hits with at least 95% ANI. All predictions were joined in an ensemble infection network that was visualized via Cytoscape v3.6.0.

To investigate whether the ribotypes of the computationally predicted phage hosts were present in the same samples, the viromes were sequenced from the 16S rDNA sequences were identified in the hit genomes using Anvi'o v.2.1.1 and matched to 16S rDNA amplicons sequences co-extracted with the viromes (blastn best hit; >=98% coverage >=97% ANI). The 16S rDNA Amplicon reads were processed as described in (Thomas et al., 2016) using mothur1.39.5 with minor adaptions to cover the longer amplified V1V2 and V3V4 regions of the 16S rRNA gene.

Viral host prediction- Result

We predicted microbial hosts of previously discovered phages *in silico* (Figure A1-I). The predicted phage hosts comprised representatives from cosmopolitan sponge symbionts such as *Poribacteria*, *Cyanobacteria*, *Chloroflexi* and *Flavobacteria* (Thomas et al., 2016). Notably, all phages that were predicted to infect sponge symbionts (Figure A1-I, bubble) occurred enriched in sponges but depleted in nearby seawater. Most planktonic phages matched planktonic bacteria, although 35 phages enriched in two of the sponges (*Chondrosia*, *Petrosia*) were predicted to infect typical seawater microbes, such as *Candidatus* Pelagibacter (TMED211) or Oligotrophic Marine *Gammaproteobacteria* (OMG; TMED95). Overall, 162 BCvir phage populations matched 156 prokaryotic genomes and 33 metagenomic scaffolds. These potential hosts were identified among sponge symbionts, planktonic bacteria from the Tara Oceans Mediterranean Sea (Tully et al., 2017) and the PATRIC genome database (Wattam et al., 2017) by mining signals from CRISPR spacers, homology and tRNA as a combination of the most prognostic approaches(Edwards et al., 2016a). To evaluate the precision/specificity of these predictions, we added ~ 97,000 genomes of expected non-target hosts from the PATRIC database as genomic background and rarely matched non-target hosts from other environments. Furthermore, 45.3% (43 of 95) of the predicted hosts where indeed present as indicated by a matching ribotype in co-extracted 16S amplicon data.

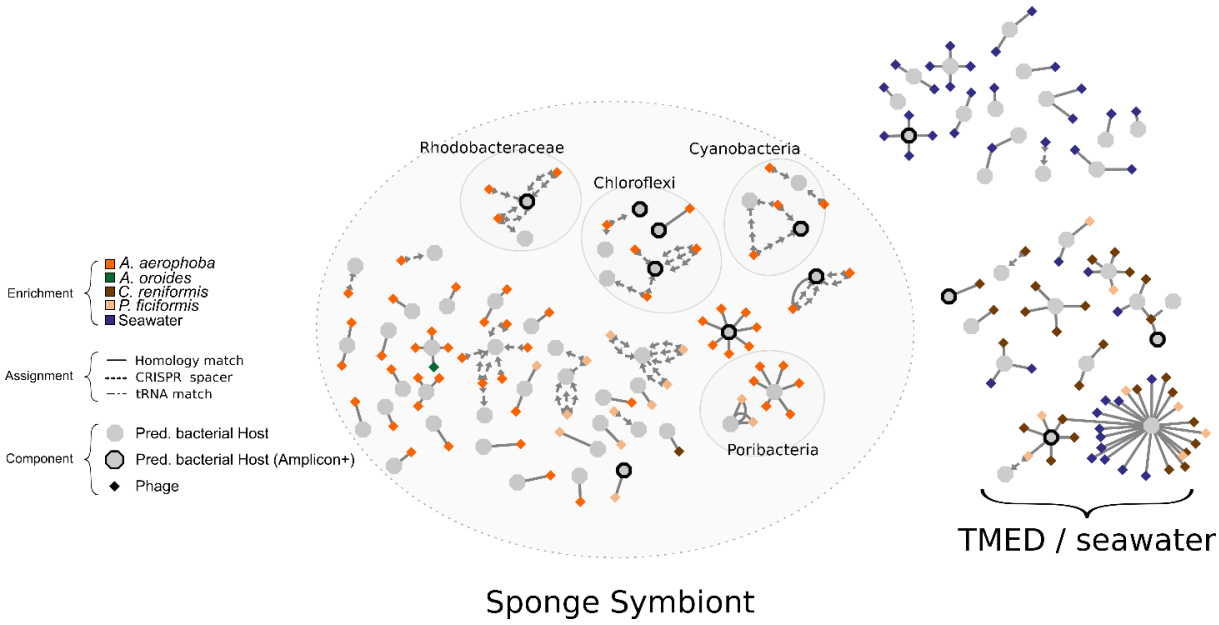

Figure A1-I: Integrative phage–bacteria infection networks. Sponge virome population contigs assigned to putative bacterial hosts by combining signals from CRISPR-spacer-, homology-, and tRNA matches against a custom database of sponge microbial sequences, PATRIC genomes(Wattam et al., 2017) and 290 Tara Oceans bins from the Mediterranean Sea (TMED(Tully et al., 2017)). Amplicon+ denotes microbial sequences that were detected by parallel 16S rRNA gene amplicon sequencing.

Appendix A2

Viral replication mode prediction- Method & Result

The lytic or lysogenic lifestyle of sponge associated phages was predicted using a combination of (i) the pre-trained supervised random forest classifier implemented in the Phage Classification Tool Set (PHACTS; (McNair et al., 2012)), and (ii) by hits to prophage machinery marker enzymes (e.g. integrase or excisionase) annotated by pVOG or InterPro (as see CHAPTER 7).

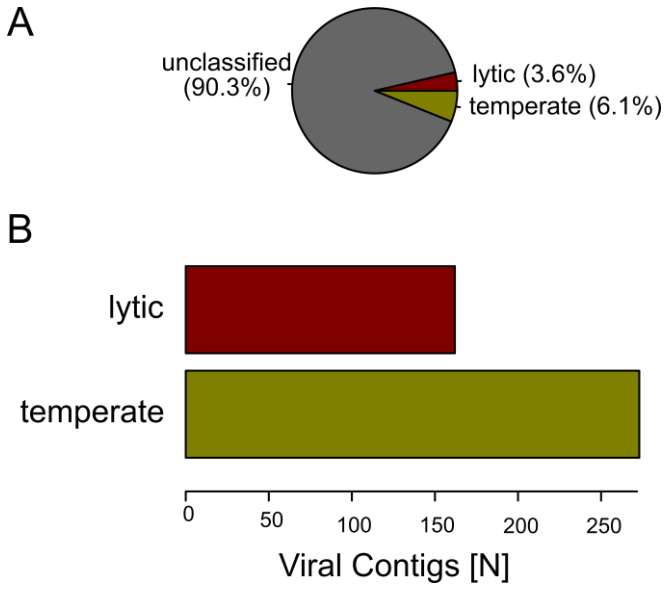

Figure A2-I: Lifestyle prediction sponge enriched viruses. (**A**) Classification proportions for N= 3936 sponge enriched phages. (**B**) Total number of phages predicted for each category.

Appendix A3

Phage *In situ* localisation - Method:

Sample processing. Sponge tissue dissection, high-pressure freezing and freeze-substitution were carried out as described in CHAPTER 3. *Phage probe design.* For each phage of interest (see Results), an RNAview probe set consisting of 30 to 54 target specific oligonucleotides (Type 1: Alexa Fluor 546) was obtained from Invitrogen (Suppl. Data 6). Undescriptive regions on the phage genomes that would not allow discrimination against the background of other viruses and microbes of the communities were identified using permissive blastn v 2.2.28+ (-e-value 100) against the X2 background database. By excluding such matched "un-specificity" sites, we used GenePROBER (http://kronos.icbm.uni-oldenburg.de/shiny/web-probe-designer/, options GC40-70; A 25; B 70; C 95; D 95; E 95; G 93, H 93; I 2; J 2; K 5; L 5; M 40; N 1; O 0.05) to design probes against structural phage genes such as for capsids *with typically lower mutation rates*. The established probe sets are available upon request. *ePhageFISH.* We modified and extended the ViewHIV approach of Chin et al. (2015) that detects HIV in laboratory

cell cultures. The modification was to localize virions and lysogens of virome-predicted bacteriophages in their natural host-associated context within cryo-immobilized and freeze-substituted sponge tissues. The extension was to augment the phage fluorescence spots with their structural context by correlative electron microscopy of the same regions. The detailed protocols for ePhageFISH are available at the open-access repository of science methods protocols.io (dx.doi.org/10.17504/protocols.io.74thqwn). The staining approach was established and validated on the test-system of (1) *Curvibacter* sp. AEP, encoding a prophage (2) *Curvibacter* sp. Hvul, not encoding this prophage (3) and the purified phage virion (Figure A3-I). Staining with the probes was performed according to the manufacturer's instructions (VIEWRNA CELL PLUS ASSAY kit; Invitrogen, Cat nr. 88-19000-99) with some modifications. Briefly, reactions were performed on 100 nm thick LR White embedded sponge tissue sections that were cut as serial ribbons on poly-L-lysine coated glass slides (Polysine slides, Thermo Fisher Scientific, Waltham, MA, USA) using the Histo Jumbo Diamond Knife (Diatome AG, Biel, Switzerland). Sections were then encircled with a hydrophobic barrier pen (Liquid Blocker, Japan) and air dried for at least 1 h. To extend the protocol for dsDNA phage targets, we added an initial denaturation step by incubating the sample with 75% formamide (Sigma) in 2x SSC for 10 min at 70°C. The samples were then dehydrated in an ethanol series of 1x 70%, 1x 85% and 2x 100% for 2 min each. Hybridization, pre-amplification, amplification and labelling were performed according to the manufacturer's instructions in a humidified chamber placed in a hybridization oven (OV5, Biometra, Göttingen, Germany). We applied the non-target AEP probe and buffer controls as negative controls for *A. aerophoba* samples in each experiment.

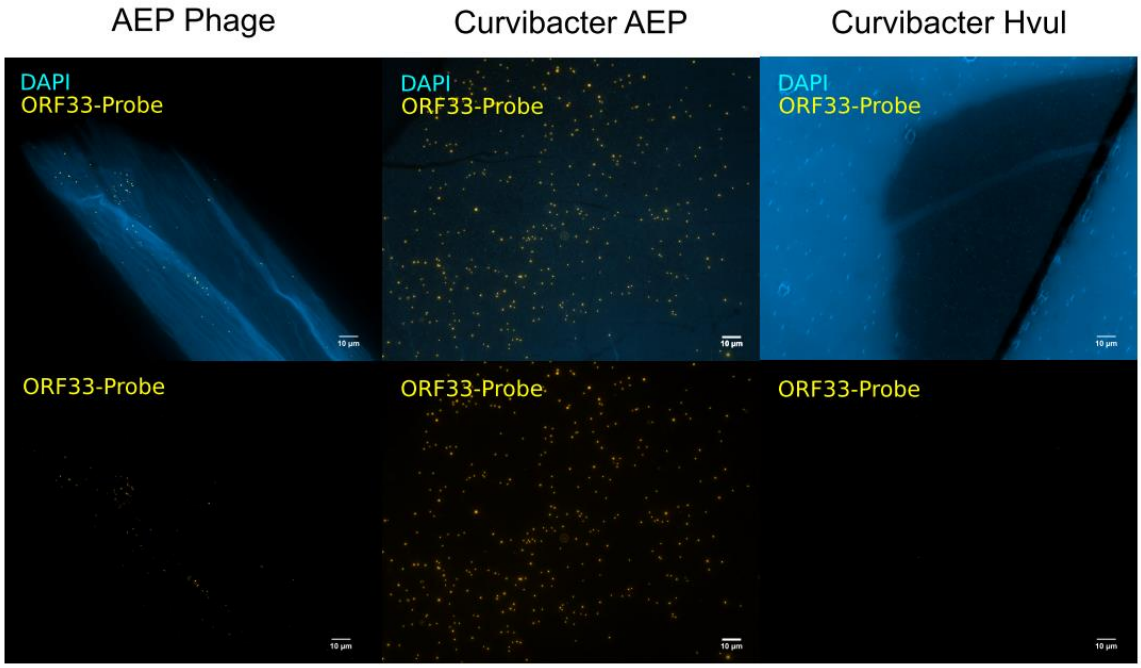

Figure A3-I: Branched-DNA fluorescence *in situ* hybridization system testing. Multiple probes (Cy3, yellow) targeting Curvibacter AEP ORF33 encoding the major capsid protein (VOG1887) were applied to Curvibacter AEP (virocells) and Hvul (no virocells) sharing 95.4% ANI and purified AEP virions.

Correlative light and electron microscopy and set correlation. FISH signals were detected using an Axio Observer. Z1 microscope equipped with AxioCam 506 and Zen 2 version 2.0.0.0 (Carl Zeiss Microscopy GmbH, Göttingen, Germany). Importantly, regions of interest were catalogued to facilitate re-observing the same regions at the electron microscope as follows: acquisition of ROI using 63x objective, acquisition of ROI using 40x objective, acquisition of ROI using 20x objective, acquisition of ROI using 10x objective, stitching of whole section using 10x objective. Slides were then processed as detailed in the supplements of (Jahn et al., 2016). Briefly, cover glass was lifted without lateral movement using a razor blade, and Mowiol mountant (Mowiol 40–88, Kuraray Europe GmbH, Tokyo, Japan) was washed off for 2 x 5 min with PBS. The sections were dried and contrasted in 2.5% uranyl acetate in ethanol for 15 min and in 50% Reynolds' lead citrate in decocted ddH_2O for 10 min. The slides were size-reduced to the region of the sections using a diamond pen and attached to a scanning electron microscopy (SEM) pin stub specimen mount. After coating the sample with a ca. 2.5 mm thick carbon layer to prevent charging of the sample (CCU-010 coating unit with CT-010 carbon thread head, safematic, Switzerland), the samples were ready for imaging using a field emission scanning electron microscope JSM-7500F (JEOL, Japan) with LABE detector (for back scattered electron imaging at extremely low acceleration voltages) directly on the microscope slides. Using the zoom-out reference catalogue described above, regions of fluorescence microscopy were identified at SEM resolution and were correlated using the eC-CLEM tool (Paul-Gilloteaux et al., 2017) using the DAPI channel mainly based on heterochromatin patterns that are visible in both imaging modalities.

Phage *In situ* localisation – Result:

The interaction of the discovered phages with their cellular environment holds the key to understanding their role and regulation in the holobiont system. To spatially resolve this, we estimated that it would require a visualization approach that allows us to spot specific virome-predicted phages *in* the holobionts' ultrastructure. Surprisingly, we realized that to the best of our knowledge, no such approach closes the gap between single molecule phageFISH and electron microscopy. Therefore, we established phageFISH-CLEM (Figure A3-II; for details find Methods), which allowed us to spot three assayed phages of cosmopolitan sponge symbionts at high lateral resolution in the hosts' ultrastructural context deep in the sponge matrix.

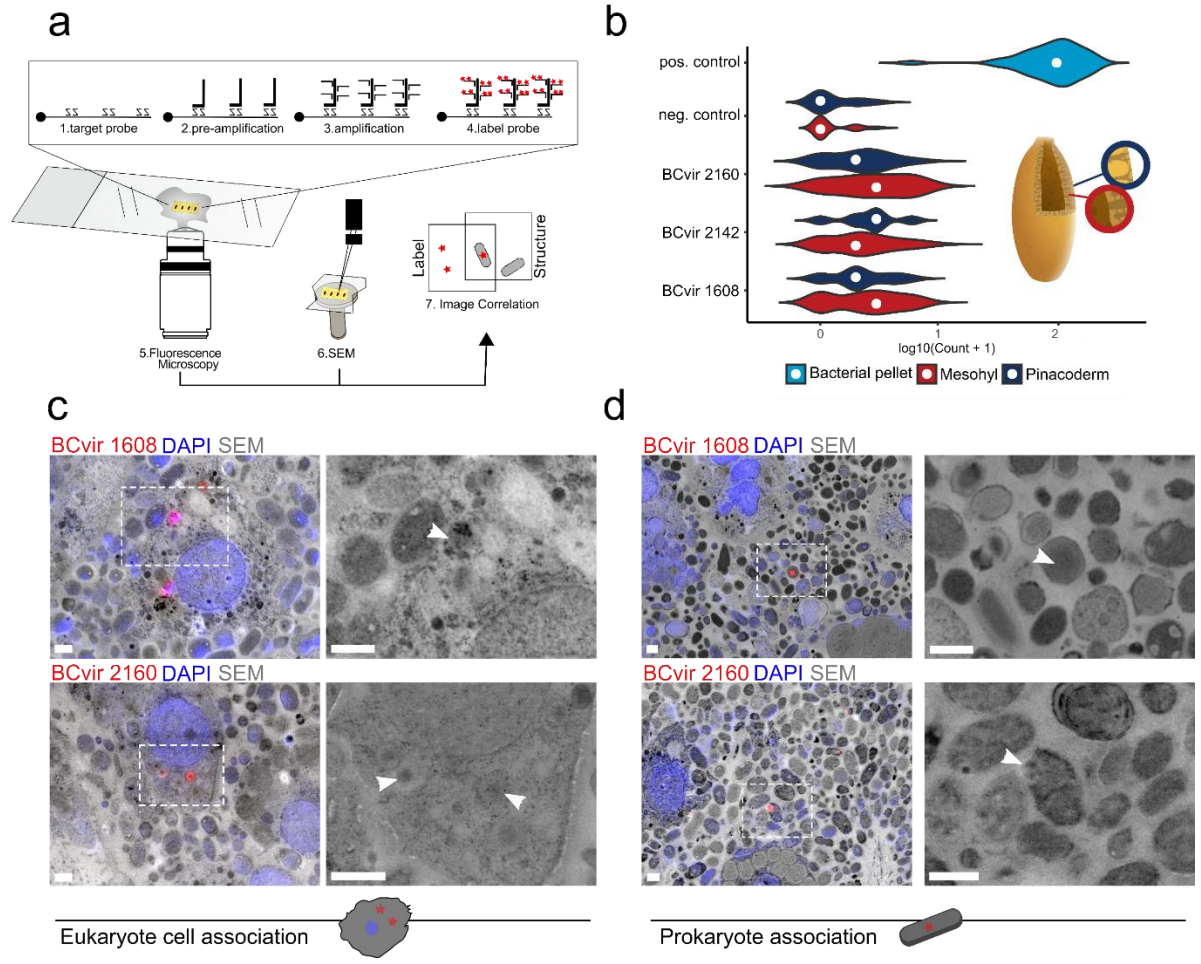

Figure A3-II: Correlative microscopy localizes phages to host ultrastructure. (**A**) Scheme illustrating Phage-FISH-CLEM. (**B**) Computer-aided image quantification of phage signals reveals abundances of different phages over tissues (pinacoderm vs. mesohyl). The graph represents values for $n = 41$ (pos.control), 43 (neg.control), 36 (BCvir 2160; Flavobacteria phage), 66 (BCvir 2142; Poribacteria phage), 98 (BCvir 1608; SBR1093;EC214 phage) measurements of 2 individuals. Representative micrographs show the association of phage signals to (**C**) the phagosomes of eukaryotic cells and (**D**) their prokaryotic host cells. White boxes indicate the regions that are magnified on the right and arrows denote positions of phage signal. Scale bars 1 µm..

To further elucidate the lifestyle of phages predicted to infect abundant, cosmopolitan sponge symbionts we applied then our established ePhageFISH approach to analyse their localisation *in situ*. These were phage BCvir 2142, BCvir 1608 and BCvir 2160 predicted to infect Poribacteria, SBR1093;EC214 and Flavobacteria, respectively. Therefore, phageFISH-CLEM was run on cryo-immobilized *A. aerophoba* sponge tissues targeting structural genes of our chosen phages. Computer-aided quantification of probe signal confirmed community-level trends from virome sequencing we reported in CHAPTER 7 showing rather homogeneous phage distribution over tissues. Specifically, signals confirmed the presence of all three phages deep in the sponges' tissue as well as in the outer pinacoderm layer (Fig. 4b, non-target probe comparison; p values$\leq$0.0007, z$\geq$3.32, df=4). There was no clear delineation of phage signal levels between the outer pinacoderm and inner mesohyl tissue, in general (Kruskal-Wallis (KW) test: p value=0.6312, chi squared=0.23044, df = 1), and when tested for the three phages separately. This similarity between tissues is in line with the community-level trends we observed from virome sequencing (previous section). Furthermore, differences in phage signals between BCvir 2142, BCvir 1608 and BCvir 2160 were marginal (KW test: kw chi squared=101.5033, df=4; p value$\geq$0.4437). This indicates a rather homogeneous distribution and abundance levels of assayed phages as derived from analysing 284 images from two individuals. We note that these estimates are not absolute but rather relative measures of abundance as stated in Chin et al. (2015).

Taking advantage of the high resolution of the correlated electron microscopy, we next showed that extracellular virion pool foraging in the mesohyl was low for the assayed phages. Signals of the three assayed phages mainly appeared as single signal spots associated with bacterial cells (Figure A3-II d), which is indicative of lysogenic or pseudo-lysogenic stages.

A temperate lifestyle of BCvir 2160 is in line with the presence of the integrase gene in its genome CHAPTER 7, while clear homologues are missing for the other two phages. Notably, morphotypes of targeted prokaryote cells differed per phage probe in line with different bacterial hosts they are predicted for. A frequently observed pattern was that BCvir 1608 and BCvir 2160 signals gravitated towards sponge cells (Figure A3-II c). CLEM of these regions confirmed their intracellular localization within phagosomes of sponge cells, which are vesicles containing engulfed particles. The size of measurable particles within the phagosomes ranged below 200 nm (average 197.7 nm, ± SD 20.4, n=5), indicating that virions rather than virocells were cleared by phagocytosis.

APPENDIX B: Thesis Introduction & Discussion

Appendix B1

```
# downloaded Porifera entries from Obis database
#"https://mapper.obis.org/?taxonid=558,146191#" OBIS (07/29/2019) Ocean Biogeographic Information System.

library(oceanmap)

dat <- read.csv("dd2d6ec7f88a65483243d48e56409438ff5785a1.csv") #  OBIS DATA (366MB file)
dat = subset(dat , dat$class!="" & dat$class!="Porifera" & dat$class!="Porifera incertae sedis") # filter for class

dat$groupCol = droplevels(dat$class)
dat$groupCol <- gsub("Calcarea", "#ff841dff", dat$groupCol) # define class coloring
dat$groupCol <- gsub("Demospongiae", "#027180ff", dat$groupCol)
dat$groupCol <- gsub("Hexactinellida", "yellow", dat$groupCol)
dat$groupCol <- gsub("Homoscleromorpha", "#bbae9cff", dat$groupCol)


# map global Porifera distribution

tiff("Porifera_world_disribution.tiff",height = 8, width = 8, units = 'in', res = 600)

plotmap(lon=range(dat$decimalLongitude),lat=range(dat$decimalLatitude),
        border='lightgray', col.bg="blue", fill.land = T, ticklabels=T, grid=F, col.land="lightgray", bwd=0)

points(dat$decimalLongitude,dat$decimalLatitude, cex=.5, pch = 21, bg = dat$groupCol, col = "black")

legend(-188,-110, col = "black", pch=21,
       legend=(c("Calcarea","Demospongiae", "Hexactinellida", "Homoscleromorpha" )),
       pt.bg=c("#ff841dff","#027180ff", "yellow", "#bbae9cff" ),
       ncol = 4, border=1, bty = "n", x.intersp=0.5, text.font=3, cex = 0.95)
dev.off()

############################   sessionInfo()


R version 3.5.1 (2018-07-02)
Platform: x86_64-w64-mingw32/x64 (64-bit)
Running under: Windows 7 x64 (build 7601) Service Pack 1
```

Appendix Code 1: Code to reproduce Error! Reference source not found.**: Global distribution of *Porifera*.**

Appendix B2

```
library("phyloseq")
library("ggplot2")
library("doParallel")
registerDoParallel(cores=20)

# load data ; source: https://doi.org/10.1093/gigascience/gix077
meta <- read.csv("sample.metadata.tsv", sep="\t") # EMP metadata table
daten = import_biom("QIIME-output.biom", treefilename="QIIME-derived_tree.tre", parallel=T)

# filter data
meta_s <- subset(meta, meta$env_package == "host-associated") # filter for sponge samples n=3571
sample_data(daten)$ENV <- rownames(sample_data(daten)) # create ID index
daten_s = subset_samples(daten, ENV %in% meta_s$sample_name_qiime_deblur) #  subset and remove seawater
daten_s_gl = tax_glom(daten_s, "Rank4" ) # collapse OTU table at order level
daten_s_gl_no0 <- prune_taxa(taxa_sums(daten_s_gl) > 0, test) # remove empty taxa
daten_s_gl_no0_mrg <-  merge_samples(test, "study") # merge samples info not needed here

# plot tree
pdf("EMP_tree.pdf", height = 30, width = 30)

plot_tree(daten_s_gl_no0_mrg, color="Rank2", size = "abundance", label.tips = "Rank2")+ coord_polar(theta="y") +
    geom_treescale(fontsize=6, linesize=10, offset=1, width=1, color='red') # label by Phylum

dev.off()
```

Appendix Code 2: Code to reproduce Figure 5: - "Sponge Microbiome Project"-prokaryote diversity.

Appendix B3

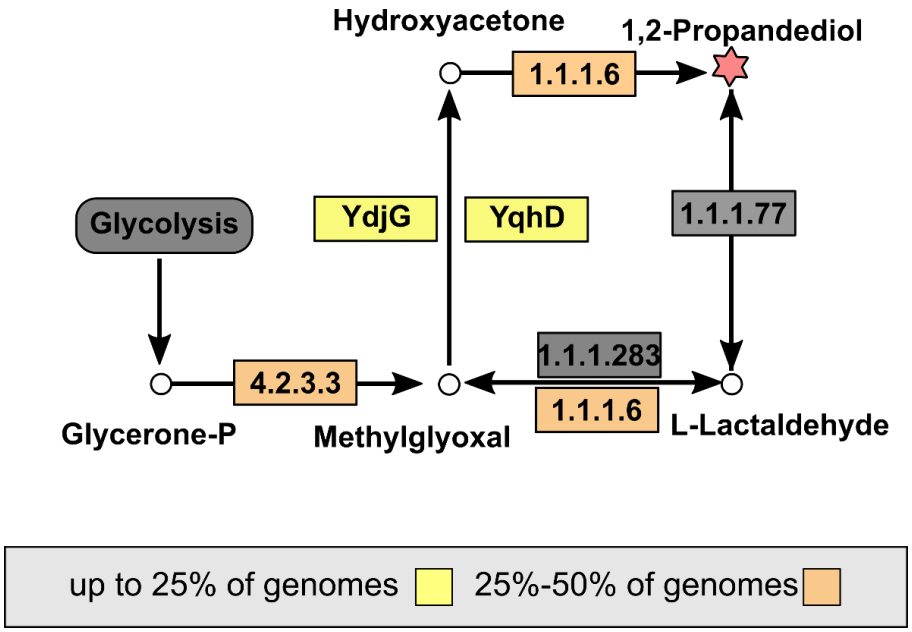

Figure B3-I: Propionate metabolism leading to 1,2 Propanediol. 145 bacterial and archaeal genomes with ecosystem annotation "Porifera" or "sponge" were selected in the IMG database (as of Oct 2019) and their annotated functions were mapped to the propionate metabolism (KEGG:map00640) using the Integrated Microbial Genomes & Microbiomes(IMG/M) system interface (Chen et al., 2019).

Appendix B4

Table: ANKp: Phyre2 3D modelling hits.

Rank	Model	Conf-idence	Sequence ID	Q start	Q end	PDBTitle
1	c5d66B_.1	0.99	25	26	184	Crystal structure of an ankyrin repeat domain (abaye2397)
2	c4rlvA_.2	0.99	33	4	184	crystal structure of ankb 24 ankyrin repeats in complex with ankr2 autoinhibition segment
3	d1oy3d_.3	0.99	28	18	184	crystal structure of an **ikbbeta/nf-kb** p65 homodimer complex
4	c1oy3D_.4	0.99	28	18	184	crystal structure of an **ikbbeta/nf-kb** p65 homodimer complex
5	c5y4fA_.5	0.99	39	5	184	crystal structure of ankb ankyrin repeats r13-24 in complex with2 autoinhibition segment ai-c
6	c3v31A_.6	0.99	21	25	184	crystal structure of the peptide bound complex of the ankyrin repeat2 domains of human ankra2
7	c5vkqC_.7	0.99	25	6	184	structure of a mechanotransduction ion channel drosophila nompc in2 nanodisc
8	c6by9A_.8	0.99	34	20	183	crystal structure of ehmt1
9	c4o60A_.9	0.99	38	25	183	structure of ankyrin repeat protein
10	c4cj9A_.10	0.99	11	4	183	burrh dna-binding protein from burkholderia rhizoxinica in2 its apo form
11	c3eu9B_.11	0.99	21	22	180	the ankyrin repeat domain of huntingtin interacting protein 14
12	c5jhqD_.12	0.99	36	5	183	arcs 1-3 of human tankyrase-1 bound to a peptide derived from irap
13	c4xd0A_.13	0.99	19	5	181	x-ray structure of the n-formyltransferase qdtf from providencia2 alcalifaciens
14	c3keaB_.14	0.99	18	5	183	structure function studies of vaccinia virus host-range protein k12 reveal a novel ankyrin repeat interaction surface for k1s function
15	c6fesC_.15	0.99	35	5	184	crystal structure of novel repeat protein bric2 fused to darpin d12

Appendix B5

Plasmid map: Synthesised ANKp-HIS tag construct

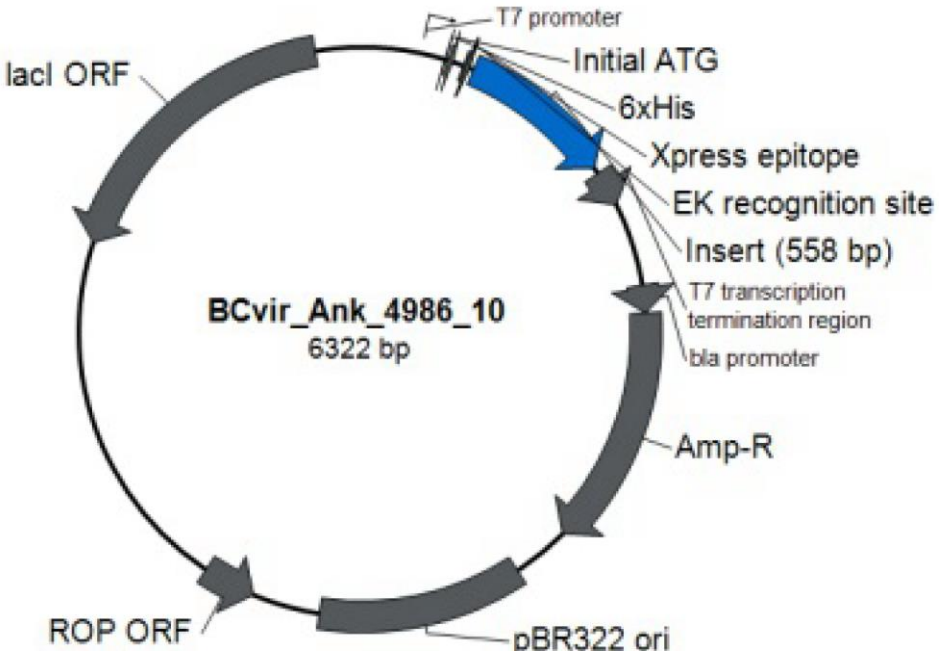

Insert Sequence name: BCvir_4986_10 (ANKp)

Express cloning vector: pET100/D-TOPO

Appendix B6

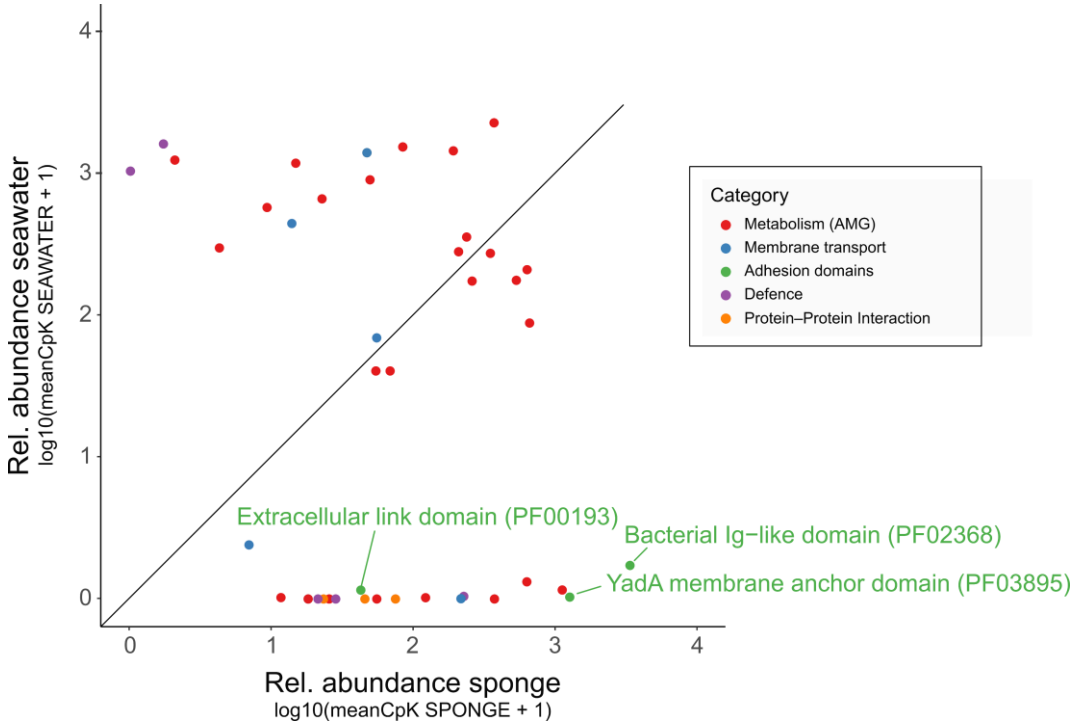

Appendix Figure: Viral adhesion domain relative abundance in sponge versus seawater. Raw data available in Chapter 7 Data S1; doi: 10.1016/j.chom.2019.08.019.

CURRICULUM VITAE

Martin Thomas Jahn

born 09.06.1988
in Biberach an der Riß

Education

Oct 2012 – Dez 2014	**Master in Biology** (MSc), University of Würzburg, Germany. Majors: Gene Regulation and Signal Transduction, Microbial and Chemical Ecology, Animal Ecology
Oct 2009 – Aug 2012	**Bachelor in Biology** (BSc), University of Würzburg, Germany.
June 2008	**Allgemeine Hochschulreife** (=qualification for university entrance), Wirtschaftsgymnasium Crailsheim, Germany.

Research Experience

since Mar 2015	**Doctoral project:** „Physiology, syntrophy and viral interplay in the marine sponge holobiont" Supervisor: Prof. Ute Hentschel
Jan 2014 – Dez 2014	**Master thesis**: "Transcriptomic analyses of poribacterial sponge symbionts" at the Department of Botany II, University of Würzburg. Supervisor: Prof. Ute Hentschel.
Sep 2013 – Dec 2013	**Research stay** working in molecular microbiology at the School of Environmental Sciences, University of East Anglia, Norwich, England. Supervisor: Prof. Thomas Mock.
Mar 2012 – Jul 2012	**Internship and Bachelor thesis**: "Immunological analysis of guttation fluid of *Bacillus thuringiensis* maize for the presence of Cry1Ab toxin" at the Department of Zoology III, University of Würzburg. Supervisor: Dr. Stephan Härtel.
Aug 2011 – Nov 2011	**ERASMUS fellowship**: "Assessing the ecological relationships determining tick (*Ixodes ricinus*) abundance and *Borrelia burgdorferi sensu lato* prevalence" at the Institute of Biodiversity, Animal Health and Comparative Medicine, University of Glasgow, Scotland. Supervisor: Dr. Roman Biek.
Feb 2011 – Aug 2011	**Student assistant** at the Department of Biochemistry, Würzburg. Work with *Danio rerio* as laboratory animals. Supervisor: Dr. Anja Hirmer.

Publications in peer-reviewed journals

1. **Jahn M.T.**, Arkhipova, K, Markert S.M., Stigloher C., Lachnit T., Pita L., Kupczok A., Ribes M., Stengel S.T., Rosenstiel P., Dutilh B.E., Hentschel U. (2019). A Phage Protein Aids Bacterial Symbionts in Eukaryote Immune Evasion. *Cell Host & Microbe*. 24,2019
2. Rausch, P., Rühlemann, M., Hermes, B. M., Doms, S., Dagan, T., Dierking, K., Domin, H., Fraune, S., von Frieling, J., Hentschel, U., Heinsen, F.-A., Höppner, M., **Jahn M. T.**, Jaspers, C., Kissoyan, K. A. B., Langfeldt, D., Rehman, A., Reusch, T. B. H., Roeder, T., Schmitz, R. A., Schulenburg, H., Soluch, R., Sommer, F., Stukenbrock, E., Weiland-Bräuer, N., Rosenstiel, P., Franke, A., Bosch, T., Baines, J. F. (2019). Comparative analysis of amplicon and metagenomic sequencing methods reveals key features in the evolution of animal metaorganisms. *Microbiome* **7**(1): 133.

3. **Jahn M.T.**, Markert S.M., Ryu T., Ravasi T, Stigloher C., Hentschel U., Moitinho-Silva (2016). Shedding light on cell compartmentation in the candidate phylum *Poribacteria* by high resolution visualisation and transcriptional profiling. *Sci. Rep.* **6**, 35860
4. Hildebrand F, Moitinho-Silva L, Blasche S, **Jahn M.T.**, Gossmann T.I., Heuerta-Cepas J, Hercog R, Luetge M, Bahram M, Pryszlak A, Alves R.J., Waszak S.M., Zhu A, Ye L, Costea P.I., Aalvink S, Belzer C, Forslund S.K., Sunagawa S, Hentschel U, Merten C, Patil K.R., Benes V, Bork P (2019). Antibiotics-induced monodominance of a novel gut bacterial order. *Gut* **68**:1781-1790.
5. Slaby B.M., Franke A, Rix L, Pita L, Bayer K, **Jahn M.T**., Hentschel U (2019) marine sponge holobionts in health and disease. In: Li Z, editor. Symbiotic microbiomes of coral reefs sponges and corals. Dordrecht: *Springer Netherlands*. p.81-104.
6. Millins C, Dickinson E. R., Isakovic P, Gilbert L, Wojciechowska A, Paterson V, Tao F, **Jahn M.T.**, Kilbride E, Birtles R, Johnson R, Biek R (2018). Landscape structure affects the prevalence and distribution of a tick-borne zoonotic pathogen. *Parasit Vectors* **11**(1): 621
7. Bayer K., **Jahn M.T.**, Slaby B.M., Moitinho-Silva L., Hentschel U. (2018). Marine Sponges as *Chloroflexi* Hot Spots: Genomic Insights and High-Resolution Visualization of an Abundant and Diverse Symbiotic Clade. *mSystems* **3**(6)
8. Moitinho-Silva L, Díez-Vives C, Batani G, Esteves A.I.S., **Jahn, M.T.**, Thomas T (2017). Integrated metabolism in sponge-microbe symbiosis revealed by genome-centered metatranscriptomics. *ISME J*.
9. **Jahn, M.T.**, Markert S.M., Ryu T, Ravasi T, Stigloher C, Hentschel U, Moitinho-Silva (2016). Shedding light on cell compartmentation in the candidate phylum Poribacteria by high resolution visualisation and transcriptional profiling. *Sci. Rep.* **6**, 35860
10. Horn H, Slaby B, **Jahn M.T.**, Bayer K, Moitinho-Silva L, Förster F, Abdelmohsen U.R., Hentschel U (2016) An enrichment of CRISPR and other defense-related features in marine sponge-associated microbial metagenomes. *Front. Microbiol.* **7**:1751
11. **Jahn, M.T.**, Schmidt K., Mock, T (2014). A novel cost effective and high-throughput isolation and identification method for marine microalgae. *Plant Methods* 10:26.

Research interests

- Ecological and molecular foundations of microbe-microbe and microbe-host interactions.

Awards and Fellowships

2017: Young Investigator Award CRC1182 Origin and Functions of Metaorganisms.

2017: Poster prize Gordon Research Conference: Animal-Microbe-Symbioses, Mount Snow, USA

2016: Poster prize EMBL-Conference: From 3D Light to 3D Electron Microscopy, Heidelberg

2015: Fellowship of the Graduate School of Life Sciences (GSLS), University of Würzburg.

Selected Posters and Talks

1. **Jahn M.T.**, Arkhipova K., Markert S. M., Stigloher C., Lachnit T., Rix L., Pita L., Kupczok A., Ribes M., Dutilh B.E., Hentschel U.: Exploring viral dark matter in marine sponges, ISME17- 17th International Symposium on Microbial Ecology. Leipzig, Germany, 2018 (Selected talk)
2. **Jahn M.T.**, Taravat A., Markert S. M., Stigloher C., Moitinho-Silva L., Baldassarre L., Fraune S., Hentschel U.: Investigating spatial relationships of host-associated microbes using correlative light and electron microscopy, Gordon Research Conference: Animal-Microbe-Symbioses, Mount Snow, VT, USA, 2017 (Selected poster)
3. **Jahn, M.T.**, Markert S. M., Ryu T., Ravasi T., Stigloher C., Hentschel U., Moitinho-Silva L.: Investigating environmental bacteria by high resolution microscopy and transcriptional profiling: A case study with *Poribacteria*, Microbiology and Infection. Würzburg, Germany, 2017 (Selected talk)
4. **Jahn, M.T.**, Markert S.M., Stigloher C., Hentschel U., Moitinho-Silva, L.: Shedding Light on the Candidate Phylum *Poribacteria* by Fluorescence *in situ* Hybridization Correlative Light and Electron Microscopy (FISH-CLEM), EMBL-Conference: From 3D Light to 3D Electron Microscopy. Heidelberg, Germany, 2016 (Selected talk)

5. **Jahn, M.T.**, Moitinho-Silva, L., Markert M.M., Stigloher C., Hentschel U.: Transcriptional profiling provides evidence for cell compartmentation in *Poribacteria*, 2nd *Planctomycetes-Verrucomicrobia-Chlamydiae Superphylum*: New model organisms, Sevilla, Spain, 2015 (Selected talk)

Scientific skills

Bioinformatics, including the analysis of high-throughput sequencing and genomic data. Experienced in Python, Pascal, HTML, Linux/UNIX shell scripting and "R".

Molecular biology methods for the isolation, manipulation and identification of DNA, RNA and proteins.

Advanced microscopy approaches to spot *in silico* detected microbial symbionts in their hosts, to analyze their gene expression and phage infection. Experienced in correlative light and electron microscopy combined with single molecule (sm)phage-FISH, smRNA-FISH, smGene-FISH, immunohistochemistry and high-resolution microscopy of model and non-model host species.

Statistics for general data analysis and analysis of spatial landscape patterns.

Languages

Native language:	German
Second languages:	English (fluent), French (basic)

ERKLÄRUNG

Hiermit erkläre ich, dass ich die vorgelegte Dissertation bis auf die Beratung durch meine Betreuer, in Inhalt und Form selbstständig und ohne Zuhilfenahme unerlaubter Hilfsmittel angefertigt habe. Ich versichere, dass diese Arbeit unter Einhaltung der Regeln guter wissenschaftlicher Praxis der Deutschen Forschungsgesellschaft verfasst wurde. Alle benutzten Quellen und Hilfsmittel habe ich vollständig angegeben und die Zusammenarbeit mit anderen Wissenschaftlern habe ich kenntlich gemacht. Weder diese noch eine ähnliche Arbeit wurden an einer anderen Abteilung oder Hochschule im Rahmen eines Prüfungsverfahrens vorgelegt, veröffentlicht oder zur Veröffentlichung vorgelegt. Mir wurde kein akademischer Grad entzogen und dies ist mein erstes und einziges Promotionsverfahren.

Martin T. Jahn
Kiel, 18. Dezember 2019